

NRL Report 7406

Criteria for Fracture Control Plans

W.S. Pellini, Metallurgy Division

May 11, 1972

Naval Research Laboratory

DOCUMENT CONTROL DATA - R & D

(Security classification of title, body of abstract and indexing annotation must be entered when the overall report is classified)

1. ORIGINATING ACTIVITY (Corporate author) Naval Research Laboratory Washington, D.C. 20390		2a. REPORT SECURITY CLASSIFICATION Unclassified	
		2b. GROUP	
3. REPORT TITLE CRITERIA FOR FRACTURE CONTROL PLANS			
4. DESCRIPTIVE NOTES (Type of report and inclusive dates) Special summary and interpretive report.			
5. AUTHOR(S) (First name, middle initial, last name) W. S. Pellini			
6. REPORT DATE May 11, 1972		7a. TOTAL NO. OF PAGES 98	7b. NO. OF REFS 2
8a. CONTRACT OR GRANT NO. NRL Problems MO1-25, MO1-24, and MO1-14		9a. ORIGINATOR'S REPORT NUMBER(S) NRL Report 7406	
b. PROJECT NO. RR022-01-46-5432 and 5431		9b. OTHER REPORT NO(S) (Any other numbers that may be assigned this report)	
c. RR022-11-41-5409			
d.			
10. DISTRIBUTION STATEMENT Approved for public release; distribution unlimited.			
11. SUPPLEMENTARY NOTES		12. SPONSORING MILITARY ACTIVITY Dept. of the Navy (Office of Naval Research) Arlington, Va. 22217	
13. ABSTRACT <p>This report presents interpretations of the significance of fracture-state criteria and their application in the development of rational fracture-control plans. A "brief" is evolved for meeting of regulatory and/or contractual requirements, based on scientific and technologically appropriate procedures. It is emphasized that the emerging issues of the 1970's center on technological application of fracture-control principles, in the total context of engineering realities and normal business relationships.</p> <p>The report is addressed to a very broad audience and focuses on primary issues. It is intended to clarify these issues for the general engineering field and also for those who are in a position to dictate requirements, i.e., those with regulatory responsibilities. The various parts are presented in a format which provides for separate reading, depending on specific interests.</p> <p>A most important feature involves initial explanation of basic aspects of constraint factors. These aspects underlie all considerations of criteria definition, selection, and validation. A physical-model approach is used for these explanations, thus avoiding the inordinate complications and limitations of mathematical expressions. As such, it should be understandable to the broadest possible audience.</p>			

(Continued)

14. KEY WORDS	LINK A		LINK B		LINK C	
	ROLE	WT	ROLE	WT	ROLE	WT
Fracture-safe design Fracture control of engineering structures Fracture tests Interpretations of fracture tests Fracture mechanics Structural mechanics High strength metals Structural reliability Metallurgical engineering Structural steels						
<p>Discussions of procedures for evolving fracture-control plans are based on a common reference to fracture states and related criteria. The common reference evolves from fracture mechanics, as a generalized subject which covers all possible fracture states. The primary issues are defined as related to the use of fracture tests which are rational, in terms of fracture-mechanics principles. It is emphasized that the statistical definition of fracture properties is essential to the engineering selection of appropriate metals from a complex aggregate of standard grades.</p>						

PREFACE

This is the third in a series of interpretive reports that were evolved for clarification of fracture-test criteria and their significance to design practices.

- The first report provided a *chronological* account of the development of fracture tests and design criteria.

- The second report described practical engineering procedures for fracture-safe design—with special emphasis on the unique *Analysis Diagrams* approach to problem solving.

- The present report extends the coverage to the primary issues of the 1970's, which focus on the *rationality of fracture-control plans*.

These broader issues require consideration of the information needs of a *new* audience—those who are responsible for imposing reliability requirements, for contractual or regulatory reasons. The report is structured in six parts, for selection as to specific interests.

The *general* reader, who is primarily concerned with state-of-practices questions, is directed to Parts 1 and 6.

CONTENTS

Abstract	v
Problem Status	v
Authorization	v
 NOMENCLATURE	 vii
 PART 1. BRIEF	 1
 PART 2. SIGNIFICANCE OF FRACTURE-MECHANICS CRITERIA	 3
Generalized Fracture Mechanics	3
Physical Significance of Constraint	4
Constraint Relaxation	8
Engineering Significance of Fracture States	10
Metallurgical Aspects of Constraint Transitions	12
Fracture-Extension Processes	16
Section-Size Effects	17
Engineering Significance of Plane-Strain Transition	21
Numerical Definition of Constraint Capacity	22
Test Methods Featuring Definable Constraint Capacities	24
 PART 3. METAL CHARACTERIZATION AND SELECTION PROCEDURES FOR TEMPERATURE-TRANSITION PROBLEMS	 28
General Requirements	28
Fracture-Test Characterization of Metal Properties	29
Statistical Aspects of Metal Quality	32
Loading-Rate Factors	33
Considerations for Compliant Structures	34
 PART 4. METAL CHARACTERIZATION AND SELECTION PROCEDURES FOR STRENGTH-TRANSITION PROBLEMS	 36
Strength-Induced Constraint Transitions	36
Principles of Initiation and Arrest	41
Case Example of Design Based on Arrest and Initiation Principles	42
Generalized Use of RAD Procedures	46
Status of Procedures for Defining the Elastic-Plastic Region	51
Metallurgical Rationale for Quality-Level Corridors	52
Statistical Variance of Mechanical Properties	55
Titanium and Aluminum Alloys	60
Critical-Edge Concept for Metal Improvement	65

PART 5. ENGINEERING APPLICATIONS OF RATIONAL FRACTURE CRITERIA .	65
Requirements	65
Availability of Rational-Criteria Data	68
The Charpy Impasse	70
Intermediate-Strength, Quenched and Tempered (Q&T) Steels	72
PART 6. RELATION TO DESIGN PRACTICES	75
Functional Requirements	75
Probability Assessment	77
Fracture Properties Rank-Level Considerations	78
Implications of Research Directions	79
Cost Factors	80
ANNOTATED REFERENCES	82
APPENDIX A -- Information of Special Interest	84

ABSTRACT

This report presents interpretations of the significance of fracture-state criteria and their application in the development of rational fracture-control plans. A "brief" is evolved for meeting of regulatory and/or contractual requirements, based on scientific and technologically appropriate procedures. It is emphasized that the emerging issues of the 1970's center on technological application of fracture-control principles, in the total context of engineering realities and normal business relationships.

The report is addressed to a very broad audience and focuses on primary issues. It is intended to clarify these issues for the general engineering field and also for those who are in a position to dictate requirements, i.e., those with regulatory responsibilities. The various parts are presented in a format which provides for separate reading, depending on specific interests.

A most important feature involves initial explanation of basic aspects of constraint factors. These aspects underlie all considerations of criteria definition, selection, and validation. A physical-model approach is used for these explanations, thus avoiding the inordinate complications and limitations of mathematical expressions. As such, it should be understandable to the broadest possible audience.

Discussions of procedures for evolving fracture-control plans are based on a common reference to fracture states and related criteria. The common reference evolves from fracture mechanics, as a generalized subject which covers all possible fracture states. The primary issues are defined as related to the use of fracture tests which are rational in terms of fracture-mechanics principles. It is emphasized that the statistical definition of fracture properties is essential to the engineering selection of appropriate metals, from a complex aggregate of standard grades.

PROBLEM STATUS

This is a special summary and interpretive report covering the results of a wide spectrum of investigations within NRL. These investigations are aimed at the general problem of metallurgical optimization and fracture-safe design. The major portions of the studies are continuing under the established problems.

AUTHORIZATION

NRL Problem Nos. M01-25, M01-24, and M01-14
Project Nos. RR 022-01-46-5432, RR 022-01-46-5431,
and RR 022-11-41-5409

Manuscript submitted March 6, 1972.

NOMENCLATURE

a	depth, or length of the crack (in.)
B or T	thickness of the plate or specimen (in.)
C _v	Charpy-V test
CAT	Robertson Crack Arrest Temperature
0.5 σ_{ys} CAT	as applied to temperature transition cases, signifies that fracture-extension stress equals 0.5 σ_{ys}
COD	Crack Opening Displacement
DT	Dynamic Tear Test — all sizes
DWT	Drop Weight Test
FTE	Fracture Transition Elastic
IAD	Instability Analysis Diagram
J _c	critical value of the J-integral for characterization of elastic-plastic or plastic-fracture states
K, K _I	stress intensity factor; the subscript I denotes the opening mode of crack extension (ksi $\sqrt{\text{in.}}$)
K _I -tests	K _{Ic} tests conducted for various controlled rates of loading
K _{Ic}	slow-load (static) plane strain fracture toughness (ksi $\sqrt{\text{in.}}$)
K _I d	dynamic-load plane strain fracture toughness (ksi $\sqrt{\text{in.}}$)
K _c	plane stress condition at crack tip for initiation; also, crack conditions in propagation as related to this fracture mode (ksi $\sqrt{\text{in.}}$)
K _Q	questionable or invalid values of K due to excessive plastic deformation of the crack tip
NDT	Nil Ductility Transition temperature obtained by DWT or indexed by DT test
Q	crack-shape parameter for semielliptical surface cracks

Q&T	quenched and tempered steel
r	plastic zone radius (in.)
RAD	Ratio Analysis Diagram
Ratio	signifies K_{Ic}/σ_{ys} or K_{Id}/σ_{yd}
R-curve	increased resistance to fracture extension, resulting from the initial development of a plastic enclave
Shelf	highest level of ductility attained at completion of constraint transition, due to temperature
ϵ_c	critical strain for crack extension
ϵ	true strain of flow-curve plot
σ	applied stress (psi or ksi)
σ_f	failure stress
σ_{yd}	yield strength for dynamic loading (psi or ksi)
σ_{ys}	yield strength for static (slow) loading (psi or ksi)

CRITERIA FOR FRACTURE CONTROL PLANS

PART 1. BRIEF

A rapidly changing situation has evolved with respect to the application of fracture-prevention principles to structural design. In former years the fracture research specialists were concerned with convincing the design field to adopt and use rational principles of fracture-safe design as normal practice, rather than as a special consideration. Present trends feature requirements for such practices, which are imposed on the design field by the user or by regulatory authorities.

The result is a dramatic broadening in the number and type of interested parties who must understand the general issues involved. Moreover, there is a broadening of issues because the design process must now be considered in the total context of engineering realities and normal business relationships.

The need to discuss broad issues is gradually being met by the emergence of a new literature which focuses on discussions of *fracture control plans, certification procedures, structural integrity programs, design validation, specification criteria, surveillance and life-time validation requirements, etc.* These terms connote formalized procedures for the translation of scientific principles to technological practice.

The rationality of these procedures depends on the understanding and appropriate application of generalized fracture mechanics principles. A distinction is made with linear-elastic (plane strain) fracture mechanics, which is restricted to considerations of the brittle state. Generalized fracture mechanics recognizes all of the three possible fracture states, as follows:

1. Plane strain
2. Elastic-plastic
3. Plastic.

The fracture state of the metal is disclosed by appropriate test procedures. Fracture tests have meaning only when they index the level of fracture resistance within the *range* of a fracture state. The fracture state defines the lower-bound reliability of a structure. For example, fracture properties of the elastic-plastic type automatically exclude plane strain (brittle) behavior. In general, the designated fracture state excludes lower orders and, therefore, places a "floor" on the expected performance.

The floor-level of structural performance is the most crucial aspect of fracture-safe design. It defines the minimum guarantee that is provided and, therefore, it is a reliability index of primary reference. In practice, the minimum guarantee evolves from

selection of an appropriate fracture criterion. The term "criterion" has a specific meaning which may be expressed in test-specimen or structural-design terms.

- It represents a fracture test *value* which defines a specific level of fracture resistance within a fracture state.
- It represents the basis on which the design is predicated, i.e., the level of fracture resistance within a fracture state, that is used in specifications.

Thus, "criterion" always signifies a specific fracture-state level, irrespective of its reference as a test value or as a structural specification index. The term "criteria" for fracture control plans implies the range of criterion levels available to meet design requirements.

There is a growing awareness that the design of engineering structures should include documentation of fracture control plans based on specific minimum criteria. Such requirements are being imposed as legally binding sections of specification documents. Thus, what was formerly a subject of general professional responsibility is rapidly becoming a matter of contractual obligation. These trends are most evident in the actions of "regulatory" governmental authorities who are becoming increasingly active in the formulation of rules for the protection of public interests. Mandatory application of rational fracture-prevention criteria should be expected for bridges, ships, aircraft, transport systems involving flammable or toxic materials, nuclear reactors, etc.

A rational fracture control plan must represent a *total* solution to a structural design problem. It includes selection of scientifically defensible fracture-safe design procedures, as well as considerations of certification factors pertaining to metal specifications, quality control, inspectability, lifetime surveillance, etc.

A design process which involves contractual responsibility for definition of a fracture control plan, with *documentation, defense, and guarantee* of all related aspects, requires searching examination and selection of metal-properties criteria. Errors in selection of the appropriate criterion may prejudice or invalidate the total plan.

Unfortunately, the literature on fracture research is highly specialized and the notable agreements which exist on fracture-state criteria are obscured by masses of detail. Moreover, the processes of metal-property surveys and sources of this information are not considered in adequate detail. Serious concern must be expressed for the paucity of statistically reliable engineering fracture data for standard grade metals that is provided by the existing literature. Developing this information is of foremost consequence at this time.

These omissions in the literature have adverse effects on the status of engineering practices. Elaborate specifications as to chemistry, section size, heat treatment, etc., are listed for the standard grades. Minimum yield strength and tensile ductility parameters are provided by these specifications. Reference to fracture properties, which would be significant for deducing the fracture state, are notable by omission. Thus, the engineer is provided with the essential information for design based on tensile properties but not for design which includes fracture control plans. He must search for this information by reference to complex literature or by consultation with those who may have experience with particular metals of specific section size, heat treatment, etc. Engineers who have

engaged in such searches will document the difficulty involved and the scarcity of reliable data.

It is important that statistical data be collected in terms of fracture-state criteria. These data are essential for defining what is attainable for specific metals and for design and specification purposes.

The engineer should be provided with unequivocal information as to the criterion that can be met by standard grade metals, for specified temperature and/or strength levels. Whether or not he elects to use a metal of lowest, intermediate, or highest fracture-state properties is an engineering question. For example, he should know how to specify a particular criterion which guarantees properties which are either low or high in the elastic-plastic fracture state, if the service conditions require such properties.

PART 2. SIGNIFICANCE OF FRACTURE MECHANICS CRITERIA

Generalized Fracture Mechanics

Fracture mechanics implies an analytical approach to defining the effective strength of structures in the presence of cracks. It does not imply that analytical treatment provides for using metals of unreliable fracture-state properties in defensibly safe structures. However, this is the primary, albeit incorrect, attraction that has evolved for its application to engineering practice. Fracture mechanics does not substantiate such unrealizable hopes; thus, clarification of the true attractive features is essential.

There are two main subdivisions of fracture mechanics theory—plane strain (linear elastic) and plane stress. The latter term is well understood by the research field but leads to complexities in communication with engineers. It is best replaced by exact definitions of the two parts of the plane stress state—the elastic-plastic and the plastic. Generalized fracture mechanics is an appropriate term for describing the totality of the subject, i.e., covering all three fracture states.

It is unfortunate that fracture mechanics has been popularly connected only with measurement of plane strain properties. Plane strain fracture mechanics, otherwise known as "linear elastic," is concerned with analytical treatment of the brittle state. This was an obvious starting point for analytical research.

Fortunately, fracture mechanics theory provides a basis for extension of analytical treatment into the elastic-plastic and plastic fracture states. The fact that little has been said in the literature relating to this aspect in recent years reflects the overemphasis that has been placed on the brittle state. This neglect is now being rectified. The primary emphasis in research is now being placed on developing improved analytical treatment for the elastic-plastic and plastic cases and on metallurgical aspects. Meanwhile, technological necessity requires using all available information within the scope of scientific and engineering realities.

It may be summarized that the development of fracture control plans must be based on

- Scientific principles derived from generalized fracture mechanics theory
- Test-specimen designs and reference criteria that are scientifically rational

- Inclusion of metallurgical considerations
- Simultaneous consideration of test practices, criteria, and metallurgical factors in problem-solving.

The foremost impediment to achieving engineering sophistication in problem-solving is the failure to understand *constraint* factors. Constraint is the basic reference; if this factor is not understood there can be no rational beginning in understanding of criteria. Thus, all other aspects of integration remain beyond reach.

Physical Significance of Constraint

Plastic flow at crack borders develops following stress-strain relationships which are distinctly different from that of a smooth section. The difference is best explained by plots of true stress vs true strain, i.e., plastic flow curves.

Exact definition of the flow curves for specific crack conditions is a subject of continuing research. We shall not attempt to explain the state of knowledge except to indicate that it suffices for generalization of constraint factors. These generalizations are well known to fracture research specialists and form the basic rationale for fracture-mechanics theory.

Schematic illustrations will be used to explain constraint factors in terms of a physical model. The first step is to discuss the origins of constraint. Figure 1 illustrates that the introduction of a circular notch in a tensile bar causes an elevation of the flow curve. We may describe the plastic flow of the smooth tensile bar as free flow, i.e., unimpeded flow. Lateral contraction occurs with a minimum of opposition, thus allowing relatively free extension in the direction of loading.

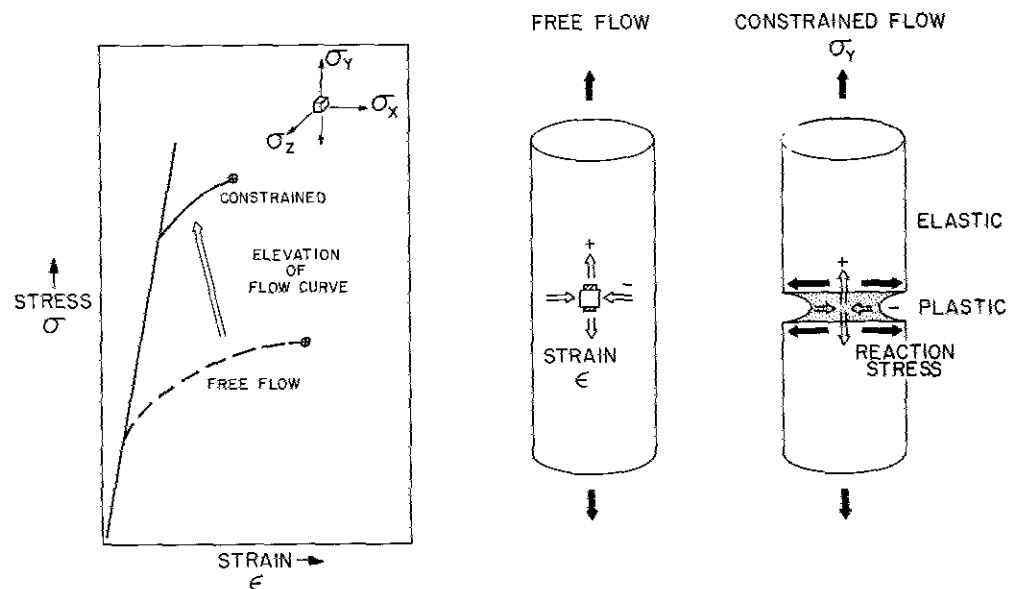


Fig. 1—Origins of constraint effects

The reduced section of the notched bar develops plastic deformation while the shoulders are stressed to elastic levels. Since the degree of elastic contraction is small compared to the plastic contraction of the reduced section, opposition is developed to plastic flow. The opposition is in the nature of a reaction-stress system, such that σ_x - and σ_z -direction stresses inhibit flow in the σ_y (load) direction. Thus, the uniaxial tension system of the smooth bar is changed to a triaxial stress system in the notched bar. Triaxiality is the factor which causes elevation of the flow curve.

Constraint may be described as the inhibition of plastic flow due to stress triaxiality. The degree of inhibition is directly related to the degree of triaxiality, i.e., the degree to which the σ_x and σ_z stresses approach the same value as the σ_y stress. Exact equality of the three reference stresses represents absolute constraint and no plastic flow can evolve. This condition is not attained in the presence of a notch because the stress system is always unbalanced to some degree. In simple terms, the σ_y -direction stress is always of higher value and thus flow will evolve in the load direction. The important factor is that flow inhibition subjects the metal grains to abnormally high stresses, compared to free flow in a tensile bar.

The origins of triaxial stress constraint may be traced to the elastically loaded metal which surrounds a volume of localized plastic flow. The effect is general, as indicated by the example of two pieces of hard steel bonded by a thin layer of soft-braze metal. If sufficiently thin, the soft-braze joint develops a strength equal to that of the hard steel. This is due to the high level of constraint imposed on the flow of the soft metal by the elastically loaded hard metal. The imposition of mechanical constraint causes metal grains to act as if they were "stiffer." Thus, the flow behavior of metal grains is not *intrinsic*; it is a function of the degree of applied constraint. For example, if the braze joint is made thicker, flow will become easier, due to decreased constraint.

The constraint level vs stiffness relationship is basic to understanding the mechanical behavior of metal grains located within crack-tip plastic zones. Increased mechanically induced "stiffness" decreases the ability of the grain structure to endure deformation without microcracking. The metal-quality parameter of interest is "crackless plasticity" under conditions of high, localized stress-systems.

Three separate stress systems are of engineering importance in analyses of fracture conditions:

- The nominal design stress which is the usual engineering reference.
- The stress which acts to "open the crack." This is a function of structural geometry. For example, stresses at nozzles of pressure vessels may be 3 to 4 times the hoop stress level. Insofar as the effects on the crack are concerned, this is the nominal stress of interest, if the crack is located in such high-stress regions.
- The localized stress at crack tips which acts to rupture the grain structure. The level of this stress can only be inferred indirectly by description of the constraint level. This is the reason why constraint factors must be understood by engineers.

Figure 2 illustrates the conditions at a crack tip. The case is that of a tensile-loaded plate featuring a through-thickness edge crack. The plastic "rod" developed at the crack tip must increase in diameter (σ_y -direction extension) with an increase in stress. However, this can only happen if through-thickness (z-direction) lateral contraction occurs.

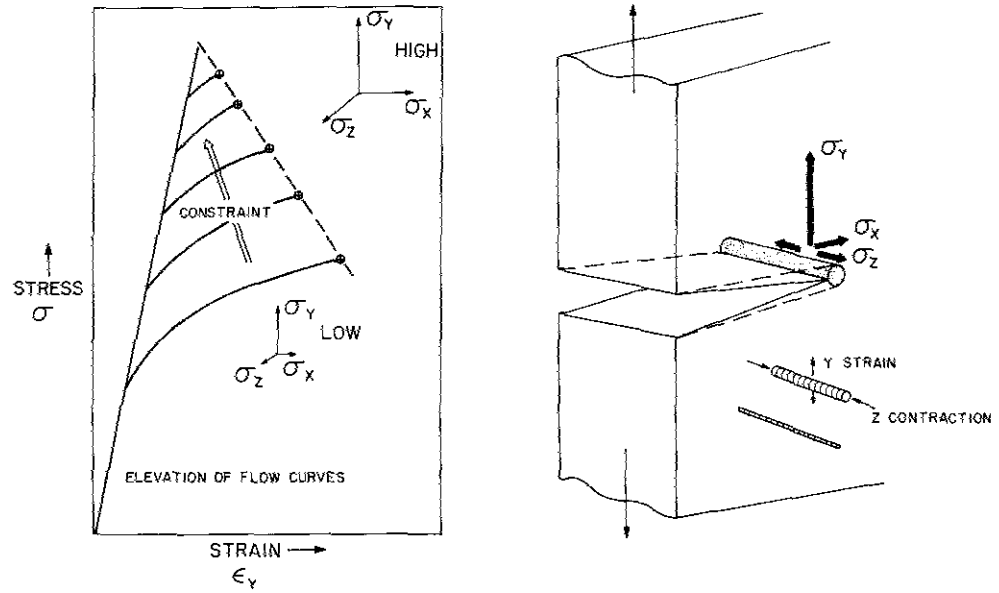


Fig. 2—Constraint conditions for through-thickness cracks. Increasing section size increases constraint because through-thickness flow must evolve with increased opposition of the larger volume of surrounding elastically loaded metal.

The elastic material which surrounds the plastic rod opposes both z- and x-direction flow, giving rise to a triaxial stress system.

The family of flow curves of Fig. 2 illustrates the effects of increasing the plate thickness. Constraint is increased (higher level flow curves) because triaxiality is increased due to higher reaction stresses in the z direction. In simple terms, the “length” of elastic material that envelops the crack is increased with crack-front size and, therefore, its capacity for opposing the enlargement of the localized plastic volume is increased. It may now be generalized that increasing crack-front size causes an increase in constraint. As a result, the stress-strain relationships are changed such that higher σ_y -stress levels are required to cause a unit increment of plastic flow at the crack tip. Thus, the metal behaves as if it were of increasing “stiffness” with increasing crack-front size.

A more generalized model of crack-front-size effects for through-thickness cracks is presented in Fig. 3. Cracks of increasing size are represented for two plate thicknesses. It is indicated that there is an increase in flow curve level (constraint) with increasing crack size to a *limit* level. This limit represents the maximum *constraint capacity* of a through-thickness crack. It is attained when the crack dimensions are approximately two times the thickness ($2T$), as a conservative estimate. The constraint capacity for such cracks increases with increases in plate thickness, because a larger crack-front size is involved for the thicker plate. The concept of a *maximum-constraint crack for a given section size* is basic to all discussions that follow.

The reason for attainment of a maximum constraint capacity for a crack of the subject geometry is explained in terms of “distance from free surfaces.” Constraint to plastic flow is always highest at the center of the crack front. This region is represented by the small “squares” in the figures. The central region is farthest removed from the free surfaces. This means that plastic contraction (z-direction flow) has the longest path

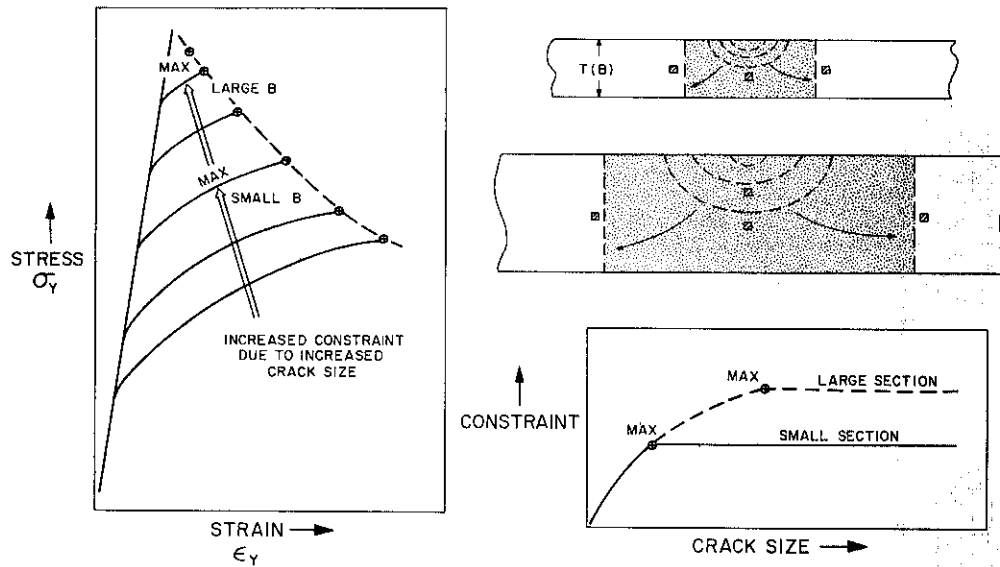


Fig. 3—Significance of maximum attainable constraint capacity for the section size as related to maximum constraint cracks. The level of maximum constraint, developed by through-thickness cracks, increases with section size because the crack-front dimension is increased.

and, therefore, senses the highest resistance to plastic flow. Conversely, plastic contraction occurs most readily close to the free surface. In effect, the metal near the free surfaces senses low triaxiality.

When a through-thickness crack attains a length dimension in the order of $2T$, the controlling (minimum) distance from the free surface is that of one-half the plate thickness. This simply reflects the fact that all other distance dimensions are now greater than $T/2$. Thus, constraint can be increased only by increasing the $T/2$ distance, i.e., increasing the plate thickness. The reference of thickness to "B" in the fracture mechanics literature arises from the fact that T represents the crack front *breadth* (B) for through-thickness cracks and, therefore, indicates the free-surface distance.

We may now generalize that maximum-constraint capacity for a through-thickness crack is attained when the crack length is such that $B/2$ is the controlling distance from the free surfaces. This generalization is important to understanding the use of edge-cracked specimens in fracture testing. The edge-cracked specimens are designed to measure the fracture resistance of a metal of specified thickness, under conditions of a maximum-constraint-capacity crack. The reason is that the lowest degree of ductile behavior which can be enforced on the metal is that which is related to the maximized condition of constraint. The metal cannot be forced (mechanically) to behave in a less ductile fashion than is measured under these conditions. Reference to the fracture resistance of the metal for this maximum level of imposed constraint then becomes independent of further increases in crack size. As such, it is the basic reference of scientific and engineering interest.

The connection between scientific and engineering aspects is illustrated in Fig. 4. The practical scientific interest is in measuring the minimal value of fracture resistance, as a standardized reference. With an increase in edge-crack depth a to approximately T

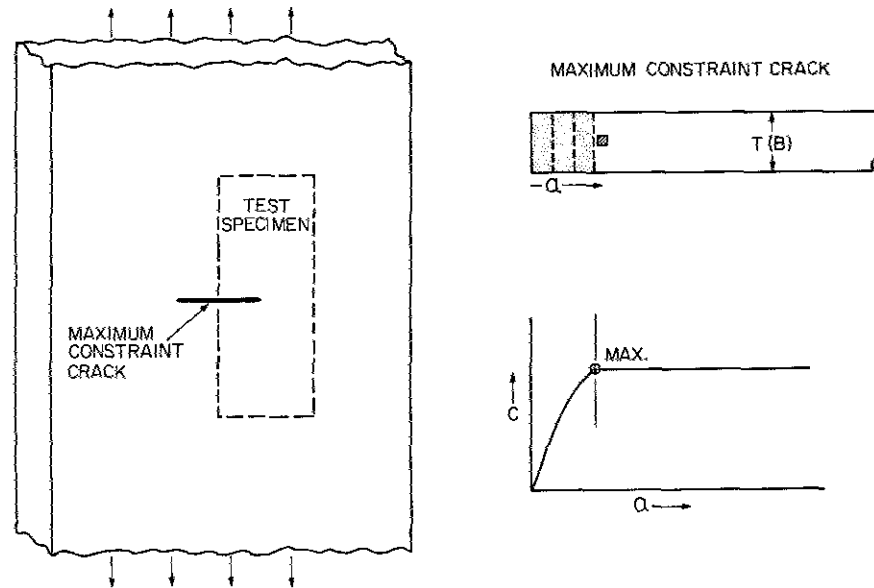


Fig. 4—Basis for design of fracture test specimens featuring maximum constraint cracks. Exact constraint-capacity correspondence is provided for a through-thickness crack in a structure

dimensions (a conservative estimate), the limiting distance from the free surfaces become $T/2$. Thus, constraint is maximized as illustrated in the C vs a plot of the figure. Fracture tests conducted with such a specimen will provide a measure of the lowest level of fracture resistance (fracture state) for the metal, in the form of a specified section size $T (B)$. As such, the test indexes the lowest level of fracture that is *allowed to develop* by the intrinsic properties of the metal grain structure.

The subject edge-crack may now be recognized as the equivalent of one-half of the maximum-constraint crack introduced in a tensile-loaded flat plate. Only one-half is required, because the two ends of the crack are fully equivalent and subject to the same constraint condition. In effect the test specimen is simultaneously a model of the maximum-constraint crack which controls the conditions of fracture extension in a structure. The lowest level (floor) fracture state that can evolve in the structure is the same as that which is characterized by the test specimen—irrespective of crack size. The metal cannot be made to behave in a less ductile fashion.

Constraint Relaxation

The objective of fracture testing is to fix the constraint conditions and then characterize the metal response as the dependent variable. These objectives are met as follows:

- The test specimen is designed to feature a maximum-constraint crack.
- Thus, the constraint capacity of the test specimen is defined by the section size.
- The metal response is the dependent variable, i.e., the aspect which is characterized.

The metal-response aspect is best understood in terms of constraint definitions provided by fracture mechanics. These include (a) degree of applied-constraint, and (b) constraint-relaxation phenomena. Constraint capacity is defined in terms of *plane strain* constraint, i.e., the capacity of the test for prevention of z-direction plastic flow. The basic reference to constraint in the fracture mechanics literature is to plane strain conditions.

In order to discuss constraint relaxation, it is necessary to consider crack acuity. The natural crack in a structure and that of a test specimen must be equivalently "sharp." Rounding off of the crack tip will decrease constraint. The development of plastic flow at a crack tip, in the course of loading, will cause some degree of rounding off. For a brittle metal, the degree of crack blunting is very slight and fracture extension will occur under conditions of continued crack sharpness. This behavior may be referred to as "fracturing under conditions of plane strain constraint." However, if the metal grain structure resists early rupture, the increase in plastic deformation will result in significant or drastic blunting of the crack tip. As a result, the limit of plane strain constraint (capacity) imposed by the mechanical system is exceeded. The effects are synergistic in that crack blunting causes constraint relaxation (exceeding the constraint limit) which causes increased plastic flow, leading to additional blunting, etc., to some ultimate fracture state in excess of plane strain conditions.

These effects are illustrated in Fig. 5 in terms of decreasing flow-curve resistance, compared to the initially applied level. The degree of crack blunting determines the course of the flow curves. In effect, constraint relaxation evolving from exceeding plane strain capacity limits decreases the effective "stiffness" of the metal at the crack tip, and lateral contraction in the crack-front-breadth (B) direction evolves.

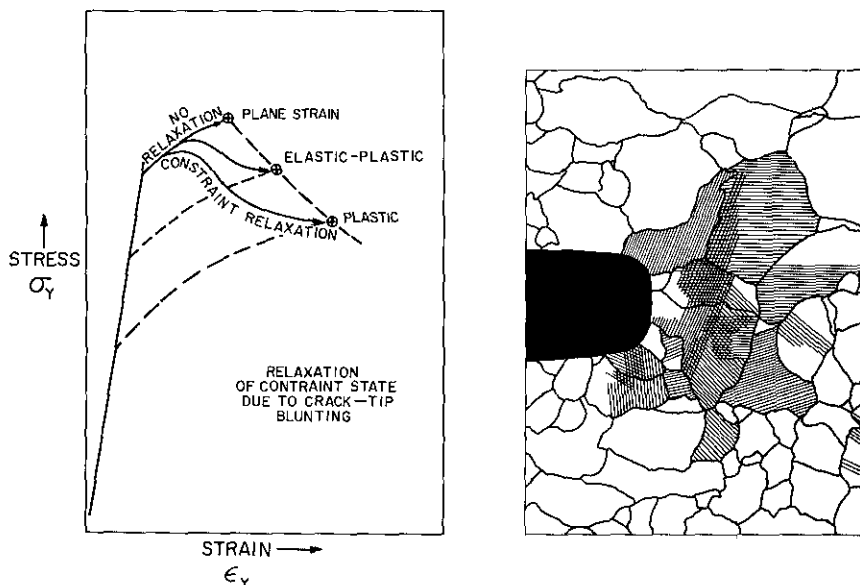


Fig. 5—Relaxation of plane strain constraint, due to metal-grain flow, which causes crack-tip blunting

The resulting fracture states (also referred to as fracture modes) are noted in the figure. Plane strain, elastic-plastic, and plastic fracture states are directly related to the flow curve behavior. Plane strain states signify fracture extension which evolves without crack blunting, i.e., no relaxation of constraint. Thus, the flow curve follows a course dictated by the degree of applied constraint. Elastic-plastic states imply significant decreases in flow-curve resistance due to constraint relaxation. Plastic states signify a major decrease or essential elimination of the applied constraint, consequent to severe blunting of the crack front.

The sketch of the grain structure indicates the micromechanical behavior at crack tips which provides for visualizing metal response effects. The dark line tracings within grains indicate slip on crystal planes, which is required to produce grain elongation. The deformation of individual grains is necessary to provide for growth of a plastic zone at the crack tip. Slip processes compete with the development of cracks and/or voids within the grains or at grain boundaries.

A brittle metal will develop microcracks or voids at early stages of plastic zone growth. For these conditions the flow curve is terminated by early rupture. The *micro-mechanical* conditions which cause grain rupture are then described as stress-induced fracture. The *macromechanical* behavior of the test specimen is defined as plane strain fracture.

A ductile metal will continue to develop grain deformation, causing enlargement of the plastic zone. If the crack tip is blunted to some degree, the grains sense decreased mechanical constraint and slip becomes easier. These descriptions indicate that a specific level of imposed constraint may be accepted or defeated by the behavior of the metal-grain structure. It should be noted that increasing constraint level also signifies increasing constraint capacity. The two terms are related mechanical expressions of the test severity for suppression of metal grain ductility. The reader should consider "level" and "capacity" as equivalent expressions of constraint.

The micromechanical features of metal response to the applied plane strain constraint determines the macroscopic fracture state of the section size under test. The macroscopic fracture state determines the reaction of the metal to loading in the presence of a crack.

Engineering Significance of Fracture States

The physical model which explains the structural-design significance of the fracture-state nomenclature is illustrated in Fig. 6. The figure indicates the full range of possible metal response to tensile loading of a flat plate, in the presence of a maximum-constraint crack. The crack is considered to be at least of $2T$ length and features a sharp edge. Two types of measurements are required—as represented by (a) a Crack-Opening-Displacement (COD) gage which indexes the elastic or plastic behavior of the crack tip, and (b) the net-section gage which indexes the rise in nominal stress.

A simultaneous plot is made of the increase in nominal stress and the COD-gage response. The nominal stress at which fracture develops, for metal of different fracture-state (mode) properties, is indicated by the crossed points with the arrow designation.

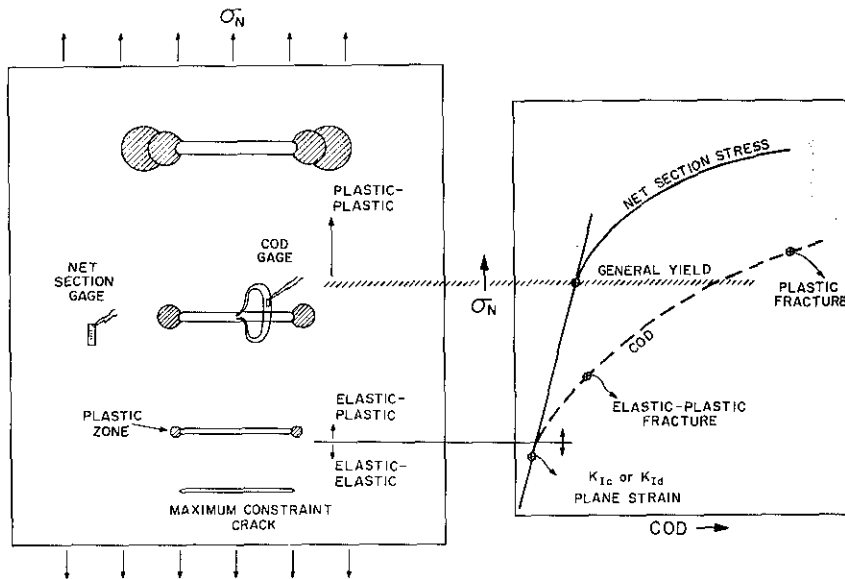


Fig. 6—Engineering significance of the fracture-state nomenclature. Note that the range of fracture-stress levels that result from the presence of a through-thickness (maximum constraint) crack is determined by the plastic behavior of the crack tip. The relative size of the plastic zones which are required for fracture extension (shaded circles) is the controlling parameter.

If fracture develops while the COD gage is indicating a linear response to increased nominal stress, it is deduced that the crack opening has been largely elastic. Since the nominal stress at failure is then forced to be of the elastic level, the combined conditions may be described as "elastic-elastic." However, this term is not used because plane strain is the conventional reference nomenclature. In effect, plane strain constraint was retained to the point of fracture instability. Calculations of K_{Ic} (or K_{IId}) may be made to define the specific level of plane strain fracture resistance. The nominal engineering stress level at the point of fracture will generally be *less than* $0.3 \sigma_{ys}$ for plane strain fracture extension, due to a through-thickness crack of 2- to 3-T length. This is an important generalization of major consequence to engineering use of all plane strain metals, i.e., those for which K_{Ic} or K_{IId} can be measured for the section size of interest.

Elastic-plastic fracture signifies that significant plasticity is developed at the crack tip, as indicated by plastic response of the COD gage. However, the nominal fracture stress remains in the elastic range. In brief, the nomenclature signifies plastic flow at the crack tip, due to constraint relaxation, of a degree that is sufficient to cause the nominal fracture stress to rise from $0.3 \sigma_{ys}$ to the limit of σ_{ys} . This fracture state is also referenced as K_c .

Plastic fracture signifies that the COD gage response is grossly plastic and that the nominal stress for fracture extension is elevated to the plastic range. In other words, plastic behavior is assured irrespective of crack size for the specific section size of interest.

Metallurgical Aspects of Constraint Transitions

The foregoing discussions have emphasized that a specifiable condition of constraint to plastic flow may be accepted or defeated by virtue of the intrinsic ductility of the metal grain structure.

The desirable attribute of the grain structure is that it must resist the development of microcracking under conditions of localized (to the crack tip) stresses of high intensity. In other words, the grain structure must respond to increasing levels of plane strain stress intensity (K_I) by continuing to activate slip systems within the grains, rather than by initiating microscopic regions of inter- or intragrain separations.

The macromechanical behavior of (a) a small test specimen featuring a maximum-constraint crack; (b) a large tensile-loaded plate featuring a crack of equivalent constraint; and (c) a structure featuring such a crack will all be controlled *equivalently* by the metal grain structure. The critical deciding factor in all three cases is the plastic flow curve of a small volume of metal which resides at the crack tip. Whether a huge structure such as a ship may be subject to fracture or is completely safe is decided by a *microscopic* volume of metal.

The inference of these relationships is that the metallurgist may adjust the microstructure of the metal so as to provide for constraint-relaxation effects, for a specified condition of imposed constraint. In other words, the structural behavior of a metal of specified section size (specified maximum-constraint capacity) can be adjusted within known limits.

The basic procedure for characterizing the fracture state of a metal and interpreting structural performance is illustrated in Fig. 7. The example may be considered to involve

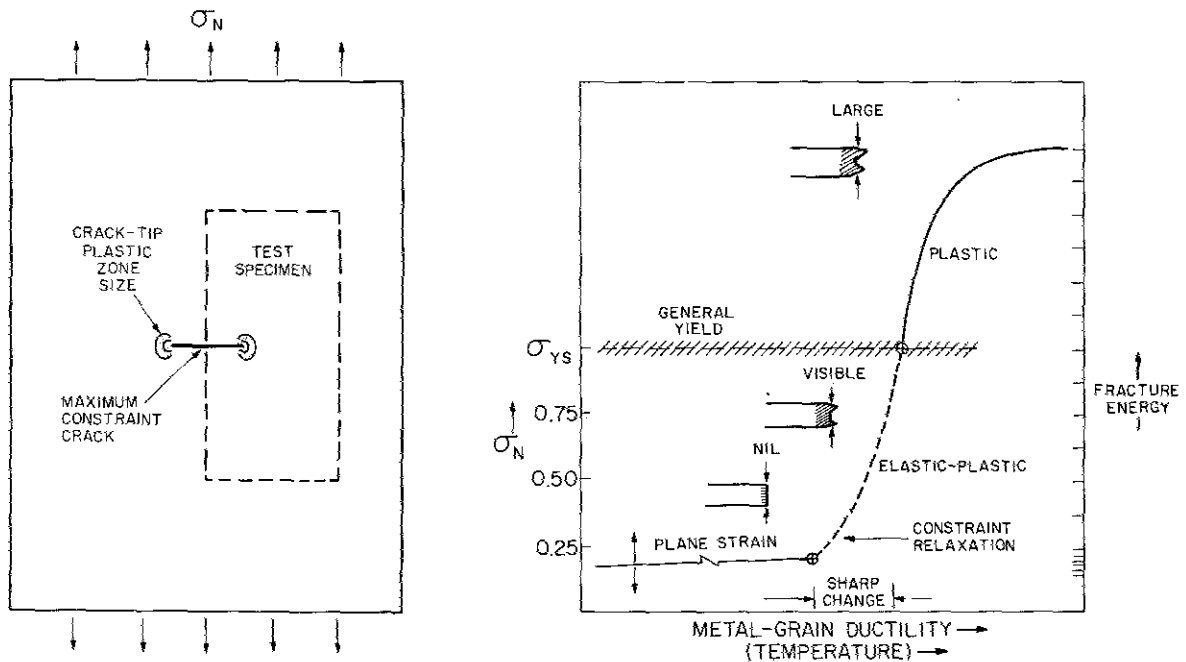


Fig. 7—Engineering significance of constraint transitions, which are developed as a consequence of temperature-induced increases in metal grain ductility.

a structural steel of say 1.0-in. (25 mm) thickness. The characterization and structural-interpretation problem for this example is to define the *temperature range of the constraint transition* for the steel and for the thickness involved.

We may proceed to do this by two equivalent routes. One is to use a large plate featuring a crack of maximum constraint ($2T$ or greater crack length). The dynamic-load constraint transition (K_{I_d} to elastic-plastic) is the controlling factor for fracture extension of rate-sensitive metals. Thus, the loading of the steel plate must be applied by impact.

If series of tests were conducted with increasing temperature, the results would be expected to follow the σ_n -temperature relationship shown in the figure. The temperature scale is, in fact, a scale of increasing metal-grain microfracture ductility. Over a long range of "low" temperatures, say -200 to 0°F (-130 to 18°C), there is little change in the fracture stress level. This is the plane strain (K_{I_d}) temperature region, which signifies that the imposed plane strain constraint was sufficient to cause cracking of the grains, with a very small degree of localized deformation at the crack tip. Conversely stated, grain ductility was insufficient to cause constraint relaxation. The fracture surfaces are flat (brittle) with nil levels (essentially zero) of thickness reduction, i.e., of plane strain fracture-mode.

At a critical temperature, specific to the steel and its section size, the effects of increasing temperature in promoting slip of the metal grains are manifested. At this point, metal ductility becomes sufficient to cause a small degree of constraint relaxation and the elastic-plastic state is entered. Accordingly, the fracture stress begins to rise, and visible evidence of lateral contraction is noted for the fracture surfaces. The first shear lips appear, indicating the start of mixed-mode fracture, characteristic of the elastic-plastic state. The constraint transition is remarkably sharp and, for the cited thickness, the fracture-extension stress is raised from less than $0.3 \sigma_{ys}$ to $0.5 \sigma_{ys}$ in a 30°F (17°C) temperature span. It is then raised to yield-stress levels, with an additional temperature increment of this order.

Obviously, it is not practical to conduct tests of large-plate type for metal characterization. A properly designed test specimen of small size serves the same purpose, provided the constraint conditions are equivalent, as described previously. A fracture-mechanics test specimen of 1.0-in. (25-mm) section size serves the purpose of following the slight rise of fracture resistance in the plane strain temperature region. The data plot will show a gradual rise of the K_{I_d} curve with temperature increase. When the critical temperature for constraint relaxation is reached, K_{I_d} measurement is no longer possible.

In order to continue using a small specimen, it is necessary to measure the fracture behavior in terms of a ductility index. This measurement may be in terms of crack-tip lateral contraction or fracture energy. Thus, the fracture mechanics K_{I_d} type specimen may be fractured and indexed in terms of ductility. However, the expense of preparing a K_{I_d} specimen is not justified. The low-cost Dynamic Tear (DT) specimen provides the same information based on identical measurements of ductility. The most practical measurement is that of fracture energy for a standardized fracture-path length. The primary requirement is that the fracture-path length should be sufficient to permit development of the characteristic fracture mode, i.e., of approximately $2T$ or greater length. (See Fig. A8 in the appendix.)

The reason that either K_{I_d} or DT specimens may be used to provide an unequivocal index of the constraint transition, in terms of fracture energy, is illustrated in Fig. 8. The photographs illustrate the change in fracture mode, associated with transition from plane strain to high-level plastic fracture. The term "high level" is used to denote a full-slant, highest ductility fracture.

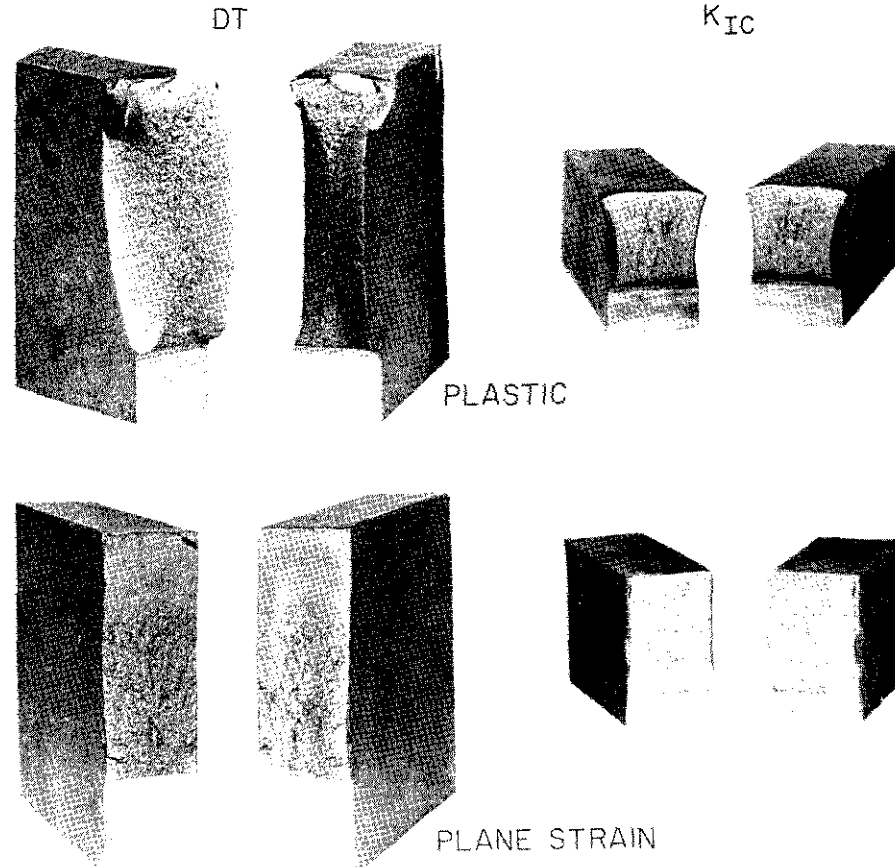


Fig. 8—Common features for the constraint transitions of 1.0-in. (25 mm) K_{I_d} - and DT-test specimens

Both specimens feature the same maximum-constraint crack (slit with sharpened edge). Thus, they feature the same constraint capacity, as determined by the section size. The metal-grain ductility response, to the identical mechanical-constraint system, is necessarily the same.

The changes in fracture mode (see Fig. 7 schematic) are the result of progressively increasing plastic deformation of the crack tip, consequent to the constraint transition. The increased volume of metal which undergoes plastic deformation prior to fracture results in an increase in the fracture-energy reading as well as an increase in the degree of lateral contraction. Thus, the fracture-energy scale of Fig. 7 (right side) may be used to index a temperature vs energy curve, which has the same flat plus sharp-rise aspects of the temperature vs σ_n curve. The energy curve may be established easily by using the DT specimen. The temperature range of the constraint relaxation, for the specific steel and section size, is thus defined exactly by a simple test procedure.

The fracture mode will change progressively from flat to full slant over the full course of the constraint transition. Thus, the constraint transition may be indexed by plotting percent of slant fracture vs temperature. This plot will show a transition from zero (full flat) at plane strain levels, to 100% (full slant) at the completion of the transition, i.e., attainment of "shelf" temperatures. This degree of fracture-mode change is characteristic of metals featuring high-level plastic-fracture states. Metals of lower levels of plastic-fracture resistance will "shelf out" with retention of a partially flat central region in the fracture surfaces.

The limiting degree of constraint relaxation determines if a metal is of high- or low-shelf features. A corresponding difference in lateral contraction, or fracture energy "on shelf," will result. These characteristics bear a close relationship to each other since they correspond directly to the degree of constraint relaxation. The important feature is that these measurements provide a faithful index of the temperature course of the constraint transition. The rapid rise in fracture energy (and the related fracture features) of either K_{Ic} or DT specimens index the entry into the elastic-plastic state with unequivocal clarity.

From an engineering point of view, the essential characterization is that of the specific temperature region of the elastic-plastic transition. Very little is gained by small increases in K_{Ic} value from very low temperatures to the temperature of constraint relaxation. The fracture-extension stress rises negligibly in the plane strain region. The exact equivalence between the sharp rise in fracture-extension energy and the sharp rise in fracture-extension stress is the important engineering aspect illustrated in Fig. 7.

Engineering practicality is achieved when the low-cost DT test is used to develop a data bank of metal properties. The various engineering grades are thus classified as to their characteristic constraint-transition temperatures, with due consideration of section size. Most importantly, the microstructural features which are required to locate the constraint transition at specific temperatures are accurately identified. Thus, it is feasible to proceed with "designing" the metal to provide for specific structural requirements as to lowest service temperatures.

The effects of increasing strength level, for all metals, is to cause a decrease in metal-grain ductility. Thus, the curve in Fig. 7 may be considered to apply in reverse fashion. With increased strength, there will be a drop from plastic to elastic-plastic and then to plane strain fracture states.

The combined effects for steels are best illustrated by a tridimensional presentation, Fig. 9. The vertical scale is the energy-scale reference of Fig. 7. It may also be considered in terms of the relative-stress scale of this figure. Accordingly, it is the index of the constraint transition for a specific section size—say 1.0 in. (25 mm). The temperature and yield-strength scales indicate the usual reference planes for plotting of constraint transitions. The important point is that the strength transition for steels must be discussed in terms of on-shelf properties, i.e., at the completion of the temperature-induced transition. Note that the high strength steels feature small temperature effects.

Nonferrous metals are relatively insensitive to temperature effects. Thus, constraint transitions develop only as the result strength-induced changes in metal grain ductility.

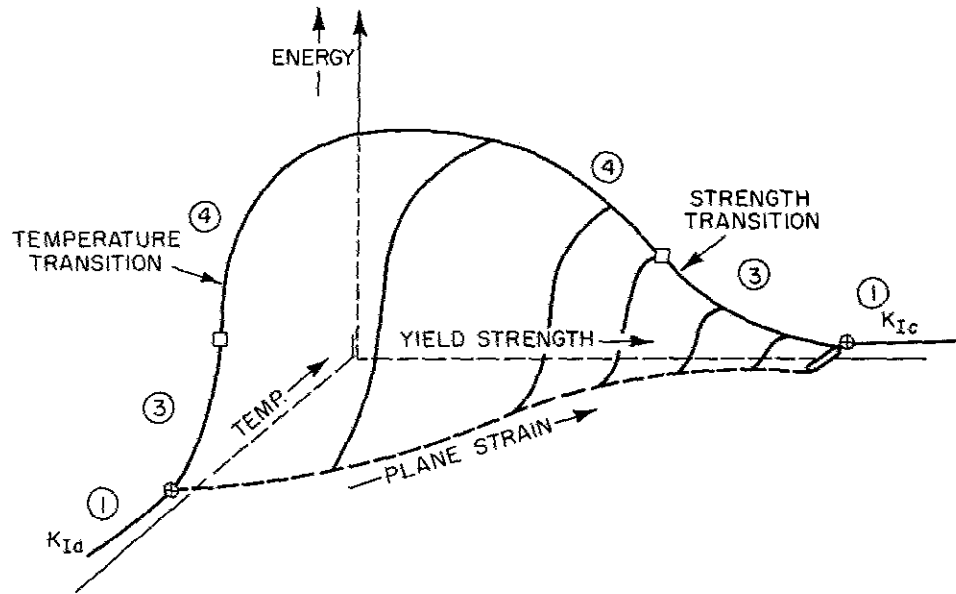


Fig. 9—Three-dimensional aspects of temperature- and strength-induced constraint transitions for steels. The notations refer to fracture states (1) plane strain, (3) elastic-plastic, and (4) plastic.

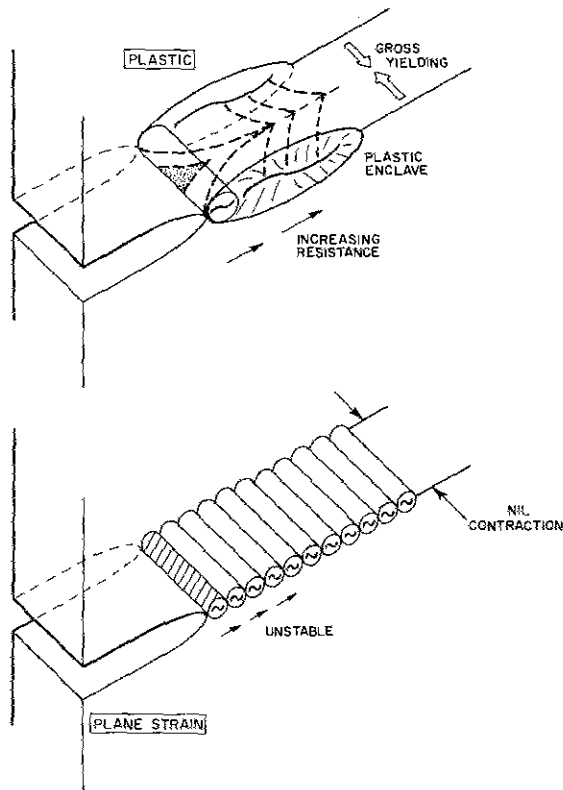


Fig. 10—Fracture-extension processes for plane strain and plastic fracture states.

Fracture-Extension Processes

Figure 10 illustrates the physical nature of fracture-extension processes for plane strain and plastic fracture states. The basic reason for the increase in fracture-extension stress during the course of constraint transitions is provided by considering these processes.

Plane strain fracture connotes brittle behavior because the extension is of an unstable type. As the first-developed, very small crack-tip plastic zone is ruptured, there is a release of elastic-strain energy—acting as if a spring were severed under stress. The crack sharpness is retained, thus the next plastic zone which forms is likewise small and ruptures immediately on being exposed to the high stress intensity (K_I) of the advancing crack tip. In effect, the fracture of the first “spring” releases elastic stress which overloads the next, leading to its rupture and continuation of this process to total fracture.

The fracture extends by repetitive overloading of the crack-tip region. The nominal elastic-stress fields of the structure are important because they represent the degree of elastic extension of the long-range "spring system" and, therefore, the level of elastic strain-energy available for continued fracture extension. Low-level elastic-stress fields provide for sufficient release of elastic strain-energy of the low order required for plane strain fracture. This is due to the small size of the plastic zones, which can only absorb small amounts of energy. Thus, the usual structural-design elastic stress fields in the order of $0.3 \sigma_{ys}$ are sufficient to provide for continued unstable extension.

As the elastic-plastic region of the constraint transition is evolved, the plastic-zone size is increased and larger amounts of energy are required for rupture. Rupturing of these plastic zones, therefore, requires increased elastic strain-energy release, which can be obtained only by raising the level of nominal stress. The extension process continues to be unstable, i.e., controlled by the elastic strain-energy release, to the point that nominal stresses of yield magnitude are required.

The plastic-zone size eventually becomes too large for unstable fracture extension. This condition is reached when the increasing constraint relaxation produces a plastic-zone size that is not subject to rupture by release of elastic strain energy. At this point the extension process cannot be induced or continued by elastic-stress fields. Stresses of over-yield magnitude must then be applied, and the rate of fracture extension becomes controlled by requirements to continually redevelop a plastic strain field, in advance of the crack as it extends.

The constraint transition to high levels in the plastic region involves growth of continually larger plastic-strain fields. The features of the plastic-strain field, which must be evolved prior to crack advancement, are illustrated by the condition termed "plastic enclave" in Fig. 10. Gross through-thickness yielding, which results in a dimple (lateral contraction), must be developed in successive unit-increment rupture steps. Translation of a fracture by such high-ductility unit-increment processes requires stress fields which become of very high plastic level.

Section-Size Effects

The very sharp transition from the plane strain state to relatively high levels of the elastic-plastic state, illustrated by Fig. 7, is characteristic of all section sizes. The primary effect of large increases in section size, say from 1.0 to 12 in. (25 to 300 mm), is to develop a K_{Ic} or K_{IId} "transition." This type of transition does not represent a change in fracture state, such as for a constraint transition. The terminology of "transition" is used to indicate that a sharp rise in K_{Ic} or K_{IId} values is developed over a relatively narrow range of temperature or yield strength. The fracture state remains that of plane strain. Thus, the proper description of this section-size effect is that it represents a *plane strain transition*.

The engineering significance of the plane strain transition, developed by large section sizes, is that the critical temperatures or strength levels for initiation of the constraint transition are shifted. In other words, plane strain constraint is lost and elastic-plastic fracture begins at higher temperatures or lower strength levels, as compared to thin section sizes. The separation of thin and thick sections is best placed at approximately 1.0-in. (25 mm) thickness.

Increases in section sizes in the order of 1.0 to 12 in. (25 to 300 mm) result in very large increases in the constraint capacity of maximum-constraint cracks. That is, the size of the $B/2$ dimension of the crack front is increased enormously with increases of section sizes in this range. Thus, metal grain ductility is suppressed to higher temperatures and lower yield strength.

Suppression signifies that plane strain conditions continue to apply, in the sense that K_{Ic} or K_{IId} values can be measured. The relatively sharp increase in K_{Ic} and K_{IId} values connotes that there is a large increase in the plane strain plastic zone size. In effect, increasing metal grain ductility in the plane strain transition region is *difficult to suppress*, which is the reason for requiring large increases in section size to provide the requisite constraint.

It should not be inferred that the plane strain transition signifies an increase in fracture resistance which is equivalent to entering the constraint transition. It is not, because plane strain measurements involve a fine-scale definition as to degree of brittleness. The plane strain transition simply means that the measurement capacity is extended by increased section size. Moreover, it does not mean that a thick-section metal is intrinsically of higher plane strain fracture resistance than a thin-section metal. K_{Ic} or K_{IId} measurement at the same temperature or strength level (provided both are valid by ASTM practices) will result in the same value for a thin specimen cut from a thick section.

The characteristic "four parts" of the temperature-transition curve for steels of very thick section are illustrated in Fig. 11. The 6- to 12-in. (150 to 300 mm) DT-test energy curves show a flat K_{IId} -related region (Part 1), followed by a modest rise in the K_{IId} -related plane-strain transition (Part 2), and then a very sharp rise in the constraint relaxation region (parts 3 and 4). The lower half of the constraint transition region locates the elastic-plastic fracture state (Part 3) and the upper half relates to the plastic fracture-state (Part 4).

The correlation to the K_{IId} curve includes a designation of the minimum section sizes (inches) that were required to track this curve experimentally. Note that tracking of the K_{IId} transition required an increase in section size from 1.0 to 8.0 in. (25 to 200 mm) in the range of 0 to 120°F (-18 to 50°C). At all temperatures below 0°F (-18°C), K_{IId} specimens of 1.0 in. (25 mm) or smaller were adequate to track the low-slope portion of the curve. This example clearly indicates the very large increases in constraint ($B/2$ crack-front dimension) that are required to retain plane strain conditions in the plane strain transition-temperature range.

Another aspect of note is the almost vertical rise of the K_{IId} curve as the constraint-transition temperature for the 12-in. (300 mm) section size is approached. This observation indicates that further increases in section size would provide a negligible increase in the temperature of K_{IId} measurement—a "wall-like" temperature limit is reached. In effect, the metal grain structure is becoming "too ductile" for continued suppression to plane strain levels, by increase in mechanical constraint. This is equivalent to stating that the constraint requirement is increasing to a hypothetical "infinity," i.e., to infinite section size.

The K_{Ic} curve for this same metal shows a similar exponential rise, displaced by approximately 70°F (40°C) to lower temperatures. The displacement is evidence of a viscoplastic effect. At the low loading rates of K_{Ic} testing, time is allowed for slow (viscous) plastic flow, i.e., the flow curve level is decreased and thus the effective metal

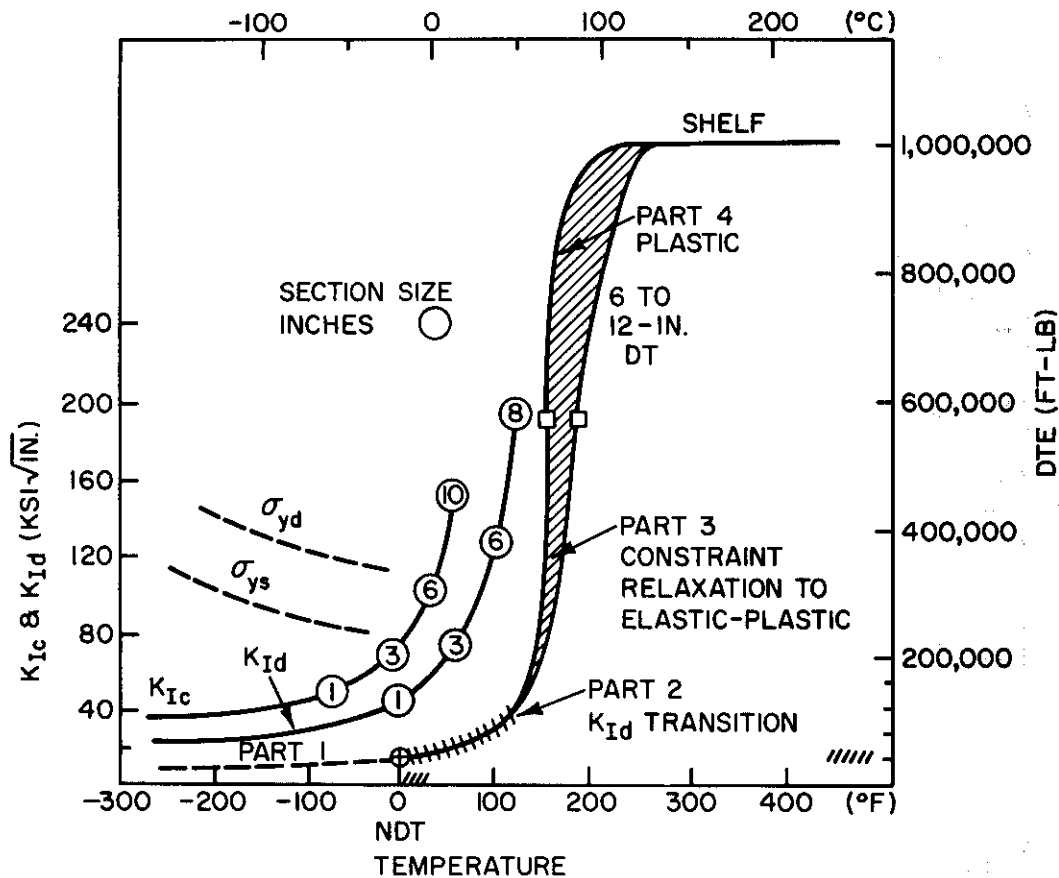


Fig. 11—Characteristic four-part constraint-transition curve for a plate 12 in. (300 mm) thick (A533-B steel), as defined by DT tests of full section size. The K_{Ic} and K_{Id} transitions are fully evolved in the toe region of the DT test curve. The circled points define the increase in section size required to track the K_{Ic} and K_{Id} transitions. The K_{Ic} and K_{Id} data were evolved by Wessel. See Ref. 2 for a full description of test details and additional references.

“stiffness” is decreased. It should be noted that the K_{Id} curve is the controlling factor for rate-sensitive metals, as indicated by failure analyses of ships, pressure vessels, bridges, etc.

The characteristic “three-part” temperature transition curves for section sizes in the order of 0.6 to 1.0 in. (15 to 25 mm) is illustrated in Fig. 12. In this case, the plane strain transition (Part 2) is essentially eliminated. This is due to the low constraint capacity of the 0.6-in. (15 mm) section size represented in the figure. For this low level of constraint, it is possible to measure only the nearly flat region of the K_{Id} curve (Part 1). The constraint transition (Parts 3 and 4) is developed with dramatic sharpness.

The experimental data of Figs. 11 and 12 are presented in generalized form in Fig. 13 (left side). In this case, the development of plane strain (K_{Id}) and constraint transitions is the result of increasing metal grain ductility due to increasing temperature. The generalized plot of section-size effects related to increasing metal grain ductility due to decreasing yield strength is illustrated in the right side of Fig. 13. The K_{Ic} scale is used

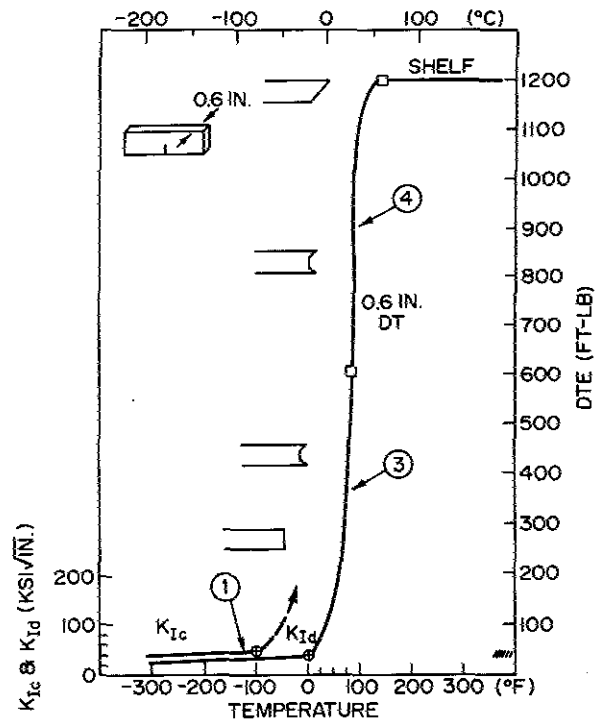


Fig. 12—Characteristic constraint transition curve for conventional mild steels of 0.6 in. (15 mm) section size. The K_{Id} and DT test scales are adjusted to provide a common plot in the toe region of the DT curve. The dashed line indicates the start of plastic COD and lateral contraction for the K_{Ic} test.

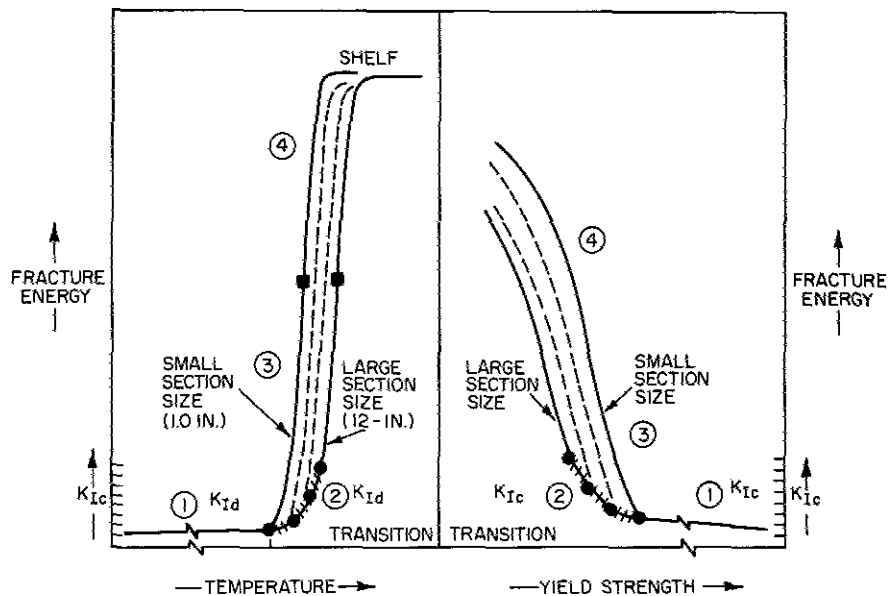


Fig. 13—Characteristic constraint-transition curves for small and very large section sizes. Illustrates the common features for temperature- and strength induced transitions. Increasing the section size results in the shifts noted by the dashed lines.

to denote that the effects are common to steels as well as to the non-rate-sensitive non-ferrous metals (aluminum and titanium alloys). The figure illustrates that a family of transition curves will develop, within the range of the two limiting curves, as the section size is increased from small to very large dimensions.

Engineering Significance of Plane Strain Transition

Discussions of plane strain transition effects in the scientific literature have centered on plotting the sharp rises in K_{Ic} and K_{Id} values that may be developed for thick-section metal >1.0 in. (25 mm). By using an expanded K_I -scale, and omitting data as to the remainder of the transition to the elastic-plastic state, the curves present the impression of large increases in fracture resistance. By additional magnification of the scale, the curve may be shown to rise as the plane strain limits of 1.0-in. (25 mm) section sizes are reached.

While these plots are defensible for scientific reasons of demonstrating the exact measurement of plane strain properties, they have led to engineering confusion. In brief, the engineering field has misread the true significance of the plots. They do not demonstrate increases in fracture resistance to attractive levels. Conversely, they document differences which are of minor engineering significance.

Fracture-mechanics calculations define that the development of a plane strain transition, for the case of thick sections, has a minor effect on the form of the fracture-extension stress curve for through-thickness cracks shown in Fig. 7. The following summations are of major engineering importance.

- The fracture-extension stress level for the plane strain state does not exceed $0.3 \sigma_{ys}$, irrespective of section size.
- Increasing K_{Ic} or K_{Id} values to the constraint-capacity limit of the section size (highest measurable value) increases fracture-extension stresses only in the range of <0.1 to $0.3 \sigma_{ys}$, as the maximum limit.
- The plane strain state always provides for catastrophic fracture extension at usual, nominal design stress levels of 0.3 to $0.5 \sigma_{ys}$.
- Protection from fracture extension through usual structural stress fields can be attained only by entering the elastic-plastic fracture state. The reason is indicated by the sharp rise of the fracture-extension stress to $>0.5 \sigma_{ys}$ in the elastic-plastic region.
- The plane strain state is always unacceptable, if design requirements include positive prevention of catastrophic fracture.

By 1950, it was known (from ship fracture studies) that small arc-strikes could cause a pop-in to a through-thickness crack condition. Catastrophic fracture-extension then evolved through the entire structure, despite the low nominal stress levels used for conservative design, in accordance with ship design Rules. At the same time Robertson CAT tests established that the fracture-extension stress in the plane strain region could be as low as 5 to 8 ksi (2 to 4 kg/mm²), i.e., below the normal design level of $0.3 \sigma_{ys}$. These tests also indicated the rise in fracture stress illustrated in Fig. 7 for the elastic-plastic temperature region. Since 1950 fracture mechanics has evolved analytical procedures

which are summarized in the above listing. These are obviously in agreement with 1950 knowledge.

The 1950 solution to catastrophic problems is perfectly valid today. It involved the application of criteria which would document the use of metals featuring elastic-plastic properties—of at least $0.5 \sigma_{ys}$ fracture-extension levels.

Numerical Definition of Constraint Capacity

Constraint capacity is best referenced to the plane strain state. In a general sense, the term means the capacity of a crack front for preventing constraint relaxation. Conversely stated, it means the capacity for enforcing plane strain conditions, i.e., essentially nil-levels of lateral contraction across the crack front.

The usual definition given in the fracture mechanics literature is, “the capacity of the crack front for enforcing a plastic-zone size which is very small in relation to the section size.” This definition is best understood in terms of a plastic zone developed at the crack front of a K_{Ic} specimen. If a K_{Ic} (or K_{Id}) value can be measured, then the plastic zone is very small because plane strain conditions apply. When constraint relaxation evolves, the plastic zone size increases rapidly and eventually becomes very large in relation to the section size.

The idealized mathematical definition of plane strain plastic zone size (r_p) is given by the formula

$$r_p = \frac{1}{6\pi} \left(\frac{K_{Ic}}{\sigma_{ys}} \right)^2 \quad \text{or} \quad r_p = \frac{1}{6\pi} \left(\frac{K_{Id}}{\sigma_{yd}} \right)^2,$$

where σ_{ys} signifies the static (slow-loading) yield strength and σ_{yd} represents the dynamic-load value. As an approximation, $\sigma_{yd} = \sigma_{ys} + 30$ ksi for steels of low- or intermediate- σ_{ys} levels. The important point is that the K_{Ic}/σ_{ys} or K_{Id}/σ_{yd} ratio is the factor which defines plastic-zone size, i.e., ductility. The limit ratio which can be measured for a specific section size represents the limit plastic-zone size (constraint capacity) of the plane strain state, for the section size.

It has been determined experimentally that the limit of plane strain measurement is conservatively indicated by the following relationship to section size:

$$B \geq 2.5 \left(\frac{K_{Ic}}{\sigma_{ys}} \right)^2,$$

where B is the crack-front breadth for a K_{Ic} specimen, i.e., the section size T, expressed in inches.

For example, a constraint capacity with ratio value of 1.0 is developed by a section size of 2.5 in. (62 mm). If the section size is less than this size, the constraint capacity becomes inadequate to measure ratio 1.0 values and constraint relaxation evolves.

The plane strain limit, expressed as a ratio, defines the constraint capacity of the section size. Table 1 lists the plane strain limit ratios for various section sizes, in entry systems that provide for reference in discussions to follow.

Table 1
Section Size vs Ratio-Limit Relationships

Section Size		Ratio Limit* (ksi $\sqrt{\text{in.}}/\text{ksi}$)
(in.)	(mm)	
SECTION SIZE AS ENTRY REFERENCE		
0.1	2.5	0.20
0.2	5	0.28
0.3	8	0.35
0.4	10	0.40
0.5	13	0.45
1.0	25	0.63
1.5	40	0.8
2.0	50	0.9
3.0	75	1.1
6.0	180	1.5
10.0	250	2.0
RATIO AS ENTRY REFERENCE		
Ratio Limit* (ksi $\sqrt{\text{in.}}/\text{ksi}$)	Section Size	
	(in.)	(mm)
0.1	0.03	0.6
0.2	0.1	2.5
0.3	0.2	6
0.4	0.4	10
0.5	0.63	16
0.63	1.0	25
1.0	2.5	64
1.5	6	142
2.0	10	254
2.5	16	386

*See ksi $\sqrt{\text{in.}}$ conversion to metric scales, Fig. A1 (appendix).

The above-described generalizations of the relationships between increased metal ductility (due to temperature or strength level effects) and mechanical constraint (provided by specific section sizes), were defined during the late 1960's. The practical implications to engineering fracture control plans are of major scope.

The ratio limit for the section size has four engineering interpretations:

1. It represents the limit of plane strain measurement for the section size.
2. It indexes the critical temperature or strength level for the plane strain to elastic-plastic, fracture-state transition.
3. It indicates that relatively small additional increases in temperature, or decreases in yield strength, have extraordinarily potent effects on fracture resistance. The change in fracture resistance is in the nature of a step function (sharp rise) at these reference points.
4. Low-reliability plane strain criteria for fracture control plans are convertible to high reliability elastic-plastic criteria, within the span of these temperature increments or strength decreases.

The critical step-function temperatures and strength levels, which relate to elastic-plastic transition for the section size, can be shifted within rather broad limits by adjustments in metallurgical quality.

Test Methods Featuring Definable Constraint Capacities

The various types of ASTM-standardized fracture-mechanics tests are specifically designed for meeting plane strain constraint conditions. Thus, the constraint capacity is defined by the formula and tables presented above.

The procedure for calculation of critical surface-crack depth vs stress relationships, is based on analyses which assumes constraint conditions of plane strain levels. A graphical illustration of these relationships is presented in Fig. 14, in terms of crack depth and relative stress, for a range of plane-strain K_{Ic}/σ_{ys} (or K_{Id}/σ_{yd}) fracture-resistance levels. The section-size scales at the top of the figure indicate the minimum B dimensions for measurement of specific ratio values.

The plot suggests that specimens featuring *surface cracks* may be used to determine K_{Ic} and K_{Id} , subject to the limitations that the plane strain constraint capacity of the crack is not exceeded. The limitations are that the crack should not exceed 0.6 T depth; the noted fracture stress should not exceed σ_{ys} ; and the COD-gage response should be elastic. This procedure is used experimentally, particularly in the aerospace industry, but has not been included in the ASTM standard practices, which are based solely on the use of maximum-constraint edge cracks. The reason is that the described procedures require expert knowledge in determining that plane strain constraint capacities of the surface cracks are not exceeded.

The K_c -testing procedure represents the extension of fracture-mechanics principles into the elastic-plastic state. The K_c tests, which are not standardized at this time, are used primarily for specimens of sheet thickness. The problem is the requirement for

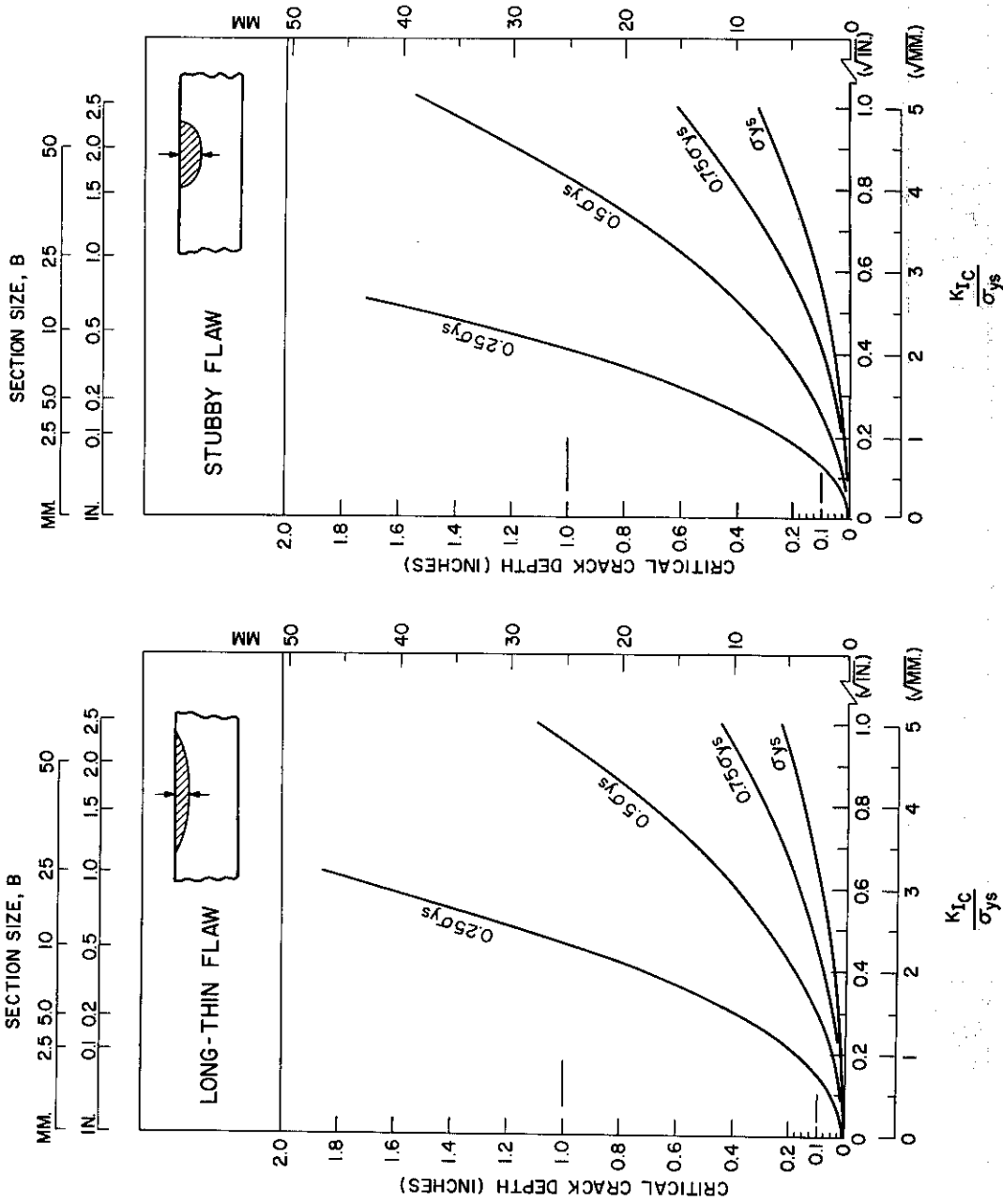


Fig. 14—Graphical presentations of flaw size (depth), relative stress, and K_{Ic}/σ_{ys} (also K_{Ic}/σ_{yd}) relationships. The calculations only apply for the plane-strain state. Note the limits of ratio measurement for specific section sizes, as determined by the constraint capacity of the section size.

defining a sheet width, in relation to the size of a through-thickness crack, which results in determination of a valid K_{Ic} value. The required sheet width increases rapidly with increase of the K_{Ic} value. Tests for metal of plate thickness would require the use of very large specimens—equal to commercial plate sizes. Obviously, this is not a practical procedure. Thus, other approaches must be used to characterize the elastic-plastic (K_{Ic}) fracture state. The only practical approach is to characterize constraint relaxation (K_{Ic}) conditions in terms of *unattainable* plane strain ratio values for the section size, as described below. This is simply a convenient means for continued reference to a standardized scale of known significance (plane strain).

Constraint relaxation of sufficient degree to cause nominal stresses to exceed yield should evolve when

$$B \leq 1.0 (K_{Ic}/\sigma_{ys})^2$$

$$B \leq 1.0 (K_{Id}/\sigma_{yd})^2 .$$

This conservative estimate of the “yield criterion” indicates that a section size which is less than 1/2.5 (0.4) of the minimum size for plane strain constraint results in exceeding yield stress for fracture extension. This is the *constraint insufficiency* criterion for attaining the plastic-fracture state. It is generally considered to be highly conservative.

In order to appreciate the meaning of this criterion, the reader should visualize measurement of a K_{Ic}/σ_{ys} ratio value using the minimum required size. Then the specimen is reduced in thickness (say by machining) so that the section size is 0.4, or less, of the original size. The yield-criterion degree of constraint insufficiency is then attained. In practice, correlations to other tests of definable constraint are used to determine when the insufficiency level is attained. This is only one of the many roles that must be assumed by other tests because of fundamental or practical restrictions on the use of existing fracture-mechanics tests.

The direct use of fracture-mechanics K_{Ic} or K_{Id} tests for purposes of defining the plane strain limit for the section size is prohibitively expensive. The tests cannot be used directly for definition of the yield-point criterion because the ratio values involved are not measurable.

At this point we shall dismiss consideration of other tests which are not fully rational in terms of generalized fracture mechanics theory. At a minimum, any attempt at correlation to fracture mechanics tests should be based on use of test specimens of definable plane strain constraint capacity.

The two practical engineering tests which meet this requirement are as follows:

Dynamic Tear - DT The geometric features of this test are the same as those of a side-bend, edge-cracked K_{Ic} or K_{Id} test specimen. Thus, the constraint capacity is definable by the thickness dimension, as is the case for fracture-mechanics test specimens. The NRL-standardized specimens (see Fig. A4 in the appendix) of 0.6 and 1.0-in. (15 and 25 mm) thickness, feature a K_{Ic}/σ_{ys} (or K_{Id}/σ_{yd}) constraint capacity of ratio 0.5 to 0.6, respectively. However, the DT test may be conducted in any size of interest, and the constraint capacity involved is definable in all cases.

Drop Weight - NDT The fixed crack size of this test provides an effective K_{Id}/σ_{yd} constraint capacity of approximately 0.5 ratio. (See discussion in Part 3.)

The other engineering test which meets constraint-definability requirements is the Robertson test. The dynamic extension of a crack, through a plate of specified thickness, provides for K_{Id}/σ_{yd} definition. For example, a 1.0-in. (25 mm) plate tested by the Robertson technique represents a K_{Id}/σ_{yd} constraint capacity of 0.6 ratio. The general form of the Robertson Crack-Arrest Temperature (CAT) curve is represented by Fig. 7. The lower toe of the CAT curve is the plane strain (K_{Ic}) region and the elastic-plastic region is the rising part of the CAT curve. In fact, the Robertson test is used specifically to determine the temperature range of elastic-plastic constraint transition for a specified section size. The CAT curve is defined by tracking the fracture-extension stress curve to the yield criterion (FTE) point.

In practice, Robertson-type tests are usually conducted at a fixed nominal stress of $0.5 \sigma_{ys}$. Several specimens are tested over a range of temperatures until fracture arrest is developed. The temperature of fracture arrest is then the $0.5 \sigma_{ys}$ CAT.

The primary problem of the Robertson test is the cost of testing. A low-cost solution for definition of CAT curves is provided by DWT-NDT and DT tests, as will be described.

The Charpy V (C_v) test features an arbitrary notch and geometry of undefinable constraint capacity. Any attempt to modify this test to fully meet fracture mechanics rationality requirements results in a configuration which is equivalent to a small DT test. In other words, it then becomes a part of the DT-test family as to geometry and test procedures.

Crack Opening Displacement (COD) tests are basically side-bend-type K_{Ic} tests carried into the elastic-plastic and plastic range. The constraint capacity of the specimens is defined by the section size. The measurement index is the plastic displacement (opening) of the crack at the point of fracture extension. Other COD procedures involve measurements of lateral contraction at the crack tip.

In effect, a COD curve would follow the course of the dashed line, which deviates from the K_{Ic} curve, as shown in Fig. 12 for the temperature-transition case. The procedure has not been extended to include *dynamic loading*, for reasons of experimental difficulties related to dynamic measurement of the COD index. For the case of the strength transition, the COD measurements would follow the course of curves in the elastic-plastic and plastic regions (Parts 3 and 4), noted in Fig. 13.

It should be noted that present research, which focuses on development of tests for indexing the elastic-plastic and plastic fracture states, is aimed at eventually evolving an analytical capability of the type shown in Fig. 14. This is a long-range goal, and such capabilities are not to be expected for at least a decade, if feasible. The following procedures are in competition:

- K_c tests
- COD tests

- J-integral tests
- Finite element analyses—reduced to test practices.

All of these focus on defining a “singularity,” that is, an index value which characterizes the metal. The value would then be used for analytical calculations. The problem is that there is presently no scientific base for such calculations.

The K_{Ic} calculations are based on the K_{Ic} singularity. The calculations are made on assumption of two-dimensional linear-elastic (purely elastic) stress fields in advance of the crack tip. The plastic case is nonlinear and must be treated as a three-dimensional matrix model. In brief, it is an exceedingly complex mathematical problem. One of the major complexities is that the plastic conditions are spatially dependent, that is to say, they depend on the crack-extension path to the point of establishing the characteristic fracture mode of the metal. This is illustrated in Fig. 10 by the notation “increasing resistance.”

The J-integral approach focuses on the use of a series of K_{Ic} -like specimens featuring different crack depths. The test procedures are in the very early stages of development. One of the J-integral objectives is to establish the energy-absorption features of the plastic enclave illustrated in Fig. 10. This is the index parameter of interest.

It should be noted that the DT specimen has been used to develop an index value of plastic fracture resistance, in R-curve terms. This is the slope of the fracture-energy curve determined by testing DT specimens of various fracture-path lengths – see Ref. 2.

PART 3. METAL CHARACTERIZATION AND SELECTION PROCEDURES FOR TEMPERATURE-TRANSITION PROBLEMS

General Requirements

The constraint transition for low- and intermediate-strength steels evolves as a consequence of temperature-induced changes in metal grain ductility. Thus, fracture-state transitions must be related to the temperature scale. The specific temperature range of the constraint transition may vary over wide limits—above, within, and below ambient service temperatures. These effects are intrinsic to the quality of the metal grain structure. The effects of section size are of two types:

- Mechanical effects due to changes of constraint
- Metallurgical effects due to changes in metal grain ductility.

These two effects interact to determine the specific temperature range of the constraint transition, for a specific section size.

The development of fracture control plans requires sequential definition of (a) structural requirements expressed in terms of an appropriate fracture-state criterion; (b) selection of metal which meets the desired criterion at specified lowest service temperatures and for the section size(s) of interest; and (c) purchasing to specifications which provide statistical guarantee that the criterion is met.

The fracture control plan requirements thus focus on the use of *standardized fracture tests*, which document that the selected criterion is met at the lowest service temperature of the structure.

Fracture-Test Characterization of Metal Properties

The requirements for using standardized fracture tests evolve from practical engineering and contractual reasons. An additional requirement is that test costs should be the minimum attainable for the intended purpose. In general, these requirements dictate the use of relatively small, economical test specimens. The size limitation demands that the standardized test be interpretable to fracture-state transitions of any other section size of interest. The interpretability factor is the crucial element which determines test rationality.

The standardized test specimen is cut to the specified dimensions from the section size of interest. The characterization of metal quality, in terms of the constraint transition temperature, is made in relation to the standardized section size. Since the constraint capacity of the test specimen is known, adjustments may then be made to represent the effects of increasing constraint capacity to the limit imposed by the section size used in the structure.

For example, if the section size is that of a 3.0-in. (75 mm) plate, a 0.6- or 1.0-in. (15 or 25 mm) DT specimen may be cut from the plate. The temperature range of the constraint transition for these standardized section sizes serve as the metal quality characterization reference. The constraint-transition temperature range is then adjusted (shifted) by a small temperature increment Δt to represent the *true* transition-temperature range for the 3.0-in. (75 mm) thickness. The adjustment procedure is of utmost simplicity.

The reason for using DT specimens of 0.6- and 1.0-in. (15 and 25 mm) section size is that these fall into the lower range of the most widely used thicknesses for structural purposes. The two standardized specimens index the true transition-temperature range directly for section sizes in the range of 0.6 to 1.0 in. (15 to 25 mm). A small difference in the order of 10°F (5°C) is developed between these two section sizes. It is difficult to detect, since the test-data reproducibility is of the same order; ordinarily, the curves superimpose. Adjustments of thickness effects to 2.0- and 3.0-in. (50 and 75 mm) section size, involve small upward shifts of the constraint-transition temperature curve, in the order of 20 to 40°F (10 to 22°C).

Metal of very thick section, say 6 to 12 in. (150 to 300 mm), presents a special case for two reasons:

- The adjustments for the constraint transition-temperature range become more significant; 80 to 120°F (45 to 65°C).
- Through-thickness gradients in the fracture properties of the metal grain structure may be present.

If it is determined that the through-thickness properties of the thick section metal are uniform, it is then possible to apply accurate adjustment procedures over the full range of 1.0 to 12 in. (25 to 300 mm). The procedure is illustrated in Fig. 15. The figure includes limited sampling for plates of 6 and 12 in. (150 and 300 mm) section

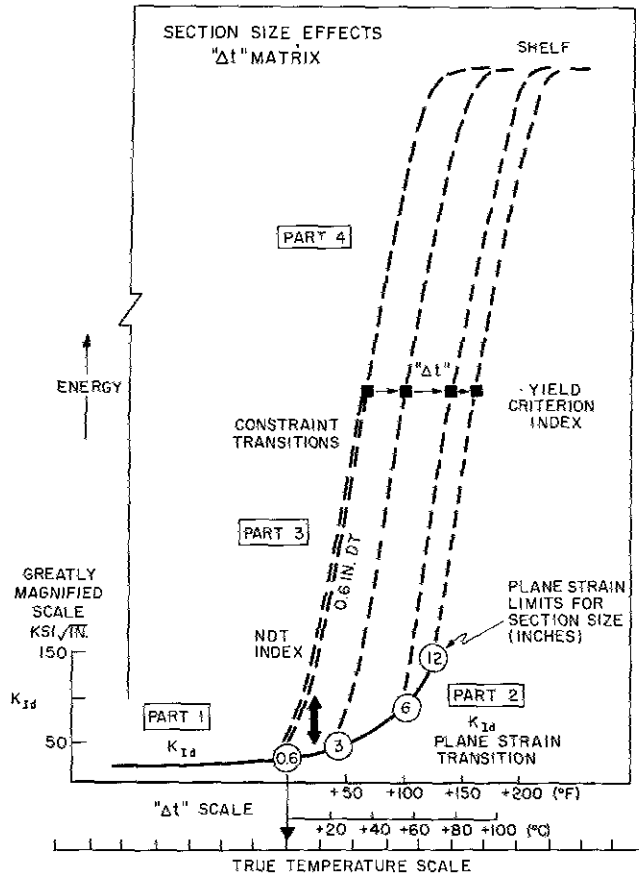


Fig. 15—Section size effects, represented by a family of transition curves which bear a fixed Δt relationship to each other. By locating a criterion's index point on the absolute temperature scale, the entire matrix is located appropriately.

(15, 75, 150, and 300 mm) section sizes. A conservative estimate of the yield-criterion temperatures for the various section sizes is provided by the midpoints of the DT test energy curve, noted by the squares.

The family of curves represents a Δt matrix which references the mechanical effects of section size. Differences in metal quality cause a shift of the total matrix up or down the temperature scale. The metal characterization objective is to locate the matrix at the correct position in the temperature scale, i.e., its absolute scale position for the metal involved.

Since the Δt relationships are fixed, the true temperature-scale location of the matrix may be determined by reference to either of the two reference criteria (circles or square points) for any section size. The specific criterion point that is selected is defined as the "entry point" for the matrix. It is the point which is indexed to the true temperature scale and, therefore, locates the matrix as a whole.

The practicality of the entry point selection now comes into consideration:

size having relatively uniform through-thickness properties. Extensive data for plates in the 1.0- to 3.0-in. (25 to 75 mm) section size range, involving a wide variety of conventional structural mild steels, provide a firm basis in the presentation. The adjustment procedures have been documented to be of high reliability and may be used with engineering confidence in determining constraint transitions for specific section sizes. The accuracy is within $\pm 10^\circ\text{F}$ ($\pm 5^\circ\text{C}$) for the lower range of section sizes. Ordinarily, the true limiting factor in the application of this information is the estimate of lowest service temperature for engineering structures.

Figure 15 illustrates the use of the constraint-capacity limits for the section size as the basic reference for temperature-scale adjustment of the constraint transition. These are the critical temperatures at which dynamic plane strain constraint is lost and constraint relaxation begins. The temperature points of rise into the elastic-plastic region are noted for 0.6-, 3.0-, 6.0- and 12.0-in.

- We may dismiss any type of entry point which requires use of large section sizes as not feasible for usual engineering characterization purposes.

- Routine testing using small K_{I_d} specimens is prohibitively expensive. Moreover, it is not possible to evolve a distinct entry point by this procedure, as explained below.

At all temperatures below the plane strain limit for small section sizes, the K_{I_d} curve is nearly flat and the K_{I_d} values are common for all conventional structural grades. In other words, a curve determined for one steel is reproduced by all others in this range of plane strain constraint level. It is not possible to determine an entry-point reference which characterizes the steel from a "nearly flat" curve. At a minimum, the K_{I_d} curve must be followed to the point that it shows a distinct plane strain transition rise (upward curvature). This determination requires the use of K_{I_d} specimens in excess of 1.0-in. (25 mm) section size, as noted in Fig. 15.

The most practical way of entering the reference matrix is to establish the specific temperature range of the elastic-plastic transition (Part 3), using a test specimen of small section size. The 0.6- or 1.0-in. (15 or 25 mm) DT specimen curve serves this purpose. All other Part 3 curves are then located at their appropriate position in the temperature scale by Δt adjustment.

The rising part of the DT-test energy curve for the 0.6-in. (15 mm) specimen denotes the full course of the constraint transition. The midpoint of the DT energy curves provides a reliable and conservative index of the temperature at which yield-criterion conditions are met. Thus, the "square point" for the first (lowest temperature) curve of the reference matrix is equivalent to the Robertson CAT curve end-point at yield-stress levels (FTE), for this section size. This point of the DT curve may be determined with ease. Because of the steepness of the curve for conventional mild steels (see Fig. 12), the selection of a point of moderately higher or lower position will result in negligible differences in the reference temperature.

The bold arrow in Fig. 15 denotes the temperature region of critical engineering interest for section sizes in the order of 0.6 to 1.0 in. (15 to 25 mm). Note that it represents the temperature region for start of the constraint transition for these section sizes, as well as the temperature for development of the *plane strain transition* for larger section sizes; the two events are related. Increasing metal grain ductility which causes constraint relaxation for these "intermediate" section sizes will require a large increase in section size, in order to maintain plane strain constraint. In other words, the plane strain transition curve must begin to rise sharply above this point because metal grain ductility is increasing sharply. This effect is well understood by metallurgists in terms of a critical temperature range T_c which activates slip systems within the grains. It then becomes very difficult to suppress metal ductility by increasing the constraint capacity of the mechanical system.

The significance of the NDT-temperature entry point is derived from the *specific size* of the surface crack that is developed by the brittle-weld bead of the DWT. The constraint capacity of the test is thus defined by the standardized crack size. The DWT develops a sharp transition from "break" to "no break" within a 10°F (5°C) temperature interval. The transition to no-break provides definite evidence of constraint relaxation, i.e., exceeding the constraint-capacity limit of the crack. This fact is most evident at 10 to 20°F (5 to 10°C) above the NDT temperature, by the grossly deformed appearance of the crack border (see Fig. A7 in the appendix).

The no-break performance is first evolved at the temperature that K_{IId} specimens are developing K_{IId}/σ_{yd} ratios of 0.4 to 0.6. The effective constraint capacity is thus defined as of approximately 0.5 ratio limit. It should be noted that the plane strain transition evolves rapidly above the NDT temperature. Thus, much larger cracks would be required to develop fracture at temperatures significantly higher than the NDT temperature.

The unusual reproducibility of the NDT determination $\pm 10^\circ\text{F}$ ($\pm 5^\circ\text{C}$) is best understood in terms of an effective constraint capacity which indexes the start of the plane strain constraint transition. In brief, the NDT temperature pinpoints the start of the rise in the K_{IId} curve noted by the bold arrow of Fig. 15. As such, it provides an excellent reference point for locating the true temperature-scale position of the matrix curves shown in the figure. Cost aspects have been cited in presenting a case for C_v -test correlation "fixes" which could provide an entry index for the subject matrix. The problems associated with C_v -test correlations are discussed in Part 5. At this point we shall simply refer to C_v costs as a known reference.

The cost effectiveness of locating the matrix curves on the temperature scale by means of the DWT-NDT temperature as the index point or by the DT midcurve temperature as the index point is closely similar. Both procedures entail costs in the same order as testing six to 10 C_v specimens. Thus, cost considerations do not enter into deducing the relative merits of these tests in comparison to C_v -test procedures. The only deciding issue is the significance of the data.

Statistical Aspects of Metal Quality

It should not be assumed that the characterization of a particular grade of structural steel is accomplished by testing a single plate to determine the temperature scale location of the constraint-transition curve. There must be statistical testing to determine the temperature range of metal-quality variance. For example, the NDT-temperature point and the "square" point denoting the yield-criterion temperature (FTE) may vary statistically (but always in close relation to each other) on the order of at least $\pm 20^\circ\text{F}$ ($\pm 10^\circ\text{C}$) from the mean. This estimate is specific to high quality steels subjected to "best" control practices as to chemistry, etc. The statistical range may be doubled for low-cost metal of "open" specification. Thus, statistical testing is required to reasonably define the "high end of the population" temperature. This is the reference temperature that should be entered in engineering tables for the steel grade and thickness involved. Only one temperature needs to be recorded. This may be reported as

- The high-end temperature for the NDT of the steel grade
- the high-end temperature for the yield criterion of the steel grade
- the high end for the midtemperature between the NDT and the yield-criterion points. This is the *half-CAT* temperature, which represents the 0.5 σ_{ys} point of Fig. 7.

While these points bear a definable relationship, the last (half-CAT) reference point is the most significant criterion for general engineering reference. Expressed statistically as the temperature for reliably ensuring that most of the population meets the 0.5 σ_{ys} criterion for fracture extension, it provides for the following direct interpretations in steel selection:

- It ensures that catastrophic fracture extension cannot evolve, irrespective of crack sizes that may be present. Since design practices focus on the use of 0.2- to 0.4- σ_{ys} levels* (for other reasons), arrest protection is always present. The engineer can then simply forget about crack sizes provided that conditions of geometric instability are not involved (see discussions of compliant structures).

- The selection of the steel is then most economical because excessive levels of fracture resistance are precluded. For most structural applications (ships, bridges, pressure vessels) the 0.5- σ_{ys} criterion is fully sufficient. Meeting of the yield criterion is an excessive requirement, if the metal features a reasonably high shelf.

Analysis of the shelf-level question is ordinarily required only for steels of greater than 60 to 70 ksi (42 to 50 kg/mm²) yield strength. The conventional as-rolled or normalized structural grades may generally be excluded from the question of shelf. The commercial Q&T steels, of 70 to 110 ksi (50 to 78 kg/mm²) yield strength, require shelf analysis. This question is treated in Part 5.

Loading-Rate Factors

The foregoing discussions centered on fracture-extension aspects of transition-temperature questions. These aspects are the primary considerations for prevention of catastrophic fracture. However, much has been written in the scientific literature with respect to

- Use of K_{Ic} rather than K_{Id} plane strain parameters for metal-characterization data and design criteria

- Use of critical surface-crack-size calculations, based on either K_{Ic} or K_{Id} , as scientific approaches to design problems.

At the outset, we shall acknowledge that all scientific aspects of plane strain fracture mechanics have been properly presented. The problem is that the engineering assumptions are totally incorrect. There is no need to belabor this aspect; a listing of points of issue derived from fracture mechanics will document the scientific aspects. The listing provides dismally adverse predictions as to reliability, as follows:

- The K_{Id} properties of the base metal generally determine whether catastrophic fracture evolves. The K_{Ic} properties of the base metal cannot be relied on because of local metallurgical and local stress conditions in structures.

- For example, the K_{Ic} values of regions, such as surround a simple arc-strike or welds, are *not* those of the base metal. The hardened material may feature very much lower K_{Ic} -values—as low as can be measured. The presence of nonmetallic inclusions in the steel provides similar circumstances; cracking of the inclusion is equivalent to metal pop-in for very low K_{Ic} values, etc.

*Stress "allowables" vary with the type of structure and refinements in design practices. Complex structures, such as ships, feature lower allowable than relatively simple pressure vessels. The range of 0.2 to 0.4 σ_{ys} reflects the usual "aim," within the allowable limits for structures.

- Thus, a base metal of, say 1.5 K_{Ic}/σ_{ys} ratio value, can be “transformed” to 0.2 K_{Ic}/σ_{ys} ratio value, in these local regions. The K_{Ic} pop-in conditions for the assumed 1.5 and the true 0.2 ratio values may be analyzed by reference to Fig. 14. The effects are enormous.

- For the above reasons, the “loading-rate effect” which leads to using the K_{Id} parameter is not necessarily related to rates of structural loading. The crucial loading rate is that of the crack-tip pop-in. The sudden separation of a few metal grains means that dynamic loading rates apply thereafter, in controlling fracture extension. K_{Id} always controls fracture extension, irrespective of initiation conditions.

- It is concluded that the use of K_{Ic} parameter values for statically loaded structures, say bridges, ships, pressure vessels, etc., is untenable. There is sufficient evidence of catastrophic failure of such structures due to local metallurgical conditions described above to document this fact.

- K_{Ic} measurement for the World War II ship failures would document *static elastic-plastic properties* at the failure temperature. That is, the K_{Ic} measurement could not be made. This applies even for the case of ships, which failed at the dock or on the ways before launching, due to arc strikes. Similar situations could be documented extensively for bridges, pressure vessels, etc.

- The concept of using something “between” the static and dynamic K_{Ic} - K_{Id} values is an illusion. Loading rates may be varied for K_{Ic} testing (known as K_I experiments), however, the test values provide no basis for engineering use.

- The controlling local stress level in structures is *not* the usually referenced nominal stress used in the scientific literature. The critical sizes of surface cracks, for the unavoidably present local stresses of high level, are exceedingly minute. Figure 14 presents these relationships and, therefore, all of the adverse predictions that evolve therefrom.

The above points explain the reasons for discussion in this section, based on dynamic fracture-extension properties. Our concern has centered on fracture control (prevention) plans—not abstract idealizations of structural conditions.

Considerations for Compliant Structures

There are broad varieties of metal-type/structure-type combinations on which fracture-safe design must be based for precluding the extension of unstable (plane strain) fracture. Thus, metals of elastic-plastic and/or plastic fracture properties provide the essential solution. However, there are special situations of metal-type/structure-type combinations for which it is important to consider differences in the level of resistance to plastic fracture.

A large and growing fraction of the structural metals in engineering use may feature low or intermediate levels of resistance to the propagation of plastic fracture. In effect, the fracture-extension stress is restricted to low, barely over-yield levels. These features may be described as “low shelf” for the case of steels and “low tearing energy” as a more general description, which applies to all metals. Such characteristics are intrinsic to metallurgical grain-structure factors which control microfracture processes. The low-shelf steels are influenced significantly by increasing temperature only to the point that

the shelf condition is attained. The full course of the constraint transition is from plane strain through elastic-plastic and then to "low-shelf" plastic fracture states.

Since the low-shelf steels are neither brittle nor highly ductile, the engineer is confronted by an in-between state of semiductile fracture. The basic problem for the semiductile state is that of possible fracture extension by low-energy tearing. Whether or not fracture may result by the extension of a low-energy tear requires consideration of the type of structure in terms of *localized force systems*. There are two basic types of structures—rigid and compliant. Rigid structures have limited force capability for release of elastic strain energy, generally sufficient only for fracture extension involving relatively brittle (plane strain) metals. Compliant structures may feature high force capability and total energy, sufficient to cause fracture extension for relatively ductile metals.

Aluminum and titanium alloys are generally characterized by low to intermediate levels of resistance to tear extension, except for the lowest strength levels. The low-strength steels generally feature high levels of tear resistance (high shelf), except for conditions of excessively preferential alignment of inclusions (e.g., weak directions of rolled or forged products). The intermediate-strength steels present a special case deserving detailed explanation (see Part 5). These metals may feature shelf levels of high, intermediate, or very low type (see discussion of corridor quality in Part 4).

There is a wide gamut of potential engineering failure conditions which involve the development of geometric instability. In general, these are conditions that result from high-compliance response to the load system. An example is the development of a flaw for internally pressurized vessels or piping, of sufficient length to cause localized bulging in the flaw area. The consequent, localized plastic loads acting on the flaw ends can cause fracture extension for metals of plastic-fracture properties. The difference in flaw length that can lead to such extension is related to the level of plastic-fracture resistance. The specific level is characterizable in terms of the R-curve slope of the metal; see Ref. 2. Very large differences in the critical flaw length (inches to feet) for initiating continued tear extension would be represented by major differences in R-curve slopes. The R-curve slope is an index of the plastic-enclave size described in Fig. 10. The significant factor is the "increase in resistance," noted in the figure, for fracture extension.

These aspects apply in a most important manner for gas transmission pipelines. In this case, the engineering consideration is the reduction in the fracture-extension velocity to the point that the gas-pressure release occurs at a rate sufficient for unloading of the hoop stress acting on the propagating tear. Low-slope R-curve metals may be expected to permit relatively high rates of fracture extension, while high-slope R-curve metals should decrease this rate dramatically, leading to fail-safe conditions. The engineering problem is the definition of the adequate (minimum) R-curve features which provide for fracture arrest (by pressure release), for the specific diameter and pressurization level of the pipe. Correlations between full-scale burst tests and laboratory test definitions of R-curve features are required.

Exact definitions should be possible by the use of full-thickness DT tests for R-curve slope determinations. An additional advantage of the DT test is that it defines the exact temperature of transition to shelf levels, for the thickness involved. R-curve slope relationships to structural requirements are discussed in a previous report (2). Engineering interpretations are provided by the Instability Analysis Diagram (IAD) which is indexed to the DT-derived R-curve slope scale. The structural force-system is defined in terms of

hoop stress vs crack length parameters. Thus, a direct relationship is established between metal properties and structural requirements.

PART 4. METAL CHARACTERIZATION AND SELECTION PROCEDURES FOR STRENGTH-TRANSITION PROBLEMS

Strength-Induced Constraint Transitions

The prior discussions focused on temperature-induced transitions in fracture state. The scientific and engineering rationality for reference to the temperature scale have been made evident.

Discussions to follow focus on the case of metals for which the fracture-state transitions evolve as a consequence of changes in strength level, i.e., are strength induced.

The factors of similarity and/or differences in characterization practices are as follows:

Temperature-induced

- The fracture-state transition is "tracked" across its pertinent temperature range using a test specimen of specified mechanical constraint capacity. A series of test specimens cut from the steel of interest suffices for this characterization—all that has to be varied is the test temperature.

- The test variable is temperature because metal grain ductility changes with temperature. Metal quality is deduced by the intrinsic temperature range of the constraint transition.

Strength-induced

- The fracture-state transition is "tracked" across its pertinent strength range using a specimen of specified constraint capacity. Test specimens are cut from samples of the metal of interest, which have been heat treated to appropriate strength levels.

- The test variable is strength because metal grain ductility changes with strength level. Metal quality is deduced by the intrinsic strength range of the constraint transition.

The fracture research literature generally avoids discussions of fracture-state transition in terms of relationship to temperature and strength scales. The reason is that the focus is primarily on the effects of changing constraint for a specific metal sample, i.e., on mechanics. However, the most elemental aspect of fracture control planning, is that of trade-off analysis between available metals. Thus we arrive at a most important generalization:

Metal selection must be based on meeting structurally required fracture-state criteria *at particular service temperatures or particular strength levels*. Reference to the fracture-state quality of the metal in terms of temperature and strength scales is the only basis by which direct rational connections may be made to the structural requirements.

In brief, the engineer must think in terms of fracture state, service temperature, and/or strength level. Metal quality should be indexed in the same manner, i.e., the fracture state for specific temperatures and/or strength levels.

Meeting of these *connective* requirements is provided by the Ratio Analysis Diagram (RAD) procedure, as introduced in Fig. 16 for the case of steels. The temperature scale is replaced by the yield-strength scale and the course of changes in fracture resistance is plotted as a function of this scale. For example, extensive test experience has determined that the best steels that can be produced (to be explained) will follow the course of the highest curve. This is the technological-limit curve which describes the present state of metallurgical achievement as a function of strength level. It is an "experience curve" derived from test data.

The poorest quality steels follow the curve described as "lower bound." Steels of intermediate quality follow other trend-line curves, as illustrated in the figure. The range of fracture resistance at any given level of yield strength is determined by the range of metal-grain ductility for the strength level. The most important feature of the plot is that the attainable range is narrowed drastically as the yield-strength level is increased above 160 ksi (110 kg/mm²). At all strength levels in excess of 230 ksi (160 kg/mm²), the range is very narrow. These ranges illustrate the limits within which steels can be produced.

The mechanical effects of section size must now be considered. Transitions in fracture state are always a combined function of the metal grain quality and constraint capacity. The effects of section size are analyzed by inserting K_{Ic}/σ_{ys} ratio lines which relate to the two critical fracture-mechanics constraint criteria. These are as follows:

- The K_{Ic}/σ_{ys} ratio which defines the plane strain limit for the section size.
- The K_{Ic}/σ_{ys} ratio, which defines a constraint insufficiency equivalent to the yield criterion for the section size.

The analysis presented in Fig. 16 is for a plate of 1.0-in. (25 mm) thickness and, therefore, the reference ratios for the plane strain limit and yield criterion are 0.63 and 1.0, respectively. The region between these two ratio lines represents the elastic-plastic fracture state. The intersections of the metal-quality trend lines with the two ratio lines define the yield strength range over which the elastic-plastic transition is evolved. Note that the specific yield-strength range is shifted to lower levels, with decrease in metal quality from the best to the lower-bound trend lines.

Test experience documents that for steels of best attainable quality, a 1.0-in. (15 mm) K_{Ic} test specimen will track the K_{Ic} curve to approximately 230 ksi (160 kg/mm²) yield strength, exactly as noted. The limit of K_{Ic} measurement is reached at this strength level. Since the 1.0-in. (25 mm) K_{Ic} specimen provides insufficient constraint for measurement of higher K_{Ic} values, it will develop elastic-plastic fracture in the yield-strength range of 230 to approximately 200 ksi (160 to 140 kg/mm²). The K_{Ic} trend-line relationship to the yield-strength scale may be determined if the section size is increased to approximately 2.5 in. (62 mm). This section size permits measurement of 1.0 ratio values. The trend line is always referenced to the K_{Ic} scale, and is the feature which provides for determination of section-size effects.

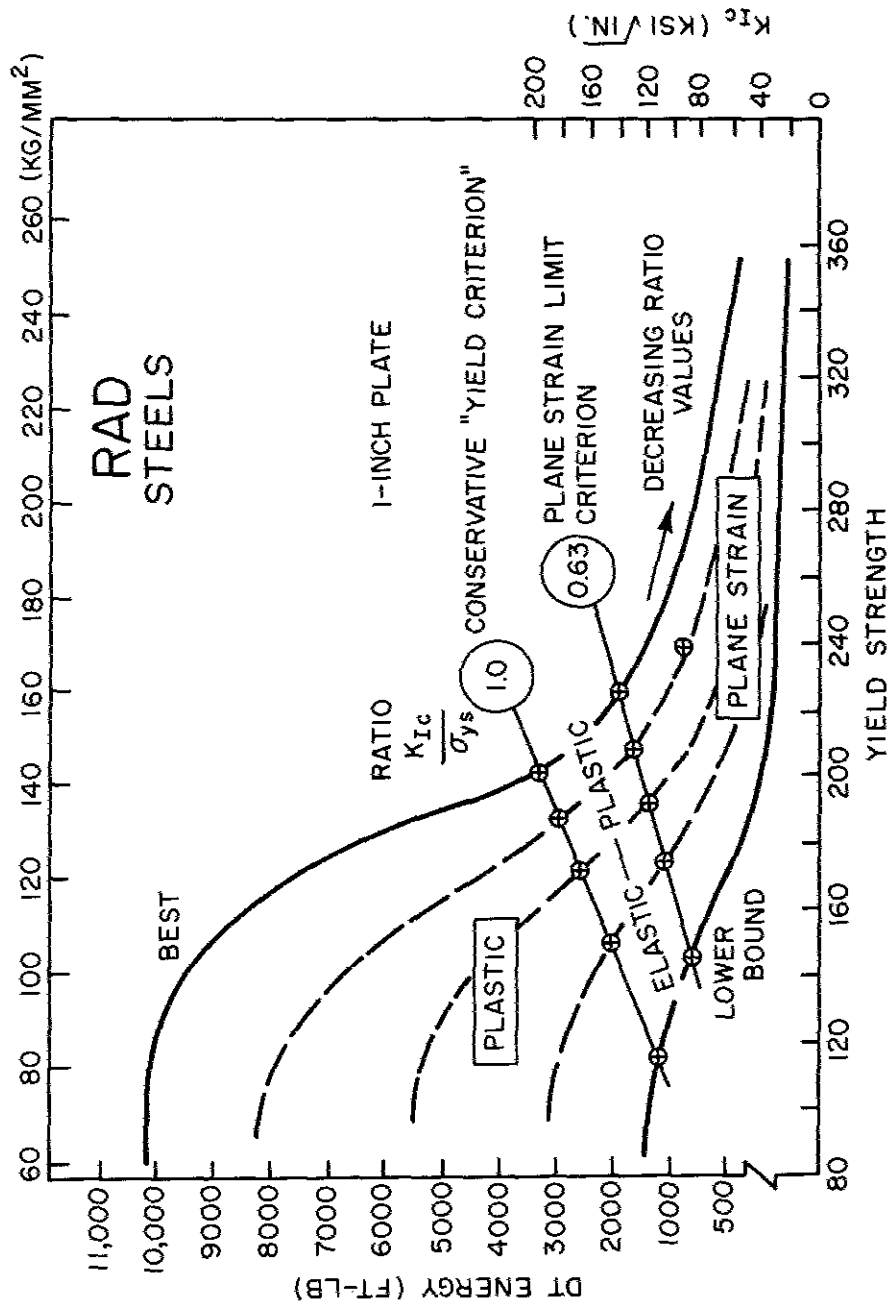


Fig. 16—Trend relationships of fracture properties applied to the yield-strength scale, as a function of metal quality. Analysis of fracture states for a 1.0-in. (25 mm) section size is provided by inserting the appropriate ratio lines, which reference the two critical criteria of foremost engineering importance.

If the trend-line characteristics (quality level) of the steel are established, it is possible to extrapolate up or down from a fixed point. For example, let us assume that a specific steel is of interest, it is of 1.0 in. (25 mm) thickness, and heat treated to 240 ksi (170 kg/mm²) yield strength. A K_{Ic} test is made and the value (which may range from 30 to 110 ksi $\sqrt{\text{in.}}$)* is actually determined to be 80 ksi $\sqrt{\text{in.}}$. This indicates a location in the RAD noted by the "+" point. The steel is of high, but not highest, quality. The trend line which applies is that of the dashed curve that it falls on. We shall now assume that it is desired that the steel of this section-size quality level should meet elastic-plastic fracture properties, as a design requirement. The trend-line extrapolation indicates that decreasing its yield strength to below 210 ksi (150 kg/mm²) by heat treatment should result in meeting the design objective. The designer is provided with a trade-off—use as a plane strain metal at the higher strength level or as an elastic-plastic metal at the lower strength level.

The regions between trend lines may be considered to be metal-quality "corridors." The metallurgical factors which determine whether a steel will fall into high- or low-quality corridors are now well understood. This knowledge is similar to that which has been developed in relationship to the temperature-transition curves. If the metal quality level (trend-line level), yield strength, and section size are fixed, it is possible to go directly to the RAD and predict the expected fracture-state properties within exceedingly close limits. All that is necessary is to locate the two proper ratio lines for the section size. As the section size is changed, it is necessary to relocate the two ratio lines, as will be described. However, the analysis as to constraint-transition effects remains invariant.

Figure 17 indicates the engineering interpretation of these analyses for a 1.0-in. (25 mm) section size. It is simply a repeat of Fig. 7 with the indefinite metal-grain-ductility scale replaced by an exact definition of the plane strain ratio-value properties of the metal. The section size effect comes into play in limiting the highest ratio that can be measured. Thus, the ratio values below this limit are noted in the figure as "true," i.e., measured. The extrapolation technique following a trend line defines plane strain ratios which are inferred (indexed). Thus, the metal properties continue to be defined in plane strain parameters by the extrapolation. The fact that they cannot be attained for the 1.0-in. plate is the feature which causes a rise in the fracture stress. The yield-level criterion is reached when the section size inadequacy is such as to indicate an extrapolated trend-line ratio of

$$B = 1.0 (K_{Ic}/\sigma_{ys})^2$$

rather than the requisite

$$B = 2.5 (K_{Ic}/\sigma_{ys})^2$$

which is the plane strain limit for the section size.

It should be noted that the fracture stress relationship to the K_{Ic}/σ_{ys} ratio, in the "true" plane strain region for the section size, is for a specific crack length. This is a crack which is three times the section size (3 T) or 3.0 in. (75 mm) in this case. The fracture stress value of $0.3 \sigma_{ys}$, cited previously for a through-thickness crack of minimum length to achieve maximum constraint (2 to 3 T) is the value attained at the ratio

*See metric conversion scale for K_{Ic} in the appendix.

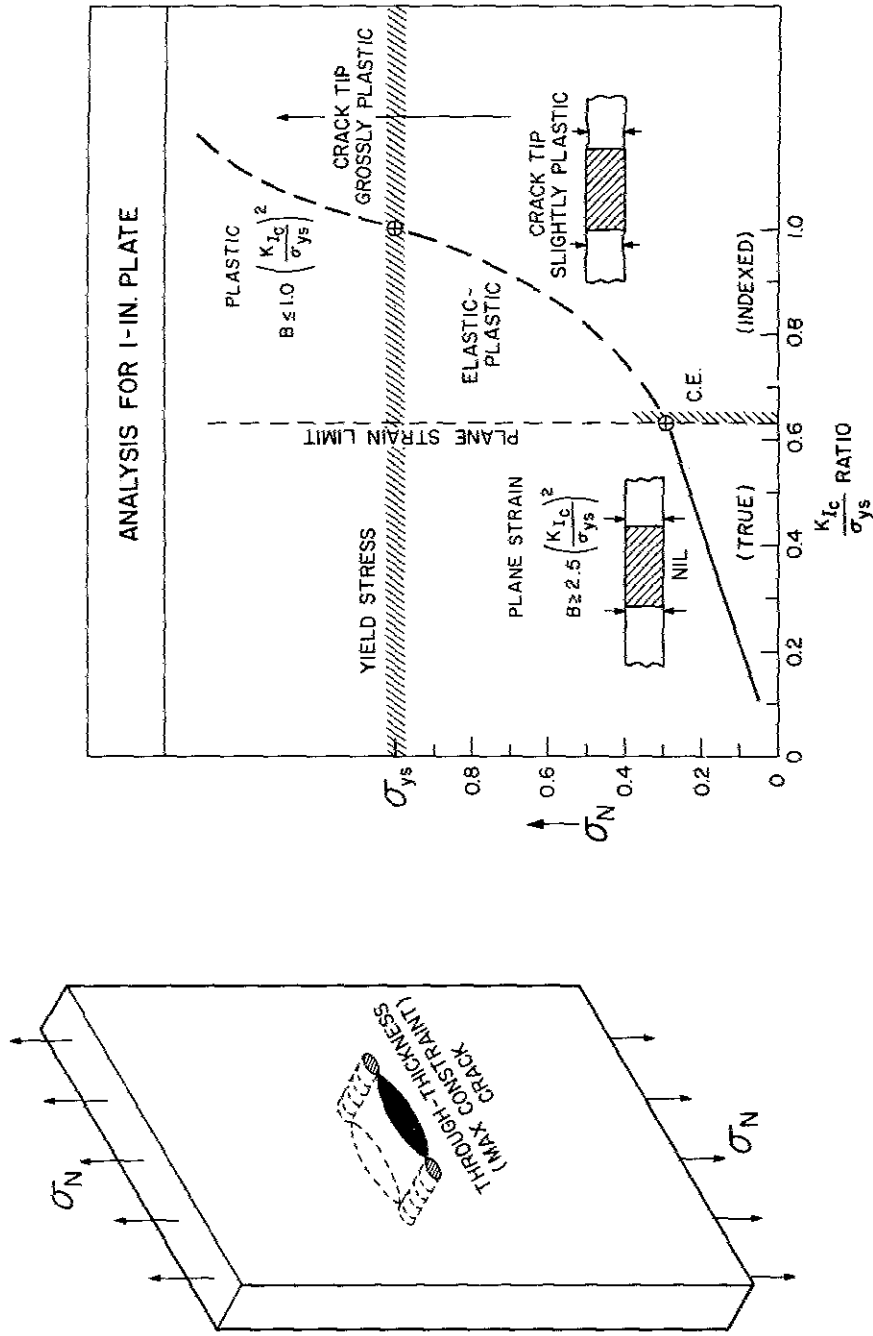


Fig. 17--General engineering significance of transition through the elastic-plastic region of the R.A.D. The fracture stress for a 3-T (3.0-in., 75 mm) through-thickness crack is defined by the curve. The solid part of the curve is derived from calculations based on the use of the measured K_{Ic} value, to its limit ratio of 0.63 for the case of a 1.0-in. (25 mm) plate. The dashed line is used to connect the limit-ratio point to the yield-criterion point.

limit for the section size. If the metal properties for this section size are of *lower* ratio value, the fracture stress decreases as shown in the figure. The basic equation which applies is

$$K_{Ic} = \sigma_f \sqrt{\pi L/2}.$$

The specific crack-length value (L) in inches must be used to calculate the fracture stress (σ_f).

Principles of Initiation and Arrest

The described graphical procedures provide relatively simple analytical tools for engineering design based on either initiation or arrest principles. These are the two choices open to the designer:

- Initiation Principle. Analyses are made of the potentials for fracture initiation due to the presence of surface cracks, which may pop in to through-thickness dimensions. These analyses are required when it is known that fracture extension can evolve.

- Arrest Principle. Analyses are made as to metal properties requirements for prevention of fracture extension, irrespective of crack size.

The initiation principle can only provide provisional protection, i.e., control is required over crack-size and stress-level questions. The arrest principle provides positive protection, which is assured without requirements (provisions) to control crack sizes. Use of the arrest principle limits design considerations to the level of nominal stress, which represents the long-range stress field. If the long-range stress field is insufficient to provide for fracture extension, cracks will be held in arrest condition. As such, they become merely a nuisance problem.

In general, $0.3\sigma_{ys}$ design-stress levels are always adequate for fracture extension in the presence of through-thickness cracks of 2 to 3 T length if plane strain conditions apply. This is the danger that evolves in using metals of plane strain fracture properties. The only protection that exists is that of preventing pop-in of a surface crack or growth of the surface crack by other mechanisms. In contrast, when the elastic-plastic state is entered, there is a rapid rise in fracture stress which brings into positive action the crack-arrest principle. This design principle provides high reliability *because the long-range stress system is then lower than the level required for fracture extension*.

The initiation principle is ordinarily related to conditions of fracture initiation from surface cracks of less than $1/2 T$ depth. The relationships of surface crack sizes to K_{Ic}/σ_{ys} ratios were presented in Fig. 14. It should be noted that these crack sizes are very small for all relative stress levels if the K_{Ic}/σ_{ys} ratio values are low. The slopes of these curves for various relative stresses are of important engineering significance. It is indicated that for regions of high relative stress, there is a small increase in critical flaw sizes with increasing ratio value. In other words, points of high stress involving geometric transitions (nozzles, etc.) may be subject to fracture initiation due to small flaws which are difficult to detect. In general, the initiation principle is of low design reliability, compared to the arrest principle.

Case Example of Design Based on Arrest and Initiation Principles

It is assumed that the case involves a thin-walled aerospace pressure vessel of 0.15-in. (4 mm) wall thickness. The first problem is to determine the maximum yield strength that may be used with retention of fracture properties sufficient to preclude bursting in the presence of through-thickness cracks. The following considerations apply:

- The desired yield strength is in the range of 240 to 280 ksi (170 to 200 kg/mm²)
- The steel is a maraging type and of high fracture quality
- The nominal design stress is $0.3 \sigma_{ys}$
- Stress corrosion cracking is possible, leading to the development of through-thickness cracks
- Leakage is acceptable but bursting is not, due to secondary-events reasons.

These considerations dictate that, for a crack which grows through the wall, the arrest principle of "leak-before-fracture" must be applied. The crack geometry may be expected to be in the range of 2 to 6 T (0.30 to 0.90 in., or 7.5 to 22.5 mm) on penetration. For reasons of reliability, a fracture stress which is at least 2 times the design nominal stress, i.e., $>0.6 \sigma_{ys}$, should be required for bursting the vessel in the presence of the subject cracks.

The solution is evolved by the use of Fig. 18 relationships, keyed to the elastic-plastic region defined by the RAD, Fig. 19. The first step is to analyze the range of possible K_{Ic} values for the yield-strength range of 240 to 280 ksi (170 to 200 kg/mm²). The RAD data bank of Fig. 19 provides for this analysis. The following aspects are noted:

- At 240 ksi (170 kg/mm²) the K_{Ic} range is from 30 to 140 ksi $\sqrt{\text{in.}}$
- At 280 ksi (200 kg/mm²) the K_{Ic} range is from 30 to 90 ksi $\sqrt{\text{in.}}$
- The high ends of these K_{Ic} ranges represent maximum recorded values. Reasonable expectations for high quality metal are represented by the trend band.
- The reasonable-expectancy K_{Ic} range is 70 to 100 ksi $\sqrt{\text{in.}}$ at 240 ksi (170 kg/mm²) and 40 to 70 ksi $\sqrt{\text{in.}}$ at 280 ksi (200 kg/mm²), as noted by the circled points.
- The mean K_{Ic}/σ_{ys} ratio value falls from 0.4 to 0.2 as the yield strength level is raised from 240 to 280 ksi (170 to 200 kg/mm²).

The significance of falling from 0.4 to 0.2 ratio value must be analyzed in terms of the specific section size involved. The plane strain limit ratio is 0.25 and the yield-criterion ratio is 0.38. These two critical ratio lines have been drawn across the diagram of Fig. 19 to locate the elastic-plastic region. It is now noted that the following fracture states are developed for the strength levels defined by the vertical bold arrows, as follows:

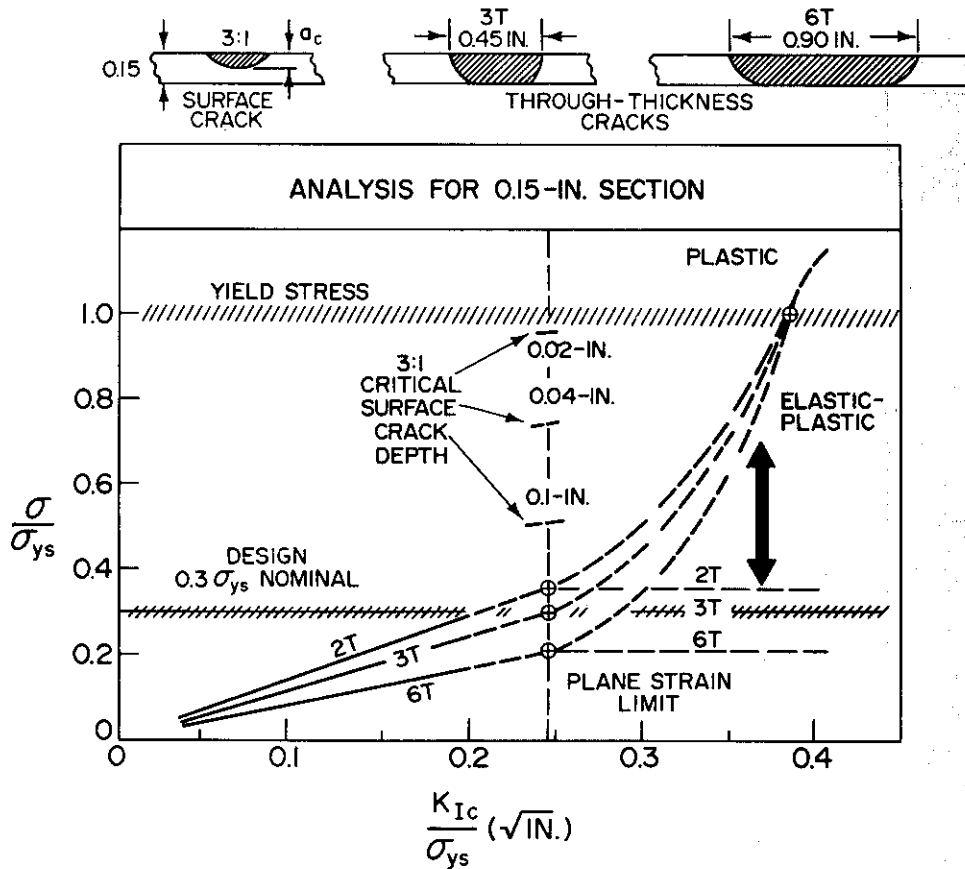


Fig. 18—Engineering analysis for a high-strength steel of thin section (see text). The most important general aspect of this plot is that the fracture-stress level for the noted crack sizes (in terms of T) is always of the level indexed by the noted crack sizes, at the plane-strain limit for the section size. This is noted by the dashed curves. The rise in fracture stress evolves only as the elastic-plastic state for the section size is entered. The difference between the two sets of curves represents the engineering benefit of the elastic-plastic state.

- <240 ksi (170 kg/mm²) — plastic
- 250 ksi (175 kg/mm²) — high elastic-plastic
- 280 ksi (200 kg/mm²) — plane strain.

The high range of the elastic-plastic state always requires stresses in excess of 0.5 σ_{ys} levels for fracture extension due to through-thickness cracks. Thus, limiting the yield strength to 250 ksi (175 kg/mm²) maximum, for metal of this quality, provides the desired “leak-before-failure” fracture control plan. The fracture stress will be at least 0.6 σ_{ys} and, therefore, meets the “two-times nominal-stress level” safety margin defined previously as the requirement.

The crack-length relationships to the relative fracture-stress scale are presented in Fig. 18. The solid curves define the effects of increasing K_{Ic} plane strain properties to

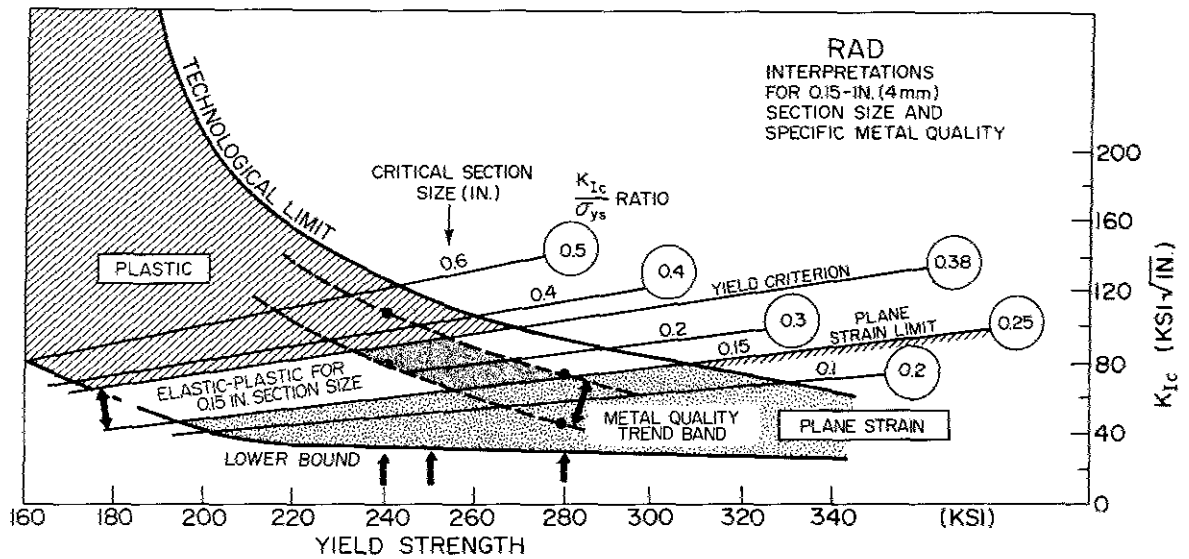


Fig. 19—Engineering analysis for the 0.15-in. (4 mm) section size. Note that the analysis is specific to the corridor quality of the metal. The reader may determine the effects of inferior metal quality by inserting a lower corridor trend band of appropriate lower slope.

the plane strain ratio limit (0.25) for this section size. Note that at the plane strain limit the fracture stresses, for these various crack lengths, are in the order of or below the stated nominal design level ($0.3 \sigma_{ys}$). Accordingly, bursting of the vessel is to be expected when the cracks penetrate the wall.

The set of rising curves denotes the effects of traversing the elastic-plastic region to the yield-criterion ratio value of 0.38. Fracture stresses in excess of $0.6 \sigma_{ys}$ are attained in the high end of the elastic-plastic range. Note that we may code the yield-strength scale to the rising values of the K_{Ic}/σ_{ys} ratios of this plot, as listed below.

Ratio	Yield Strength	
	ksi	kg/mm ²
0.20	280	200
0.25	270	190
0.30	260	185
0.35	255	180
0.38	250	175

This relationship is traced by the midcourse of the quality band of Fig. 19.

Proof of the validity of the trend-band curve will be required for quality control and purchase specifications. This requirement is met by conducting K_{Ic} tests for the metal, using section sizes that provide for valid K_{Ic} tests in the elastic-plastic region of the 0.15-in. (4 mm) section size, i.e., specimens of 0.2- to 0.3-in. (5 to 7.5 mm) thickness. Alternatively, measurements are made

for the metal in the 0.15-in. (4 mm) thickness, at the high yield strength levels which provide for valid K_{Ic} values. The trend band deduced by either of these procedures validates control of the metal to the desired trend-band quality level.

We shall now illustrate the undesirable effect of increasing the wall thickness slightly, and with continued use of metal of 240-ksi (170 kg/mm²) maximum yield strength. Consideration is often given to increasing the wall thickness for possible "added safety."

Increasing the wall thickness, which raises the plane strain ratio limit, causes the metal of 0.3- to 0.4-ratio value to have plane strain properties. Now the course of the fracture stress curves of Fig. 18 for 2-T, 3-T and 6-T flaws (referenced to a length in inches which is related to the increased wall thickness) remains in the 0.2- to $0.3\sigma_{ys}$ stress level. This fact is represented by the flat curves with the 2-T, 3-T, and 6-T notations. Comparison of the fracture stresses for plane strain state and for the elastic-plastic state is provided by the two sets of curves in the figure. The bold arrow emphasizes the dramatic differences. The importance of entering the elastic-plastic state is graphically evident from this comparison. The added "safety" assumptions for increasing wall thickness *are not justified*.

Ordinarily, increased wall thickness is used to reduce nominal stresses from maximum "allowable" ($0.5\sigma_{ys}$ for pressure vessels) to lower levels. The calculations presented in Fig. 18 indicate that the reduction must be to $0.25\sigma_{ys}$ levels or less, in order to be effective for fracture prevention when cracks penetrate the pressure vessel wall. Reductions from, say, $0.5\sigma_{ys}$ to $0.3\sigma_{ys}$ do not provide added safety for such cases. Paradoxically, reductions in wall thickness which result in increasing stresses above "allowables" to 0.6 or $0.7\sigma_{ys}$ do provide safety if the reduction in thickness results in metal of high elastic-plastic fracture properties. We may summarize:

In developing fracture control plans, the engineer must develop completely new "thinking" with respect to factors of safety. Adherence to past conventions is dangerous.

Finally, we shall illustrate the low reliability which evolves for design of this vessel to initiation criteria, i.e., by control of surface-crack sizes. Again, "new thinking" is essential. We shall first assume that procedures are available for detecting the initial presence, or "monitoring" the growth of a surface crack in service. The validity of this assumption is the question involved.

The effect of relative stress level on the critical size of surface-cracks of 3 to 1 (length to depth) geometry is indicated in Fig. 18 at the plane strain limit value. Note that the critical crack depths are in the undetectable range of 0.02 to 0.1 in. (0.5 to 2.5 mm) at a nozzle (high stress) location. In the hoop-stress region of the vessel ($0.3\sigma_{ys}$), surface cracks in excess of wall thickness would be required for fracture initiation at the plane strain limit for the section size. For ratios of lower value, the critical surface crack sizes would decrease rapidly at this stress level, as illustrated in Fig. 14. In fact, they decrease to the same values cited above for the nozzle, i.e., to undetectable dimensions. It is concluded that

- Reliable protection cannot be provided at nozzles for metal of the highest measurable plane strain fracture properties for the section size.
- Similarly, reliable protection cannot be provided for all other locations of the pressure vessel if the plane strain value is significantly less than maximum for the section size.

We may now summarize a most important and often neglected consideration in fracture control planning based on initiation-prevention principles:

The critical crack size for any structure is that which is defined by stress levels in the range of 0.75 to σ_{ys} , *not* by nominal design-stress levels.

The reason is that such high stress levels are generally present in structures due to regions of geometry transition. The most refined designs, say, nuclear reactor pressure vessel nozzles, result in stress-concentration effects of approximately 2.5. Thus, 2.5 times the allowable $0.5 \sigma_{ys}$ results in exceeding yield levels. A gradient of stress from σ_{ys} to $0.5 \sigma_{ys}$ obviously exists in the nozzle-transition region. The reader should now recognize the true engineering significance of the lower curves of Fig. 14. They define the usual and not the unusual requirements for crack-size surveillance. The usual reference to nominal stress of less than $0.5 \sigma_{ys}$ level, used in the research literature, represents an unrealistic idealization of structural design problems.

Generalized Use of RAD Procedures

The RAD procedures are based on the use of fracture mechanics principles to evolve an analytical "grid system" of K_{Ic}/σ_{ys} ratio lines. The grid is superimposed on a data bank of metal properties, separated according to three levels of metal quality.

Figure 20 illustrates the first step in evolving the complete RAD procedure. Metal properties are represented by three metal quality corridors—low, intermediate, and high.

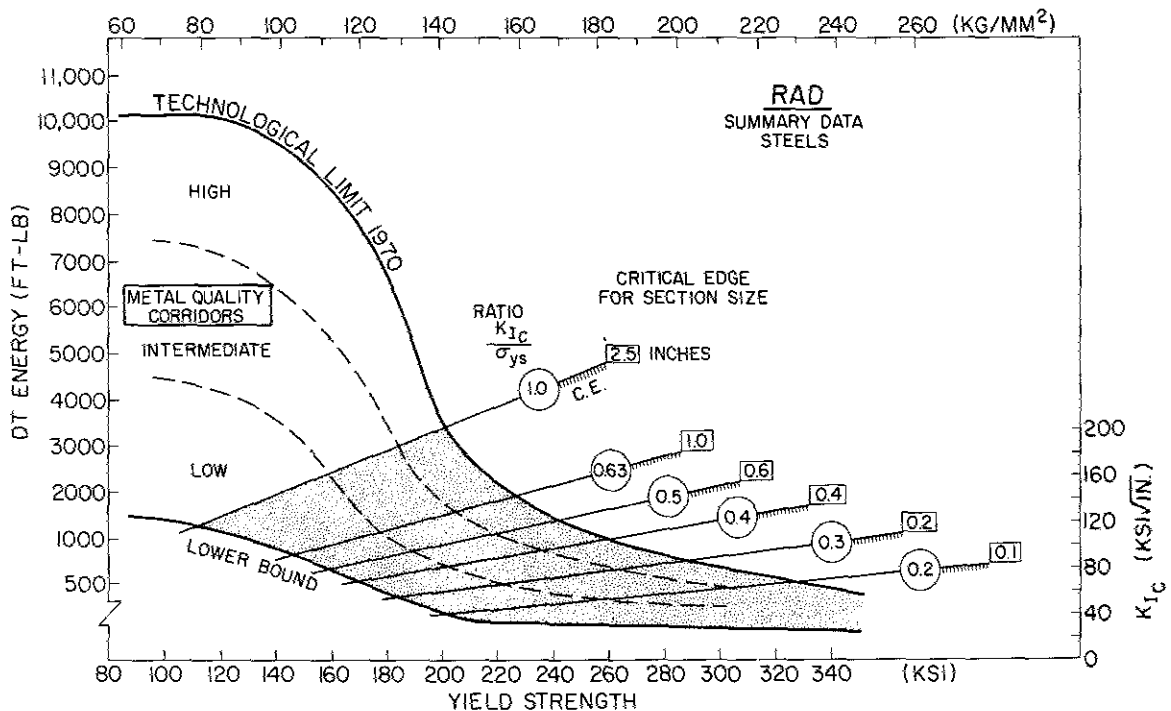


Fig. 20—Standardized ratio grid system which provides for analysis of the plane-strain limits of specific section sizes. Each of the ratio lines represents a "critical edge" of transition to elastic-plastic fracture for the noted section size.

The K_{Ic} scale provides for overlay of the ratio-line grid by reference to the yield-strength scale. The ratio lines chosen are the plane strain limits (constraint capacities) for a range of section sizes, as noted in the figure. The terminology of "critical edge" (C.E.) is used to emphasize that the transition from plane strain to elastic-plastic evolves as the constraint capacities of the specified section sizes are exceeded.

Figure 21 presents an analysis which is specific to a plate thickness of 1.0 in. (25 mm). The critical edge has a 0.63 ratio value, and yield-criterion conditions are reached at the position of the ratio 1.0 line. Thus, the location of the elastic-plastic region is identified, as well as the plane strain and plastic regions. For metal of highest corridor features (technological limit), the elastic-plastic region is developed in the 230 to 200 ksi (160 to 140 kg/mm²) yield-strength range. Note that the strength range for this transition decreases to lower levels of yield strength, with decreases in metal quality to lower corridors.

The rising stress scale of Fig. 17 is inserted to denote the significance of crossing through the elastic-plastic region. The fracture stress for a 3-T through-thickness crack (3.0 in. or 75 mm) will rise from 0.3 to σ_{ys} levels, as shown. If a line is visualized across the elastic-plastic region at its midpoint (parallel to the critical-edge ratio line) it will indicate the 0.5 σ_{ys} fracture-extension stress for the subject crack.

There should be little concern for the absolute accuracy of this inserted scale. Note that the technological-limit curve indicates that the increase from 0.3 to 1.0 σ_{ys} levels must evolve in a 30-ksi (20 kg/mm²) strength range. Since the elastic-plastic transition region is very narrow, any attempt to provide more exact definitions will require analyses of statistical variances of metal properties (to be discussed). In brief, the scale suffices for the analysis of behavioral trends to be discussed and for a generalized description of the structural significance of the elastic-plastic region.

The notations of critical surface-crack depths for 0.5 σ_{ys} and σ_{ys} relative stress levels are coded to ratio lines which lie below the C.E. ratio value. The crack depths are deduced from Fig. 14. The fracture mechanics calculations for surface cracks only apply for the plane strain state. The choice of high-stress levels for reference is made deliberately, to emphasize that the high-stress regions of structures (geometric transition points) determine the minimum critical crack sizes for the structure. Note the rapid decrease in crack size with decreasing ratio value, i.e., with increasing strength level. In all cases, in making these analyses it is necessary to follow the trend of a specific corridor, which is related to the metal quality of interest.

The significance of the DT scale is that it provides for a full-span definition of fracture properties, up to the highest plastic fracture levels. Moreover, the DT energy value can be used to index the K_{Ic}/σ_{ys} ratio of the metal. The RAD can be entered either from the DT energy scale or the K_{Ic} scales. The major importance of the DT scale is that it provides an *inexpensive method* for determining the metal quality corridor level of the metal. With this determination, the ratio-line grid system can then be used for further detailed analysis.

The RAD interpretations for 0.5- and 2.5-in. (12.5 and 62 mm) plate thickness are presented in Figs. 22 and 23. The notations are the same as above. Thus, quick reading of the significant features can be made.

The reader may analyze conditions for any section size in the range of 0.1 to 2.5 in. (12 to 62 mm), starting from the relationships presented in Fig. 20. For example, let us

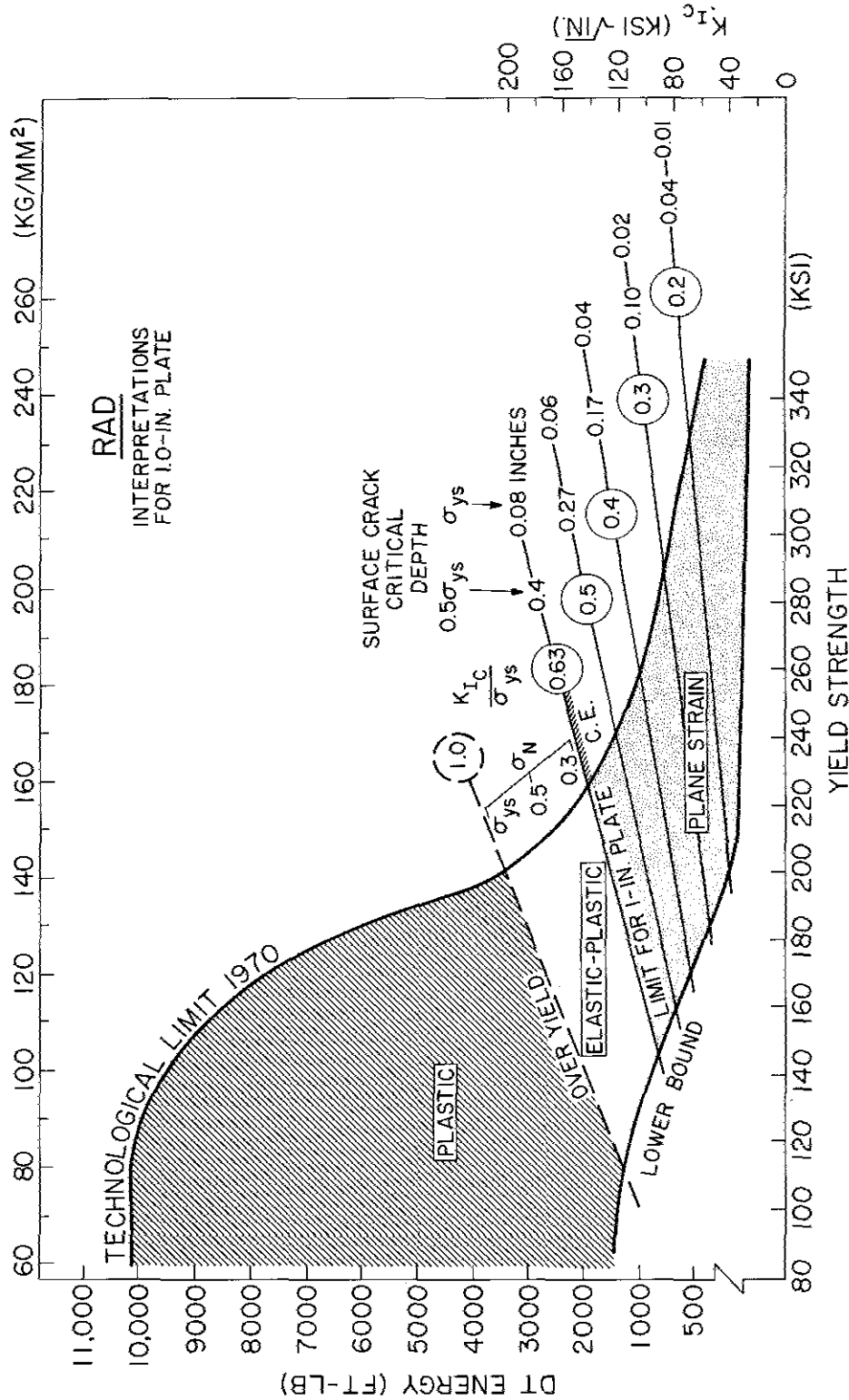


Fig. 21—Expansion of the analytical capabilities of the ratio grid system; example for a 1.0-in. (25 mm) section size. The ratio lines for the plane-strain and yield criteria are drawn in specific relationship to the section size involved; 0.63 and 1.0, respectively, in this case. The increase in fracture stress for a through-thickness crack (3.0 in. in this case) is indexed to the elastic-plastic region. Critical flaw sizes in the plane-strain region are deduced from Fig. 14 for two levels of relative stress.

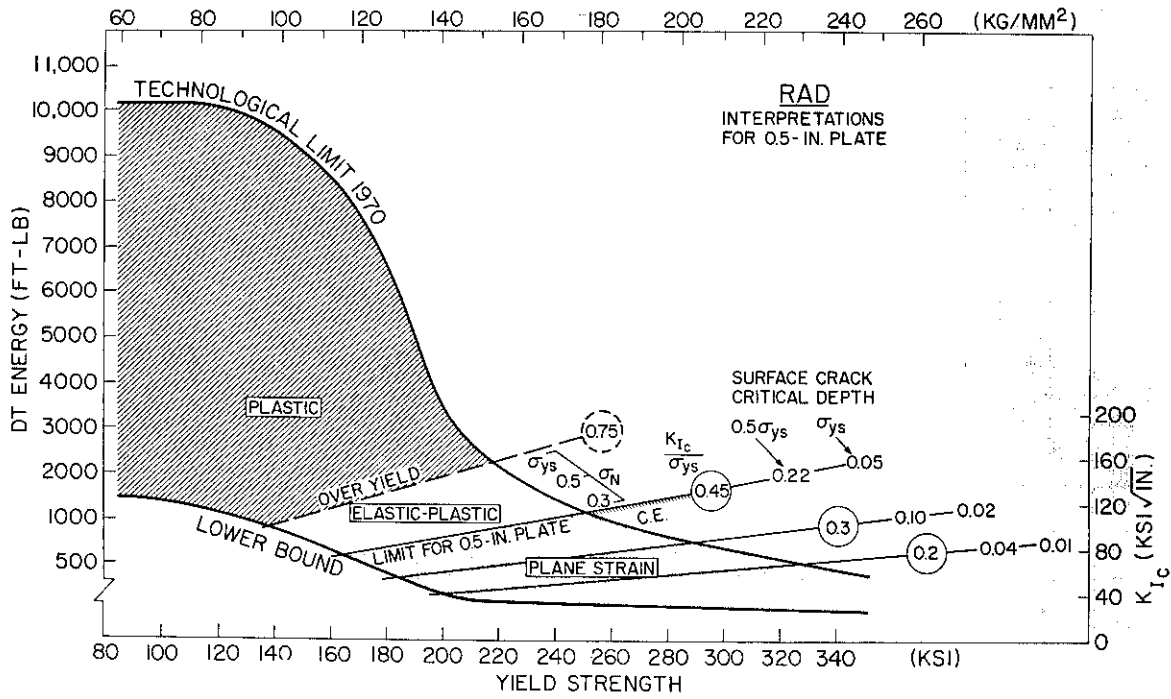


Fig. 22—Analysis for 0.5-in. (12.6 mm) section size

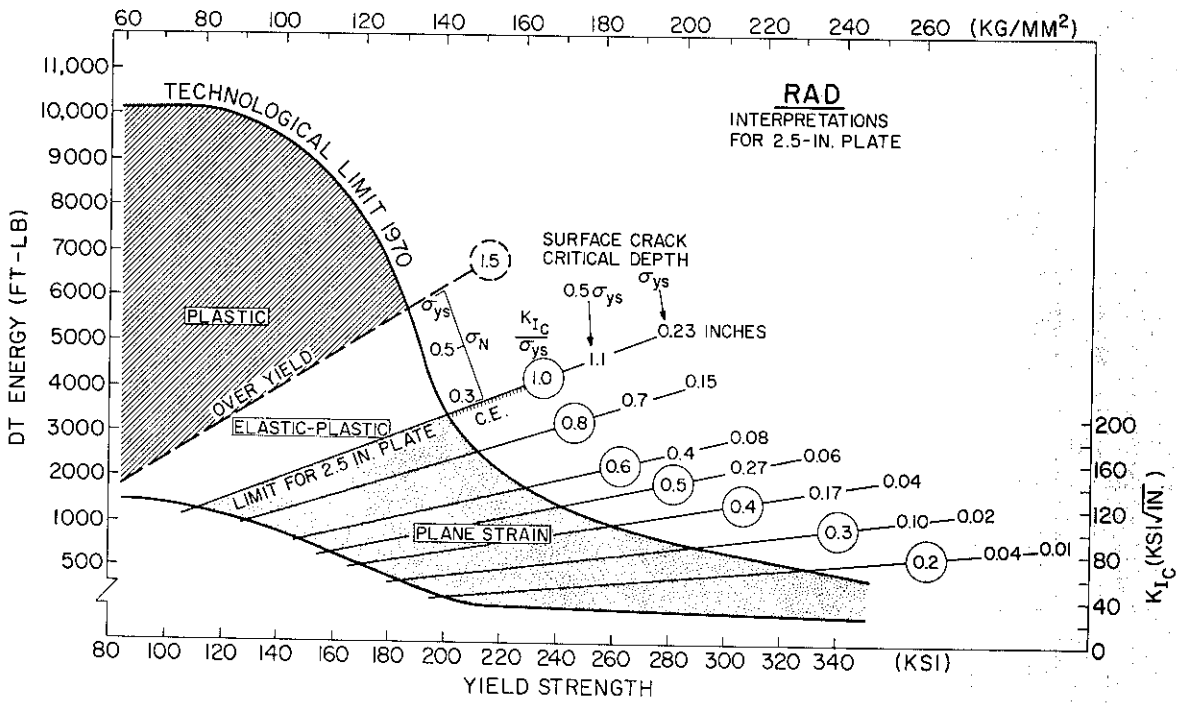


Fig. 23—Analysis for 2.5-in. (62.5 mm) section size

assume that the section size of interest is 0.3 in. (7.5 mm). The C.E. for this section lies at the 0.35 ratio level, as deduced by interpolation between the C.E. ratio lines for the 0.2- and 0.4-in. (5 and 10 mm) section sizes. The interpolated C.E. ratio line is drawn across the diagram. The span of the elastic-plastic region for this section size has a ratio value of approximately 0.2 (see Table 2 below). Thus the yield-criterion ratio value is $0.25 + 0.20 = 0.45$. Another line, denoting the yield criterion, is then drawn at the 0.45 ratio level. The elastic-plastic region for this section size is thus located in the diagram. The standardized scale, which denotes the fracture-extension stress levels (0.3 to 1.0 σ_{ys}), is then inserted in the elastic-plastic region.

Calculation of the ratio-span difference between the C.E. of $B = 2.5 (K_{Ic}/\sigma_{ys})^2$ and the yield criterion of $B = 1.0 (K_{Ic}/\sigma_{ys})^2$ for the section size indicates the following ratio span above the C.E.

Table 2

Section Size (inch)	Approximate Span (ratio)
0.3 to 0.5	0.2
0.5 to 1.0	0.3
2.5 to 3.0	0.5

In the example cited above, the elastic-plastic region of the 0.3-in. (7.5 mm) section size was indexed as having a 0.2 ratio span, in accordance with these generalizations.

The definition of "conservative" for the ratio span of the elastic-plastic fracture state implies that the $B = 1.0 (K_{Ic}/\sigma_{ys})^2$ method of deducing the yield criterion is conservative. In effect, this means that the span of the elastic-plastic range may be somewhat less than that deduced by these procedures. Concern for the exactness of this definition is eliminated if the narrow width of the yield-strength range is considered. For any metal-quality corridor, the yield-strength range is only in the order of 20 to 30 ksi (15 to 22 kg/mm²) for all section sizes below 3.0 in. (75 mm). The range decreases with decreases in section size. In other words, the transition in fracture state is "as sharp" for the strength-induced transition as for the temperature-induced transition.

Because of these relationships, the elastic-plastic transition may be referenced to a critical strength range. That is, the elastic-plastic transitions may be defined as evolving over specific strength ranges, which are very narrow. Metal quality is the factor which moves the critical strength range up or down the yield-strength scale. Thus, knowledge of metal quality trend relationships provides for absolute determination of the scale position.

The simplicity of these analysis procedures results from combining of mechanical and metallurgical factors. Discussions of metal properties solely in terms of continuum mechanics leads to an impasse, wherein the high accuracy of K_c measurement becomes the dominant issue. In fact, it is the accuracy of yield-strength measurement which becomes the limiting factor because of the narrow ranges involved. The reader should ponder on this statement because, if understood, it will clarify the absolute requirement for combined thinking of mechanical and metallurgical aspects of fracture-state transitions.

The lack of discussion of these intrinsic relationships in the *mechanics* literature is the source of its confusion to engineers, as well as unending debate between mechanics-oriented specialists.

Status of Procedures for Defining the Elastic-Plastic Region

Considerable research attention is being directed to eventual quantification of flaw size vs stress relationships in the elastic-plastic regions which apply to specific section sizes. The objective is to evolve a complete flaw-size calculation procedure which is similar to that which applies to the plane strain state, Fig. 14. This is a long-range goal because there is presently no analytical base which provides for such calculations in the elastic-plastic state.

The trend-line extrapolation approach which is used to define the elastic-plastic region of the RAD should be understood in terms of being "a pragmatic engineering solution which must be taken because no other analytical procedures are available." It is based on two factors:

1. Continued reference to metal properties in terms of plane strain parameters. This form of reference avoids the problem of inability to determine K_{Ic} values. It should be noted that K_{Ic} testing, which is necessary for the elastic-plastic region, requires the use of large plates featuring through-thickness cracks. This is similar to the K_{Ic} test procedure for sheet metal. The use of small specimens of K_{Ic} type results in the literature-quoted K_Q values, when plane strain limits are exceeded. K_Q is best defined as "K-question mark" in that its only significance is that K_{Ic} levels are exceeded. It cannot be used for K_{Ic} calculation, i.e., as being equivalent to K_{Ic} ; it is not.

2. Use of metal-quality trend bands to define the extrapolation slope for the plane strain parameter. This is the basis for the solution. Since the extrapolation slope is known, it is possible to characterize the metal in terms of unattainable (for the section size) plane strain ratios. Thus, fracture mechanics and metallurgical aspects are combined to arrive at the solution. It is presently the only solution which is available.

The role of the DT test is simply that of providing an additional aspect of test practicality. The ratio-line grid is superimposed over a data bank of valid K_{Ic} values. Thus, the RAD could be presented without use of the DT scale. Correlation of the DT scale to the K_{Ic} scale simply affords entry into the RAD by use of the inexpensive DT test.

The reason for the existence of a correlation between the two scales is explained in terms of constraint factors. Figure 8 illustrates the close similarity of the Navy-standardized 1.0-in. (25 mm) DT test to a side-bend K_{Ic} test of the same section size. (Also see Fig. A4 in the appendix.) The same section size and maximum-constraint crack are used; therefore, the same mechanical constraint is applied in testing the metal. In the region below the 0.63 ratio line, the 1.0-in. (25 mm) DT test fractures in plane strain. In the region above the 0.63 ratio line, the fracture becomes of mixed-mode and then of full-slant type. The energy-to-fracture reading is a faithful reflection of the degree of constraint relaxation that has evolved, above the limit of plane strain (0.63 ratio line) for metal of 1.0-in. (25 mm) section size.

Extensive correlations have been evolved between DT-energy values and K_{Ic} -test data, leading to positive documentation that an entry point from the DT energy scale *easily*

predicts the K_{Ic} value (measured by valid ASTM procedures) well within a $\pm 15 \text{ ksi}\sqrt{\text{in.}}$ range. In fact, these correlations, for the standard 1.0-in. (25 mm) DT test, have been extended for specimens of 2.0 to 3.0 in. (50 to 75 mm) thickness. Thus, it is possible to index K_{Ic} values which would require the use of K_{Ic} specimens in excess of 1.0-in. (25 mm) thickness.

The empirical documentations that the fracture energy of 1.0-in. (25 mm) DT specimens, cut from 2.5- to 3.0-in. (62 to 75 mm) plates (or thicker), can provide for plane strain fracture toughness indexing for these section sizes should not be surprising. It is simply a reflection that the degree of constraint relaxation (mixed-mode fracture) for the 1.0-in. (25 mm) section size bears a direct relationship to the constraint level for the thicker section. If the constraint level of the thicker section results in plane strain fracture (K_{Ic} can be measured), then the degree of constraint relaxation for the 1.0-in. (25 mm) section size, is determined by the "closeness" to which the K_{Ic} value approaches the limiting K_{Ic}/σ_{ys} ratio for the thick section. For example;

- If the K_{Ic} value for the thick section metal is below 0.63 ratio the 1.0-in. (25 mm) DT test will provide sufficient constraint to fracture in plane strain.
- If the K_{Ic} value is close to the ratio limit (highest possible) for the thick section, then the 1.0-in. (25 mm) DT test will develop a specific degree of mixed-mode fracture which is relatable to the constraint-level difference between the two section sizes.
- If the K_{Ic} value of the thick section is slightly above 0.63 ratio, then the 1.0-in. (25 mm) DT test will show a small degree of mixed-mode fracture.

These various degrees of mixed-mode fracture of the standardized 1.0-in. (25 mm) DT test, will be reflected in the level of the energy reading. Thus, the fracture energy bears a direct relationship to the K_{Ic}/σ_{ys} ratio that could be measured for section sizes that provide the necessary level of plane strain constraint. Briefly, a specific intrinsic increase in metal ductility results in

- Increased K_{Ic}/σ_{ys} ratio, if adequate constraint is imposed, or
- Increased mixed-mode fracture energy, if the constraint is inadequate.

The two effects are relatable and rationalizable in fracture mechanics terms.

Metallurgical Rationale for Quality-Level Corridors

The metal-quality corridors represent trend bands of fracture property relationships to the strength-level scale. The trend-band relationships may be of high, intermediate, or low corridor type, depending on the cleanliness level of the metal. Cleanliness refers to the density of nonmetallic particles such as oxides, sulphides, carbides, etc. The non-metallic particles are either brittle and/or noncoherent in comparison to the metal grain structure. As such, early cracking or separation from the surrounding metal grains, evolves in the process of crack-tip deformation. The microcracks or grain boundary separations join to cause plastic-zone rupture. In effect, the deformation capability of the grain aggregate is decreased.

Increasing the strength level increases the flow-curve resistance of the metal grains. Thus, the metal grain aggregate becomes more sensitive to the presence of nonmetallic phases, as the strength level is increased. The metallurgically "dirty" metals, therefore, develop transitions from plastic to plane strain levels at lower strength levels than the "cleaner" metals. In effect, increasing metal cleanliness results in a shift of fracture-state transitions up the scale, i.e., to higher strength levels.

The corridors define the connection between the fracture states and metallurgical quality. The specific fracture state for any given level of yield strength is a combined function of the section size and the metallurgical quality. The origins of section-size effects have been explained previously in terms of constraint-capacity factors. We shall now explain the origins of the metallurgical aspects.

There are two basic origins for void-site nucleation phases in steels. These are

- Extrinsic (foreign) nonmetallic particles, which may be traced to melting and de-oxidation practices
- Intrinsic (inherent) nonmetallic particles, resulting from the formation of carbide phases during solidification, particularly for steels of high carbon contents.

The improved steels which were developed during the past decade, and notably during the past five years, provide a basis for discussion of factors related to melting and deoxidation practices. These steels feature intermediate or low carbon contents in order to promote improved weldability. Hardenability and strength aspects are controlled by sophisticated use of alloy elements, with avoidance of excessive dependence on the use of high carbon contents—characteristic of the "older" steels. As such, the problems of intrinsic carbide phases were eliminated from consideration.

These steels have the potential of attaining high metal-quality corridor positions if the introduction of other types of nonmetallic phases is avoided. Figure 24 presents a summary of data reported previously (2) for the "modern" steels, melted according to various practices, as follows:

- Conventional air-melt. Limited slag treatment results in relatively high phosphorus and sulphur contents ($>0.015\%$). On solidification, phosphide and sulphide phases are formed. Presence of aluminum, or other deoxidation practices to remove oxygen, results in the Al_2O_3 or other nonmetallic phases. Thus, the void site density is high.
- Special slag, plus vacuum-arc remelting. Multiple slag melting practices are used to lower phosphorus and sulphur levels. Vacuum-arc remelting lowers oxygen content, thus eliminating the need for other deoxidation treatments cited above and causing a degree of metal grain refinement. The void-site density is decreased to intermediate levels.
- Vacuum-induction melting, plus vacuum-arc remelting. Melting generally starts with an air-melt charge of special low-phosphorus and -sulphur iron. Three slags or more may be used to lower phosphorus and sulphur to very low levels. Alloy additions are made under vacuum and the oxygen content is controlled by carbon-deoxidation effects. The metal which undergoes the final vacuum-arc remelt is of very high purity. If properly processed, these steels are very clean, even when examined under the microscope at high magnifications. Very few nonmetallic particles can be seen.

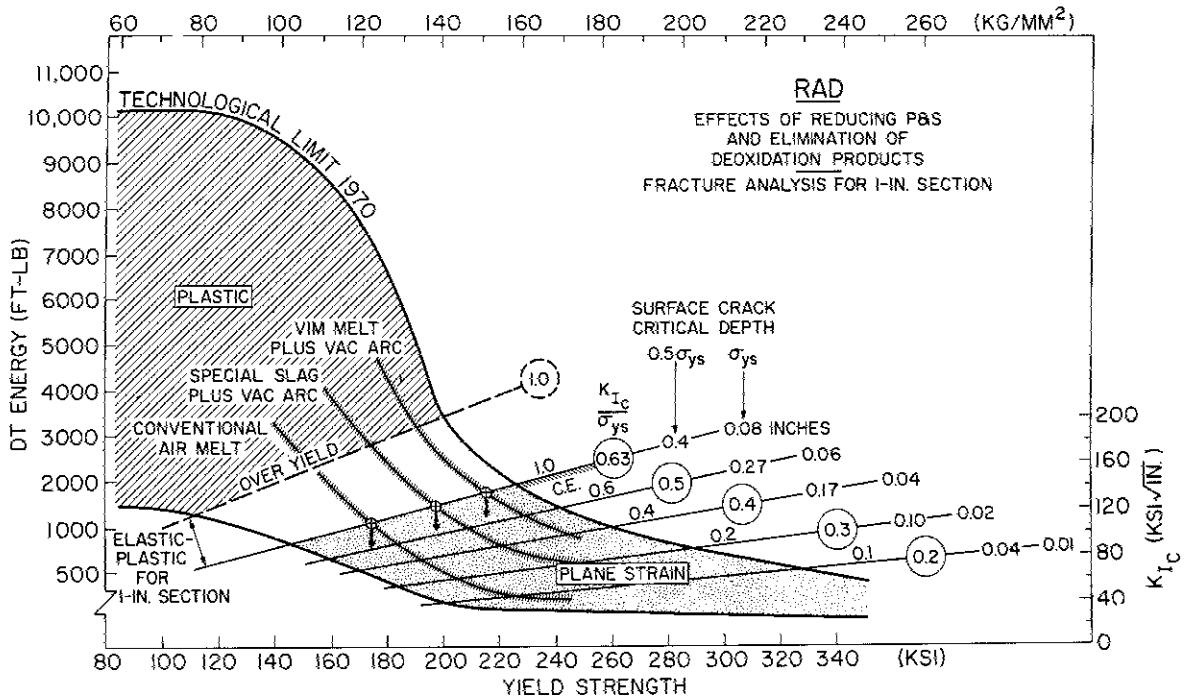


Fig. 24—Trend bands which illustrate the effects of relative metallurgical cleanliness relating to furnace-melting and deoxidation processes. Fracture analysis, for a 1.0-in. (25 mm) section size provides an index of the significance of the metallurgical improvements.

The data presented in Fig. 24 represent a plot of the trend-band properties for these steels. In fact, the lines represent the *ceiling level* developed by optimizing heat treatments to produce the highest possible fracture properties for the strength level involved. These data disclose that the ceiling level is built into the metal by the melting and deoxidation procedures. The relative cleanliness of the metal "in the ingot" becomes the determining ceiling factor thereafter.

This is a most important deduction. It signifies that a small section of an ingot may be forged and evaluated as to "corridor quality." Since a large ingot may be priced at \$1.00 per lb and a large forging at \$10 to \$20 per lb, rejection of undesirable material at the ingot stage is an economically justifiable procedure.

The tremendous effects of metal quality on the fracture resistance properties of steels in the 180- to 220-ksi (125 to 155 kg/mm²) yield-strength range is made clearly evident by Fig. 24. For example, at 200 ksi (140 kg/mm²) yield strength, a 1.0-in. (25 mm) plate may be of

- Elastic-plastic properties, if of high cleanliness
- 0.63 ratio properties, if of intermediate cleanliness, and
- Very low 0.3 ratio properties, if of conventional cleanliness.

The corresponding effects on critical flaw sizes are enormous, as indicated by the RAD indexing of this aspect.

The reader may analyze the larger range of effects for the 180-ksi (125 kg/mm²) level of yield strength. At this level, a 1.0-in. (25 mm) plate may vary between plastic, elastic-plastic, and low plane strain ratio values, as a function of corridor quality.

In general, the older types of forging steels feature high carbon contents, coupled with strong carbide-forming alloy elements. The carbide particles which form during ingot solidification are difficult to place back in solution during high-temperature heat treatment. Accordingly, they remain to enforce low ceiling properties. Therefore, vacuum melting and other modern improvements in deoxidation practices cannot be expected to produce desired results, such as raising the metal quality to the high corridor level.

Statistical Variance of Mechanical Properties

When a steel is purchased to a specified minimum value of yield strength, a range of yield-strength and fracture properties will be present in the population of the production lot or lots. The range of statistical property variations depends on the specification controls which are applied:

- O Ordinary metallurgical control, based on specification of composition and heat treatment—wide range
- T Test control, aimed at narrowing the property range by rejection — within feasible limits, relatable to cost
- TL Test-limit control, established by test reproductibility.

For example, yield-strength values for steels of over 170-ksi (120 kg/mm²) level, may range as follows:

- O 20 to 30 ksi (15 to 22 kg/mm²)
- T 10 ksi (7 kg/mm²) — strict control
- TL 5 ksi (3 kg/mm²).

In the discussions to follow we shall consider ordinary (O) limits. The reader may further analyze the effects of reducing the range to T or TL limits on decreasing the sizes of the "statistical boxes" to be described. For guidance it may be cited that K_{Ic} -test variations, in ASTM round-robin tests by different laboratories, were determined to be in the order of $\pm 10\%$. This range is, therefore, representative of the TL limits for K_{Ic} control.

Figure 25 presents a typical (O) ordinary-variance statistical box which may be expected if a forging-grade steel is procured to minimum yield-strength specifications of 200 ksi (140 kg/mm²) and if one of the following additional aspects apply:

It should be noted that there is little increase in the lower bound values for the low-corridor steels, with decrease in yield strength, until levels of less than 180 ksi (125 kg/mm²) are used as specification-minimum values. On the other hand, there is a rapid increase of the lower bound K_{Ic} value caused by decreasing the yield-strength minimum below 230 ksi (160 kg/mm²) for the high-quality, clean steels. Decreasing the yield-strength range by test control does not change these conclusions.

The increases become most significant when the lower bound K_{Ic} value approaches the ratio measurement limit for the section size. However, this means that steels featuring a lower bound K_{Ic} which lies close to limiting ratio values, may be used (and purchased) only if most of the population has fracture resistance properties such that K_{Ic} measurements are not possible. This is the case if the plate section sizes are used as such in the structure. If considerable machining is performed, ratio values in excess of the final section-size limits may be specified and measured. However, the fracture characteristics of the thinned sections may then be of the elastic-plastic type.

These analyses of metallurgical variance pose practical questions which emphasize the value of close control of metal-quality factors and heat-treatment procedures. If the O metallurgical control limits are not adequate, then it is necessary to resort to metal rejection procedures.

Irrespective of the point of rejection, prior to or after purchase, the cost of rejection must be assumed by the user. These analyses indicate that close to 50% rejection is necessary if K_{Ic} values equal to or exceeding the + mean points are established as the purchase criteria. Decreasing the size of the statistical box only results in shifting the + point; on a relative basis the rejection statistics will continue to apply.

It should be noted that decreasing the K_{Ic} requirements to 20 ksi $\sqrt{\text{in.}}$ below the + points will reduce rejection rates markedly—to an estimated 20% or less. However, the effects of such reductions on critical crack sizes and, therefore, inspection costs must now be considered. In general, the related decrease in critical crack depths for regions of high stress are of minor order. In other words, relatively little is lost. While this conclusion may appear appealing, it also indicates that the small differences are due to the fact that the critical flaws are exceedingly small if stress levels are high. Little is lost because there is little to lose if inspection limits are exceeded.

The analyses for regions of low stress are entirely different. Decreases of 20 ksi $\sqrt{\text{in.}}$ may be highly significant with respect to inspection requirements. The related decreases in critical crack depths may be in the order of tenths of inches, depending on the population + level. The most direct procedure for analyzing the effects of decreasing (or increasing) lower bound K_{Ic} values is by reference to the ratio. Decreases which signify a 0.1 ratio drop from 0.6 to 0.5 have completely different meaning from those of 0.3 to 0.2. The RAD coding to critical crack-sizes clearly indicates these effects for intermediate and high relative stress levels.

These analyses also disclose the benefits derived by shifting from low-level-corridor metals to the high-cleanliness metals of highest corridor features. Again, the benefits derived from such increases in K_{Ic} values, for the regions of high stress, are not particularly appealing.

The reasons for such unfortunate projections do not evolve solely from metallurgical variance factors. They are basic to fracture mechanics theory (see Fig. 14).

The benefits that evolve in the case of metallurgical improvements which result in exceeding the ratio-line limit for the section size can be analyzed in terms of traversing the elastic-plastic regime. The structural significance of entering, and then exceeding, this regime is best considered by reference to the stress level required for extension of a through-thickness crack, as discussed previously.

The degree of metallurgical improvement, which results in crossing through the elastic-plastic regime for a specified section size, pays high dividends in terms of rapidly raising the nominal stress required for extension of through-thickness cracks. The resulting benefits to structural reliability become evident in this context because the nominal design stress is a readily definable structural parameter. Moreover, the high costs evolving from attempts to locate minute flaws, which are critical for high stress regions, are eliminated. Modest increases in metal costs for purposes of avoiding the plane strain state can pay high dividends, costwise as well as safetywise.

The types of trade-off analyses that may be made between yield strength and metal-corridor levels are indicated by the metallurgically zoned RAD presented in Fig. 27. The options which may be examined by the engineer are indicated by the solid black squares and the arrows. The design-strategy "plotting board" aspects of the RAD are thus indicated. The analyses can be performed in a few minutes, once the RAD is understood.

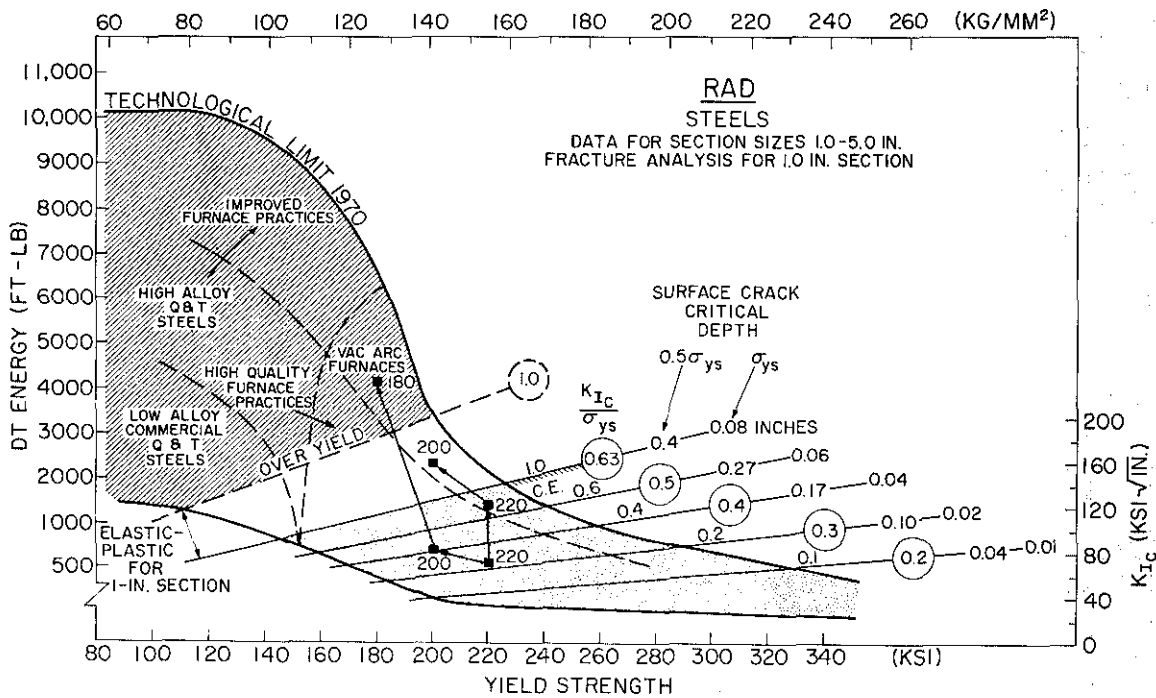


Fig. 27—One form of more detailed metallurgical zoning of the RAD. Finer zone definitions, of primary interest to metallurgists, can be evolved, depending on the metallurgical analysis purpose. The trade-off analyses that may be made in design are indicated by the lines with arrows. Combining these two types of analysis leads to highly sophisticated decisions in metal selection and/or improvement for specific purposes.

Figure 28 compares the location of the statistical-expectancy box for the low-corridor ceiling steels of Fig. 25 with those of a "chain" of the new premium steels of high-ceiling features (see Tables 3 and 4). The chain evolves by modification of alloy contents to provide increasing levels of strength. The steels are strength limited by the basic alloy formulation, i.e., they are specifically designed for the strength range indicated. In general, it is not feasible to evolve compositions which span a very broad range of strength levels because off-optimum microstructural conditions result.

It should be noted that the mechanical-state analyses presented in Fig. 28 are specific to a 1.0-in. (25 mm) section size. However, the noted K_{Ic} -scale-referenced properties for these steels are attainable over the range of 0.5 to 3.0 in. (12.5 to 75 mm). Specific types may be alloy adjusted to provide the same properties for greater thickness.

The reader may now "exercise" the RAD by defining the elastic-plastic regions for different section sizes. For example, the elastic-plastic region for the 0.5-in. (12.5 mm) section size moves to considerably higher yield-strength ranges, compared to that of the Fig. 28 plot. The specific section size, *as used* in the structure, should be the basis for these deductions. Thus, different parts of a structure may feature different fracture-state properties, if the section size varies. In aircraft wing box-structures, the variations may be from 0.5 to 3.0 in. (12.5 to 75 mm) or greater. Thus, the fracture state can vary from plane strain to plastic, depending on strength-level selection.

Titanium and Aluminum Alloys

The RAD summarizations of commercial titanium and aluminum alloys are presented in Figs. 29 and 30. The significance of the ratio lines is exactly the same as for steels because fracture mechanics definitions of fracture properties are not dependent on metal type.

The metallurgical transition from high to low levels of fracture resistance is, as for steels, strength related and may be modified considerably by metal quality factors.

The primary metal quality factor for titanium alloys is oxygen content because this metal is ordinarily "highly clean" due to vacuum arc-melting production practices. The metallurgical "problem" is to avoid embrittling effects due to oxygen. The use of oxygen in small amounts to promote increased strengthening in the 120- to 140-ksi (85 to 100 kg/mm²) yield strength range is catastrophic to fracture resistance. The "zones" in Fig. 29 illustrate the expected fracture properties of titanium alloys produced to conventional C.P. (commercial purity) oxygen levels, as compared to low-oxygen (less than 0.10%) alloys of slightly lower yield strength.

A special note should be made of the combined effects resulting from decreases of 10 ksi (7 kg/mm²) in minimum yield strength, 115 vs 125 ksi (80 to 87 kg/mm²) and using low-oxygen metal. Section sizes of 1.0 in. (25 mm) will show constraint transitions from plane strain to elastic-plastic (or better) material as the result of these combined changes—as may be deduced from Fig. 29.

The dashed line in Fig. 29 represents the boundary between conventional (present production) metal of C.P. grade and the new low-oxygen metal. The span between the dashed line and the 1970 technological limit represents the improvements which have been identified since 1967. There are sound metallurgical reasons for believing that

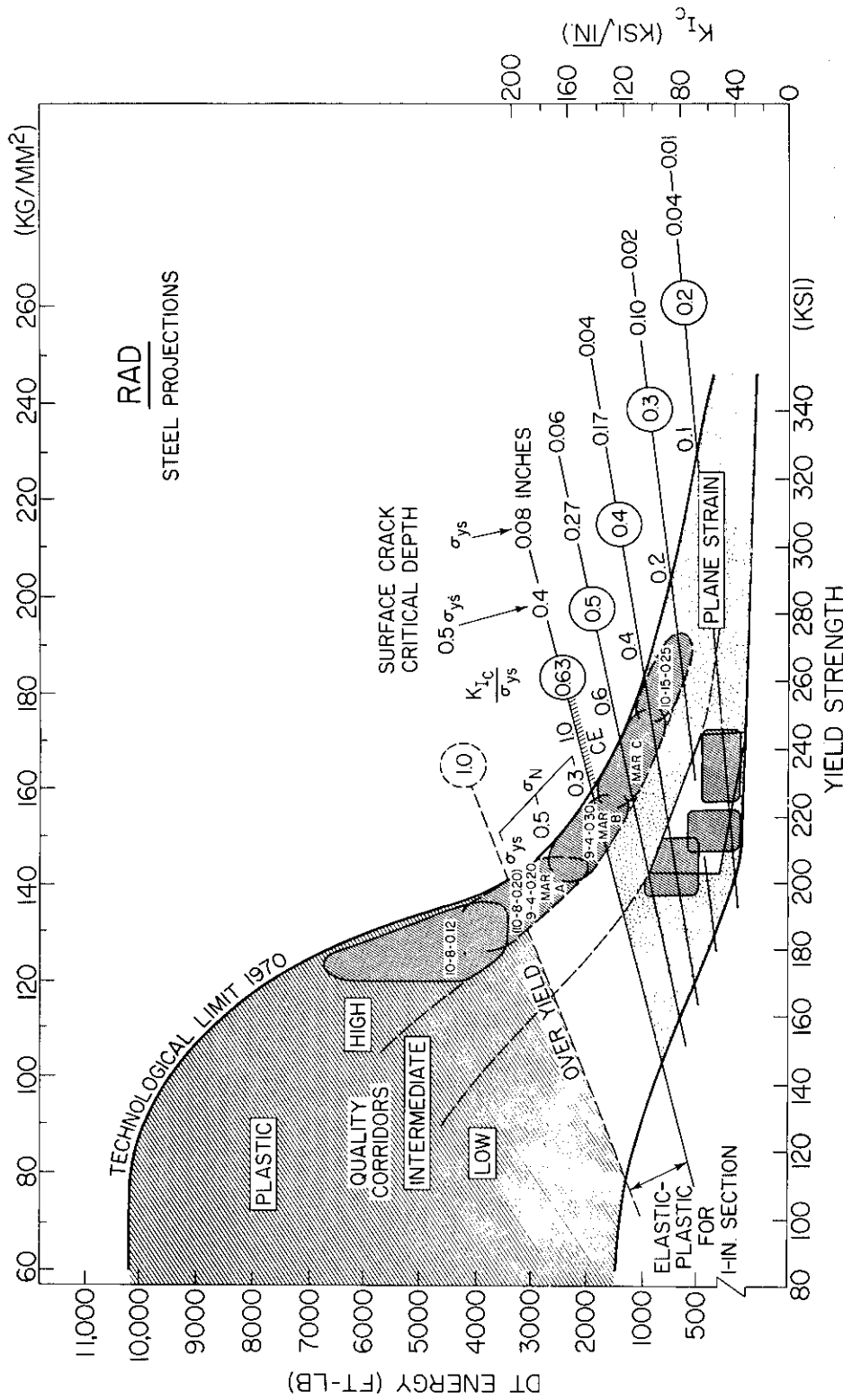


Fig. 28—RAD zoning for the new, premium-quality, high-strength steels

Table 3
Representative High-Alloy Q&T Steels*

Specification	Section Size		Minimum σ_{ys}		Minimum/Maximum Range of Primary Alloy Elements, Percent									
	Inch	mm	ksi	kg/mm ²	C	Mn	Si	Ni	Cr	Mo	Co	V		
ASTM A543 Gr. A and B [†] Class 1 (3Ni-Cr-Mo)	<4.0	<10	85	60	— 0.23	— 0.40	0.20 0.35	2.60 3.25	1.50 2.00	0.45 0.60		— 0.03		
	>4.0	>10	85	60	— 0.23	— 0.40	— 0.35	3.00 4.00	1.50 2.00	0.60 0.60		— 0.03		
Class 2 (3Ni-Cr-Mo)	<4.0	<10	100	70	— 0.23	— 0.40	— 0.35	2.60 3.25	1.50 2.00	0.60 0.60		— 0.03		
	>4.0	>10	100	70	— 0.23	— 0.40	— 0.35	3.00 4.00	1.50 2.00	0.60 0.60		— 0.03		
AMS 6523 (9Ni-4.5Co-0.20C)	<4.0	<10	175	123	0.17 0.23	0.20 0.40	— 0.10	8.50 9.50	0.65 0.85	0.90 1.10	4.25 4.75	0.06 0.10		
	<4.0	<10	175	123	0.24 0.30	0.10 0.35	— 0.10	7.00 9.00	0.35 0.60	0.35 0.60	3.50 4.50	0.06 0.12		
AMS 6524 (7.5Ni-4.5Co-0.30C)	<4.0	<10	200	140	0.29 0.34	0.15 0.35	— 0.10	7.25 7.75	0.90 1.10	0.90 1.10	4.25 4.75	0.06 0.12		

*RAD summarizations provide reliable predictions of fracture-state properties, if the metal-quality corridor level is determined and shelf-level conditions are known to apply.

[†]Grade A and Grade B relate to different maximum percentages of P and S levels.

Table 4
High-Alloy Steels of Maraging Type*

Specification	Section Size	Minimum σ_{ys}		Min/Max Range of Primary Alloy Elements, Percent							
		ksi	kg/mm ²	Max C	Max Mn	Max Si	Ni	Mo	Co	Ti	Al
ASTM A538-70 Grade A (18Ni-8Co-4Mo)	†	200	140	—	—	—	17.00	4.00	7.00	0.10	0.05
				0.03	0.10	0.10	19.00	4.50	8.50	0.25	0.15
Grade B (18Ni-8Co-5Mo)	†	230	160	—	—	—	17.00	4.50	7.00	0.30	—
				0.03	0.10	0.10	19.00	5.10	8.50	0.50	0.15
Grade C (18Ni-9Co-5Mo)	†	275	195	—	—	—	18.00	4.60	8.00	0.55	—
				0.03	0.10	0.10	19.00	5.20	9.50	0.80	0.15

*RAD summarizations provide reliable predictions of fracture-state properties if the metal-quality corridor level is determined.

†Signifies section size limited by ability to attain *specified* mechanical properties.

additional improvements may be made by control of texture and microstructure. Heat-treatment and metal-processing factors are particularly important for titanium alloys and, as yet, are only partly explored.

The RAD for aluminum alloys is presented in Fig. 30. The effects of increased strength level on decreases in fracture resistance are again evident. In this case, it is not possible to present a "prior" vs a 1970 technological limit. No significant improvement in these respects has been recorded to date.

Aluminum alloys are metallurgically "dirty," in the sense that vast amounts of brittle intermetallic compounds are present to serve as initiation sites for microcracking and void initiation. As such, the true potential of aluminum alloys has not been disclosed. Deliberate research aimed at producing relatively clean metal should show marked improvements in the strength-transition range of 45- to 65-ksi (32 to 46 kg/mm²) yield strength.

Critical-Edge Concept for Metal Improvement

The foregoing discussions and analyses, based on the RAD data summarization and interpretation system, converge to several important conclusions:

- If the deciding factor in metal selection is the critical crack size for regions of high stress concentrations (K_t of 2.5 or greater) — then plane strain properties are undesirable. The reason is that the critical crack sizes will be below reliable inspection limits if the ratio value is 1.0 or less.
- Metallurgical improvements which simply increase the measurable K_{Ic} value for a section size will provide small benefits for the above-cited case.
- In order to effect large returns for the metallurgical improvement, it is essential to raise the intrinsic fracture resistance to above the K_{Ic}/σ_{ys} ratio for the section size. This is the "critical edge" concept of transition from plane strain to elastic-plastic fracture properties.

The critical-edge concept provides important guidance to metallurgical research. It defines that highly significant improvement in metal properties may be made over the region of the "strength transition." This is the region of rapid falloff of the RAD plot for each metal system. The improvement which is highly significant must be related to specific section sizes. Thus, the improvement possibilities must be limited to lower yield-strength ranges for thick section metal. With decreases in section size, higher yield-strength ranges provide the improvement challenge.

PART 5. ENGINEERING APPLICATIONS OF RATIONAL FRACTURE CRITERIA

Requirements

It is a popular misconception that the application of fracture research information in engineering is inherently limited by knowledge of details. This is not the case. The primary aspects can be made abundantly clear if the confusion of details is stripped away.

Moreover, the requirements for profound attention to details emphasized in publications and the first-order requirements for engineering practice are not necessarily comparable. The difference evolves from the fact that additional aspects emerge as the determining factors in engineering practice.

The sequential steps in evolving knowledge which expands capabilities for engineering application of rational criteria are as follows:

First Step. Development of scientific information relating to mechanical constraint factors and to the definition of test-specimen rationality requirements.

Second Step. Standardization of test methods and development of rational reference criteria.

Third Step. Assembly of a statistical data bank for specific metals in terms of rational criteria.

Fourth Step. Evolving simplified analysis procedures which connect mechanical and metallurgical aspects. The connection process is crucial because rational metal selection is the ultimate aim.

Final Step. Total synthesis in evolving trade-off analyses for specific fracture control plans. All other pragmatic considerations in design must be added; for example, structural redundancy, whether single or multiple fracture paths are required for structural failure, criticality of failure events, etc. (This aspect is discussed in Part 6.)

Specialists' interests and publications may cut off at the first or second steps. The engineer must practice at the final step because total synthesis must be attained, in the context of usual engineering practices.

We shall now redefine the factors which are involved in establishing a chain of rationality, from metal characterization to structural certification, in reverse order.

- Certification means meeting of documentation requirements, as established by regulatory bodies or by basic legal responsibilities.

- Fracture control plans mean a total pragmatic solution to problems of preventing catastrophic failure. While design, fabrication practices, quality control, etc., are involved, the most basic element is the choice of an appropriate design criteria.

- Design criteria mean specification of the minimum level of fracture resistance that is appropriate for the particular structural problem, whether plastic, elastic-plastic, or plane strain. Each of these fracture states may be considered to be subdivided into high and low levels for the state.

- Fracture-test criteria mean the identification of test-specimen values, in terms of the fracture state and level in the state involved, as follows:

<u>Fracture State</u>	<u>Significances to Fracture Extension Stress (σ_f)</u>
1. Low-level plane strain (< ratio 0.6)	<0.3 σ_{ys}
2. High-level plane strain (ratio 0.6 to 2.0)	<0.3 σ_{ys}
3. Low-level elastic-plastic	0.3 to 0.5 σ_{ys}
4. High-level elastic-plastic	0.5 to 1.0 σ_{ys}
5. Low-level plastic	Slightly over σ_{ys}
6. High-level plastic	Considerably over σ_{ys}

If the fracture-test value does not provide a clear relationship to one of the six levels in terms of minimum guaranteed fracture properties, it is not rational. That is to say, its significance is not deducible for design purposes. The state of engineering application of rational fracture criteria is necessarily determined by the availability of metal characterization data, which are rational in the above context.

If the engineer is to make a rational selection of metals, he must use statistical data which indicate the commercial production range for the reference criteria. Such data must be readily available. This is important for reasons of reliability, economics, and purchase specifications. The producer cannot be expected to accept specifications that are uncertain as to rejection rates.

Gathering of such data may be unappealing to investigators of fracture phenomena. However, this is the function of test laboratories and they should be employed for this purpose. A reasonable partition of effort for continued research and for statistical characterization appears to be in order.

Availability of Rational-Criteria Data

The status of information which is available in *organized statistical form* is best defined in terms of generic metal types and is in the following rank sequence.

1. High-strength aerospace metals of moderate or thin section
2. Reactor-grade pressure vessel steels of thick section and moderate strength levels
3. Intermediate strength Q&T steels of high alloy content and high production quality, section sizes 1.0 to 4.0 in. (25 to 100 mm)
4. Aluminum alloys of intermediate strength levels
5. Low- and intermediate-strength structural steels for general fabrication purposes

6. Low-alloy commercial Q&T steels of 90 to 115 ksi (65 to 80 kg/mm²) yield strength, in the thickness range of 0.5 to 2.0 in. (12 to 50 mm)

7. Thick-section Q&T steels of all types.

In general, rankings of 5, 6, and 7 signify an unsatisfactory state of affairs in which confusion rather than clarity predominates. The separation between rankings 1, 2, 3, and 4 vs 5, 6, and 7 is related to dependence on or avoidance of the use of the C_v test for engineering reference purposes.

It should not be surprising that the most advanced engineering use of generalized fracture mechanics principles has evolved for high-strength metals; see Tables 3 and 4. This is due to the absolute need for certification of reliability in critical applications for aerospace structures and components. The RAD discussions document the availability of a large body of rationally determined fracture data. The data were obtained largely from K_{Ic} tests and supplemented by DT tests in the intermediate-strength and thick-section range.

Another area which is highly systematized as to availability of rational data is that of the high-alloy Q&T steels of 80 to 130 ksi (58 to 95 kg/mm²) yield strength. Because of their intended application in critical structures, criteria of high plastic-fracture states for the section size were used consistently in metal development, dating from 1955. In this case, the data were obtained by relatively low-cost DT test procedures (1,2). The test is ideally suited for characterizing plastic-state properties.

The status of rational properties characterization for metals of intermediate yield strength, 65 to 80 ksi (45 to 55 kg/mm²) and very thick sections, which are used in pressurized water reactors, is likewise in excellent shape (1,2). The governing design principle in this case was that of enforcing the meeting of the yield criterion as the minimum acceptable level for the section size. This criterion is applied in the temperature transition range and may be recognized as related to the 6- to 12-in. (150 to 300 mm) dynamic constraint-transition curves shown in Fig. 15. The adjustment procedure is based on the NDT temperature point, plus a Δt correction to provide meeting of over-FTE properties which equate to the yield criterion. The requirements for this case evolve from the absolute need for preventing fragmentation, which could result in projectiles piercing the secondary containment vessel, with release of isotope contamination. Environmental protection was the deciding issue in the choice of the subject criterion.

Recently this criterion ($> FTE$) was reaffirmed by the AEC. It is required to apply for the neutron irradiation-embrittlement case, during the service life of the vessel. A shift of the constraint transition for the section size to higher temperatures results from neutron exposure. In all cases it is required that the metal does not fall below the yield criterion (FTE) value at pressurization temperatures.

Representatives of industry and technical society committees have presented proposals to the AEC for modification of the design practices based on *plane strain* constraint-transition criteria (see Fig. 15). The proposal is that the rise of K_{Ic} values in this range should provide sufficient, although less conservative, criteria for fracture control plans. The discussions presented in this paper contradict this thesis, particularly in relation to metal properties' statistics. Moreover, acceptance of K_{Ic} properties is equivalent to acceptance of frangibility, even if the reference K_{Ic} value is maximum for the structural section size.

The status of rational properties characterization, for the wide spectrum of standard grades of low- and intermediate-strength structural steels, is in poor condition. Table 5 illustrates "best estimates" of the wide variations in fracture-state properties that evolve within grades due to metallurgical and section size variables. The poor state of available information is due to the general dependence on C_v values, for reference to transition-temperature properties, for the very wide range of steels involved.

It is not to be inferred, however, that the many alloy grades, section sizes, heat treatments, etc., which are represented in standard specifications are characterized systematically by C_v value. This is not the general case, and the lack of any systematic characterization may be traced to perplexities as how to use the C_v test for this generalized purpose.

The Charpy Impasse

An impasse as to the use of the C_v test has existed for over ten years, and committees of specification societies have not been able to arrive at a consensus solution. Meanwhile, research advances have documented that the desired generalized solution is not attainable. Continued debate will only perpetuate the impasse; a change to rational test procedures must be made. It is inevitable and cannot be postponed.

The C_v test has provided dependable fracture-state definitions, for specific grades of steels which were subjected to intensive statistical surveys, based on correlation indexes to other tests of definable constraint capacities. The correlations to the C_v test evolving therefrom are reliable. The problem is one of unending development of such specific correlations, plus engineering confusion which evolves from the myriads of such correlations. It is simply not practical to use C_v -test fracture-properties index values whose meaning changes with the type of metal involved.

Paradoxically, the evolution of rational plane strain characterization procedures over the past ten years has contributed to the C_v impasse. This is not due to scientific reasons, but to the lack of appreciation of the implications of what plane strain fracture characterization implies to the engineering use of metals.

The promise that standardization of plane strain fracture tests would provide the required engineering characterization led to "waiting" for this scientific development to mature. At that point there would be a shift to new rational methods and away from the C_v test, or a new basis for C_v -test indexing would be evolved.

The fallacy of this expectation is clear from the previous discussions. Generalized fracture mechanics principles do not predict that plane strain properties should be the reference criteria. Conversely, they lead to definition of the six fracture-state levels cited previously, of which plane strain levels are the lowest two of the ascending series.

At this point, the implications of test practices with respect to the rationality of fracture control plans should be evident. The foremost hindrance to evolving defensible fracture control plans may be traced to the status of characterization practices for the metal involved. The main problem for the conventional structural grades is the continued reliance on the Charpy V test for characterization and engineering text reference. The interpretive complexities arising therefrom are insuperable. There simply are too many

Table 5
Conventional* Low-Strength Structural Steels—ASTM Grades

ASTM Specification	Number of Grades	Minimum σ_{ys}		Maximum Thickness		Heat-Treat Condition†	Range Estimated NDT**	Range Estimated $0.5 \sigma_{ys}$ CAT**
		ksi	kg/mm ²	Inch	mm			
A36-70a	Strength— minimum†	36	25	Not specified		AR	Not definable†	Not definable†
A131-70a	6	32	22	0.5 1.0 2.0	13 25 51	AR or N§ " "	-20° to 80°F (-30° to 30°C) " "	0° to 130°F (-20° to 55°C) " "
A441-70a	Strength— minimum	50 46 42 40	35 32 29 28	0.75 1.5 4.0 8.0	19 38 102 203	AR or N§ " " "	-60° to 80°F (-50° to 30°C) " "	-30° to 140°F (-35 to 60°C) " "
A442-70a	2	30 32	21 22	1.0 1.5	25 38	N¶	-30° to 40°F (-35° to 5°C)	0° to 70°F (-20° to 20°C)

*Widely used grades for welded construction—selected from a very wide variety.

†Chemical composition not specified for this grade.

‡AR — AS-Rolled; N — Normalized.

§Heat-treatment related to section size limits.

¶Fine-grain practice if purchase-specified—normalizing of coarse-grain practice steels results in small improvement in transition temperature, compared to as-rolled state.

**Estimates cover full range of grade, section sizes, and heat treatment applied, if any. The purpose is to illustrate the need for specific characterization in terms of these aspects.

possible C_v correlations (fixes) to the true elastic-plastic transition temperature range of the standard steel grades.

The "fix" problem cannot be evaded by changing from a fracture-energy-value index to a specimen-deformation index. Proposals are pending, and isolated initial use has been made of measurements based on the C_v -test lateral expansion (see note, Table 6). This procedure involves measurement of the bend-induced plastic expansion of the specimen, i.e., in the region opposite the notch. It is proposed, on the thesis that the backside expansion bears a direct relationship to the lateral contraction which evolves at the notch. While experimental data support this premise, it is likewise true that energy, lateral contraction, and lateral expansion *rise together* as a function of temperature. Any one infers the others; thus, no case can be made for improved "fixes" or for basic rationality. The fact that changes from fracture-energy values to specimen-expansion measurement are being considered and applied by specification society committees speaks volumes as to the engineering-criteria status of the C_v test.

Intermediate-Strength, Quenched and Tempered (Q&T) Steels

The intermediate-strength Q&T steels require special discussion because of their extensive and growing use in engineering structures. The range of yield strength is from 80 to 120 ksi (58 to 87 kg/mm²). There are two general types:

- The high-alloy types, as typified by HY-80 and its commercial derivatives, the A-543 ASTM Grade (Table 3). It should be noted that MIL-SPECS criteria enforce intermediate-corridor quality for HY-80. This does not signify that the commercial derivatives are necessarily of equivalent properties; note that there are two classes which permit melting practices that can result in low-corridor properties. These steels should easily meet the over-yield criterion at ambient temperatures for section sizes to 4.0 in. (100 mm), if the alloy content is adjusted to provide the required hardenability. The principal problem involves inadequate information for thick sections.

- The low-alloy, low-corridor quality types, as typified by the A514 and A517 ASTM Grades (Table 6). Their development was strongly influenced by economic competition to provide higher strength at minimum possible cost.

The thick-section problems of the high-alloy types provide a classical example of failure to understand constraint factors, plus incorrect assumptions as to hardenability considerations. There is a popular assumption that the relatively high Ni-Cr-Mo contents of these steels provide generally for "HY-80" levels of plastic-fracture resistance. In fact, a composition which provides for such properties in 4.0-in. (100 mm) section size may result in plane strain fracture properties for section sizes to 6 or 12 in. (150 to 300 mm). Increases in alloy elements are required to avoid plane strain behavior. Inadequate alloy contents result in metal grain brittleness and, therefore, in a shift of the true transition temperature, so that expected on-shelf (plastic) properties at room temperature decrease to plane strain levels. The true fracture-state properties of the A543 Grade, Class 1 or 2, for section sizes over 4 in. (100 mm) are not definable without resorting to rational fracture tests.

These combined mechanical and metallurgical aspects explain the confusion which results when C_v temperature-transition curves are used for characterization. C_v on-shelf properties may be indicated at temperatures for which the true transition state is that of

Table 6
 Proprietary Low-Alloy Q&T Steels of Intermediate Yield Strength* Levels
 ASTM A514 and A517 Steels†

Grade or Type	Thickness Limit		Chemical Composition						Other Percentages‡
	Inch	mm	Max %C	%Mn	%Ni	%Cr	%Mo		
A	1.25	32	0.23	0.75/1.15	—	0.46/0.84	0.15/0.31	Zr-B-0.34/0.86Si	
B	1.25	32	0.23	0.65/1.05	—	0.36/0.69	0.12/0.28	V-Ti-B	
C	1.25	32	0.22	1.05/1.55	—	—	0.17/0.33	B	
D	1.25	32	0.22	0.36/0.74	—	0.79/1.26	0.12/0.28	Ti-Cu-B	
E	4.0	102	0.22	0.36/0.74	—	1.34/2.06	0.36/0.64	Ti-Cu-B	
F	4.0	102	0.22	0.55/1.05	0.67/1.03	0.36/0.69	0.36/0.64	V-Cu-B	
G	2.0	51	0.23	0.75/1.15	—	0.46/0.94	0.36/0.64	Zr-B-0.44/0.96Si	
H	2.0	51	0.23	0.90/1.35	0.27/0.73	0.36/0.69	0.17/0.33	V-B	
J	1.25	32	0.23	0.41/0.74	—	—	0.46/0.69	B	
K	2.0	51	0.22	1.05/1.55	—	—	0.42/0.58	B	
L	2.0	51	0.22	0.36/0.74	—	1.09/1.71	0.22/0.43	Ti-Cu-B	
M	2.0	51	0.23	0.41/0.74	1.15/1.55	—	0.41/0.64	B	
N	0.75	19	0.23	0.75/1.15	—	0.46/0.84	—	Zr-B-0.34/0.96Si	
P	4.0	102	0.23	0.41/0.74	1.15/1.55	0.79/1.26	0.41/0.64	B	

*Minimum of 100 ksi (57 kg/mm²) to 2.25 inch (57mm) and 90 ksi (63 kg/mm²) to 4.0 inch (100mm).

†Estimates of statistically reliable fracture-state properties are not possible from available data. See ASTM A593 for C_y test requirement of 15 mils minimum lateral expansion (opposite the notch) for A517 Grades. No C_y test requirements are established for A514 types.

‡Nominal 0.15/0.35Si except as noted.

plane strain for the section size. The "fix" for the NDT temperature of A543 grade steels is related to high-energy positions of the C_v curve—ordinarily over 50 ft-lb. Accordingly, lateral contraction or expansion of the C_v specimen would likewise indicate very high ductility. To compound the quandary, sampling is often made of surface or corner-edge metal from large forgings. These positions may feature a ductile metal grain structure, as compared to brittle for the subsurface regions.

It should not be surprising that situations have arisen in which expensive thick-walled pressure vessels were belatedly discovered to feature low-level plane strain properties (NDT level) at service temperatures. The amazement of the design engineer, that selection-criteria based on high-value C_v properties should lead to such conditions, is worth noting. When rational tests were applied, the true fracture state was disclosed — a lesson was learned somewhat late. The lesson is twofold:

- A Q&T steel which develops a premium reputation for use in a specific section size may be highly brittle in thicker sections.
- Rational characterization is essential. It is easy to be misled by high-value C_v -test characterization of metal properties, for many reasons.

The discussions to follow will focus on the low-alloy types because of their widespread use. Inappropriate selection by users has resulted in service failure experiences of serious consequence. These steels may provide excellent and low-cost solutions to fracture control problems, if rational selection is made and specification guarantees are enforced.

In general, these steels may reside close to the lower bound curve of the RAD for a specified minimum yield-strength range of 90 to 100 ksi (65 to 73 kg/mm²). The average expected strength properties are moderately higher and follow the low-corridor trend (see Fig. 21). There are 14 proprietary (patented) commercial varieties (Table 6), covering a range of metallurgically designed thickness limits (hardenability adequacy) ranging from 1.25 to 4.0 in. (32 to 100 mm). It is important to recognize that the modest alloy contents of these steels enforce strict thickness limits; the latitude is much less than for the high alloy steels. Depending on type, the high end of the thickness range may become marginal as to hardenability adequacy. In brief, these steels require good metallurgical heat-treatment control to provide desired properties at the enforced minimum cost. The user should refrain from attempting to buy strength-thickness combinations at lowest possible prices because metallurgical margins are reduced thereby. User pressure in this respect may be traced as one of the major contributing factors involved in adverse experiences.

The literature on these steels (as a whole) tends to imply that all are designed to provide over-yield criterion properties for the section size and at ambient temperatures. The few grades that are reasonably characterized as meeting the yield criterion tend to carry over this connotation to competing grades. The usual reference to fracture properties is in terms of difficult-to-interpret Charpy V values. The true elastic-plastic transition temperature range for specific types may vary widely from below to above ambient. A systematization of the true fracture properties of these 14 grades, in their various thickness ranges, is simply not available.

Some of these steels have been extensively investigated by the producers and designed metallurgically to provide properties which specifically meet the over-yield criterion.

However, even for these there is scattered service evidence of plane strain fracture which indicates a perplexing situation as to metallurgical quality-control factors. The grades which are produced with sufficient control and alloy content for the section size, to provide guaranteed yield-criterion performance, are not known with confidence. It is essential that rational test procedures of a modern type be applied to statistical surveys of these grades. The development of this information should not be delayed. For example, bridges and large tanker-type ships are being constructed using these steels. The experience of World War II ships should not be repeated, before rational fracture-testing procedures are applied.

The other major problem of these steels is the possibility that the heat affected zone (HAZ) of welds may be greatly inferior to that of good quality plate. This possibility is a function of welding heat-input parameters (cooling rate). There must be adequate control based on fracture properties information, related to welding variables for the grade and thickness involved. With notable exceptions, this information for the 14 grades involved is in a rudimentary state. Moreover, it is an aspect which falls in the domain of the welding engineer, who may not be adequately impressed with the need for exercising strict control, for cases in which information is available.

The problem is described in terms of the RAD plot. The HAZ properties are known to fall below the lower-bound curve, when welding conditions are not proper. Analysis of the elastic-plastic region for a plate of 1.0-in. (25 mm) thickness (see Fig. 21), will indicate that falling below the lower bound curve, for steels of 100 to 115 ksi (70 to 80 kg/mm²) yield strength, is equivalent to dropping into the plane strain region. The various recorded HAZ-path failures are rationalizable in this context. Thus, fracture extension at nominal design stresses becomes possible.

It is emphasized that desired properties for plate and HAZ can be attained with confidence for many of these steels. The problem is to provide assurance of this fact and/or eliminate those that do not. For critical structures, purchasing to rational-criteria specifications is essential. There is no question that costs will rise thereby and that some of the low-cost appeal will be lost. However, fracture control plans should be based on lowest cost which provides the desired service guarantee. New thinking on this point is needed by those who are in a position to dictate required guarantees.

PART 6. RELATION TO DESIGN PRACTICES

Functional Requirements

The design function is to meet imposed requirements within pre-established limits. The general structural arrangements may be relatively fixed (pressure vessels) or subject to considerable adjustment (aircraft, ships, bridges, etc.). Reliability requirements may dominate or they may be relaxed by preference to economic constraints.

In all cases, the foremost dedication of the designer is to the application of "deterministic" processes for evolving structural reliability. These processes imply calculation of the load-bearing characteristics of the structure.

The evolution of welded construction with emphasis on monolithic features resulted in unexpected failures at relatively low elastic-stress levels. These failures were alarming

because they disclosed glaring inadequacies in design procedures. In effect, classical design had failed to guarantee strength reliability.

The random aspects of these failures, such as for ships, disclosed that reliability could not be expressed in terms of statistical probabilities. The true control was exercised by stochastic (purely random) events. Fracture research made the inexplicable performance understandable, in terms of the effects of cracks in reducing strength reliability.

The appeal of fracture mechanics to the designer is that it provides analytical tools for deterministic design, for structures containing cracks. These procedures

- Establish whether or not catastrophic failure is possible
- Characterize metals in distinct fracture-state levels
- Define lowest levels of fracture resistance in an analytical scale of plane strain fracture properties
- Document that unstable (fast) fracture, at low levels of elastic stress, is intrinsic to plane strain metals.

However, the procedures of plane-strain fracture mechanics do not provide direct solutions to questions of probabilities. The solutions must be found by application of crack-control procedures involving fabrication quality, inspectability, lifetime surveillance, etc.

Thus, the use of plane strain metals poses continued problems of structural-reliability certification to the designer. These metals are implicitly documented to have fast-fracture potential. Accordingly, failure probabilities exist, but the control of these is not in the province of the designer. The burden falls on "others" who must verify fracture prevention by control of crack conditions. In effect, the designer cannot specifically verify structural reliability in the design process. The design solution becomes an "it depends" question.

The paradox of plane strain fracture mechanics is that it provides (a) the desired deterministic procedures, and (b) a glaring insight into the direct assurance provided by the design process *per se*.

The inadequacies of classical tools based on safety factors could be cited previously as the cause of unexpected failures. Plane strain fracture mechanics removes this "excuse." Thus, the designer must seriously consider whether the imposed requirements permit defensible use of plane strain metals or not.

There are three aspects to be considered:

1. Failure-probability assessment, i.e., what must be done to prevent fracture of plane strain metals, and the costs arising therefrom
2. Recourse to other design procedures for plane strain metals (structural redundancy, etc.), if permissible

3. Documenting that the use of plane strain metals is unacceptable for the intended purpose, and thereby deciding other metal choices consistent with generalized fracture-mechanics criteria.

The probability question emerges as the first major point of issue, from which other aspects are decided.

Probability Assessment

A design may be considered "probabilistic" if probabilities of failure by fast fracture exist. Ordinarily, failure rates are expected to be very low, which implies statistics of small numbers. If failures can evolve due to purely random events (related to fabrication and quality-control deviations, or any other nonpredictable circumstances), then probability definitions become stochastic. Proof that structural performance is not potentially controlled by stochastic circumstances should be part of a fracture control plan.

There is a distinct separation between fully deterministic solutions and probabilistic solutions. However, there is no definable point at which probabilistic solutions become stochastic. Thus, the design solution is either distinctly deterministic or potentially stochastic.

The use of plane strain fracture mechanics, for purposes of controlling probabilistic events for plane strain metals, is feasible only under idealized conditions. In practice, statistical aspects of metal-property variances and crack size vs stress variances become the controlling factors. The analyses and control of these variables may result in expenses that make the added cost of using elastic-plastic metals insignificant by comparison. Thus, it is the *cost limitation* aspect which tends to drive probability definitions down to essentially stochastic levels.

Plane strain fracture mechanics implicitly defines that the use of plane strain metals must be based on failure-probability control. It also defines the limits that must be applied for such controls. Documentation that the requirements are met is the engineer's problem. Plane strain fracture mechanics analyses do not specifically imply that plane strain metals can be used safely. Conversely, the analyses may dictate consideration of other choices for certification of the design. These choices may be intrinsic to the design configuration or to the metal selection process.

The designer has the choice of various fallback positions, as follows:

- Fracture control plans may be based on *redundancy assurance*, if feasible to the configuration. This principle involves introducing multiple-load (fracture) paths, so that the failure of any one part does not result in large reduction of residual structural strength.
- If redundancy assurance is not feasible, the next alternative is to provide *fail-safe assurance*. This principle involves use of crack-arrest provisions, such as geometric interruptions (aircraft) or inserts of highly ductile metal (ships).
- If neither of these two procedures is feasible, the remaining alternative is to provide *safe-metal assurance*. This principle involves the selection of metal that does not permit extension of fast fracture at the levels of nominal design stresses.

All of the above-listed design procedures may be classified as deterministic. The design process, and not other factors, determines that the structure will not be subject to "unexpected" failure due to unstable fracture. The solution is fully developed in the design process.

Fracture Properties Rank-Level Considerations

Table 7 presents a summary of fracture properties rank-levels, coded to structural-design aspects discussed in this report. The most crucial aspect to the design engineer is that of the fracture-extension stress. It should be recognized that providing safe-metal assurance requires selection of metal of rank 4 or higher, depending on specific requirements. Most structural applications are satisfied by the rank 4 level (see Part 3 discussions of exceptions for compliant structures).

Table 7
Rank-Level Relationships

Rank Level	Fracture State	Fracture Mode	Test-Specimen Characterization Criteria	Structural Design Significance
6	High plastic	Full slant	CR-E	(Fracture extension stress) $\gg \sigma_{ys}$
5	Low plastic	Mixed mode	CR-E (COD/ J_c)	$> \sigma_{ys}$
----- Yield criterion -----				
4	High elastic-plastic	Mixed mode	CR-E (K_c /COD/ J_c)	0.5 to 1.0 σ_{ys}
3	Low elastic-plastic	Shear lips	CR-E (K_c /COD/ J_c)	0.3 to 0.5 σ_{ys}
----- Plane strain-limit criterion -----				
2	High plane-strain	Flat	$\frac{K_{Ic}}{\sigma_{ys}}$ or $\frac{K_{Id}}{\sigma_{yd}} = 0.6$ to 2	$< 0.3 \sigma_{ys}$
1	Low plane-strain	Flat	$\frac{K_{Ic}}{\sigma_{ys}}$ or $\frac{K_{Id}}{\sigma_{yd}} = 0.1$ to 0.6	$< 0.3 \sigma_{ys}$

CR-E — Constraint relaxation index, based on fracture energy or equivalent.
(K_c /COD/ J_c) — see text.

The rank ordering indicates that metal selection does not have to be based on a semi-infinite scale of fracture properties. The six levels are easily definable by presently available test practices. Correlating these levels to the fracture-extension stress scale indicates that the designer cannot use "finer cuts" in practice. This is clear for the plane strain case because the fracture-extension stress levels are below those of the normal nominal-design levels. Control based on critical crack size has been defined as nondeterministic, insofar as the design process is concerned.

Finer cuts for the elastic-plastic rank levels may be appealing, but the temperature or strength ranges for crossing through this fracture state are very narrow. Thus, the true limits of useful definition are decided by statistical data for the metal population in the structure, exactness of estimates as to lowest service temperatures, etc. The two rank levels fully suffice for most practical purposes.

Requirements for finer scale definition for the plastic fracture state are highly specialized. In general, the yield-criterion definition is fully adequate. The exceptions should be treated on a case basis by specialists in the present state of knowledge.

Implications of Research Directions

Test-specimen criteria for rank levels above the plane strain state are indicated by Table 7 to be based on energy or related ductility references. There is no apparent possibility for generalized definition of these levels in terms of stress intensity parameters, such as the K -singularity of plane strain fracture mechanics. K_c characterization is feasible only for thin sheet, and then only for the elastic-plastic region.

Thus, research attention for improvement of characterization procedures centers on COD or J_c concepts. The COD procedure has been investigated extensively and found to be applicable to specialized cases. It requires direct empirical correlation of crack-tip plasticity to structural configurations. Its lack of potential for generalization has caused a decrease in research interest.

The J -integral approach is based on measurement of plastic strain fields in the general area of the crack. J_c signifies the critical value of J (energy) absorbed at the point of fracture extension. Even though it is in the early stages of development, it is the only attractive approach which is now evident. The engineer should expect a rapid transition from K - to J -interest in research-field publications and conferences. The reasons are that (a) plane strain research has run its course and now provides diminishing practical returns, and (b) the important technological transfer problems now center on improved analytical capabilities for definition of the higher rank fracture states.

This need is particularly important for metals of thin section and for the relatively unexplored high-temperature metals area. The reasons are as follows:

- Relatively small absolute crack lengths may result in fracture extension due to geometric instability, for highly compliant sheet-metal structures — even for the case of relatively ductile metals. Thus, exact ranking of plastic fracture properties becomes essential.
- High temperatures may reduce plastic-fracture resistance to relatively low levels. The above-stated conditions of geometric instability often apply. In any event, fracture properties data are practically nonexistent.

The introduction of fracture mechanics principles in high-temperature design has been delayed too long. There should be an accelerated attention to this aspect of fracture control plan requirements. Present design practices are not rationally deterministic with respect to fracture-related events.

Cost Factors

In the final analysis, all aspects of the application of fracture mechanics in structural design will be influenced by cost factors. The degree to which such issues become deciding depends on the intent of fracture control plans and their specific contractual requirements.

The genesis of plane strain fracture mechanics in the mid-1950's was stimulated by cost issues. In the early literature, it was cited as "procedures that would provide for fracture-safe design using brittle metals." In effect, the hope was that least expensive metals of plane strain properties could be utilized, based on analytical procedures for calculation of critical crack sizes for fracture initiation. The issues at that time involved shifting the transition-temperature range for steels to lower temperatures to provide metals of elastic-plastic (arrest) properties. The cost-incentive aspect was related to the additional costs for shifting the transition temperature.

During the 1960's an additional cost issue emerged, which was related to maximum levels of yield strength. If plane strain criteria could be applied reliably, increased costs for using elastic-plastic metals at particular strength levels could be avoided.

Paradoxically, the engineering application of plane strain fracture mechanics principles has provided documentation of the fact that the cost issue is exactly opposite to the original concept. The cost of using metals of plane strain properties may be *prohibitive* because of the test costs, quality control, inspection and lifetime surveillance aspects that are implied by the plane strain state. The inversion evolves from acceptance of plane strain fracture mechanics definitions of critical crack sizes by users of the structures and by regulatory authorities. If a serious intent exists for requiring structural reliability assurance, and such requirements are reduced to contractual obligations, it then evolves that

- Statistical definition of plane strain properties must be made at very high test costs
- Quality-control practices must be applied to limits that greatly exceed requirements for flaw-tolerant metals
- Inspection requirements will generally exceed capabilities for achieving the specified purposes.

Thus, costs for structural certification will escalate to levels that reduce questions of metal costs to relative insignificance.

The imposition of contractual obligations, for validation of structural performance in terms of fracture mechanics principles, enforces the use of elastic-plastic metals as the low-cost solution in most cases. Thus, the rank-sequence of Table 7 emerges as crucially related to structural certification costs.

The certification cost-barrier aspects of traversing the elastic-plastic regions of the strength transition are illustrated in Fig. 31 for steels and Fig. 32 for titanium alloys. In each case, structural certification considerations cost-decide the strength limits. These aspects apply to nonredundant, single-load-path, critical components of all structures. The message provided by these two figures is that the selection of metals of highest

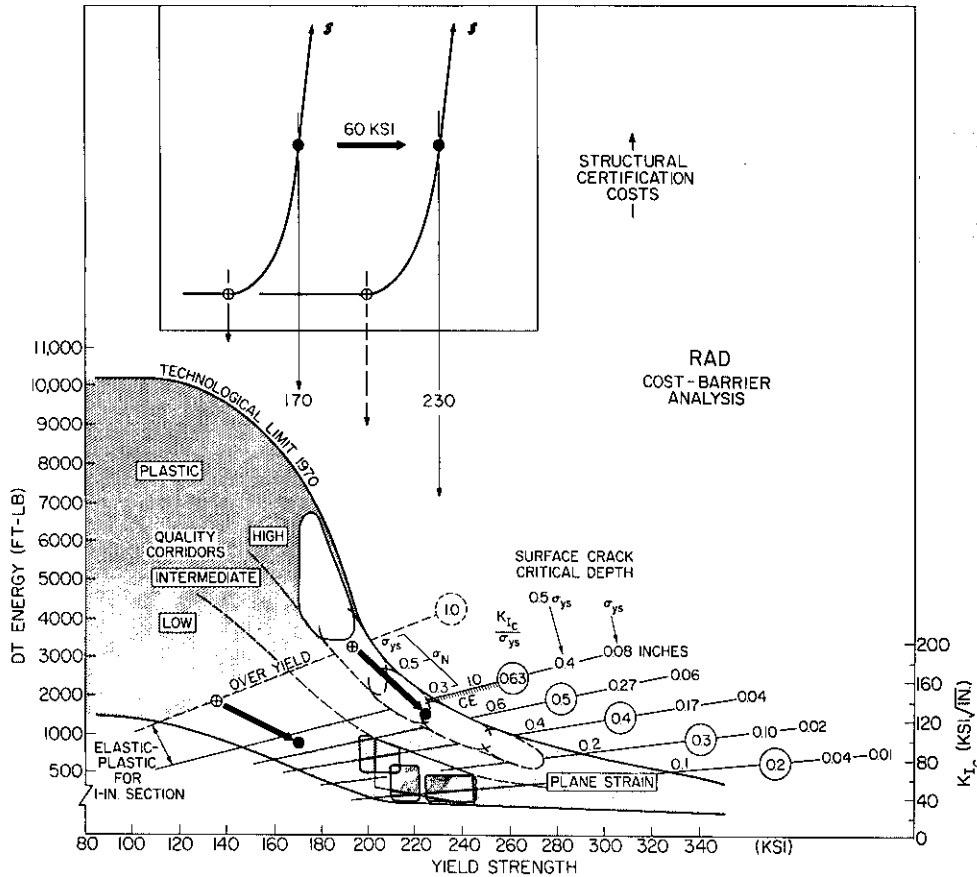


Fig. 31—RAD and cost-barrier analyses for structural certification involving high strength steels. Note that metal quality and specific section sizes, 1.0 in. (25 mm) in this case, must be considered as establishing the strength range for cost escalations.

corridor quality extends low-cost certification procedures to higher levels of yield strength. Exceeding these limits results in cost escalations to a degree that depends on the criticality of the structure and potential sequential effects of structural failures. That is, the more serious the consequences, the greater the cost escalation required to *seek assurance* that critical crack sizes are not developed in the structure. Ordinarily, this becomes a lifetime surveillance problem of potentially staggering proportions (for example, in high-performance aircraft).

The analyses of Figs. 31 and 32 are specific for a 1.0-in. (25 mm) section size. Adjustments for section size effects may be made from the procedures described in Part 4.

The cost-barrier aspect for transition-temperature problems is illustrated in Fig. 33. Two section size ranges are considered. The analyses are general and may apply to a wide range of structures, if these are of critical importance as to failure.

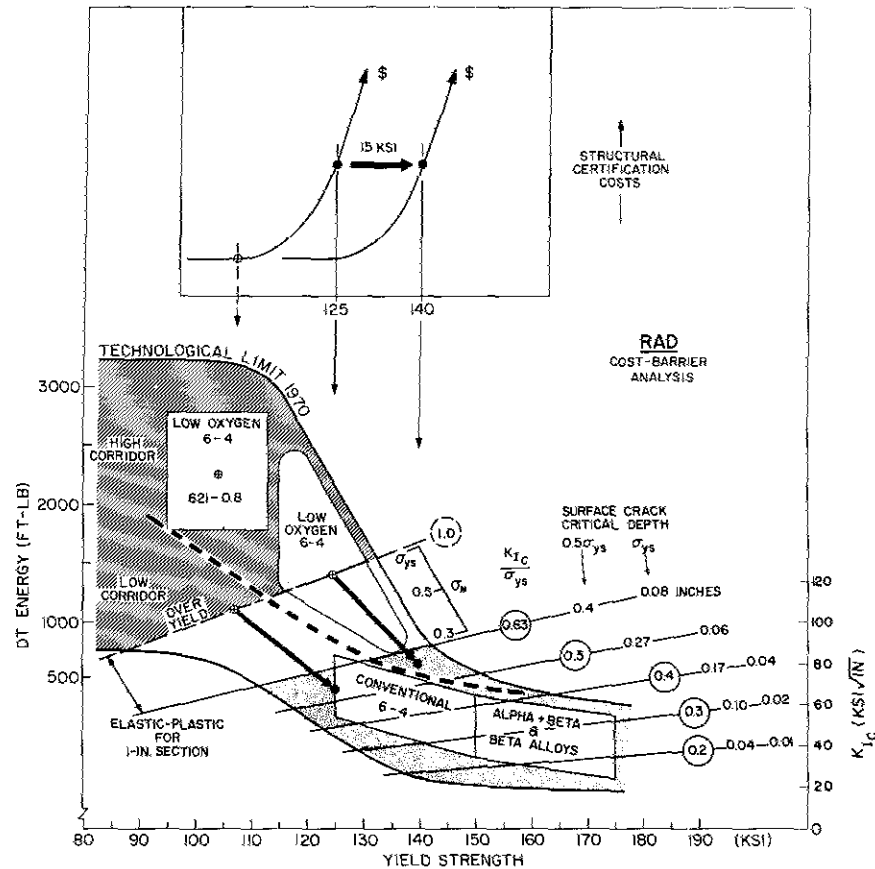


Fig. 32—RAD and cost-barrier analyses for structural certification involving titanium alloys. Analyses for 1.0-in. (25 mm) section size; comparisons of quality corridors relate to oxygen content factors.

ANNOTATED REFERENCES

1. W. S. Pellini, "Evolution of Engineering Principles for Fracture-Safe Design of Steel Structures," NRL Report 6957, Sept. 23, 1969.
2. W. S. Pellini, "Integration of Analytical Procedures for Fracture-Safe Design of Metal Structures," NRL Report 7251, Mar. 26, 1971.

These reports provide an extensive bibliography of references, separated as to types of tests and procedures for their interpretation. Report (1) features a special section on "Elementary Aspects of Fracture Mechanics" plus a comprehensive listing of "Fracture Mechanics Terms and Equations." These features are not repeated in the present report because joint use of the three reports provides the equivalent of a textbook treatment of the subject.

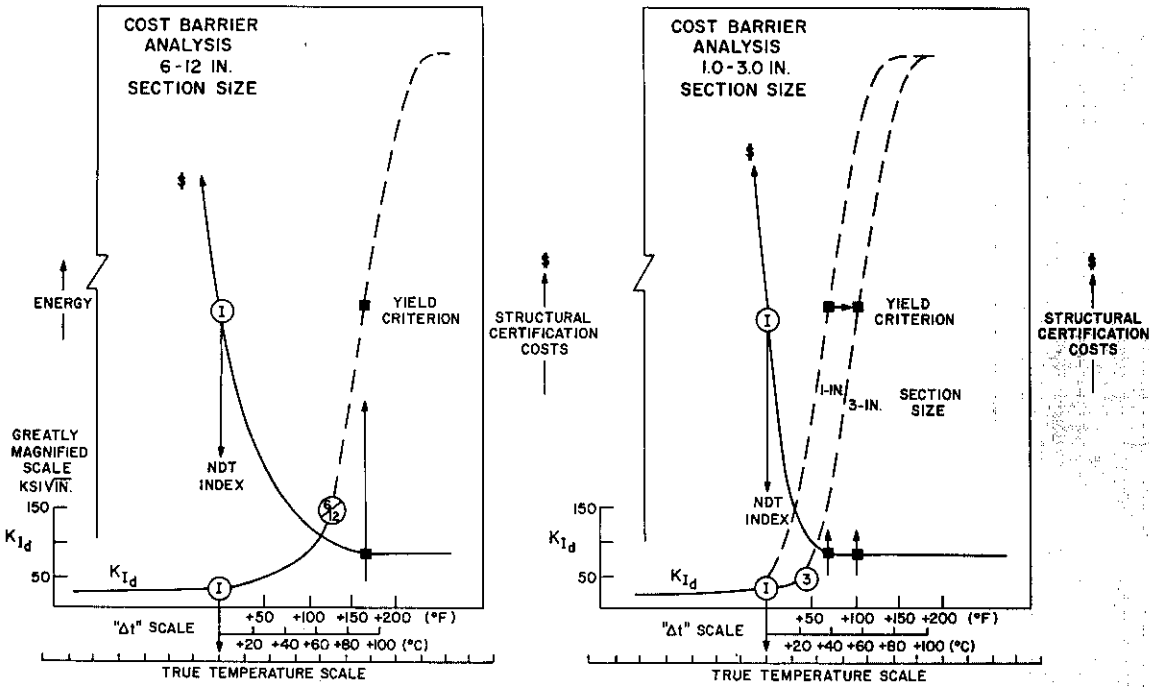


Fig. 33—Cost escalation for structural certification resulting from reducing selection criteria from elastic-plastic to plane strain levels. The importance of requiring elastic-plastic properties to the lowest service temperatures is emphasized by the sharp temperature effects on the certification-cost curves.

Appendix A

INFORMATION OF SPECIAL INTEREST

This section is intended to provide additional information including—

- Metric scale conversions of plane strain reference parameters (Fig. A1)
- Fracture mechanics plane strain tests, configurations and K_{Ic} calculation procedures (Figs. A2, A3)
- Configuration and test procedures for engineering tests which provide constraint capacity definition—DT, DWT, and Robertson CAT (Figs. A4, A5, A7)
- Critical crack-size calculation procedure, as related to engineering use of surface-crack specimens for K_{Ic} determination (Fig. A6)
- Requirements for adequate fracture-path extension features, for tests intended for characterization of the true fracture-mode state (Fig. A8).

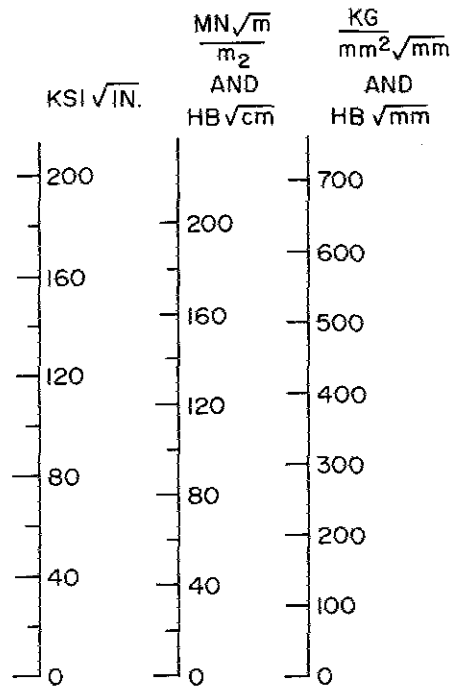
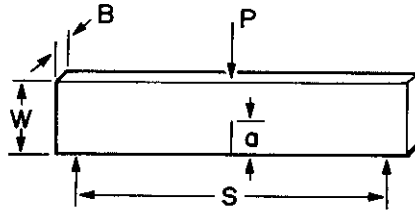


Fig. A1—Indexing of $ksi \sqrt{in.}$ parameter to metric scale units

BEND SPECIMENS



$$K_I = Y \cdot \frac{6Ma^{1/2}}{BW^2}$$

WHERE $Y = A_0 + A_1(a/W) + A_2(a/W)^2 + A_3(a/W)^3 + A_4(a/W)^4$
 AND VALUES OF A VARY WITH LOADING:

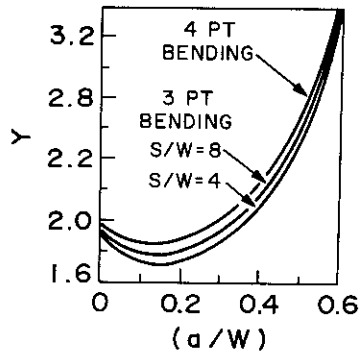
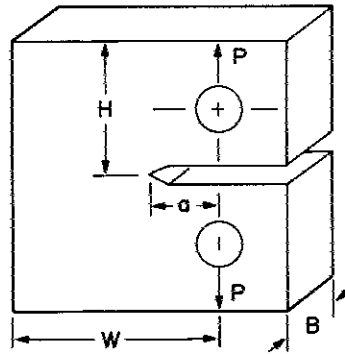


Fig. A2— K_{Ic} -determination procedures for bend-type plane strain tests

COMPACT TENSION SPECIMEN



$$K_I = Y \cdot \frac{Pa^{1/2}}{BW}$$

WHERE $Y = A_0 + A_1(a/W) + A_2(a/W)^2 + A_3(a/W)^3 + A_4(a/W)^4$

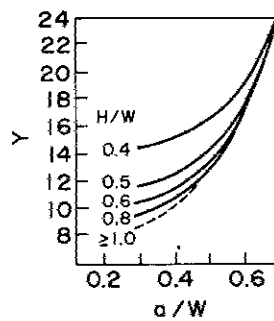


Fig. A3— K_{Ic} -determination procedures for compact tension plane strain tests

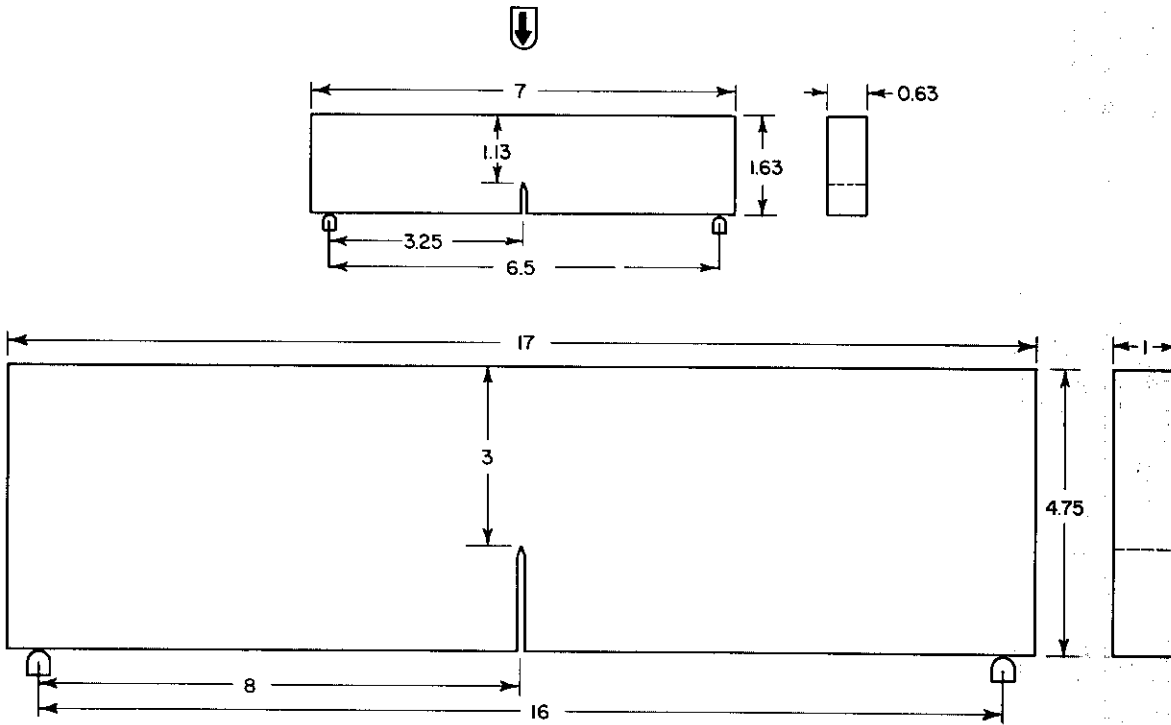


Fig. A4—Specimen dimensions for NRL-standardized DT tests. A sharp crack tip is provided by a brittle electron-beam weld or a pressed-knife edge. In both cases, maximum constraint conditions for the section sizes are attained.

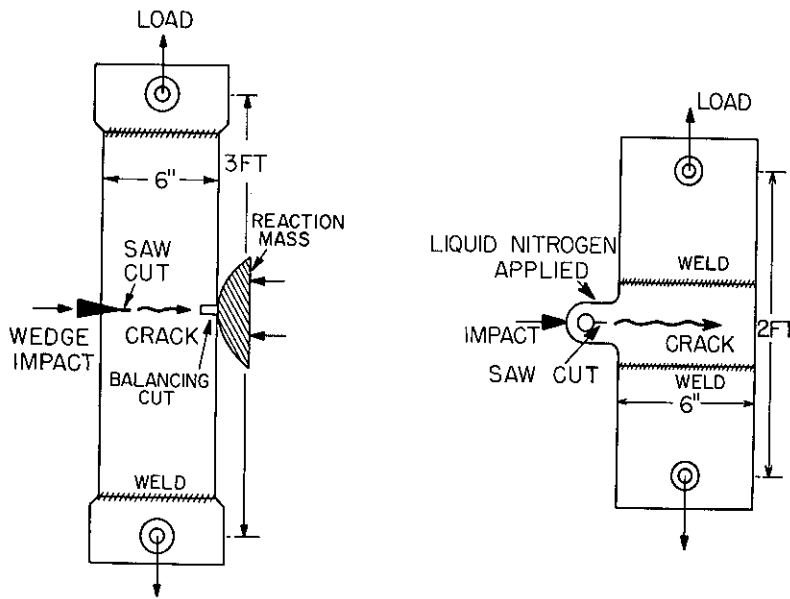
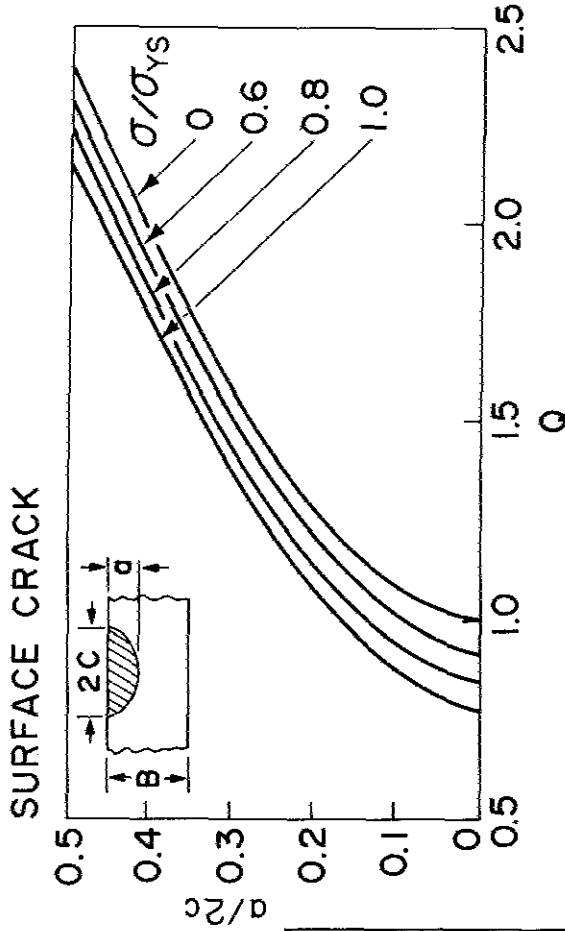


Fig. A5—Features of Robertson test for plates of approximately 1.0-in. (25 mm) section size



LIMITATIONS

$$a \leq 1/2 B$$

$$\sigma \leq \sigma_{YS}$$

$$B \geq 2.5 \left(\frac{K_{Ic}}{\sigma_{YS}} \right)^2$$

$$K_{Ic} = 1.1 \sigma \sqrt{\pi a}$$

$$\left(\frac{K_{Ic}}{\sigma_{YS}} \right)^2 = 1.21 \pi \left(\frac{\sigma}{\sigma_{YS}} \right)^2 \left(\frac{a}{Q} \right)$$

RATIO $\frac{K_{Ic}}{\sigma_{YS}}$	CRITICAL CRACK DEPTH a			
	10:1		4:1	
	$0.5 \sigma_{YS}$	σ_{YS}	$0.5 \sigma_{YS}$	σ_{YS}
0.2	0.044	0.009	0.058	0.013
0.3	0.098	0.021	0.131	0.029
0.4	0.175	0.037	0.234	0.051
0.5	0.272	0.058	0.365	0.080
0.6	0.393	0.083	0.525	0.116
0.8	0.700	0.150	0.934	0.206
1.0	1.09	0.232	1.46	0.321
1.5	2.45	0.522	3.28	0.723

Fig. A6—Calculation of critical crack sizes for plane strain conditions. The K_{Ic} value of a surface-cracked specimen may be calculated also from fracture stress and crack geometry relationships.

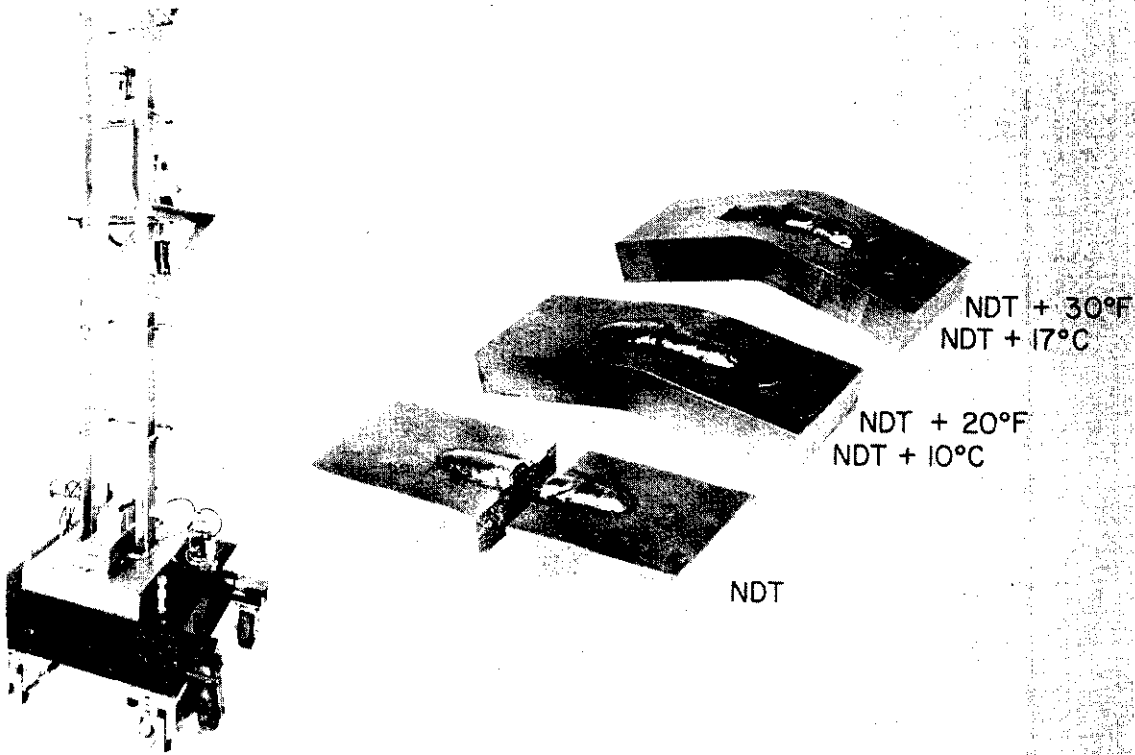


Fig. A7—Drop Weight-NDT Test. Standardized according to ASTM Designation E208-69.

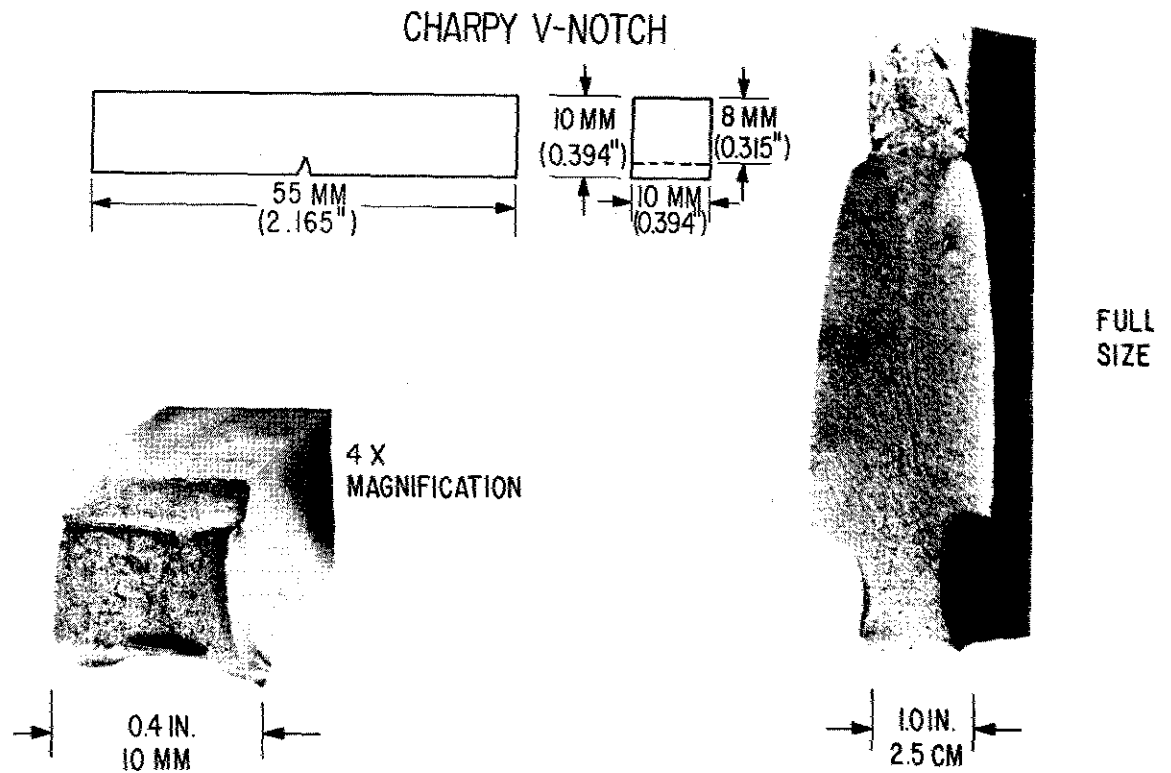


Fig. A8—The true fracture mode of a 1.0-in. (25 mm) steel plate is defined exactly by a DT-test specimen of the same section size (right side of figure). The full-slant fracture is typical of the plastic fracture state of highest attainable levels. The C_v test can never develop slant fracture due to geometric effects. Note the difference in fracture appearance for the same steel (left side of figure).

Load Shock Spectra

The load shock spectra are in more comforting circumstance. The 73-Hz reed, although removed from the fundamental frequencies to a greater or lesser degree, is close enough to indicate that this is the dominating feature of the load motions. The shock spectra demonstrate the limit to constant acceleration above this frequency and try to show the velocity shock region to the best of the reed gage's ability. As the shock machine control parameters are varied, the peak at 73 Hz rises and falls but largely continues to be the salient feature of the shock spectrum. This variation could be due to the fundamental oscillation frequency being shifted around in the selectivity band of the 73-Hz reed as much as to actual variation in its strength.

Effects of Hammer Drop Height

Increase in the height of hammer drop has the effect of raising the level of the shock spectrum without changing its shape. The level of the spectra for blows representing the higher drops of the standard shock test specification is about 150% that of the lower drops, roughly in the same ratio as peak load velocities and accelerations (Fig. 69).

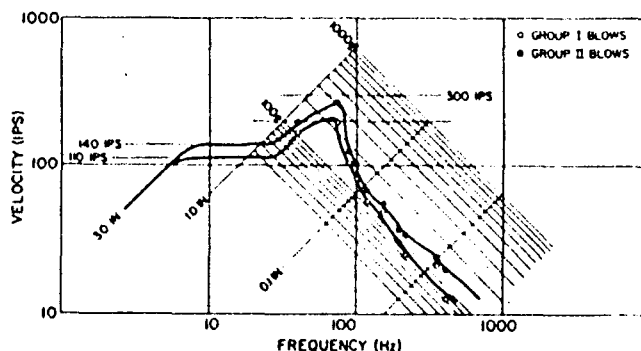


Fig. 69 — Effect of hammer drop height. Shock spectra of Group I (1.5 ft) and Group II (2.5 ft) blows for a 2051-lb load, mounting dimension 16 in.

Effects of Load Weight

Interestingly enough, increasing the load weight seems to increase the shock spectrum level, almost entirely at the high-frequency end, which is presumably due to the waveform distortion noted previously for high drop and heavy loads (Fig. 70). This might be somewhat alarming in view of the intention of the MWSM to provide less severe shock to heavier equipments. However, the frequencies which are most affected are from 353 Hz and beyond, while those below 200 Hz may decrease, and the 73-Hz level definitely decreases, as it should. The region between 200 and 353 Hz remains a mystery since no reed was located there. In any event, the frequency range below 200 Hz is certainly the only area of consequence for shipboard equipments, and it is reasonably safe to say that for practical purposes the shock severity does decrease with increasing load.

Effects of Mounting Dimension

Increasing the distance between mounting points also has the effect of selectively raising the shock spectrum levels at high frequencies (Fig. 70). This is in accord with the increased stiffness of the mounting arrangement indicated by the increase in fundamental oscillation frequency. The effect is probably not significant for practical test equipments.

Effects of Anvil-Table Travel

The anvil-table travel has no consistent effect. With the heavier loads, there is some tendency for the high-frequency (>200 Hz) end of the spectrum to be a trifle greater for 1.5-inch travel blows than for 3.0 inch. This tendency is reversed in the more important region of the fundamental oscillation frequency (Fig. 70). Such variations are much smaller than those due to the other machine variables. It is interesting that a parameter which can affect the load motion's waveform so strongly has so little influence on its shock spectrum. It is also noticeable that when the change in load velocity due to reversal is large, the time in which it takes place is relatively short, which would tend to stimulate the higher-frequency reeds more than the lower.

Reproducibility

The specification shock test calls for three groups of two identical blows. Comparison of the load shock spectra for these pairs of blows, plus two additional groups of three identical blows, shows the reproducibility to be generally good (Fig. 71). The variations above 200 Hz are commensurable with the uncertainties in reading the reed gage records. Variations below 200 Hz may be attributed to random variations in machine performance probably deriving from such sources as slight differences in bolt tightness.

Correlation with Model Predictions

The model used to calculate load shock spectra was the undamped mass-spring-mass system with rigid stops, and allowing for gravity. Spectra were computed for mass ratios of 0.45 and 0.9, corresponding approximately to the loads of 2051 lb and 4423 lb, and were computed for the epochs before and after the reversal event. The agreement between these curves and the measured spectral points is reasonably good for frequencies below about 2.5 times the fundamental oscillation frequency. Above this value, it remains fairly good for the lighter load, but the measured points are much higher than the theoretical curve for the heavier load (Fig. 72). This indicates the inadequacy of the simple model to express the actual mass distribution when the load mass is close to that of the anvil table, as was also exemplified by the departure of the load-velocity waveform from the simple shape predicted by the model.

Nonstandard Operation

Like the LWSM, the MWSM has also been used to generate special waveforms. These waveforms and the methods used to produce them do not form part of the standard shock test or its specification.

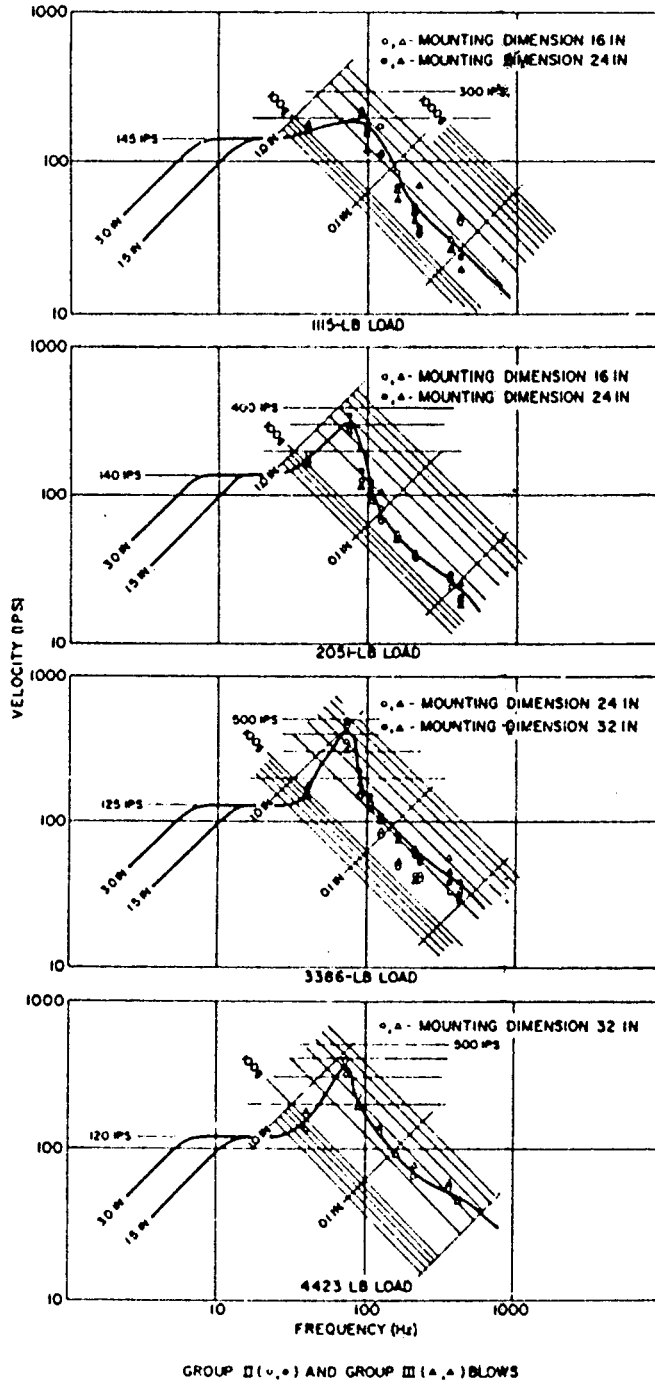


Fig. 70 - Shock spectra for Group II and Group III blows

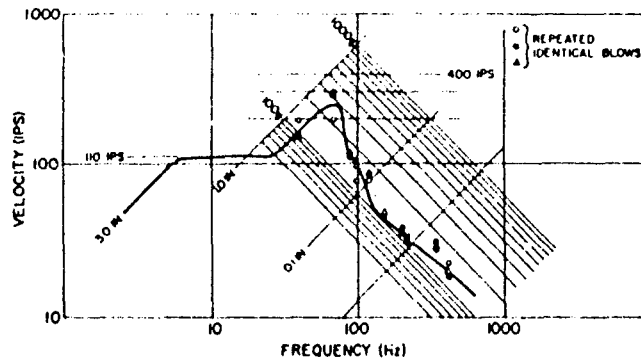


Fig. 71 — Shock spectra for repeated Group I (1.5 ft) blows with a 2051-lb load, mounting dimension 24 in.

Simple Pulse Shock (30)

The MWSM may easily be used to provide the commonly required initial ramp sawtooth and half-sine pulse shock waveforms. The test equipment is attached directly to the anvil table, with no flexible fixtures intervening unless they are considered part of the test equipment. All impacting surfaces of the MWSM (anvil-table impact pad, anvil-table travel top limit stops and bottom stops) are padded with appropriate shock moderating material. For sawtooth pulses the material, shown in Fig. 73, is plastic (lead or solder), and for the half-sine pulses it is elastic (polyurethane).

The plastic element attached to the anvil-table impact pad is a cone whose weight is appropriate to the desired pulse duration. When the hammer impacts, the anvil table accelerates for 6 to 8 ms, until the velocities of the anvil table and hammer are matched. The acceleration then drops to -1 g in 1 or 2 ms. This represents an elastic contribution mostly from the machine, setting a lower limit to the possible buildup time and imparting a slight velocity difference between hammer and anvil table. The anvil table rises until it strikes the elements at the top limit stops, which are also padded plastically, and decelerates over a period of some 25 to 30 ms. During this epoch, the hammer may catch up with the anvil table and impact again. It then swings back and the anvil table drops onto the bottom stops. The material for the bottom stop elements may be plastic or elastic since these elements do not play a significant role in the shock production. Elastic elements are more convenient since they need not be replaced. Peak accelerations from the primary hammer impact of up to 60 g (Figs. 74 and 75) may be produced. The peak accelerations from the secondary hammer impact (if any) may run from 10 to 20 g (Fig. 74).

The elastic elements, shown in Fig. 76, used for half-sine pulses are formed from polyurethane with a Shore A durometer reading of 65. The loading on the anvil-table impact pad element is so great that it is quite nonlinear, and the resulting anvil-table acceleration waveform departs seriously from half-sine if drops above a few inches are used. However, drops of up to 3 inches can produce reasonable half-sine pulses of up to about 7 g, with durations of 20 to 30 ms (Fig. 77).

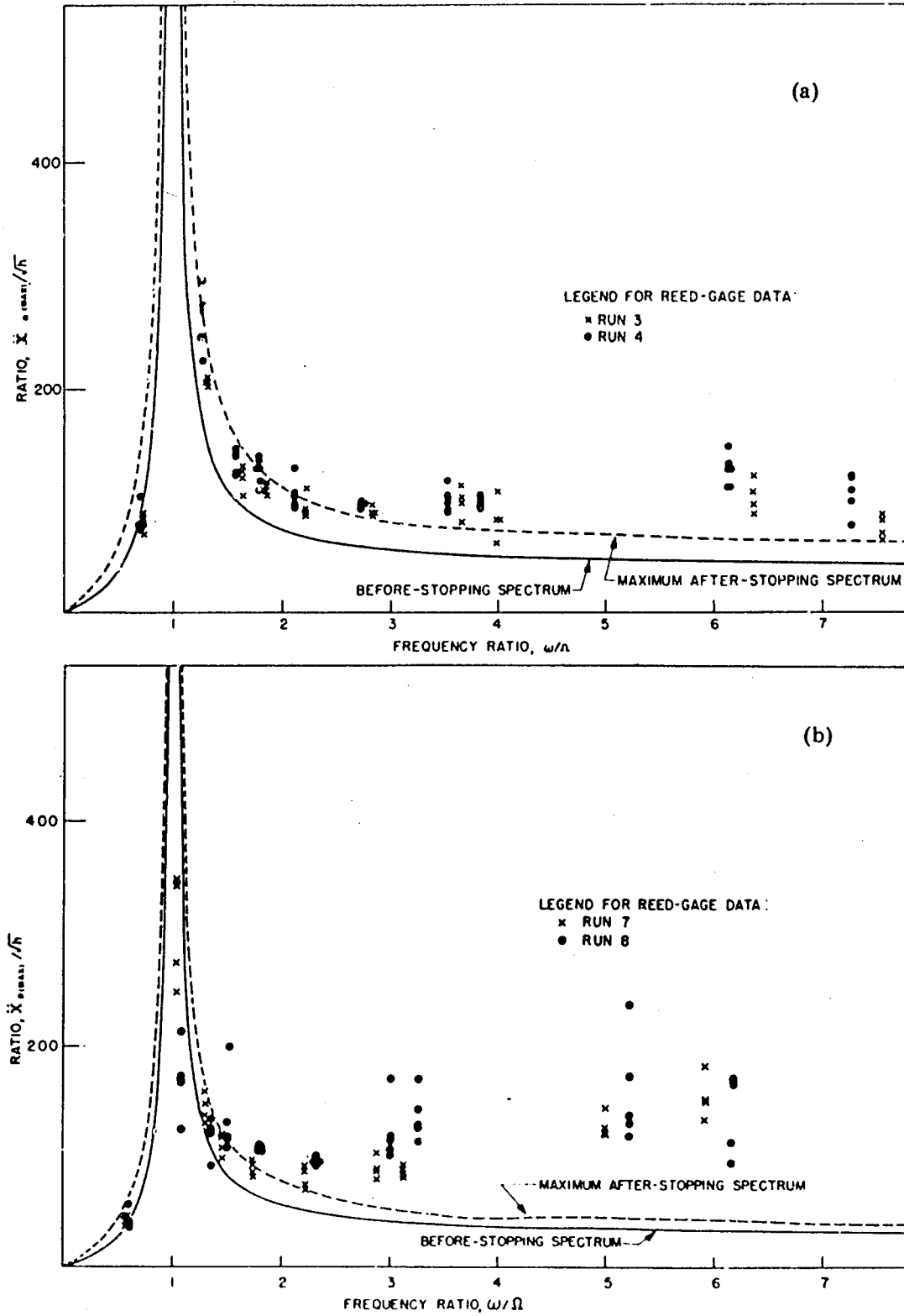


Fig. 72 — Theoretical and experimental shock spectra for mass-ratios of 0.45 and 0.9. These are plotted as equivalent static acceleration. Ω is the frequency of the fundamental oscillation.

47342

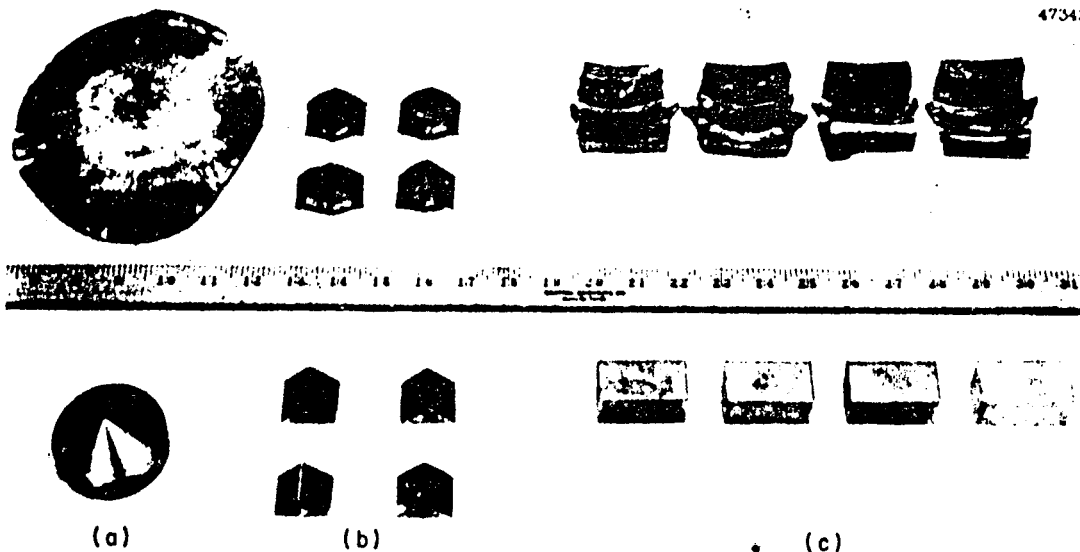


Fig. 73 — Plastic (solder) elements for generating sawtooth pulses with the MWSM. Shown (lower) before deformation and (upper) after, these elements are attached to (a) the anvil, (b) the bottom stops, and (c) the top stops.

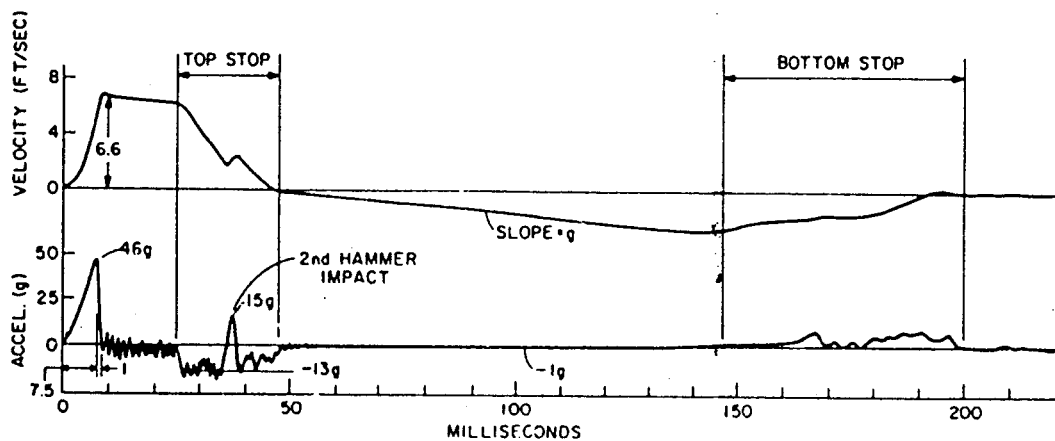


Fig. 74 — Anvil-table motion for a 4-ft hammer drop with a 21-oz plastic (solder) element

Plate Mounting

Some types of equipment, such as reactor components, are required or permitted to be shock-tested by procedures different from those of MIL-S-901. Typically, these shock tests are required to provide a mounting system such that a specified fixed-base natural frequency shall result and that hammer drop heights and table travels shall be as given by the schedule of MIL-S-901 for the all-up weight on the anvil table. Another type of specification might require that a mounting system and machine operation procedure shall be such that a specified fundamental oscillation frequency and peak load velocity shall be

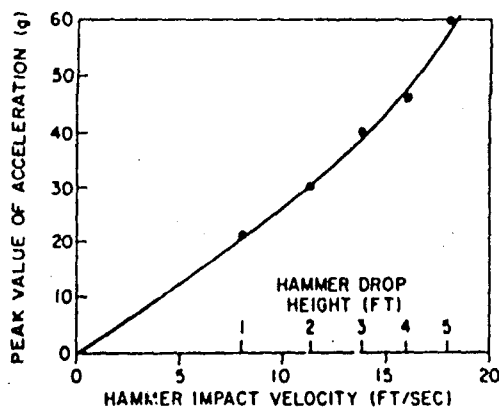


Fig. 75 — Sawtooth pulse amplitude as a function of hammer impact velocity

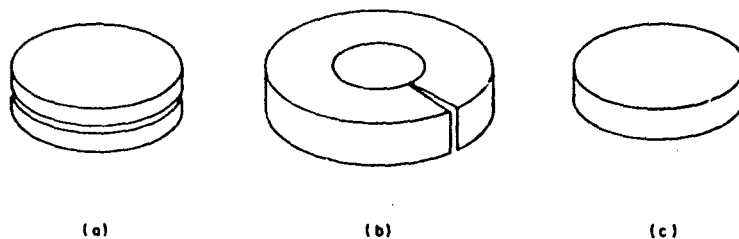


Fig. 76 — Elastic elements (polyurethane) used between the impact surfaces: (a) anvil, (b) top stops, and (c) bottom stops. All are 1 in. thick, (a) and (c) have 4-in. diameters, and (b) has a 5.2-in. O.D. and a 2.3-in. I.D.

produced. Still another may require that a specified shock spectrum envelope shall be produced at the load mounting points. This last procedure was once fairly common, then fell into abeyance as the complexities of interpreting shock spectra properly became appreciated. It is now reappearing. Since its renascence is largely localized in fields with little previous acquaintance with shock and shock design, there seems little reason to hope that the present practitioners are any more knowledgeable than the last.

The frequencies specified for tests of the two former types are generally too low to be provided by the usual support channels. The dynamic stresses are entirely too high, and bending may be so rapid that the fundamental oscillation persists for only a cycle or less. A convenient way around this problem is to interpose a steel plate between the support channels and the test equipment, which is arranged so that its long axis lies parallel to the support channels. This system may be tuned by moving the support channels in and out to vary the effective free span of the plate and by such traditional tricks as judicious use of spacers. The plate will still yield somewhat, but the depth of plastic penetration is vastly less than would occur in the support channels alone and has no noticeable influence on the load motions. In time, the deformation may accumulate to an unsightly extent, whereupon the plate can be turned over for the next test.

Deck Motion Simulation

NSRDC is investigating ways to modify the operation of the MWSM to provide the large displacements and low frequencies characteristic of deck motions. The projected technique would not entail the extensive modifications of the machine structure that

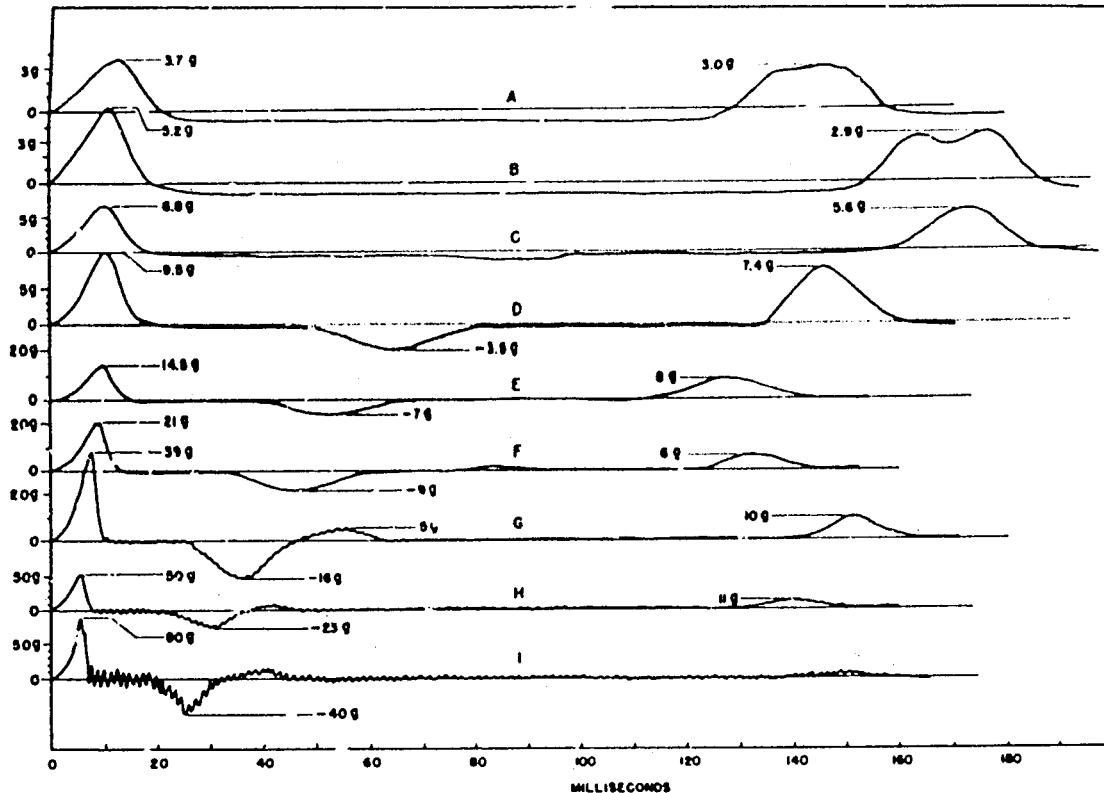


Fig. 77 — Acceleration curves using polyurethane elements of the dimensions shown in Fig. 76 and with a 65 Shore A durometer hardness. Hammer drop heights were (a) 1 in., (b) 2 in., (c) 3 in., (d) 5 in., (e) 8 in., (f) 1 ft., (g) 2 ft., (h) 3 ft., and (i) 4 ft.

were used with the LWSM but would constitute an elastic mounting system to be placed between the anvil table and the test equipment. The displacements involved would accordingly be limited to much less than the 12 inches permitted by the modified LWSM.

30° Corner Bulkhead

The 30° corner bulkhead (Fig. 55) is an auxiliary mounting adapter which permits shock motion to be induced along all three axes of a test equipment simultaneously. It is intended as an adjunct to the standard mounting arrangement, not as a replacement for it.

The bulkhead is a stiff and massive structure which is attached to spacer rails mounted on the anvil table. It has so many response modes of its own that the response of an equipment mounted in it is difficult to forecast, but by and large the normal modes of the overall structure will be those of the bulkhead, little influenced by those of the test equipment. The velocity measured at the corner of the bulkhead (the most compliant part of its structure) has the same character as that of the anvil table with strong, well-sustained sinusoidal components at 250 Hz and integral multiples, and a minor 150-Hz component. The displacements associated with these components are small. A severe input to the test equipment may be the racking occasioned by the motion of the bulkhead's

sides, which flap considerably. However, there are equipments which have inadequacies that are best revealed when shock is directed along two or three axes simultaneously, and for this reason it is desirable that some blows of the shock test should be delivered with the equipment on a 30° mounting.

Excessive Load Weights

The original schedule of specification blows provided peak load velocities of 11.5 ft/sec. Equipments weighing up to 4800 lb still receive tests of this severity. Dead-weight loads in excess of 4800 lb cannot be given this velocity; since the hammer is 5.5 ft long, it cannot be dropped from a height greater than 5.5 ft. With the current standard load limit of 6000 lb the peak attainable load velocity is 9.5 ft/sec at best, and usually lower. In view of this decrease in test severity at the high end of the load range, it may be desirable to modify the test procedure for items in the 5000- to 6000-lb range. For example, tests of such items could simply be transferred to the Floating Shock Platform, or light-weight mounting components could be fabricated from high-strength alloys. In any event, it would be well to hold the total load on the anvil table to around 6000 lb.

THE NAVY FLOATING SHOCK PLATFORM

History (31)

In the absence of suitable shock machines for testing equipments weighing in excess of about 4500 lb, actual shock testing of heavy shipboard items was limited to what could be installed on board a ship undergoing a series of shock tests. The situation largely involved calculating shock response plus occasional spot checks by actual test. Although capable of providing the best proof test imaginable, a ship undergoing shock tests is not a convenient device for equipment development. The expense is great and the shock severity is usually limited to a level which assures survival of the ship.

In 1959 the first Floating Shock Platform (FSP) was designed and built by the Underwater Explosion Research Division (UERD) of NSRDC at the Norfolk Naval Shipyard. It consists of an open steel barge capable of handling all-up loads to 30,000 lb (40,000 lb with restrictions on the location of the center of gravity) which is exposed to a series of underwater explosions. Test equipments are installed as they are on shipboard, and the test hopefully approaches the actual service conditions while providing the conveniences of accessibility, controlled shock environment, and economy obtained with a laboratory test machine. Since 1959, additional FSP's have been built, most of them somewhat larger than the original. The larger version has a total load capacity of 40,000 lb (or 60,000 lb if the center of gravity is not too high), and plans are in progress for the construction of a similar device for loads up to 320,000 lb.

A somewhat similar shock test device is the Submarine Test Vehicle (SSTV), which has recently been placed in service. This is essentially a submersible FSP, consisting of a segment of submarine hull in which equipments are attached with their normal foundations. The SSTV is then submerged and exposed to a series of underwater explosions.

Description

The original FSP is a rectangular double-bottomed barge 22 ft long by 16 ft wide; the double-bottom structure is heavily reinforced and 3 feet deep. Sides 3 feet high and 1 foot thick enclose the usable workspace of 20 x 14 ft. Freeboard is further increased by the addition of 3-ft-high bulwarks atop the sides for a total height of 9 ft. The structure is topped with a canopy which provides protection from weather and plume spray and can be removed to permit free access to the workspace for installation and removal of test equipments. The larger version is similar except for its 6 ft greater length. The deck and bottom reinforcing members are 20.4-lb HY-80 plate, the bottom and sides are 40-lb STS plate, and the bulwark structure is 5.1-lb mild steel plate. The waterproof cover of the original FSP is steel-framed canvas, but this item is irrelevant to the shock characteristics and wide design variations are permitted.

The unloaded FSP weighs about 85,000 lb, draws about 4 ft of water, and provides an internal volume of 20 (or 26) ft long by 14 ft wide by roughly 15 ft high to the center of the canopy (Fig. 78).

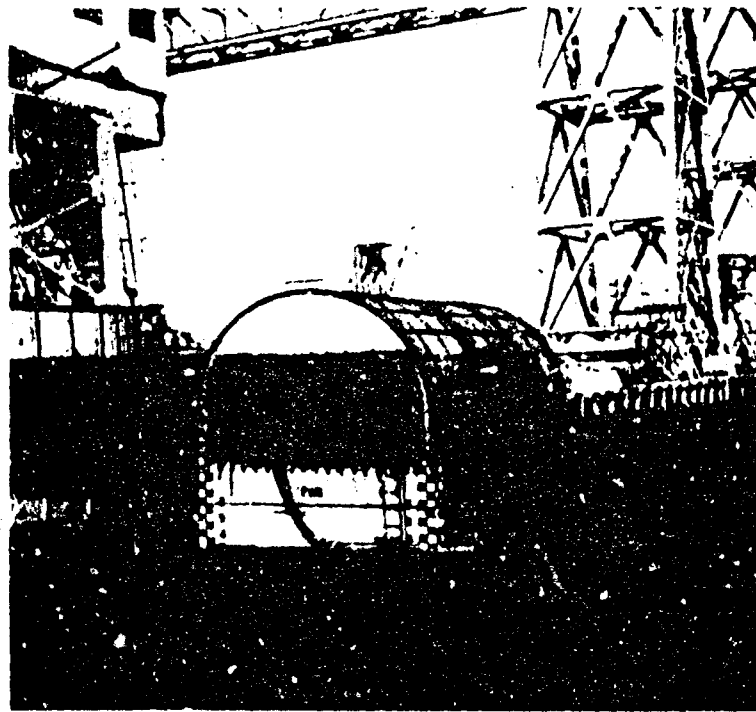


Fig. 78 — The Navy Floating Shock Platform (FSP). This FSP is one of the larger version (28 ft x 16 ft) and is located at the West Coast Shock Facility (WCSF), Hunters Point Naval Shipyard, San Francisco, California.

Mounting Arrangements

The test equipment should be mounted on a foundation structure which duplicates that of its shipboard mounting or approaches this ideal as closely as possible. For most equipments this may be done simply by bolting or welding their standard shipboard mounting foundations to the FSP deck. For some it is necessary to first erect a structure which simulates a particular region of the ship and to attach the shipboard mounting foundation to this structure.

Operating Procedure

The normal test procedure is to tow the loaded FSP to the test area and subject it to a series of underwater explosions at increasing proximity, the last being close enough to cause shock motions on the FSP which approximate those found on ships during severe shock attack (Fig. 79). The charge weight is standardized at 60 lb, the depth of detonation at 24 ft below the surface of the water, and the orientation such that a straight line from the charge to the center of geometry of the FSP bisects its long axis at right angles. The shock test control variable is "standoff," the horizontal distance from the near side of the FSP to the charge. The shots of the test series are detonated at standoffs of 60, 40, 30, 25, and 20 ft, in that order. A recent modification of this procedure requires the second (40-ft standoff) shot of the test series to be performed with the charge located forward of the FSP and on its projected center line. It is anticipated that this requirement for a fore-and-aft input will be retained in future editions of MIL-S-901.

After each shot the test equipment and installation are inspected, and mounting fasteners are retightened as necessary. As with the LWSM and MWSM equipment, performance is evaluated on the basis of its assigned category of importance. Water depth is not specified but should be around 35 to 40 ft at least. The maximum radius of the gas bubble on the first expansion is slightly less than 15 ft so that the bubble does not vent and the first bubble pulse is radiated. During the contraction phase the bubble's velocity toward the surface is greatly increased, and the bubble vents on the second expansion.

Calibration of Shock Outputs (32)

The shock motions of the FSP are considerably different from those of the LWSM and MWSM in several important respects. First, the shock input is not unidirectional but has strong vertical and athwartship, or vertical and fore-and-aft, components, which depend on the test orientation. Second, the rigid-body displacements are not limited by travel stops but by the characteristics of the detonation and the FSP response. These displacements are sizable in vertical and athwartship or vertical and fore-and-aft translations and in the rotations which couple them. Third, the relative strengths of vertical and athwartship input components are not the same for all shots since they are given at constant depth but varying standoff. Fourth, the test-item/shock-machine interactions are much more significant. Test loads in this weight range are so large, and the FSP structure required to support them must be so rigid, that its test load cannot be considered as simply a rigid dead-weight load. These differences add great complications to the calibration procedure, and the last prevents output descriptions as simple as those for the LWSM and MWSM. To reduce the data from the FSP to the same basis, it is necessary to compensate for the reactance of the test structure, which is unfortunately ill defined.

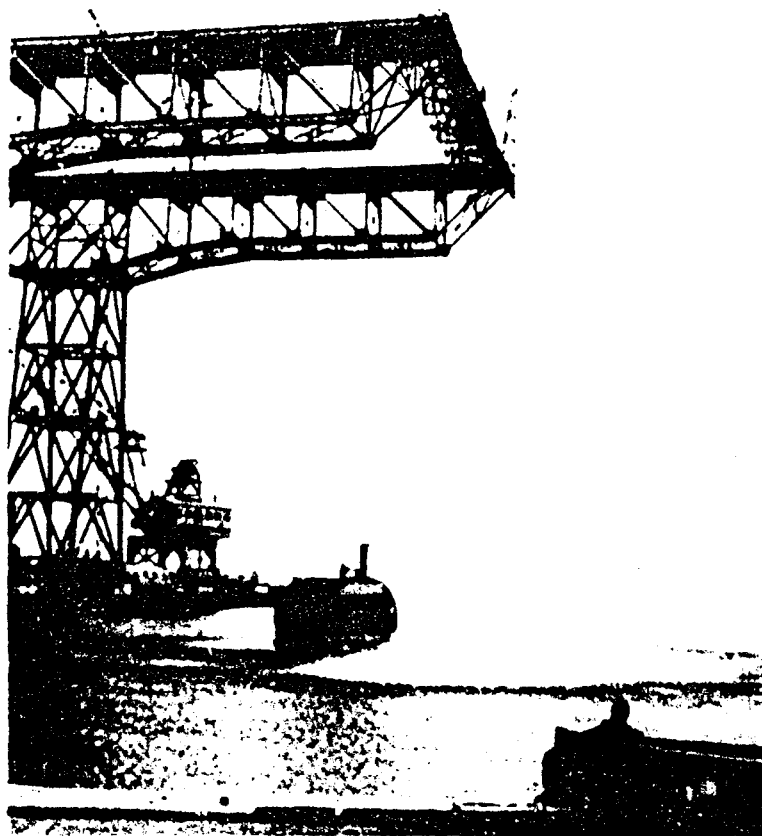


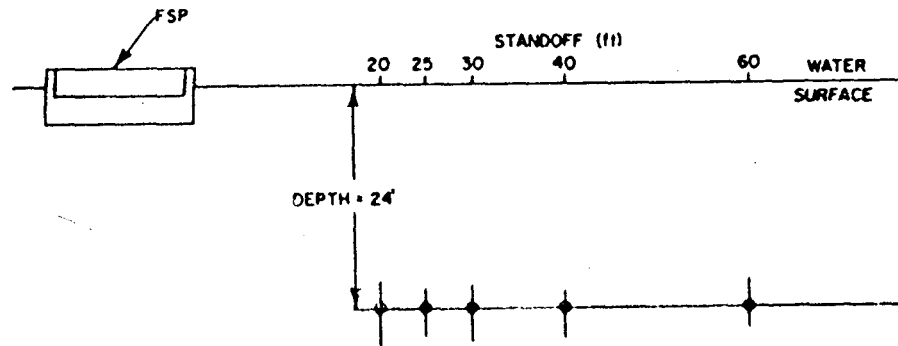
Fig. 79 -- The FSP at an early stage of a close-in shot

Test Arrangement

The factors which influence the shock behavior of the FSP are the test-load weight, the charge weight, and the geometry of the test setup. Three test-load weights were selected: 35,800 lb, 18,400 lb, and 9,000 lb. Charge weights were mostly the standard 60 lb, but some were 90-lb charges. Some of these were placed at locations chosen to produce the same shock severity as the standard 60-lb charges (to check the shock factor scaling law) and others were placed close in to provide higher shock severities than those of the standard test specification. The test geometry was varied by changing the standoff (20, 30, 40, 60, and 80 ft) and depth (10, 15, 20, 25, and 30 ft) of the charge and also by moving the charge forward so that the line connecting it to the FSP's center of geometry formed a 39° angle to the normal (Fig. 80). Some pairs of identical shots were made to reveal shot-to-shot variations.

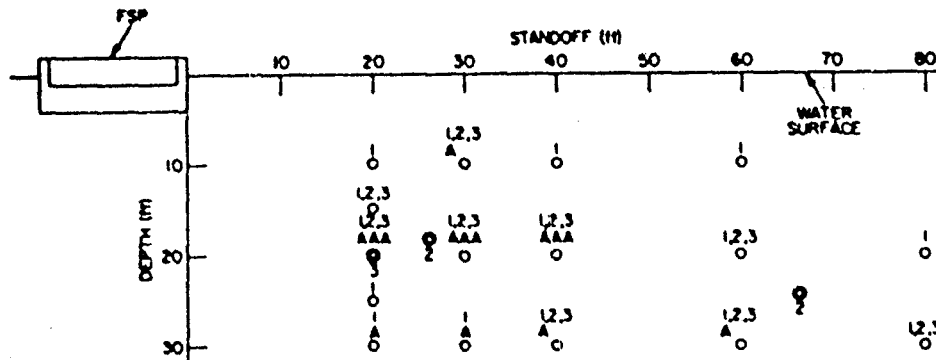
Test Procedure

The test load consisted of a damaged diesel engine and its shipboard foundation, together weighing 35,800 lb. When all removable parts had been stripped off, the weight was 18,400 lb. The lightest load, 9000 lb, consisted of two sections of 2-inch steel plate bolted to half of the engine foundation (Fig. 81). It was felt that since the reactance of



(a) The standard test series specified by MIL-S-901 requires five 60-lb charges to be exploded at a depth of 24 ft and distances of 60, 40, 30, 25, and 20 ft from the near side of the FSP.

○ 60 lb CHARGE
 ⊙ 90 lb CHARGE
 1 35,800 lb LOAD
 2 18,400 lb LOAD
 3 9,000 lb LOAD
 A 30° INCIDENCE



(b) The FSP calibration test series was more comprehensive. This schematic locates the shots in the depth-standoff plane. The load configurations for which shots were fired are indicated by the numbers above (60-lb charges) or below (90-lb charges) the shot indicator. In addition to the normal incidence shots, some were made with 30° incidence, where the normal array geometry was maintained but rotated 30° forward about the depth axis through the center of the FSP. These shots are indicated by the addition of an A below the load indicator for the corresponding normal shot. For example, the indicator at standoff 30 depth 10 reads that 60-lb charges were detonated at normal incidence with test loads of 35,800 lb, 18,400 lb, and 9,000 lb, and that a 60-lb charge was also detonated at 30° incidence with a test load of 35,800 lb. The indicator at standoff 20 depth 20 reads that 60-lb charges were detonated at normal incidence and at 30° incidence with all three test loads, and that a 90-lb charge was detonated at normal incidence with a test load of 9000 lb.

Fig. 80 — Schematic of the shot geometry for FSP tests

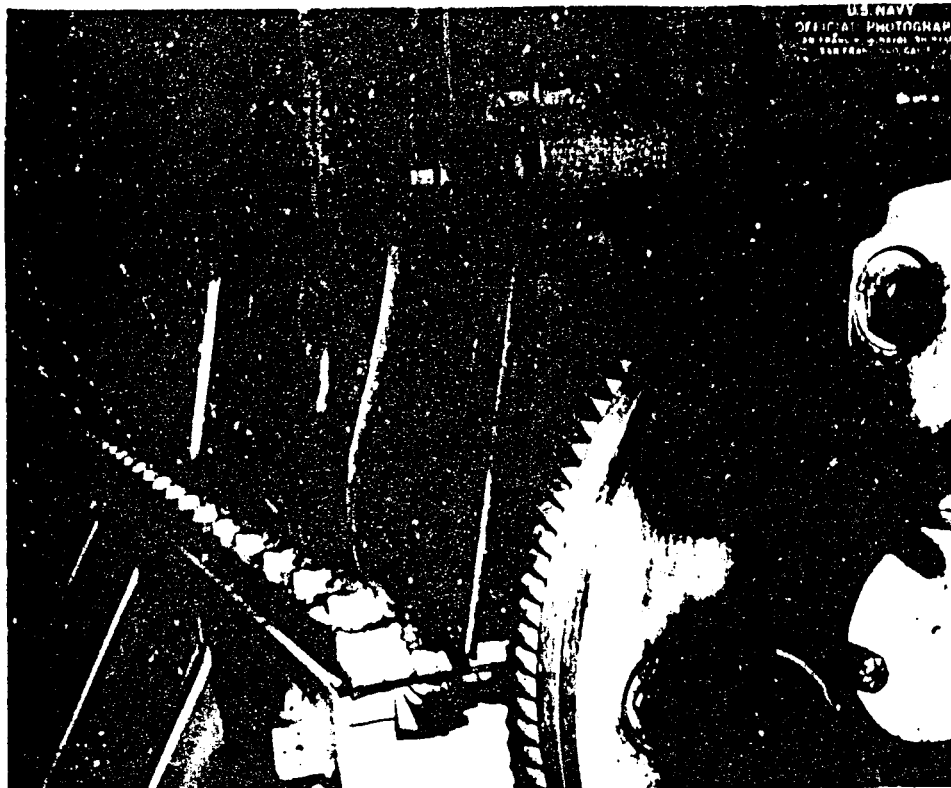


Fig. 81 — The test load for the FSP calibration series. This is an inoperable submarine diesel engine weighing 35,800 lb. After being stripped of all removable parts, its weight was 18,400 lb. The final test load of 9000 lb was attained by removing the engine, cutting its foundation in two, and attaching steel plates to one of the halves.

the load would have to be considered anyway, the convenience and economy of using an object at hand would outweigh the analytical conveniences of using specially designed load structures. It was realized that the diesel engine foundation had not been designed for shock resistance, except for the use of static multipliers ("shock design numbers"), which are intended to ensure that sufficient bolts are used to prevent flight. This procedure represents shock design at its crudest level, and foundation structures based on it may be expected to deform plastically and move about under shock since these factors are not considered at all. It was hoped that by starting with one of the more severe shocks and with maximum test load, the inadequacies of the design would be revealed immediately, and that when appropriate renovations had been made the new foundation structure would be suitable for the purpose.

Inadequacies did indeed become apparent immediately, but after renovation new ones continued to appear. After a time the information available on the spot indicated no further deterioration, and no new repairs were necessary. Later analysis of the recorded data revealed that in fact deformations were still occurring at a magnitude sufficient to cause the characteristics of the foundation structure to be constantly changing. It was only for the lightest load configuration that the test load structure could be considered the same for all shots.

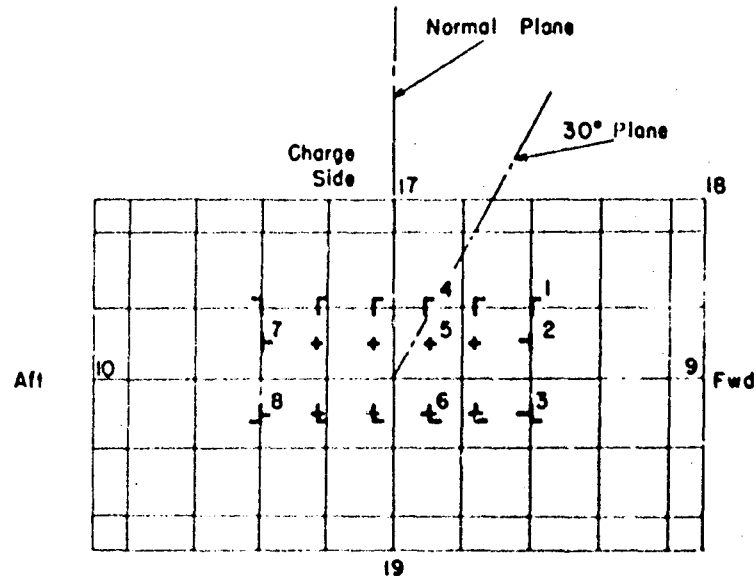


Fig. 82 — Schematic of the FSP structure and test load foundation showing the locations of input transducers. Note that locations 2, 3, 7, and 8 lie atop athwartship stringers, location 4 lies above a longitudinal stringer, and location 1 lies above an intersection. Locations 5 and 6 lie over the centers of cells. The line marked 30° indicates the axis of the test array for 30° incidence shots.

Measurement Instrumentation

The motion transducers used were seismic-magnet-type velocity meters (natural frequency 5 Hz, displacement capacity 5 inches) and an assortment of accelerometers, mostly of the strain gage type and mostly with natural frequencies of about 2 kHz. These were attached in various combinations to the base of the engine foundation at selected points or to the adjacent deck (Fig. 82). The arrangement of transducers attached at specific points to measure various shock motion components was varied from shot to shot. This technique allowed extrapolation of the values measured to give an estimate of those which were not. Considerable difficulty was experienced with the poor shock resistance of the transducers themselves. The test was intended primarily for uniaxial shock, and the cross-axis shock proved highly deleterious. After appropriate signal conditioning, the outputs from the transducers were recorded on magnetic tape and later analyzed for peak velocities and accelerations. Shock spectra were then calculated by digital computer.

In a later series of standard specification tests, the rigid-body displacements (athwartship, vertical, and the coupled rotation) were evaluated from dockside high-speed movies. The test loads ranged from about 30,000 to 40,000 lb, the variation having little influence on the motion.

Output Shock Motion Waveforms (33,34)

Description

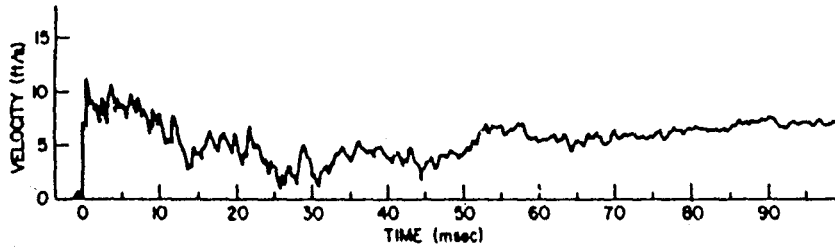
The most significant part of the FSP response to the primary shock wave occurs within about 50 ms after its arrival. By this time the rigid-body motion due to the surge of water displaced by the gas bubble is considerable, and this remains the most important feature until about 600 ms after the arrival of the primary shock wave. The rigid-body displacements (vertical and athwartship) have the basic form of a half-sine pulse of 600-ms duration. At about the time this displacement has returned to zero, the first bubble pulse arrives but is insignificant in shock effect compared to the primary shock wave. The motion tails off with undershoot from the rigid-body displacements, and finally the FSP rocks from the surface waves excited by venting of the gas bubble. The important epoch of the entire process occurs when the effects of the primary shock wave are in full force. There may, of course, be individual cases when other epochs will also be important.

The timing of the sequence outlined above is that for a 20-ft standoff and will be somewhat different for the less severe shots. The general features will remain the same.

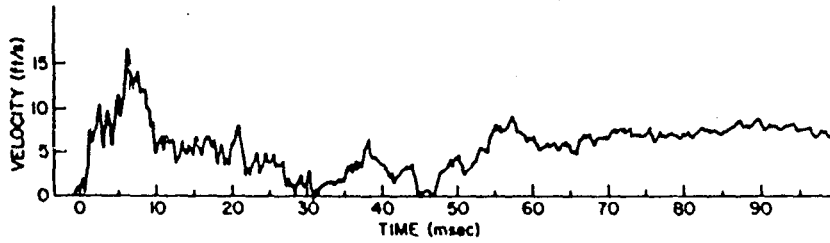
The character of the deck motion waveform is strongly affected by the structure of the FSP at the point of measurement, more strongly than by the test control parameters. Vertical velocities measured above the stiffeners feature a very sharp initial rise of about 1 ms or less, followed by a gradual decay with fairly strong sinusoidal components of 21, 47, 500, 1000, and 2000 Hz (Fig. 83a). Those measured at the center of the unsupported span show very nearly a damped $(1 - \cos)$ wave at 100 Hz carried on a basic 18 Hz and in turn carrying a 1000-Hz rider (Fig. 83b). Athwartship velocities are less distinctive. Both locations have sharp rise times and $(1 - \cos)$ -type waveform with a dominant frequency of about 200 Hz. This component is rapidly (2-3 cycles) damped to the same footing as the other major components, 100 Hz and 15 Hz. In addition, there is a component at 1000 Hz which is small and rapidly damped in the center of the span and strong and well sustained over the stiffeners (Figs. 83c and 83d).

Some estimates have been made of the natural frequencies which might be expected from the FSP. The rigid-body modes — heave, pitch, and roll — are around 1 Hz. The free-free beam frequencies calculate to 120 Hz (fore and aft) and 310 Hz (athwartship). No serious attempts have been made to calculate plate frequencies since the reliability of the answers would hardly justify the difficulty of the calculation, but the lowest plate mode may be somewhere in the range 50 to 100 Hz. The frequency associated with the unloaded deck plating between stiffeners might run from about 100 Hz to 140 Hz, depending on the loading condition of adjacent areas of the plating. The presence of a concentrated load in an unsupported space could reduce its membrane frequency to practically any value, however.

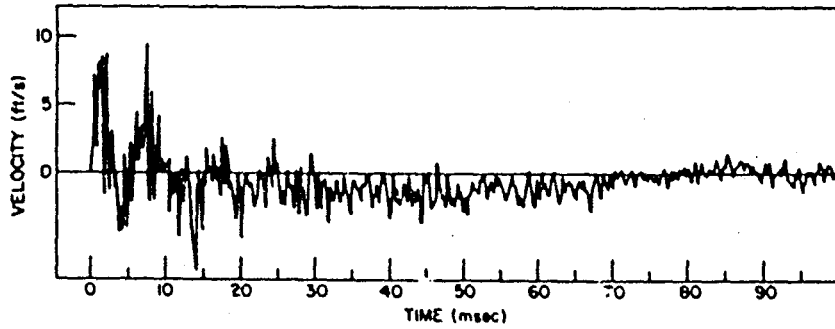
The effects of the test control parameters are largely to vary the amplitudes and fine structure of the velocity waveform, while its basic character remains primarily determined by the FSP deck structure. In this respect the FSP deck is very much like the LWSM mounting-plate/anvil-plate combination. The presence of the engine foundation itself has little influence except for the lower frequencies, as would be expected. As in the LWSM, the higher-frequency components are decidedly localized and in any event have little significance to shipboard equipments.



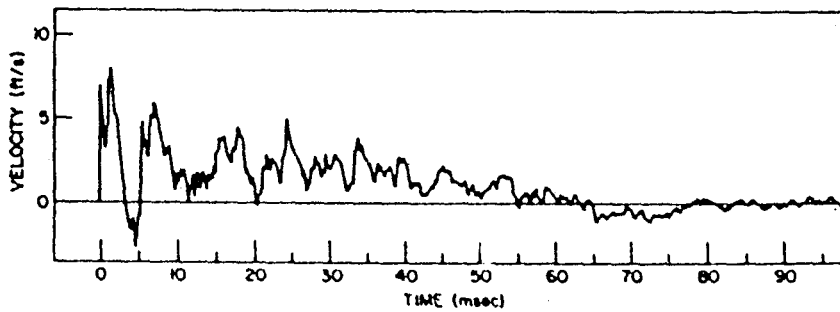
(a) Vertical velocity vs time measured above an athwartship stringer (location 3, load 18,400 lb)



(b) Vertical velocity vs time above a cell (location 5, load 18,400 lb)



(c) Athwartship velocity above an athwartship stringer (location 3, load 18,400 lb)



(d) Athwartship velocity above a cell (Location 5, load 35,800 lb)

Fig. 83 - Influence of FSP structure on velocity waveforms

The recorded transducer outputs were restricted to the significant range by filtration before peak accelerations and velocities were read. The cutoff frequency was set at the value which gave agreement between peaks read from filtered acceleration recordings and graphically determined slopes of velocity recordings. This value was 250 Hz, in reasonably good agreement with the traditional 300 Hz generally used for shipboard shock analysis. Both velocity and acceleration records were filtered with this cutoff before the peak values were read.

Effects of Measurement Location

The magnitudes and relative magnitudes of the peak velocities in the three component directions are influenced not only by the test geometry but also by the structure of the FSP at the point where the measurement is made and the structure of the test load. With so many variables, the pattern of FSP shock motions is somewhat confused. Some simplification can be made by averaging the values measured at the various locations to provide a measure of the overall shock input to the test load. This was done to the measured values of peak and spectral velocities to provide the values plotted in Figs. 84 through 86 and Figs. 91 through 93. Averaging is complicated by the variation of transducer locations from shot to shot. Of the input locations, only locations 3, 4, 5, and 6 were monitored consistently. Comparison of the averages found from this set alone with those found from the complete set of input locations (available for some shots) indicates that the overall averages lie quite consistently at 0.91 of the restricted averages. Accordingly, when a reasonably complete set of input values were not available, the averages from 3, 4, 5, and 6 were used after multiplication by 0.91.

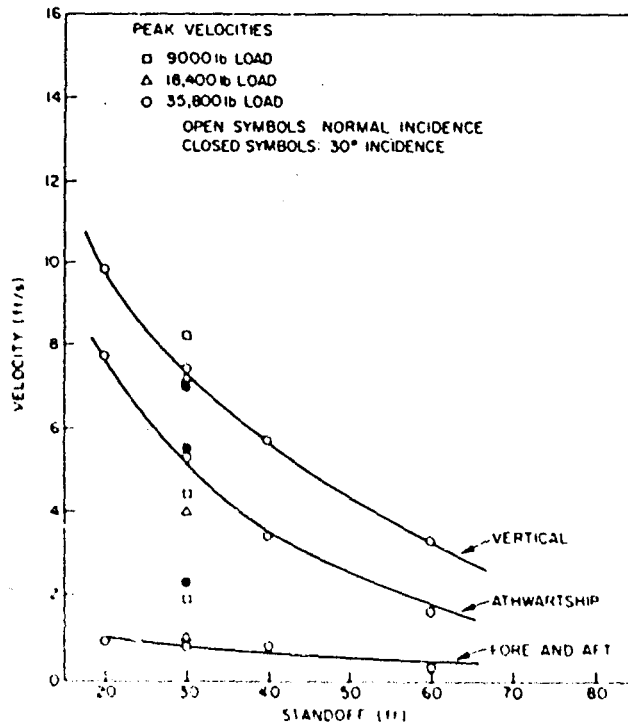


Fig. 84 — Peak velocity vs standoff for a 10-ft depth. The trend lines are given as a fiducial convenience and do not represent any particular formula for shock factor. They have been drawn to correspond roughly with the data for normal incidence tests with a 35,800-lb load.

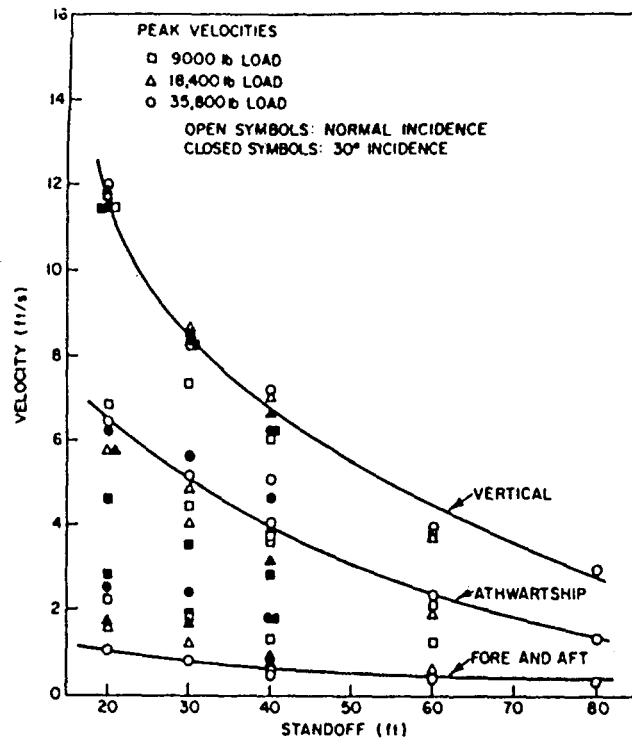


Fig. 85 — Peak velocity vs standoff for a 20-ft depth

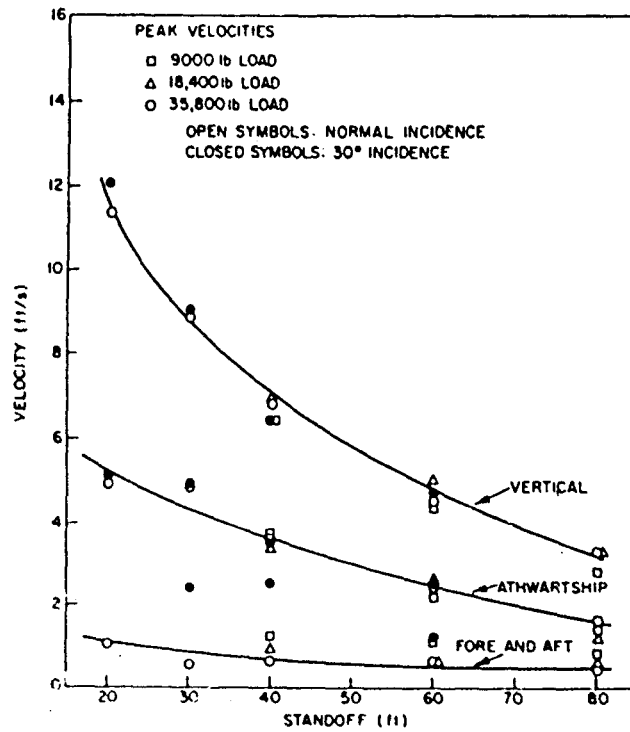


Fig. 86 — Peak velocity vs standoff for a 30-ft depth

The highest peak velocities are associated with the more flexible measurement locations because the stiffer locations have motions richer in high-frequency components and are more affected by the filtration. Since the vertical and athwartship stiffnesses at the stiffer locations are more nearly comparable, the shock motions are more nearly alike. This is reflected by the relative magnitudes of the peak athwartship velocities with respect to the peak vertical velocities being larger than at the softer locations. Moreover, the spread of peak vertical velocities is somewhat greater ($\pm 20\%$) than that of peak athwartship velocities ($\pm 15\%$) (Figs. 84 through 88). Evidently, then, the FSP is relatively stiff in the athwartship and fore-and-aft directions, of somewhat less stiffness in the vertical direction at the hard spots, and considerably less stiff in the vertical direction at the soft spots.

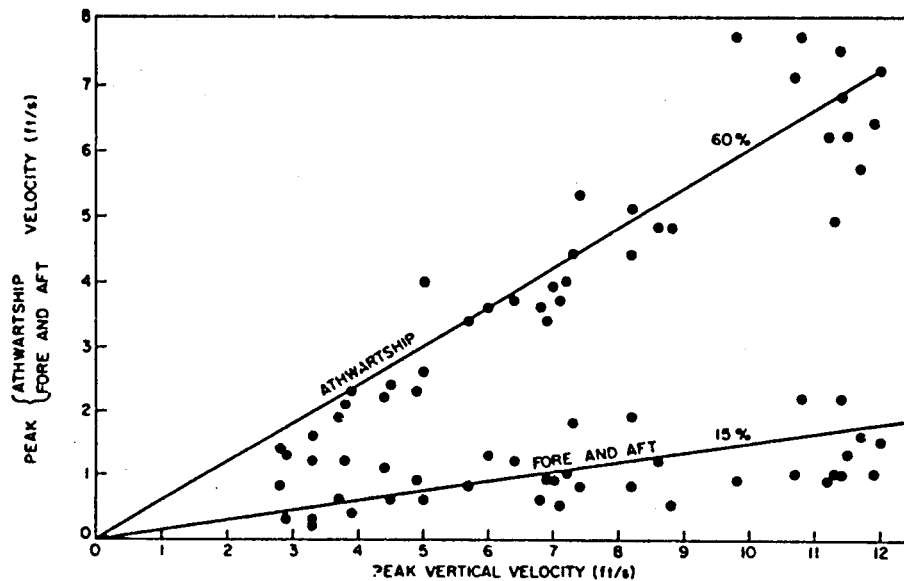


Fig. 87 — Peak athwartship and fore-and-aft velocities as functions of peak vertical velocity for normal incidence shots. Note that athwartship peaks cluster along the 60% line, and fore-and-aft peaks cluster along the 15% line.

Effects of Measurement Orientation

Peak velocities in the vertical direction are greatest, and those in the fore-and-aft direction are smallest, even for the angled shots. The latter are so small as to be negligible, but special cases may arise where the nature of the test equipment requires that they be considered. Peak athwartship velocities average about 60% of the vertical peaks, although the relationship between the magnitudes is not truly linear due to the changing geometry of the test setup (Fig. 87). The higher velocities occur with short standoffs, where the vertical component is more pronounced. The fore-and-aft peak velocities are about 15% of the vertical and are a more-or-less constant fraction. It is interesting that the peak accelerations in the athwartship direction are larger than those in the vertical direction for shallow, close-in shots with the 35,800-lb load (although not for the lighter loads), indicating the substantial high-frequency content of the athwartship motions.

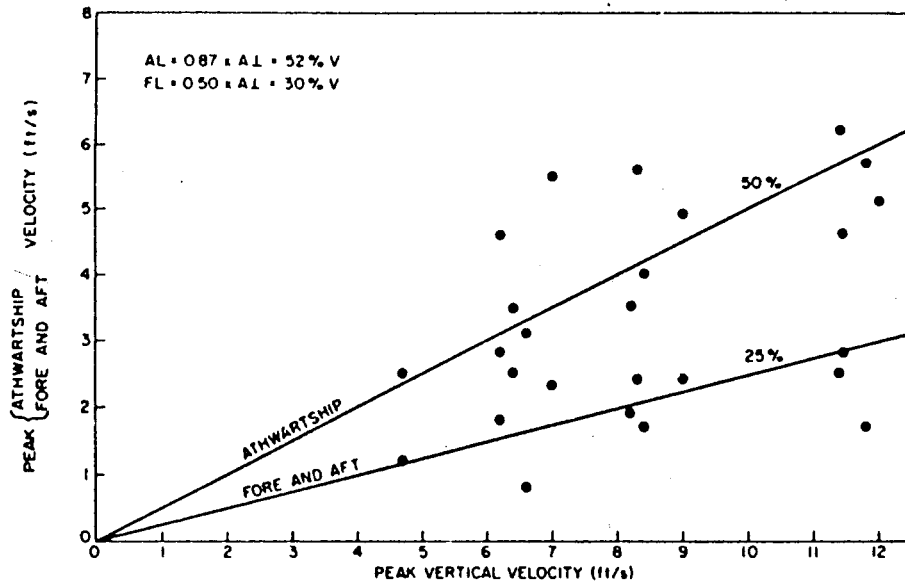


Fig. 88 — Peak athwartship and fore-and-aft velocities as functions of peak vertical velocity for 30° incidence shots. Here the athwartship and fore-and-aft peaks cluster around the 50% and 25% lines, respectively.

Effects of Load Weight

The variation of load weight in the calibration test series was only 24% of the average total. While load weight is thus not a dominating parameter, it does have some effect, and this may come from two conflicting actions. The first is simple presence of additional mass which tends to decrease the shock severity. The second is additional draft which tends to increase shock severity for shallow shots. The latter factor is presumably responsible for the excess of peak athwartship accelerations over peak vertical accelerations for the heaviest load weight with appropriate shot geometry. These two actions combine to the end that the shock is usually most severe with the 18,400-lb load, followed more often than not by that with the 9000-lb load. The overall variation of peak velocity with load weight runs about 10% (Figs. 84 and 86).

Effects of Charge Orientation

Placement of the charge along a line at 30° off the perpendicular to the FSP axis has no significant effect on the vertical motions and little on the athwartship motions, but it does about double those in the fore-and-aft direction (Fig. 88). Even so, they are considerably smaller than those in the two other directions, being about half as great as the athwartship motions. The peak athwartship velocities show the slight decrease to be expected from geometry, dropping to about 52% of the vertical. The fore-and-aft peak velocities rise to about 25% of the vertical, while the geometry would indicate a fraction of 30%. There is considerable scatter, however.

Effects of Charge Depth

The depth of the detonation is not a strong influence on the shock intensity, being more noticeable for its effect on the relative magnitudes of peak velocities in the component directions. Shots with the charge at a 10-ft depth yield somewhat lower peak velocities than the others, but little change is observable for depths of 15 ft and greater (Figs. 84 and 86).

The peak velocities in the vertical and athwartship directions are comparable for shallow shots (although the vertical peak is always the greater). As the depth is increased, the peak vertical velocity increases and the peak athwartship declines until the depth is about equal to the standoff, after which time their values remain essentially constant. The fore-and-aft peak velocities are totally indifferent to shot depth.

Effects of Standoff

Charge standoff is the control variable of the specification shock test and by far the most significant in its effect on the shock motions induced. The peak velocities for an 80-ft standoff are only about 30% of those for 20 ft (Figs. 84 through 86 and Table 4). The character of the motions remains essentially unchanged, and other than the decrease in magnitude the only effect is variation in relative magnitudes due to the change in geometry of the test arrangement.

Table 4
Multiplication Factors Relating Shock Inputs
by Charge Standoff

Standoff (ft)	Multiplier		
	Vertical	Athwartship	Fore and Aft
20	1.0	1.0	1.0
30	0.7	0.8	0.8
40	0.6	0.7	0.7
60	0.4	0.5	0.5
80	0.3	0.4	0.4

Effects of Charge Weight

Charges of 90 lb rather than the specified 60 lb produce greater shock severity, but the increase is slightly less than that predicted by the shock factor. Placement of 90-lb charges at standoffs calculated to provide the same shock factor also resulted in slightly lower peak velocities and accelerations than the specified 60-lb charges.

Reproducibility

Duplicate shots result in very similar peak velocities (Figs. 84 through 86). The spread is nil at some measurement locations, perhaps 20% at others, which is due to the mechanical details of the test load installation and the condition of the FSP. The FSP is not an elastic machine, as welds crack and plates bulge with use, but the normal maintenance procedures seem adequate to preserve predictability of shock output.

Rigid-Body Motions (35)

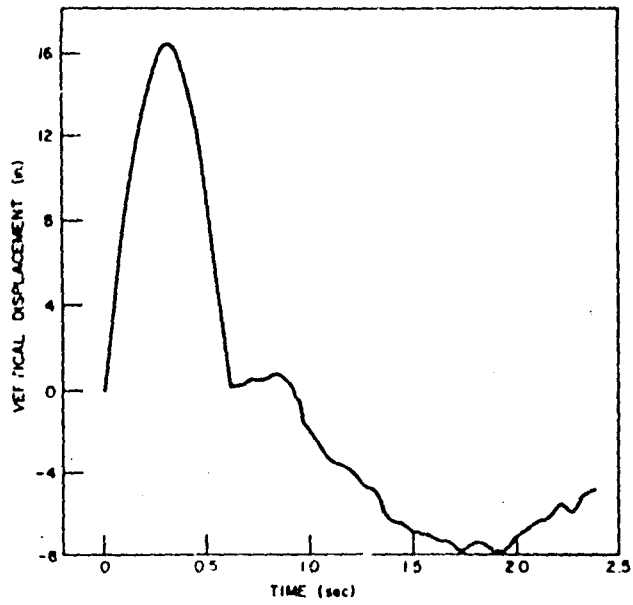
On a subsequent series of specification tests the FSP rigid-body motions were determined from high-speed movies. Test loads ranged from 29,300 lb to 41,100 lb but made little difference in the motions. Since the 20-ft standoff, 24-ft depth shot is the most severe, only the motions produced by it will be described. Because of the symmetry of the specification test arrangement, the rigid-body motions may be adequately described by the vertical and athwartship displacements of the center of gravity and the rotation about the roll axis through it.

The largest displacement occurs in the vertical direction (as the athwartship displacement is limited by the pressure buildup on the lee side), reaching a maximum of about 16.5 inches at 300 ms after the arrival of the shock wave (Fig. 89a). At about this same time the athwartship displacement reaches its maximum of 5 inches (Fig. 89b), and the rotation its maximum of 40 mrad (Fig. 89c). These motions are well described by a half-sine displacement pulse of 600-ms duration, implying a peak "bodily" velocity of 7.2 ft/sec. After this initial pulse has passed, there is some undershoot, amounting to 8 inches in the vertical direction (about 1.9 seconds after the arrival of the shock wave) and 5 inches in the athwartship (a little earlier than the vertical minimum). The rotational undershoot is small (6 mrad) and occurs somewhat earlier than those of the displacements, about 1.4 seconds after the shock wave arrives.

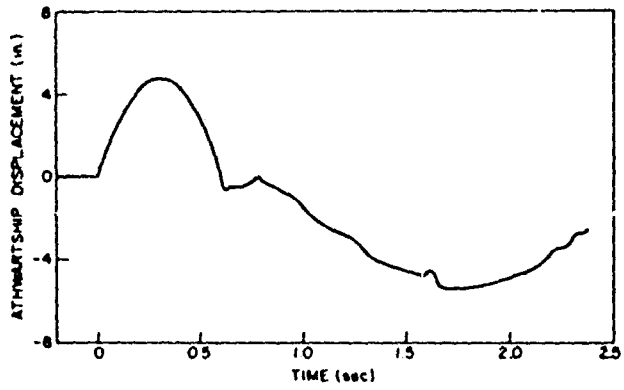
Output Shock Spectra (33,34)

Overall and residual shock spectra were calculated by digital computer for natural frequencies every 2 Hz from 0 to 150 Hz. The velocity recordings were used as inputs since this parameter is less influenced by the local properties of the measurement location, and a few acceleration records were processed to provide a cross check. Shock spectral values below about 20 Hz should be regarded with some reserve for two reasons. First, the nature of the velocity meter itself, with its 5-Hz natural frequency, seriously distorts the importance of motions in this region. Second, the spectra were calculated from the first 200 milliseconds of the velocity record, making it difficult to distinguish frequency components of a few hertz from each other or the dc bias of the magnetic tape recorder. A slight error in the estimate of this dc bias has a substantial effect on the shape of the shock spectrum at the low-frequency end.

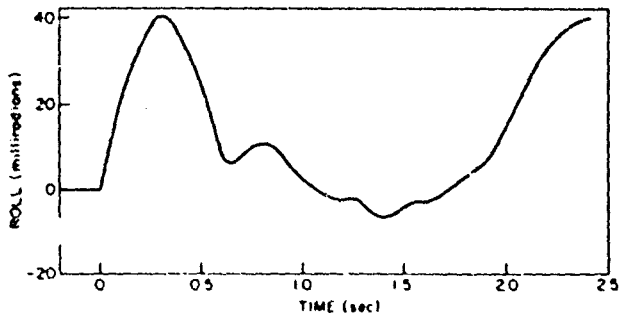
Even so, it is possible to extract some of the desired information, viz., the frequencies for which the residual spectrum has minima. The velocity level cannot be evaluated in this region but must be extrapolated from higher frequencies and the displacement limit set from other measurements. The ill-defined and changing characteristics of the load structure render these spectra considerably less useful than could be desired. Possibly due in part to the multiple-support nature of the foundation, the expected effect of load weight cannot be seen to any extent, and like the waveforms the shock spectra are largely characteristic of the measurement location. Averaging the spectral parameters measured at the several measurement locations provides an inkling of the behavior which may be expected with relatively nonreactive test loads. It is hoped that more data will be accumulated which will permit the influence of modal weight to be more apparent.



(a) Vertical displacement vs time



(b) Athwartship displacement vs time



(c) Roll vs time

Fig. 89 - Rigid-body motions of FSP: the center of mass displacements for a 20-ft standoff specification test shot

The shock spectra presented in the sections on the LWSM and MWSM were of the motions of dead-weight loads attached to rigid machines by flexible mountings. The shock spectra from the FSP are of motions measured at the interface of a load-foundation structure and a machine which are reactive and have comparable compliances. The shock spectra have highly individualistic shapes which are governed by the local peculiarities of the overall load-foundation-machine structural ensemble, and their most significant content lies in their values at the fixed-base natural frequencies of the load-foundation system. When the test load has been designed for a specific purpose, its modal frequencies and weights are (in principle) known. Therefore, enough spectral points can be extracted to define the design shock spectrum completely, although it may require several test load structures to provide an adequate range of modal weights and frequencies.

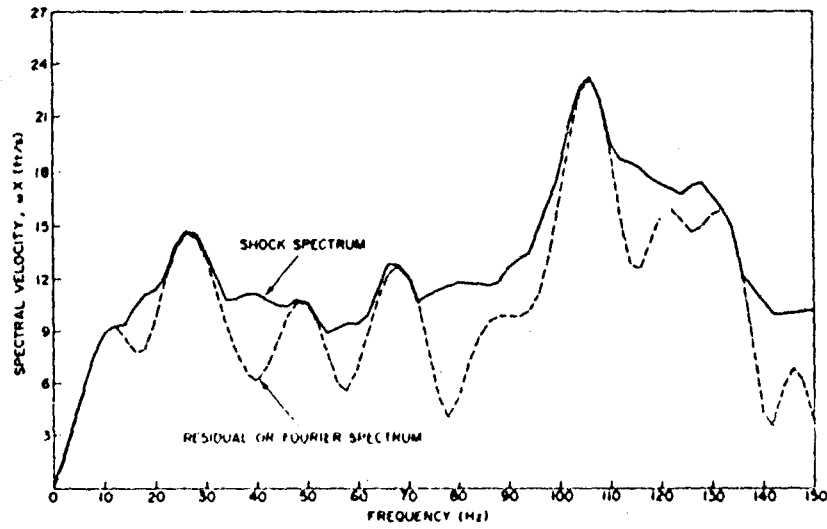
Unfortunately, this procedure cannot be applied to the shock spectra which have been obtained since the load structure is an unknown quantity. It is possible to make a fairly good guess at the frequencies of the first mode or two, as has been done, but the modal masses remain a mystery. The best estimate that can be made is based on the observation that for simple structures, where only translatory motions are involved, the modal mass of the first mode will be about 80% of the total mass.

Description

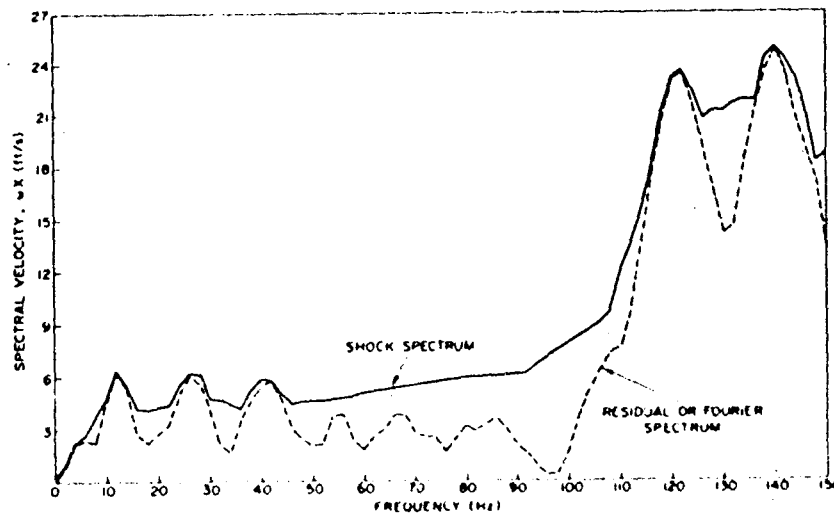
The basic character of the shock spectra is velocity shock. Interactions dominate above about 130 Hz, although some may occur at lower frequencies. The spectra probably become acceleration limited around 100 to 300 Hz, depending on the direction of the motion component and the measurement location. The residual shock spectrum shows its dips in the area of 20 Hz and multiples, indicating the natural frequencies of the test load-foundation structure. In this region the overall spectrum is substantially flat, and the shock spectrum value is taken as the average of the values of the overall spectrum at the frequencies of the first few well-defined residual dips (Fig. 90). This procedure essentially forces the shock spectrum of the FSP deck motion to a form similar to the MWSM anvil-table motion — a low-frequency, displacement-limited region at the maximum displacement of the motion; a high-frequency, acceleration-limited region at the highest acceleration of the motion; and an intermediate velocity shock region where the equivalent velocity change is taken from the average of the values at the individual measurement locations. There is, naturally, a different shock spectrum applying to each component direction of motion.

The cutoff frequencies can be estimated by fitting the measured displacements, equivalent velocities, and peak accelerations to this pattern. The upper cutoff frequencies (the transition from velocity shock to acceleration limited) are 67 Hz, vertical; 220 Hz, athwartship; and 125 Hz, fore and aft. The lower cutoff (transition from displacement limit to velocity shock) is 1.15 Hz, from the displacements measured in the vertical and athwartship directions. This implies a peak fore-and-aft displacement of about 3 inches. Since the lower cutoff is so low, the usual design shock spectra assumed for dynamic analysis (which extend the velocity shock region to zero frequency) are valid for soft-mounted equipments as well as rigid mounted.

In general the shock spectrum velocity values so derived are fairly close to the peak velocities read from the waveforms. They tend to be somewhat higher, indicating that the filtration performed on the velocity waveforms before the peak values were read did in

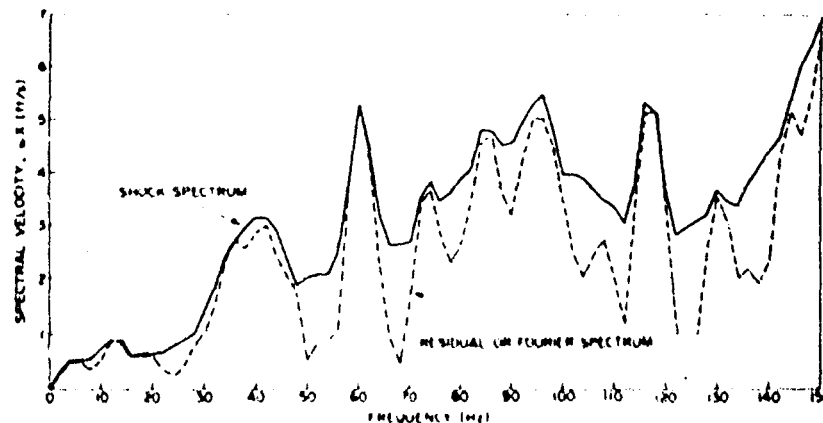


(a) Vertical, location 3



(b) Athwartship, location 5

Fig. 90 — Representative overall and residual shock spectra for shots at 20-ft standoff, 15-ft depth



(c) Fore and Aft, location 2

Fig. 90 (Continued) — Representative overall and residual shock spectra for shots at 20-ft standoff, 15-ft depth

fact remove some of the pertinent frequency components.* In view of this, it is hardly surprising that the shock spectrum values should exhibit the same reaction to variation in test parameters that the peak velocities do.

Effects of Measurement Location

The shock spectrum velocities show much the same pattern as the peak velocities but with some interesting variations of questionable importance. The first is that the scatter of athwartship and fore-and-aft shock spectrum velocities is generally less than the scatter of the peak velocities. The scatter of most of the locations' vertical shock spectrum velocities is also less than that of the peak velocities, but one or two locations will be far enough out of line with the rest to make the overall scatter comparable to that of the peak velocities.

Effects of Measurement Orientation

The vertical shock spectrum velocities are comparable to and slightly larger than the peak velocities. The athwartship shock spectrum velocities are considerably smaller than the peak velocities (about 35-50%), and the fore-and-aft shock spectrum velocities are larger than the peak velocities (about 50%). Therefore, the shock spectrum velocities of the athwartship and fore-and-aft motions are much more comparable than are the peak velocities. The athwartship shock spectrum velocities average about 35%, and fore-and-aft 20%, of the corresponding vertical shock spectrum velocities (Figs. 91 through 95). Since the athwartship direction seems to be the stiffest, more of the velocity waveform will be supplied by high-frequency components which will not be noticed by the load-foundation system and will not contribute to the shock spectrum. In the fore-and-aft direction the waveform does seem to contain a substantial component in the area of the load-foundation fixed-base fundamental.

*Even so, the agreement is far better than was shown by the reed gage values on the MWSM anvil table, demonstrating the improvements in measurement and analysis capabilities in the intervening years.

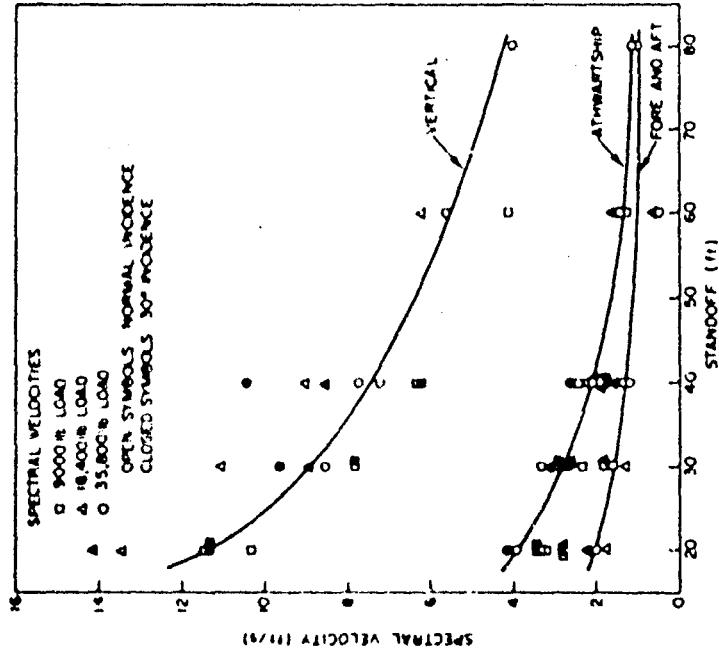


Fig. 92 - Spectral velocity vs standoff for 20-ft depth

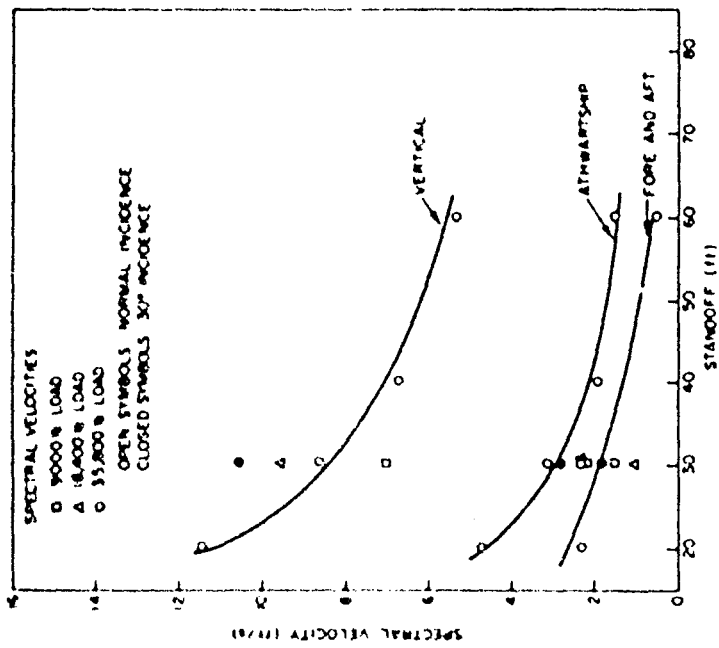


Fig. 91 - Spectral velocity vs standoff for 10-ft depth. As in Figs. 84 through 86, the trend lines of figs. 91 through 93 are of a fiducial character and roughly correspond to the behavior of the data for shots with a 35,800-lb load.

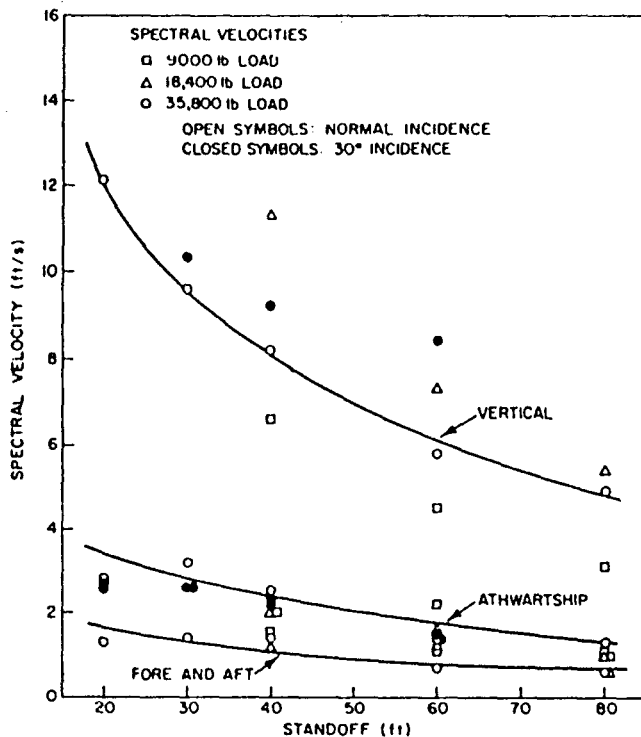


Fig. 93 - Spectral velocity vs standoff for 30-ft depth

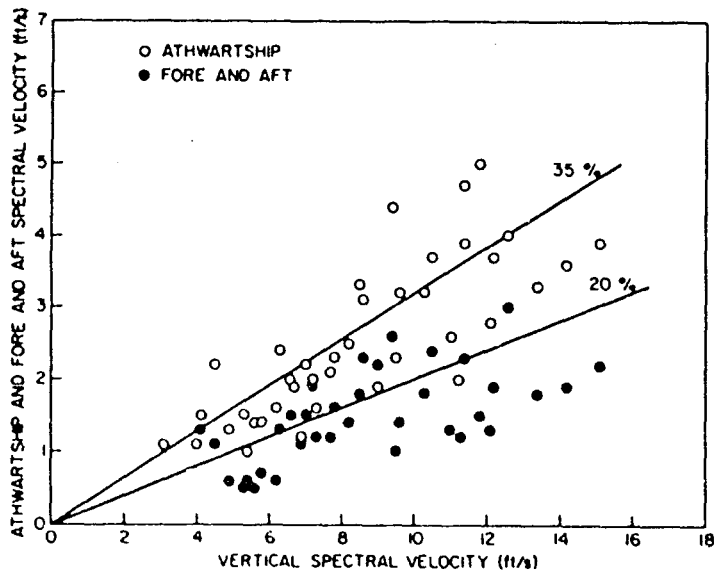


Fig. 94 - Athwartship and fore-and-aft spectral velocities as functions of vertical spectral velocity for normal incidence shots

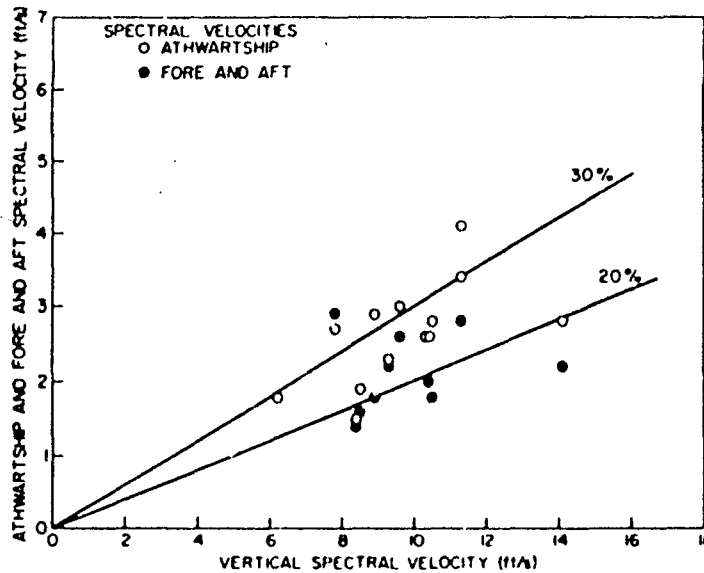


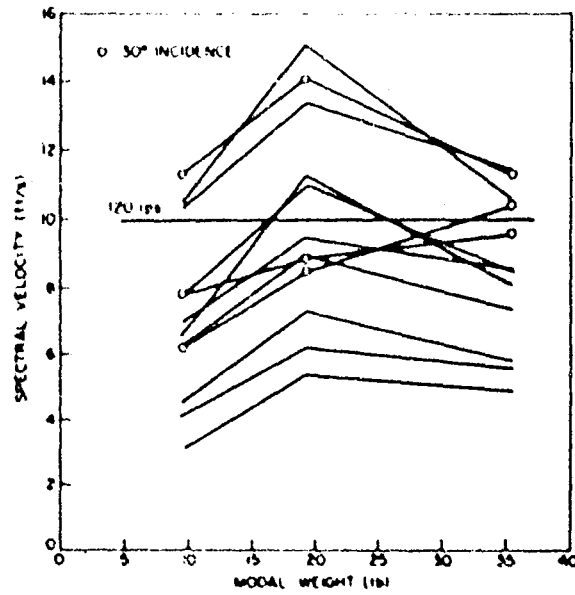
Fig. 95 — Athwartship and fore-and-aft spectral velocities as functions of vertical spectral velocity for 30° incidence shots

Effects of Load Weight

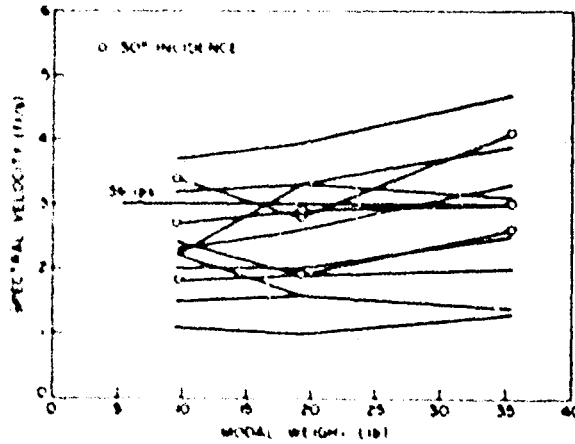
Dynamic analysis of structural shock response predicts that the shock spectrum velocity shock value should decrease smoothly as the modal mass increases. In the calibration tests, this did not occur (Figs. 91 through 93). If the modal mass associated with the first mode of each test load structure is taken as 80% of the total mass, the vertical shock spectrum velocity was found to peak at a modal weight of 14,720 lb and to decrease at 28,640 lb to a value which was still higher than that for 7200 lb. The athwartship shock spectrum velocity showed a similar action, though much less pronounced, and only the fore and aft exhibited the predicted uniform decline (Fig. 96).

Two possible contributing factors are that the shock input to the FSP is not entirely independent of load weight and that the load foundation deforms plastically for shots with the heavier loads. Investigations of a s.d.o.f. system with a yielding spring indicate that the shock spectrum value is higher than for a system of the same natural frequency with a linear spring. A similar effect may apply to more complicated structures. Other factors might include the imponderable action of multiple supports. The analysis of these factors involves enormous difficulties, and it is doubtful that a structure such as this test load will ever be feasible to model satisfactorily. A test series using loads designed specifically for the purpose would be more profitable.

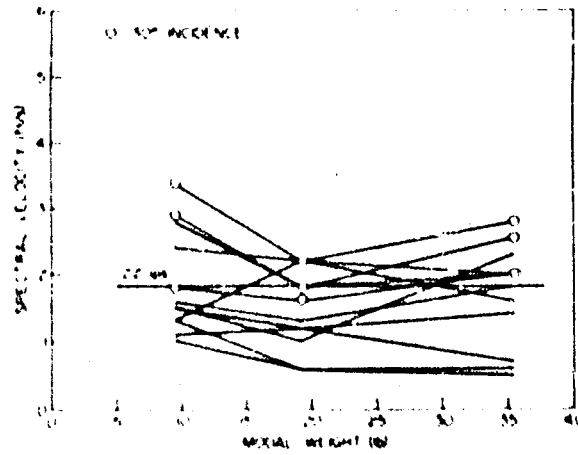
Since no clear trend for the influence of modal mass is discernible in the present data, the spectral parameters indicated in the design shock spectra for the most severe specification test shot (Fig. 97) represent the average values found over the range of calibration test loads. These spectra should be considered to apply to modes of any mass.



(a) Vertical



(b) Athwartship



(c) Fore and aft

Fig. 96 - Spectral velocities vs modal weight. The lines at 120 ips (vertical), 36 ips (athwartship), and 22 ips (fore and aft) represent the averages for the most severe shot of the specification test series.

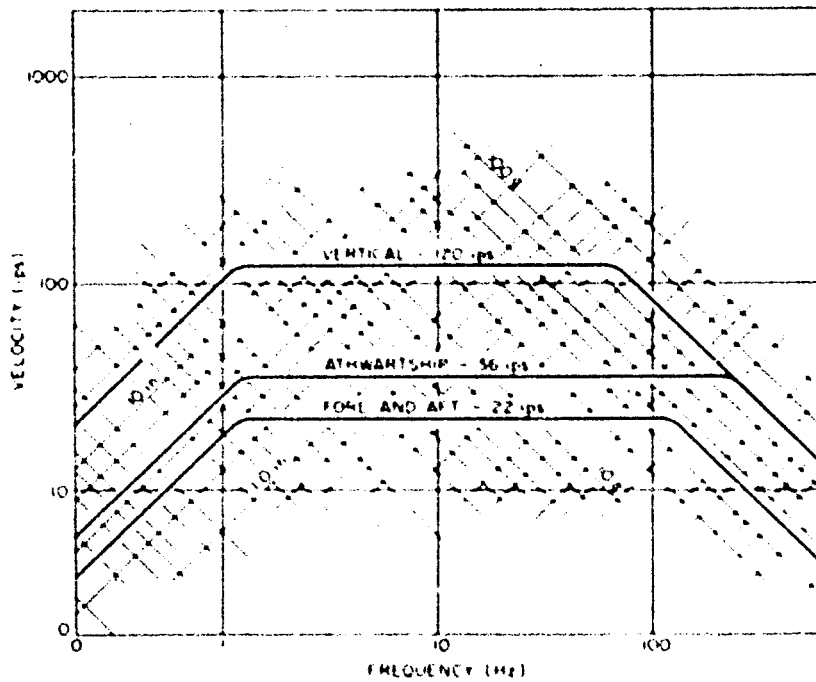


Fig. 97 - Design shock spectra for the FSP. The lower cut-off frequency for all directions is 1.15 Hz. The upper cutoffs are: vertical - 67 Hz, athwartship - 220 Hz, fore and aft - 125 Hz. These spectra should be used for all modal weights.

Effects of Charge Orientation

The effect of detonating the charge at 30° to the normal standoff direction is to enhance the fore-and-aft motions somewhat while decreasing those in the athwartship direction. This is demonstrated by the shock spectrum velocities, which drop to 30% of the vertical for athwartship and rise to something over 20% for fore and aft (Fig. 95).

Effects of Charge Depth

The effects of varying the depth of the detonation are predominately the geometrical changes in the aspect of the FSP. There are, of course, some differences due to venting of the gas bubble for the very shallow shots, but these are relatively minor so far as the shock environment aboard the FSP is concerned. Like the peak velocities, the shock spectrum velocities increase somewhat as the depth is increased to a value equal to the standoff, then are fairly constant. The athwartship shock spectrum velocity becomes a small fraction of the vertical until about the same depth, then also remains fairly constant. The fore-and-aft shock spectrum velocities do not seem to depend on the depth (Figs. 91 through 93).

Effects of Standoff

Charge standoff, the control parameter of the specification shock test, controls the shock spectrum velocities in the same way that it controls the peak velocities. It varies their magnitudes so that those at 80-ft standoff are about 30% of those at 20 ft and varies the relation of the component direction magnitudes by the change in geometrical arrangement (Figs. 91 through 93 and Table 4).

Effects of Charge Weight

As noted in the peak velocities, increasing the weight of the charge is slightly less influential in the shock severity than the shock factor indicates it should be done. Placement of 90-lb charges to produce both shock factors duplicating those of 60-lb charges and shock factors higher than those of 60-lb charges resulted in shock spectrum velocities about 6% lower than expected.

Reproducibility

Occasional shots were performed under test conditions duplicating those of earlier shots, with as many as 18 shots of various descriptions intervening. The variation in shock spectrum velocities at a particular measurement location was usually small but could be fairly large, possibly due to the constant rebuilding of the test load-foundation structure. When averaged over the measurement locations, the worst-case variation in shock spectrum velocity for duplicate shots was 16%, occurring in the spectra for the vertical motions. The variation for the other component directions was lower (Figs. 91 through 93).

DYNAMIC DESIGN FOR SHOCK RESISTANCE

Items weighing up to 40,000 lb (or in some cases 60,000 lb) can be tested for resistance to shipboard shock environments with the Navy shock testing device appropriate for their weights. This range will soon be extended to 320,000 lb. In the interim, items in excess

of 40,000 lb must rely largely on the calculated response as an indicator of shock resistance. Several methods for calculating these responses have been specified by the Navy at various times and have had various degrees of success.

Shock Design Numbers

One of the earlier methods of dynamic design required the use of "shock design numbers." These were presented as a set of three curves (for vertical, athwartship, and fore-and-aft shock) of static acceleration vs equipment weight. These curves seem to have been derived by starting at the average equivalent static acceleration found for loads on the LWSM, passing through values found for some ship tests, and proceeding to values considered to represent the feasible limit to construction of support structures for heavy propulsion components (Fig. 98).

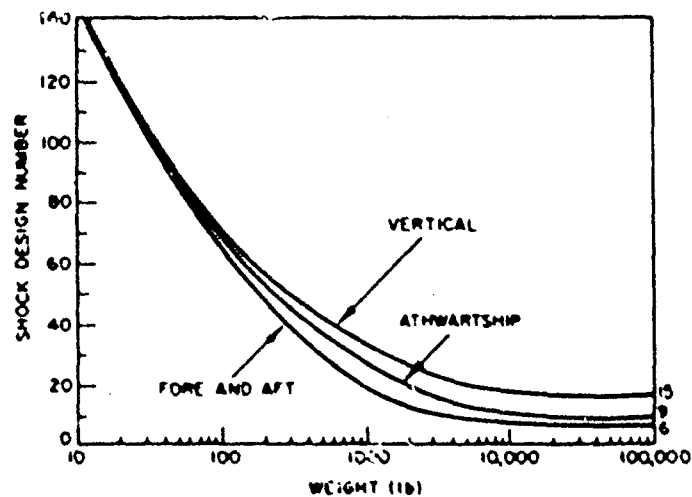


Fig. 98 - Shock design numbers. The numbers read from these curves were applied as weight multipliers at the equipment center of gravity to provide loading for a static analysis of hold-down bolts and supports.

In use, the static acceleration applying to a given equipment weight for each direction of shock was extracted from the appropriate curve and multiplied by the equipment weight to yield an equivalent force. This force was assumed to act at the center of gravity of the equipment, and a static analysis of the equipment mounting feet, hold-down bolts, and major structural members performed. Each shock direction was analyzed separately, and coupling between directions was not considered. This procedure could presumably be extended to include design of the foundation structure to which the equipment was attached, but this was not required and was not usually done.

Since this method ignores the interactions of equipment and ship, and the design curves were established on the basis of few data from outmoded vessels, the designs resulting were not realistic. Some equipments were undoubtedly overdesigned, and ship

shock tests revealed many to be underdesigned. Few, however, took leave of their mountings and traveled through the ship, which was what the method was originally intended to assure.

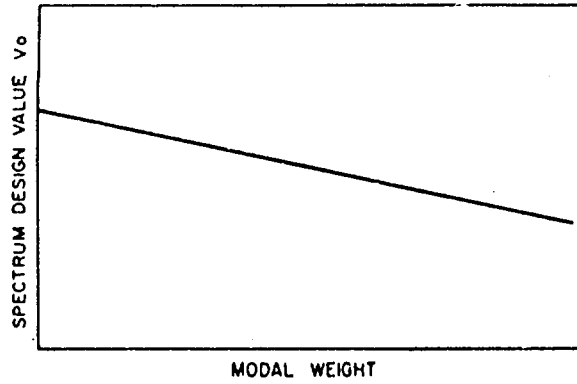
Dynamic Design Analysis Method (7)

Due to these inadequacies the shock design number procedure was supplanted by the Dynamic Design Analysis Method (DDAM). DDAM requires that the equipment be modeled and analyzed by a dynamic procedure using normal mode theory. Usually the models will be different for the three directions of shock input, but cross coupling is included by computing responses in all three directions to inputs in each direction. The inputs to be used for the shock analysis are presented as a design shock spectrum and curves of spectrum design value and of limiting acceleration vs modal weight. Since the primary application was intended to be to rigid-mounted equipments and few field data were available regarding ship displacements, the shock spectrum is represented as a velocity shock with an acceleration limit. In use, the input for each mode of the equipment model is determined by reading off the spectrum design value and limiting acceleration for the modal weight from the curves, then reading off the appropriate shock input at the modal frequency from the shock spectrum so defined (Fig. 99). Different curves and spectra are provided for each shock direction and for various locations on the several ship types. These were derived from measurements of ship tests by analysis of shock spectra and normal mode analysis of the equipments on which the measurements were made.

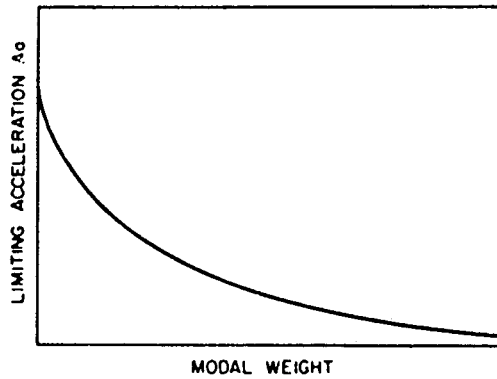
In general, this method has been very successful, but its users have not been uniformly proficient. The Navy has had to provide close guidance in the application of DDAM, and in some instances contractors have encountered difficulties in performing analyses which have contributed to extending ship lead times.

g Values

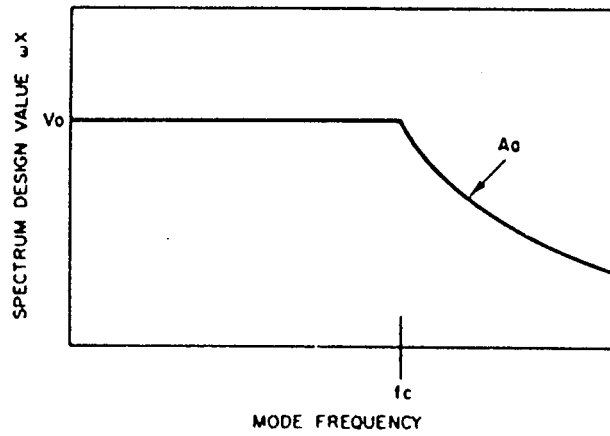
In view of the time required for dynamic analysis of some equipments, the present Navy approach to shock design separates items into two categories. The first consists of items whose dynamic analysis is expected (from past experience) to be straightforward and present little difficulty. For this category the shock design requirement is the application of the DDAM as outlined above. The second category consists of items for which detailed DDAM guidance cannot be provided, or for which production scheduling denies adequate time for dynamic analysis. For these items the Navy specifies a set of g values derived from previous analyses of similar equipments and from other appropriate sources. Like the earlier shock design numbers, the g values are to be used as center-of-gravity weight multipliers in a static analysis, the major difference being that the multipliers are provided for closely defined subsections of the equipment. In addition to designing to these static levels, the contractor is required to perform a concurrent dynamic analysis and identify any potentially unsatisfactory areas revealed by it. Dollar and time estimates of the cost of design fixes are to be furnished to the Navy and may be implemented at the option and expense of the Navy.



(a)



(b)



(c)

Fig. 99 — Examples of DDAM design curves. In part a the spectrum design value V_0 is read off corresponding to the modal weight. This is the value of the velocity shock region in part c, which shows how the spectrum design value ωX varies with frequency. Part b gives the limiting acceleration variation with modal weight.

SUMMARY

The Navy Shock testing devices for test items weighing up to 60,000 lb are the High-Impact Shock Machine for Lightweight Equipment, the High-Impact Shock Machine for Mediumweight Equipment, and the Floating Shock Platform. All provide about the same shock intensity to test loads, as shown by shock spectra and peak velocities. The major differences in the shock motions they generate are that the LWSM is rich in high-frequency components, that the motion of the FSP is triaxial, and that they have different displacement limits. The LWSM and MWSM are displacement limited at 1.5 inches and 3 inches respectively by mechanical stops. The FSP is displacement limited at 16.5, 5.1, and 3.0 inches in the vertical, athwartship, and fore-and-aft directions respectively by exhaustion of the driving energy. This large difference in displacement capability between the machines is of less consequence than it might seem. The bulk of shipboard items falling in the weight range of the LWSM and MWSM have mounting frequencies above the lower cutoff frequency of these machines (7-10 Hz), and the bulk of those items with mounting frequencies below this value are within the FSP weight range or heavier.

The anticipated addition of the large Floating Shock Platform to this family will extend the shock testing capability to 320,000 lb and perhaps higher in special cases. Over this entire range, the only gap in testing capability lies between 4800 and 6000 lb. The MWSM was designed for a maximum load of 4500 lb and can generate a shock environment of the full intensity with test loads of 4800 lb. For loads higher than this the test severity decreases. It would be advisable to consider ways in which the total load on the MWSM anvil table could be held to no more than 6000 lb, including transfer of shock testing to the FSP for items in the 5000- to 6000-lb range.

ACKNOWLEDGMENTS

The information presented here has been extracted principally from the publications of Conrad (20,23,24,28), Dick (21), Dick and Blake (29), Vigness (18), Belsheim (33), and unpublished material by Kaplan (34).

The publications given in the References span a period of approximately 25 years. During this period, the following people have figured prominently in NRL efforts toward the calibration of the Navy's shock testing devices by measurement and analysis of the motions they produce under standardized conditions. Most of these people did this work while at NRL; the others have their affiliations noted: J. L. Bachman, R. O. Belsheim, R. E. Blake, R. L. Bort, F. J. Bury, R. W. Conrad, K. C. Cowan, P. Cunniff, R. Daugherty (WCSF), A. F. Dick, H. M. Forkois, J. J. Harris, D. M. C. Hurt, E. Judd, R. E. Kaplan, C. L. Lamb, W. McDermott (WCSF), G. J. O'Hara, M. W. Olesen, L. P. Petak, R. J. Peters, P. Pida, G. Remmers, H. M. Schauer (UERD), C. Schrader (WCSF), R. Q. Tillman, I. Vigness, J. P. Walsh, J. W. Whyte, R. A. Willem, and S. E. Young.

Much of this work has been performed under the continuing sponsorship of the organization which is now the Ship Hardness Section, Code 6105G, of the Naval Ship Engineering Center: J. R. Sullivan and coworkers. A great deal of the research and development in the areas of shipboard shock and shock simulation has been rooted in the concern of this group with the combat effectiveness of Navy ships and its efforts to increase this effectiveness.

REFERENCES

1. C. M. Harris and C. E. Crede, editors "Shock and Vibration Handbook," McGraw-Hill, New York, Vol. 3, 1961.
2. R. H. Cole, "Underwater Explosions," Princeton U. Press, Princeton, 1948; reprinted by Dover, New York, S1384, 1965.
3. J. P. Walsh and R. E. Blake, "The Equivalent Static Acceleration of Shock Motions," NRL Report F-3302, June 1948.
4. L. S. Jacobsen and R. S. Ayre, "Engineering Vibrations," McGraw-Hill, New York, 1958.
5. Lord Rayleigh, "The Theory of Sound," MacMillan, New York, 2nd edition; reprinted by Dover, New York, 1945.
6. R. E. Blake and E. S. Swick, "Dynamics of Linear Elastic Structures," NRL Report 4420, Oct. 1954.
7. R. O. Belsheim and G. J. O'Hara, "Shock Design of Shipboard Equipment, Part 1 — Dynamic-Analysis Method," NRL Report 5545, Sept. 16, 1960.
8. J. P. Walsh and R. E. Blake, "The Determination of Shock Isolator Performance," NRL Report 3596, Jan. 6, 1950.
9. R. O. Belsheim and R. E. Blake, "Effect of Equipment Dynamic Reaction on Shock Motion of Foundations," NRL Report 5009, Oct. 23, 1957.
10. G. J. O'Hara, "Shock Spectra and Design Shock Spectra," NRL Report 5386, Nov. 1959.
11. L. P. Petak and R. E. Kaplan, "Resonance Testing in the Determination of Fixed Base Natural Frequencies of Shipboard Equipment," NRL Report 6176, Dec. 15, 1964.
12. G. J. O'Hara and L. P. Petak, "The Effect of a Second Mode and Nearby Structures on Shock Design Values," NRL Report 6676, Apr. 5, 1968.
13. C. T. Morrow and H. I. Sargeant, "Sawtooth Shock as a Component Test," J. Acoust. Soc. Am. 28, 959 (1956).
14. R. Lowe and R. D. Cavanaugh, "Correlation of Shock Spectra and Pulse Shape with Shock Environment," Environ. Eng. 1, No. 1 (1959).
15. G. J. O'Hara, "Effect Upon Shock Spectra of the Dynamic Reaction of Structures," NRL Report 5236, Dec. 16, 1958.
16. R. H. Oliver, "The History and Development of the High-Impact Shock-Testing Machine for Lightweight Equipment," Shock and Vibration Bull. 3, NRL Report S-3106, May 1947, pp. 3-8.
17. S. E. Young, "Effect of Modifications on the Performance Characteristics of the Lightweight, High-Impact Shock Machine," NRL Report V-2666, Oct. 1945.
18. I. Vigness, "Navy High-Impact Shock Machines for Lightweight and Mediumweight Equipment," NRL Report 5618, June 1, 1961.
19. R. G. Lorraine, "Lightweight Class HI Shock Machine Characteristics," Symposium on Shock, Vol. II, BuShips, Oct. 30, 1943.

20. R. W. Conrad, "Characteristics of the Lightweight High-Impact Shock Machine," NRL Report 3922, Jan. 23, 1952.
21. A. F. Dick, "Reed-Gage Shock-Spectrum Characteristics of Navy Lightweight High-Impact Shock Machine," NRL Report 4749, June 28, 1956.
22. G. W. Dorr, "Investigation of Characteristics of Mechanical Shock on HI Shock Machines," NRL Letter Report 3853-323A/ :GWD:mlhb, S and V Folder 502.
23. R. W. Conrad, "Class High-Impact Shock Machines for Lightweight Equipment: Comparison of Characteristics of Material Laboratory's and I-T-E Circuit Breaker Company's Machines," NRL Letter Report 6251-386A/56 mb, S and V Folder 707, Nov. 26, 1956.
24. R. W. Conrad, "Class High-impact Shock Machines for Lightweight Equipment: Investigation of Performance of I-T-E Circuit Breaker Company and Material Laboratory Machines," NRL Letter Report 6251-236A:RWC:mb, Aug. 19, 1957.
25. W. E. Carr, "Extension of Performance of Navy Lightweight HI Shock Machine," Bull. 33, Shock, Vibration, and Associated Environments, Part I, Feb. 1964, pp. 49-56.
26. T. P. Kirkpatrick, "Medium-Weight High-Impact Shock Machine Characteristics," Symposium on Shock, Vol. II, BuShips, Oct. 30, 1943, p. 48.
27. MIL-S-901C (NAVY), "Military Specification. Shock Tests, HI (High-Impact); Shipboard Machinery, Equipment, and Systems, Requirements for," Jan. 15, 1963.
28. R. W. Conrad, "Characteristics of Navy Medium-Weight High-Impact Shock Machine," NRL Report 3852, Sept. 14, 1951.
29. A. F. Dick and R. E. Blake, "Reed-Gage Shock-Spectrum Characteristics of Navy Medium-Weight High-Impact Shock Machine," NRL Report 4750, July 10, 1956.
30. I. Vigness and E. W. Clements, "Sawtooth and Half-Sine Shock Impulses from the Navy Shock Machine for Medium-Weight Equipment," NRL Report 5943, June 3, 1963.
31. "The Floating Shock Platform for Shock Testing Equipment Up to 30,000 Pounds," David Taylor Model Basin, Underwater Explosions Research Division (UERD) Report 7-61, May 1961.
32. M. W. Oleson, "Calibration Study of (SFNSY) Floating Shock Platform, Part 1 — Operations and Instrumentation," NRL Report 6069, Mar. 17, 1964.
33. R. O. Belsheim, "Preliminary Shock Design Criteria for Floating Shock Platform," NRL Letter Report 6260-7A:ROB:kep, Feb. 18, 1964.
34. R. E. Kaplan, "Calibration Study of (SFNSY) Floating Shock Platform, Part II — Analyses and Results," written in Dec. 1964, but unpublished.
35. R. A. Willem and R. L. Port, "Measured Rigid-Body Motions of the Floating Shock Platform for Testing Heavyweight Shipboard Equipment," NRL Letter Report 8440-114A:RLB:dd.

principal findings are: (1) The effect of various environments on crack growth in fatigue are qualitatively the same as those for crack growth under sustained loading. For example, water (liquid or vapor) increases the rate of crack growth both in fatigue and under sustained loads, the severity being dependent on the alloy composition and fracture toughness. Dehumidified hydrogen produces considerably more embrittlement than water vapor; however, the effect of hydrogen is nullified by the introduction of water vapor. The mechanism for environment-enhanced crack growth under both types of loading may then be the same. (2) Fractographic evidence, which shows the fracture paths are the same for fatigue and for sustained loading, tends to support the observation above. Other evidence, which shows that the fracture paths for crack growth in water, or water vapor-containing environment, and in dehumidified hydrogen are different, raises questions regarding "hydrogen embrittlement" as the mechanism for environment-enhanced crack growth in these environments. (3) The rate of fatigue-crack growth for high strength steels in an inert environment is nearly independent of the test frequency. In aggressive environments, it can be quite sensitive to the test frequency depending on the stress-corrosion susceptibility of the material. A prediction procedure for environment-enhanced fatigue-crack growth has been developed and will be discussed below. The influence of gaseous hydrogen on crack growth in a 18 Ni (250) maraging steel is being studied as a function of test temperature. Companion experiments were made on 18 Ni (300) maraging steel and AISI 4340 steel at room temperature. The results indicate that rate limiting speeds were attained in these steels. At room temperature, these speeds were in the range of 0.1 to 0.5 inch per minute. For the 18 Ni (250) maraging steel, the maximum rate-limiting speed occurred at 0 to 25 C; and severe crack branching occurred at temperatures below about -40C.

Correlation between Sustained-Load and Fatigue-Crack Growth. Based on previous observations that the mechanism for environment-enhanced crack growth under sustained loads and in fatigue may be the same, a simple superposition procedure for predicting the rate of fatigue crack growth in an aggressive environment is suggested. In this procedure the rate of fatigue-crack growth in an aggressive environment is considered to be equal to the algebraic sum of the rate of fatigue-crack growth in an inert reference environment and an environmental component, computed from sustained-load growth data and the load profile. This procedure permits characterization of "corrosion fatigue" from two sets of experimental data: (1) fatigue-crack growth data for an inert reference environment, and (2) sustained-load crack growth data in the appropriate aggressive environment. Results with Ti-8Al-1Mo alloy in salt water, H-11 steel, and AISI 4340 steel in distilled water and/or in humid environments, and 18 Ni (250) maraging steel in hydrogen, show that this procedure correctly predicts the influence of test frequency and qualitatively predicts the effect of mean load. Recent results on sustained-load crack growth for AISI 4340 steel in distilled water and other data indicate that the effect of mean load is also quantitatively correct. The procedure is only a first order approximation and does not take account of the "delay phenomenon" for fatigue due to overload, and is applicable only to specific alloy-environment systems. At stress intensity K levels below the apparent threshold level for stress-corrosion cracking, there appears to be some cooperative effects of fatigue and corrosion, and the proposed super-position procedure should not be applied. The possible mechanism(s) for this interaction are being studied.

Publications

"Fatigue-Crack Propagation in a High-Strength Aluminum Alloy," R. P. Wei, Intl. J. Fracture Mech. 4, 159 (1968)

"The Effect of D₂O on Fatigue-Crack Growth in a 7075-T6 Aluminum Alloy," R. P. Wei and J. D. Landes, Intl. J. Fracture Mech. 5, 69 (1969)

"Environmental Fatigue in Commercial Aluminum Alloys at Low Stress Intensities," J. A. Feeney, J. C. McMillan and R. P. Wei, Boeing Document No. D6-60114, May 1969, available from The Boeing Corporation

"Application of Fracture Mechanics to Stress Corrosion Cracking Studies," R. P. Wei, Proc. Intl. Conf. Fund. Aspects of Stress Corrosion Cracking, 104 (1969)

"Some Aspects of Environment-Enhanced Fatigue-Crack Growth," R. P. Wei, J. Eng. Fracture Mech. 1, 633 (1970)

"Fracture Mechanics and Corrosion Fatigue," A. J. McEvily and R. P. Wei, to be presented at the International Conference on Corrosion Fatigue, University of Connecticut, June 14-18, 1971 and published in the proceedings of the conference

"Crack Propagation Behavior in Steels," J. P. Gallagher and R. P. Wei, to be presented at the International Conference on Corrosion Fatigue, University of Connecticut, June 14-18, 1971 and published in the proceedings of the conference

"The Influence of Gaseous Hydrogen on Subcritical-Crack Growth in High-Strength Steels," R. P. Wei (to be published, 1971)

Lehigh University

ENVIRONMENT-ENHANCED FATIGUE

P. C. Paris and R. Bucci*

(*Graduate student)

Objectives

Environment-enhanced fatigue-crack growth in a titanium alloy is being studied as a function of load-time characteristics.

Approach

Sustained loading and fatigue characteristics of mill-annealed titanium-8Al-1Mo-1V in dry argon, distilled water, and 3.5% salt solution are being measured. Variations in frequency, load profile, and mean load are investigated to determine their effects on fatigue behavior of the alloy in the three environments.

Achievements

Fatigue results are plotted as the conventional cyclic growth rate, da/dN , vs. stress intensity amplitude, ΔK . In dry argon and in distilled water environments both load profile and frequency effects are slight and the only loading parameter which significantly alters fatigue behavior of the Ti-8-1-1 alloy is mean load. In contrast, Ti-8-1-1 fatigues in a 3.5% salt solution showed a considerable influence of frequency, mean load, and load profile on fatigue behavior. Data accumulated thus far indicates that the rate of fatigue crack growth of Ti-8-1-1 in a salt water system can be represented by the algebraic sum of the rate of fatigue-crack growth in an inert reference environment (dry argon) and an environmental component computed from sustained-load-crack-growth data obtained in salt water. This component is a quantity integrated over one cycle of fatigue loading and incorporates the effects of stress intensity factor variation with time. Environment-enhanced fatigue-crack growth has also been observed to occur at K levels below K_{scc} and work is currently under way to account for this effect.

Publication and Thesis

"Environment-Enhanced Fatigue in a Titanium Alloy and a Simple Model for the Assessment of Environmental Influence on Fatigue Behavior," R. Bucci, J. Eng. Fracture Mech., forthcoming

"Environment-Enhanced Fatigue in Titanium Alloys," Ph.D. thesis, Robert Bucci, June 1970

Invited Talks

Talk at ASTM E-24 Subcommittee 4, 1969

ASTM meeting, Philadelphia, March 23-25, 1970

Lehigh University

GENERAL FRACTURE MECHANICS

P. C. Paris

Objectives and Achievements

Articles on various aspects of fracture mechanics are being written for publication.

The major evidence bearing upon subcritical flaw growth in structural materials is reviewed and discussed, and the applicability of fracture mechanics concepts to flaw growth is demonstrated. Environmental cracking under static load, fatigue crack growth, and the combined effects of fatigue and aggressive environments are considered from a fracture mechanics point of view. Finally, engineering applications of the techniques and considerations discussed are indicated.

Publications

"Sub-Critical Flaw Growth," H. H. Johnson and P. C. Paris, Eng. Fracture Mech. 1, 1968 p. 3

Lehigh University

ELASTIC FIELD EQUATIONS FOR BLUNT CRACKS

P. C. Paris and M. Creager*

(*Graduate Student)

Objective

The elastic stress field equations for blunt cracks were derived and employed in analyzing a dissolution model for the arrest of stress-corrosion cracks by crack tip blunting.

Approach

Pertinent equations were developed and tabulated. The equations were employed in analyzing possible models for crack arrest in stress-corrosion cracks.

Achievements

The elastic stress field equations for blunt cracks were presented in a form equivalent to the usual sharp crack tip stress fields for each of the three loading modes. When these elastic stress field equations are incorporated into a stress-corrosion cracking model based upon material dissolution, indications are that for accelerated stress-corrosion cracking to occur the dissolution velocity should be more strongly dependent upon stress than a one-half power law. The relationship of dissolution velocity to stress is equally correct if there is a plastic zone in the vicinity of the crack tip, and therefore it may represent a "minimum criterion" for stress-corrosion cracking with material dissolution. The stress field equations presented have other applications as well.

Thesis

"The Elastic Stress Field Near the Tip of a Blunt Crack," M. Creager, M.S. Thesis, October 1966

Lehigh University

STRESS-CORROSION MODELS

P. C. Paris and M. Creager*

(*Graduate Student)

Objective

Theoretical models of stress corrosion at a macroscopic level were developed and investigated. Results were compared to experimental data generated elsewhere.

Approach

General models which involve changes in elastic constant, or which involve changes in maximum supportable stress were studied. Particular models of stress corrosion were then developed and the boundary value problems which arose were studied. A particular model having bulk diffusion as the rate-controlling process was investigated in detail and comparisons were made with the stress-corrosion behavior of steel and glass in water environments. The boundary-value problems describe the stress distribution in an infinite bi-material parabolic cylinder and the stress-assisted diffusion from the surface of a growing blunt crack.

Achievements

Some general descriptive models of stress corrosion in which the bulk material is treated as a continuum were derived with no assumptions being made as to rate-controlling processes. Various diffusion or reaction processes were subsequently considered. The stress distribution in an infinite bi-material parabolic cylinder, subjected to anti-plane loads on the free surface was found in closed form. The solution to the associated in-plane load problem was determined by the numerical solution of two coupled first-order ordinary differential equations. Using a modified form of Fick's law which includes the effect of a stress field, some concentration distributions were determined for the problem of diffusion from the surface of a growing blunt crack. For the diffusion model used and over the range of parameters investigated, the velocity of crack growth and the stress intensity factor are the most important parameters affecting the distribution of concentration of the diffusion species. The crack-tip radius is a less important parameter than either the stress intensity factor or the velocity. Stress-corrosion models which are based upon bulk diffusion as the rate-controlling process must consider the effects of both the stress intensity factor and the velocity of crack growth on the diffusion process itself. The model in which bulk diffusion of a damaging species is considered as the rate-controlling process describes the general character of the relationship between crack-growth velocity and stress-intensity factor as found experimentally for both glass and steel in water. Additional understanding of diffusion phenomena in the crack tip vicinity is necessary to describe clearly the role of hydrogen in stress corrosion of steels.

Thesis

"Stress Corrosion Models and Some Associated Boundary Value Problems,"
M. Creager, Ph.D. Thesis, Lehigh University, 1969

Lehigh University

STRESS-CORROSION CRACKING IN THE COPPER-GOLD SYSTEM

R. Bakish

Objective

Information relating to the effect of composition on the kinetics of cracking of copper-gold alloys was determined.

Approach

As-cast and homogenized specimens of Cu-Au alloys containing 97, 70, 50, 40, 35, and 25 wt-% copper were subjected to immersion tests in 2% FeCl_3 aqueous solution at room temperature and at 100°C for from 2 hours to 12 days. All tests were repeated using specimens which differed from the above only in having been plastically deformed by indentation. Specimens were examined metallographically after immersion, and their ductility was tested by indentation.

Achievements

After treatment at 100° , 97% copper alloys suffered general dissolution. Intermediate composition alloys showed copper leaching and oxidation within the alloy, accompanied by loss of ductility. Low copper content alloys were not attacked. After treatment at room temperature, the most consequential loss of strength was shown to take place with 70:30 and 50:50 alloys. General attack of the 97:3 alloy was observed, but embrittlement was lacking. The 60:40 alloy also did not show embrittlement although the reason for this behavior is not at all clear. No changes in behavior as a result of pre-indentation could be determined.

Lehigh University

STRAIN ELECTROMETRY OF ALUMINUM

H. Leidheiser, Jr., and E. Kellerman

Objective

The potential changes of aluminum wires in various electrolytes were observed after abrupt straining, and the effects of changing experimental parameters relating to stress-corrosion cracking problems were determined.

Approach

Annealed commercially pure aluminum wires immersed in sodium chloride solution or other electrolytes were abruptly strained 1.5-12%. The potential before straining and the changes in potential for one or more seconds after strain were recorded. Studies were made of the effects of varying the pH, altering the oxygen content of the solution, changing the anion or cation of the electrolyte, and anodizing or boiling the wires before stretching.

Achievements

The maximum potential achieved after straining in 0.1 M NaCl solution decreased with decrease in pH, but the rate of decay to the initial steady state value (-0.66v) was independent of pH over the range of 1.5 to 6.5. In deaerated solutions, decay to within 100 mv of the steady-state value occurred in less than 120 seconds, while in the presence of oxygen decay occurred much more rapidly. The oxygen content of the solution did not affect the initial portions of the potential-time curve. Increasing the amount of strain up to 6% increased the maximum potential. Above 6% strain the potential remained constant at V_{max} for periods of time which increased with increase in total strain. Boiling the wires before straining decreased the potential changes observed; the curves obtained at large strain were similar to the curves obtained at small strain with non-boiled wires. Anodizing the wires caused curves subjected to moderate strain to have the appearance of curves obtained at large strain with reference wires. Curves measured in NaCl, Na₂SO₄, sodium tartrate, and Na₂Cr₂O₇ solutions of equal ionic strength were similar under conditions of similar pretreatment of the wire. The following metallic cations were added in concentrations up to 1 M: aluminum, sodium, magnesium, zinc, cadmium, nickel, iron, lead and copper. Copper, above .01 M, and lead and iron at the highest concentrations reacted with the aluminum wire. Aluminum, sodium, and magnesium ions had little effect on the decay curves. For other added ions, the maximum potential change was decreased greatly, and plateau regions were observed in the decay portions of the curve. No change in the pH of the solution close to the wire could be determined. High purity aluminum wire gave standard strain electrometry curves very similar to those obtained with the commercially pure materials. An annealed 7075 alloy (T6 could not be strained as required for these experiments) gave a much smaller potential anodic shift after strain (400 mv at pH 5.5 compared to 900-1000 mv for the commercially pure aluminum).

Publications

"Strain Electrometry Studies of Aluminum," H. Leidheiser, Jr., and E. Kellerman, *Corrosion* 26, 1970, p.99

Invited Talks

"Basic Studies of Surface Phenomena and Their Relation to Corrosion", Henry Leidheiser, Jr., presented at ASTM meeting, Atlanta, Georgia, October 4, 1968

"Electrochemical Studies of Stress Corrosion Cracking of Aluminum Utilizing Strain Electrometry and Synthetic Cracks," H. Leidheiser, Jr., E. Kellerman, and V. V. Subba Rao, Presented at NACE Symposium on Fundamental Corrosion Research in Progress, Houston, March 1969

Lehigh University

FERROMAGNETIC STUDIES OF NICKEL

M. M. P. Janssen

Objective

The nature of the compressive stresses in thin nickel films deposited in UHV was studied. The amount and mechanisms of stress relief caused by gas adsorption on the films were investigated.

Approach

Thin nickel films were deposited at room temperature at better than 5×10^{-10} torr onto glass substrates. Ferromagnetic measurements on the films before and after admission of gases to the system were used to study the compressive stresses in the films and their relief upon admission of gas.

Achievements

Oxygen adsorption on clean films resulted in essentially complete stress relief. N_2O had the same effect indicating it decomposed on the Ni surface to nitrogen and oxygen. N_2 had no effect on the surface free energy, but γ_{Ni} was changed from 2500 dyne/cm to 200-500 dyne/cm in partial stress relief by CO, H_2 , H_2O or pyridine, and then to less than 100 dyne/cm by O_2 , N_2O or air. Films less than 100 Å thick were shown to have an island structure. Annealing thicker films at 250°C for 20 minutes resulted in apparent stress release. O_2 adsorption produced the same stress relief resonance shifts with either annealed or unannealed films. This last observation, coupled with the fact that for about 500 Å thick films 250°C is a good annealing temperature, is excellent evidence for the correctness of a surface tension model for the observed compressive stress. Any other form of stress would be removed by annealing.

Publications

"Release of Compressive Intrinsic Stress in Ultraclean Thin Nickel Films as a Result of Adsorption of Gases, "M. M. P. Janssen, J. Appl. Phys. 40, 1969, p. 3055

"FMR Study of Surface Tension Related Stress Effects in Ultraclean Nickel Thin Films, " M. M. P. Janssen, J. Appl. Phys. 41, 1970, p. 384

"Observation of Spin Wave Resonance in Nickel Thin Films after Adsorption of Oxygen, "M. M. P. Janssen, J. Appl. Phys. 41, 1970, p. 399

Lehigh University

CREVICE CORROSION OF ALUMINUM

H. Leidheiser, Jr., and V. V. Subba Rao

Objective

Potential differences between the sides and tip of a synthetic crack were investigated under a variety of conditions thought to relate to the conditions existing during crack propagation in stress-corrosion cracking experiments.

Approach

Synthetic cracks were constructed by sandwiching aluminum between glass cover slides. Two pieces of aluminum, not in electrical contact, were used, one corresponding to the base of the crack and another corresponding to the side of the crack. In some cases the aluminum corresponding to the base of the crack was a wire which could be stretched externally. Potential differences between the two pieces of aluminum were measured in sodium chloride solution as described below.

Achievements

The more interesting results are: 1) After several days the base of the crack became anodic to the side of the crack, probably reflecting the formation of an oxygen concentration cell with the base of the crack being oxygen-deficient. 2) Additions of acid to the base of the crack with a hypodermic needle caused the base to become anodic with respect to the side of the crack. The potential difference decayed over 24 hours when the acid became distributed evenly throughout the crack by diffusion and convection. 3) Addition of aluminum ions to the base of the crack made the base anodic to the side of the crack. 4) Straining the wire corresponding to the base of the crack caused an immediate and large anodic shift in the potential of the wire. In some cases the base of the crack remained significantly anodic to the side of the crack for several days after straining; in others, the potential difference tended towards zero after 24 hours.

Invited Talks

"Electrochemical Studies of Stress Corrosion Cracking of Aluminum Utilizing Strain Electrometry and Synthetic Cracks," H. Leidheiser, Jr., E. Kellerman, and V. V. Subba Rao, Presented at NACE Symposium on Fundamental Corrosion Research in Progress, Houston, March 1969.

Lehigh University

FERROMAGNETIC STUDIES OF IRON THIN FILMS

H. Leidheiser, Jr., and R. Kellerman*

(*Graduate student)

Objective

Studies are being made to determine the applicability of ferromagnetic resonance techniques to investigations of the interaction between clean iron surfaces and various gases.

Approach

The basic techniques of depositing a metal film in ultrahigh vacuum and observing its ferromagnetic resonance spectrum follow the nickel work done in this laboratory by Janssen (see his report). Iron, however, presents both physical and chemical problems not associated with nickel. In particular the very high demagnetizing field of iron has necessitated modification of the spectrometer to increase the magnetic field strength, and the very high chemical reactivity of iron has demanded rather elaborate cleaning techniques be applied to the iron wire from which the films are evaporated.

Achievements

A UHV apparatus, adapted for rigorous cleaning of the iron wire before evaporation of a thin film, has been constructed. The position of the ferromagnetic resonance is a function of film thickness for clean films; these observations are not in accord with published information. Multiple-line resonances have been observed with very thin films. The explanation for this observation is still being sought.

Changes in the position of the ferromagnetic resonance occur upon admission of either oxygen or hydrogen. Hydrogen gas, in the pressure range of 10^{-8} to 10^{-7} torr, causes a small irreversible and a larger reversible change in the resonance field upon varying the gas pressure. This observation is in accord with what is presently known about chemisorption in the iron-hydrogen system.

Radiotracer studies of adsorption on the very thin films are being carried out in an attempt to gain information about the morphology of these films.

Invited Talks

"Studies of Iron Surfaces Using Ferromagnetic Resonance," Henry Leidheiser, Jr., and Richard Kellerman, 44th National Colloid Symposium, Lehigh University, June 22, 1970.

"Ferromagnetic Resonance Techniques as a Means for Studying Chemisorption," Henry Leidheiser, Jr., Gordon Conference on Corrosion, July 27, 1971.

Lehigh University

CHEMISORPTION ON CLEAN METAL SURFACES

K. Klier

Objective

Interactions of carbon monoxide with bulk and single crystal metal surfaces have been studied to determine the structure, equilibria, and rates of surface reactions in adsorbed layers.

Approach

^{14}C -labeled carbon monoxide is adsorbed on UHV-cleaned metal surfaces. The measured quantities are: equilibrium amounts adsorbed, effective molecular cross sections at saturation, collision efficiencies ("sticking probabilities"), and the rates of exchange reactions between adsorbate and gas. Derived quantities are: heat of chemisorption (binding energy), lateral interaction energy, mobility, chemical potential, and actual molecular cross sections in the adsorbed state. A statistical mechanical theory developed by the author permits the determination of these quantities.

Achievements

The measurement of ^{14}C on small surfaces has been performed at pressures from 1×10^{-10} torr up, with a sensitivity of detecting adsorbates on areas of 0.1 mm^2 . The method is readily applicable to systems containing any organic adsorbate. Under the UHV conditions employed, metal surfaces studied remain clean (if made clean by ion and electron bombardments) and exhibit reproducible properties. The instrument used contains a UHV Geiger counter. On nickel single crystal planes of (100) and (110) orientation, the following results were obtained: The full description of state (p , V , T) was determined for the systems carbon monoxide plus (100) nickel and (110) nickel between 200 and 300°K and 10^{-9} - 10^{-1} torr. The effective molecular cross section of carbon monoxide on single crystal nickel surfaces was found to be 9 \AA^2 . The rates of adsorption and exchange were measured over a wide range of pressures and interpreted by a statistical mechanical theory which permitted three conclusions: 1) The binding energy of carbon monoxide on both planes is 25 - 26 kcal/mole, and the lateral interaction energy is of the order of 2 - 3 kcal/mole; 2) the adsorbate is mobile, and its chemical potential sharply rises at coverages of 9 - 11×10^{14} molecules/cm 2 , leading to extremely fast exchange between adsorbed and gaseous carbon monoxide molecules; and 3) the adsorbate is uniform if the crystal planes are clean and well annealed. If the crystal planes are chemically clean but geometrically rough, the adsorbate is heterogeneous, and its binding energies range probably from 40 kcal/mole to 25 kcal/mole. If the crystal planes are covered by chemisorbed oxygen or surface oxide, the chemisorption of carbon monoxide is reduced by approximately two orders of magnitude. The theory of adsorption and exchange rates also quantitatively explains the adsorption equilibria. Clean surfaces behave differently if they are atomically smooth or if they are rough. The adsorbate on rough surfaces is tightly bound and fixed while the adsorbate on smooth surfaces is weakly bound and mobile. This may be of some importance to stress-corrosion cracking in that the chance for weak chemisorption in cracks will increase if the crack surface can be made smooth by some annealing procedure. On bulk polycrystalline iron and iron single crystal planes of (111), (110), and (100) orientation the behavior of rough iron surfaces is similar to that of nickel. On

smooth iron surfaces, no matter whether in single crystal or polycrystalline form, carbon monoxide chemisorption saturates at about 10% of the saturation value for nickel, and the sticking probabilities are generally very low. This may be an ultimate manifestation of the relative inertness of smooth surfaces but may also be due to some undetected contamination of the iron surface. Great care was taken to avoid carbon, oxygen, and water contamination. Some of the iron surfaces were cleaned for hours by argon bombardment in UHV, but their "inertness" towards CO after temperature annealing did not change. Work is continuing on maraging steels.

Publications

"A Geiger-Muller Counter for Ultrahigh Vacuum Systems," K. Klier, Rev. Scientific Inst. 40, 1969, p. 372

"Chemisorption of Carbon Monoxide on (110) and (100) Nickel Crystal Faces," K. Klier, A. C. Zettlemoyer and H. Leidheiser, Jr., J. Chem. Phys. 52, 1970, pp. 589-602.

Invited Talks

"Interaction of Carbon Monoxide with Clean Nickel Surfaces," K. Klier and A. C. Zettlemoyer, presented at 156th National ACS Meeting, Atlantic City, Sept. 1968

"Exchange Reactions at Interfaces," invited lecture at Dept. of Chemistry, The Johns Hopkins University, Nov. 1968

"Radiotracer Studies of Adsorption on Ultraclean Surfaces," Kamil Klier, Gordon Conference on Corrosion, July 1969

"Adsorption of Carbon Monoxide on Iron Using Radiotracer Techniques," Kamil Klier, 44th National Colloid Symposium, June 22, 1970

Lehigh University

RARE GAS (ARGON) ION BOMBARDMENT

R. Coughlin, H. Leidheiser, Jr., and E. Chornet*

(*Graduate Student)

Objective

The binding energies and ion-sticking probabilities of argon atoms on nickel, iron, and titanium are being studied.

Approach

Argon atoms, previously incorporated in a wire as a result of ion bombardment, were thermally released by a 2 to 10 second flash. Ultrahigh vacuum conditions (less than 3×10^{-10} torr), a hot tungsten filament and molybdenum grid bombarding unit, a Bayard-Alpert ionization gauge pressure sensor, and a quadrupole residual gas analyzer were used. The polycrystalline specimens were chemically polished, sealed into the vacuum system, and degassed thoroughly until the pressure in the system with the wire hot could be maintained in the 10^{-10} torr range. Maximum degassing temperatures were: nickel, 1000°C; iron, 875°C; titanium, 900°C. The wires were ion bombarded in 5 minute intervals. Each bombardment was followed by a 30-minute annealing period, and the total bombarding time before any flash was about 1 hour. Nickel and iron were also reduced and decarburized by heating specimens in hydrogen at temperatures between 600° and 800° during two cycles of 16 hours each.

Achievements

For nickel the number of impinging ions ranged from 3×10^{13} to 10^{17} ions/cm², that of desorbing argon atoms from 2×10^{12} to 10^{14} atoms/cm² from which the sticking probability of argon on nickel was obtained. The pressure spectra on raising the wire temperature revealed six different peaks for a high number (more than 10^{16} ions/cm²) of incident ions and only three distinct peaks at 10^{14} ions/cm² or less. The energies of the binding states (peaks) are being calculated. On titanium, experiments with a high number of incident ions were carried out. The presence of three binding states was observed. Analysis of the first two peaks showed energies of 32 and 56 kcal/mole. The third peak, of a higher energy, is poorly resolved and did not allow quantitative estimation. For iron, only one peak has been found although the cleaning procedure has not yet been completed. The nickel calculations will be continued, a complete set of iron experiments will be performed, and the titanium behavior at a low incident number of ions will be studied.

Invited Talks

"Flash Desorption of Argon Imbedded Within Iron, Nickel and Titanium," E. Chornet, R. N. Coughlin, and Henry Leidheiser, Jr., 44th National Colloid Symposium, Lehigh University, June 22, 1970

Lehigh University

FLASH FILAMENT STUDIES

R. Goughlin, H. Leidheiser, Jr., and E. Chornet*

(*Graduate student)

Objective

A comparative study of the chemisorption of hydrogen on clean surfaces of nickel, iron and titanium, with extension to the methanol-titanium system, has been carried out.

Approach

The flash filament technique gives information concerning the rates of adsorption and desorption, and the nature and binding energies of the adsorbed species.

Achievements

Sorption and desorption rates and sorption equilibria of hydrogen have been investigated on polycrystalline filaments of nickel, iron, and titanium under ultrahigh vacuum conditions using the flash desorption technique. The wires were cleaned by argon-ion bombardment followed by heating.

On nickel, hydrogen atoms exist on the surface at 298°K. as a single phase. The dissociated hydrogen recombines upon desorption with a constant activation energy of 17.5 kcal/mole up to the maximum coverage explored, 0.5×10^{15} atoms/cm². A low sticking probability of 3×10^{-3} was explained by the presence of a weakly-bonded precursor state.

A single phase of adsorbed hydrogen atoms was also found on iron. Desorption follows a second-order reaction with an activation energy of 20.3 kcal/mole, which value remains constant up to 0.2×10^{15} atoms/cm² and then decreases with further coverage. Entropy calculations indicate that the adsorbate is mobile and its behavior approaches that of an ideal two-dimensional gas. The initial rates of adsorption are explained in terms of an activated complex, molecular in nature, which loses rotational freedom with respect to the gas phase and requires about 0.5 kcal/mole to dissociate. Lateral interactions are included in the interpretation.

On both nickel and iron, a second, small desorption peak appears at high temperatures at long exposure times, suggesting diffusion of hydrogen into the interior.

Hydrogen readily penetrates titanium at room temperature; the penetration is appreciable at 130°K. Sorption at 400°K. and higher temperatures follows the solubility laws of hydrogen in titanium. Two distinct peaks were found upon desorption. The peak at 100°K. is consistent with a first-order reaction with an activation energy of 4 kcal/mole. A second broad peak at higher temperatures is indicative of both surface and bulk hydrogen. At 298°K. and lower temperatures, the sorption rate is a linear function of pressure.

The initial heats of adsorption of hydrogen on nickel, iron, and titanium are consistently lower than values reported by other workers who used evaporated films. The low and nearly constant heats of adsorption are a characteristic of the clean and smooth surfaces used in this work.

When a clean titanium surface is exposed to methanol, hydrogen penetrates into titanium. Upon flashing, there is a violent reaction accompanied by a substantial decrease in the amount of carbon monoxide as determined mass spectrometrically. This reaction contaminates the surface and subsequent adsorption of hydrogen proceeds at a much lower rate than in the case of a fresh surface.

Pretreatment of metal wires by argon-ion bombardment, followed by annealing, produces a clean reproducible surface on nickel, iron, and titanium. Small quantities of carbon monoxide in the gas phase (5×10^{-9} torr partial pressure) results in contamination of the surfaces during argon-ion bombardment as judged from the negligible amounts of hydrogen adsorbed. Hydrogen chemisorption provides a useful criterion of cleanliness of a surface.

Thesis

"Flash Desorption of Hydrogen on Clean Nickel, Iron and Titanium Wires,"
Esteban Chornet, Ph.D. Thesis, Lehigh University, submitted to the faculty for
action, June 1971

Lehigh University

⁵⁷MOSSBAUER SPECTROSCOPY OF SURFACES

H. Leidheiser, Jr., G. W. Simmons, and E. Kellerman

Objectives

The purpose of this study is to determine the applicability of ⁵⁷Mössbauer Spectroscopy to analysis of very thin surface films on iron and steels.

Achievements

⁵⁷Mössbauer spectroscopy is a form of resonance spectroscopy involving gamma-rays with energies of 10-100 keV. The iron isotope, Fe-57, present in natural iron to the extent of approximately 2%, is a ⁵⁷Mössbauer-active species and resonantly absorbs the 14.4 keV gamma-ray emitted by the activated state of Fe-57. Information about the chemical environment of an iron atom and its magnetic properties can be obtained from such experimental parameters as the chemical shift, quadrupole split, the magnetic hyperfine splitting, and the superparamagnetic characteristics.

Techniques have been developed for improving the applicability of ⁵⁷Mössbauer spectroscopy to the study of iron surfaces. The K-conversion and Auger electrons which are emitted following resonance absorption of the 14.4 keV incident gamma-ray are detected in 2- π geometry. Further enhancement of the sensitivity for detection of species at the surface is made by enrichment of the surface of the sample with electro-deposited Fe-57.

The passive film on iron, 15-50 Å in thickness, formed by immersion in sodium nitrite solution or by anodic treatment in sulfuric acid or borate electrolytes, is readily studied by the electron-detection technique. The experimental results obtained to date suggest that the major component in the passive film on iron is gamma-Fe₂O₃. The thinner films exhibit superparamagnetic behavior whereas the thicker films show magnetic hyperfine splitting.

⁵⁷Mössbauer spectroscopy is proving to be a powerful tool for surface studies of iron and steel.

Invited Talks

"Studies of Surfaces Using ⁵⁷Mössbauer Spectroscopy," H. Leidheiser, Jr., First Conference on Colloid and Surface Chemistry, Hungarian Academy of Sciences, Matrafüred, Hungary, May 24, 1971

"⁵⁷Mössbauer Spectroscopy of the Passive Film on Iron," Gary W. Simmons, Elsie Kellerman, and Henry Leidheiser, Jr., to be presented at meeting of the Electrochemical Society, Cleveland, October, 1971

Lehigh University

HYDROGEN ABSORPTION BY ALUMINUM

H. Leidheiser, Jr., and N. Das*

(*Graduate student)

Objective

The hydrogen which passes into aluminum during reaction with various aqueous solutions is being determined. Correlations between hydrogen dissolution and stress-corrosion cracking and fatigue properties are being sought.

Approach

Vacuum extraction at 600°C and 10^{-6} torr is used to measure the amount of hydrogen present in aluminum after exposure to aqueous solutions at 60° and 100°. After vacuum treatment, aluminum samples with various surface/volume ratios are exposed to water for several minutes to 24 hours. The hydrated oxide formed during corrosion is removed with a chromic acid-phosphoric acid solution before extraction. Differentiation between the hydrogen formed as a consequence of reaction with water and the hydrogen formed by the reaction of the hydrated film with aluminum during extraction is made by appropriate use of D_2O and H_2O in formulating the reactive solutions. The extracted gas is then analyzed mass spectrometrically.

Achievements

The total amount of hydrogen which penetrates into aluminum during reaction with water at 100° is linearly related to the surface area. A typical result for a sample exposed to pure water for 24 hours at 100° is 0.00017 ml./cm². For this particular sample, the total amount of hydrogen is equivalent to 0.056 ml./100 g. of aluminum.

Lehigh University

REVIEW OF THE ALUMINUM-HYDROGEN SYSTEM

R. D. Iyengar and H. Leidheiser, Jr.

Objective

A review of the literature concerning the aluminum-hydrogen system was prepared.

Achievements

Published data for the aluminum-hydrogen system were reviewed. The adsorption of hydrogen on aluminum and the effect thereon of the oxide layer were considered. In addition, reports of the diffusion of hydrogen in aluminum and of the solubility of hydrogen in aluminum and its alloys were listed and discussed.

Publication

"The Aluminum-Hydrogen System: A Review", R. D. Iyengar and H. Leidheiser, Jr., report distributed to ARPA participants.

Lehigh University

REVIEW OF HYDROGEN IN IRON

H. Leidheiser, Jr., and E. Kellerman

Objective

An annotated bibliography of the literature concerning the effect of environment on the diffusion of hydrogen in iron and steel is being prepared.

Achievements

Published data for the diffusion of hydrogen in iron were surveyed. Reports in the literature of the effect of solution composition on the penetration of electrolytically generated hydrogen into iron and steel were collected.

Lehigh University

THE FRACTURE OF MICA

P. C. Paris and R. Leonesio*

(*Graduate Student)

Objective

The influence of moisture on the fracture energy of mica crystals is being studied.

Approach

The use of double cantilever beam specimens permits the fracture energy of uniformly thick mica crystals to be determined from $G = 3 \Delta^2 / 2bKL^4$ where G is the splitting energy in ergs/cm², Δ is the total displacement of the ends of the beam, L is the crack length, b is the width of the specimen, and K is a constant representing the elastic stiffness of the beams. The value of K varies from specimen to specimen and is found experimentally for each specimen used. Muscovite mica was split in water, in air with varying humidity, in helium with varying humidity, and in dry helium. The crack tip was located with a travelling microscope, and Δ was measured with another microscope. The water experiments were done by immersing the bottom of the specimen so that the water surface was above the crack tip. The experiments at various relative humidities were done in a glass chamber. Varying amounts of moisture were introduced by heating the bulb. The dew points of the gas leaving the chamber was measured with a dew point hygrometer, and the relative humidity was then calculated from the corresponding vapor pressures. Zero humidity conditions were reached by first baking the system at 200°C for at least one hour under mechanical pump vacuum, and then passing high purity helium through a liquid nitrogen cold trap and into the chamber.

Achievements

The fracture energy of mica in water varied between 150 and 250 ergs/cm² for the several specimens tested. This energy is virtually independent of crack velocity from 0.1 micro-inch/sec to 10,000 micro/inches/sec. When tested as a function of relative humidity in both helium and air, the fracture energy varied uniformly from 350 ergs/cm² at 100% relative humidity to 600 ergs/cm² at 2 to 5% relative humidity. Further testing is being done to determine any shift in energy with a change in temperature. Below 5% relative humidity and especially at 0% relative humidity the data points showed much scatter. Values for the fracture energy varied from 600 ergs/cm² to 3,000 ergs/cm² at atmospheric pressure and room temperature, and from 1,000 ergs/cm² to 14,000 ergs/cm² in a vacuum of about 10⁻² mm. of mercury. These results indicate that for very low humidity the fracture energy of mica is strongly dependent on impurities within the system. A unique feature which mica possesses is its ability to reheel itself upon load release. The crystal can then be resplit and a new fracture energy measured. For mica resplit in water and in moist helium or air, the energy for refracturing is always lower than that of the original fracture. This is to be expected because adsorbed moisture trapped between resealed layers will lower the energy needed for the second fracture. In a dry environment in many cases the energy for resplitting was found to be greater than the

original fracture energy. This phenomenon was observed in environments of air, helium, hydrogen, and carbon dioxide, and also under mechanical pump vacuum. That the energies for refracturing were sometimes two or three times higher than the original fracture energy was totally unexpected and is as yet unexplained.

Thesis

"Environmental Effects on the Fracture of Mica Crystals," Robert B. Leonesio, Ph.D.
Thesis, June 1970

Lehigh University

GLASS CRACKING

E. Sommer and G. Irwin

Objective

New apparatus, experimental techniques, and mathematical methods of analysis applicable to fracture mechanics studies of glass were investigated.

Approach

An apparatus was designed and constructed for propagating cracks in glass, and an interference method was developed whereby the opening displacement of the cracks can be accurately and simply determined. Experimental results were compared to analytical predictions.

Achievements

Using a travelling microscope mounted on an optical bench associated with an eccentric loading apparatus, simple measurements of the interference fringes produced by monochromatic illumination of a crack tip were used to determine accurately the opening displacement of cracks in glass. Some studies of plastics were also attempted. Results of glass cracking under eccentric tension load were compared with analytical prediction from the boundary collection method and from Westergaard analysis as detailed in the second publication listed below. Additionally, since the crack opening displacement is analytically related to the stress intensity factor, K , a K -calibration curve for the crack-line-loaded, single-edge notched plate was established. Finally an original method for crack initiation in glass was investigated.

Publications

"A Remark on Crack Initiation in Glass Plates," E. Sommer, Eng. Fracture Mech., to be published.

"An Optical Method for Determining the Crack-Tip Stress Intensity Factor," E. Sommer, Eng. Fracture Mech., to be published.

Lehigh University

RUTILE STUDIES BY ELECTRON SPIN RESONANCE

R. D. Iyengar

Objective

Further characterizations of the oxygen species produced by oxidation of outgassed rutile powders were made.

Approach

Standard ESR techniques were used to determine spectra of powdered rutile samples which had been outgassed and then treated with oxides of nitrogen under various conditions.

Achievements

Nitrogen dioxide restored the oxygen deficiency at the surface of outgassed rutile, and produced a signal which has been attributed to O_2^+ . Nitrous oxide reacted with rutile to produce the same signal. Neither oxide of nitrogen produced O_2^- on interaction with vacuum-outgassed high-area rutile.

Publications

"An ESR Study of the Nature of the Surface Oxygen During Oxidation of a Non-stoichiometric Rutile Surface with Oxides of Nitrogen," R. D. Iyengar, M. Codell and J. Turkevich, *J. Catalysis* 9, 1967, p. 305

Lehigh University

ELECTRON SPIN RESONANCES STUDIES OF ZINC OXIDE

R. D. Iyengar and V. V. Subba Rao

Objective

Identification of the chemical species formed by surface interaction of zinc oxide with oxygen, chlorine, nitrobenzene, oxides of nitrogen, and tertiary butyl hydroperoxide was sought.

Approach

Electron spin resonance spectra were recorded after treatment of vacuum-outgassed ZnO with NO_2 , NO, N_2O , O_2 , Cl_2 , nitrobenzene, and tertiary butyl hydroperoxide. From variations in the spectra with further treatments such as outgassing, heating and/or cooling, as well as from power variation studies, the ESR results were correlated with species formed on the oxide surface.

Achievements

Both NO_2 and NO were found to be adsorbed as rigid neutral molecules. Confirmation of the assignment was provided by the use of the two adsorbates enriched in ^{15}N . The origin and identity of the signals produced by N_2O , NO, or Cl_2 were investigated, but no final conclusions concerning the species involved could be reached. Nitrobenzene on the oxide surface was converted to the anion radical. With tertiary butyl hydroperoxide two signals are formed which can be understood in terms of oxygen ion vacancies and interstitial zinc ions.

Publications

"Electron Spin Resonance of Nitrogen Dioxide (NO_2) Adsorbed on Zinc Oxide," R. D. Iyengar and V. V. Subba Rao, *J. Am. Chem. Soc.* 90, 1968, p. 3267

"ESR Studies of the Interaction of O_2 , NO_2 , N_2O and Cl_2 with Zinc Oxide," R. D. Iyengar, V. V. Subba Rao and A. C. Zettlemoyer, *Surface Science* 13, 1969, p. 251

"An ESR Investigation of Nitrobenzene Adsorbed on Zinc Oxide," V. V. Subba Rao, R. D. Iyengar, and A. C. Zettlemoyer, *J. Catalysis* 12, 1968, p. 278

"Electron Spin Resonance Study of Hydroperoxide on Zinc Oxide," M. Codell, H. Gisser, J. Weisberg, and R. D. Iyengar, *J. Phys. Chem.* 72, 1968, p. 2460

Lehigh University

ELECTRON SPIN RESONANCE STUDIES OF TITANIUM DIOXIDE

R. D. Iyengar and R. Kellerman*

(*Graduate Student)

Objective

Identification of the source of two of the more frequently observed ESR signals from oxygen-treated rutile and anatase was sought.

Approach

Standard ESR techniques including determinations of hyperfine splitting and isotopic substitution were employed. Sample pretreatments (e.g., outgassing and oxygen exposure) were varied, and the source and preparation method of the samples (ammonia-precipitated TiO_2 was compared to other types of TiO_2) were changed to determine the cause of the observed signals.

Achievements

The two signals were shown to be due to impurity centers. Final identification of these centers was not made, but by a comparison of the known hyperfine splitting associated with the ^{14}N nucleus and the change in the spectrum when ^{14}N was replaced by ^{15}N , they were shown to involve nitrogen. The origin of the nitrogen impurity was established as being the ammonia precipitation stage of rutile manufacture.

Publications

"Formation and Nature of Radical Species in the Oxidation of Precipitated Titanium Dioxide," R. D. Iyengar and R. Kellerman, *Z. Phys. Chem., N. F.* **64**, 1969, p. 345

"The Nature of Paramagnetic Species Observed in Ammonia-Precipitated TiO_2 Powders," R. D. Iyengar and R. Kellerman, *J. Catalysis* **12**, 1968, p. 107

Yale University

LOW ENERGY ELECTRON DIFFRACTION

W. D. Robertson, J. V. Florio, D. G. Fedak*, and Robert Zimmer*

(* Graduate Student)

Objective

Determination of the atomic structure and composition of surfaces.

Approach

Surface structure, unit cell parameters and unit cell contents, are determined by low energy electron diffraction (LEED) observations. Surface composition is determined by Auger electron spectroscopy. Reactivity of surfaces and identification of reaction products are studied by flash desorption into a mass-spectrometer. All these determinations are carried out on the same surface, in the same vacuum space, as functions of pressure, temperature, and time.

Achievements

1. To perform the operations outlined above, it is first of all necessary to develop techniques for transforming measured LEED intensity into surface structure. An optical simulation technique was first developed for this purpose (see bibliography). The results of the optical technique led to a reconsideration of the scattering mechanism, and a complete computer program for simulation. Subsequently, the entire physical process of multiple elastic and inelastic scattering of low energy electrons was formulated and is now being programmed on the Yale Computer by Dr. Brian Holland and Dr. Richard Hannum. It appears that this program, and that of C. B. Duke (at General Electric) are the only two physically realistic treatments of the LEED interpretation problem.
2. The combined operation of structure and composition analysis has been performed on silicon by Dr. John Florio with the following results, which are being submitted for publication. Auger electron emission spectroscopy has been used to identify and, with suitable calibration, to quantitatively specify chlorine surface concentrations on Si(111) surfaces. Adsorption rates of Cl_2 on Si(111)7 and Si(111) $\sqrt{19}$ surfaces have been measured as a function of substrate temperature, and sticking probabilities have been subsequently calculated. The initial sticking probability is in the range 0.1 to 0.2. Adsorbed chlorine is observed to exist in two states, one, weakly bound and the other, strongly bound to the surface.

Electron beam desorption of chlorine from Si(111) surfaces can be significant with a focussed electron beam. Starting with an ordered (1x1) chlorine structure, the result of beam desorption is a disordered surface. The electron beam desorption cross-section for chlorine was calculated to be $2 \times 10^{-19} \text{ cm}^2$.

Various LEED structures were observed for chlorine on Si(111) surfaces. These include two with chlorine monolayer concentrations, Si(111)7*-Cl and Si(111)1*-Cl, and a third with only a trace (4-5% of a monolayer) of chlorine present, Si(111)1. The 1x1 structures at high and low coverage are different, as shown by the voltage dependence of the reflected beam intensities.

The reaction between chlorine and the Si(111) surface follows second order kinetics in its dependence on chlorine surface concentration. The desorption reaction product is SiCl_4 . From the temperature dependence of the rate constant, an activation energy of ~ 35 kcal/mol for the desorption process was measured. A reaction mechanism, involving the surface species $[\text{>SiCl}_2]$ which is formed on the surface ledge at the junction of (001) and (111) planes, is suggested.

Detailed analysis of the structure of silicon surfaces in different states, which can be obtained from LEED intensity data, is currently being performed. This data will also be employed to test the new formulation of the scattering problem and the computer program which calculates the intensity from an assumed structural model.

Publications

D. G. Fedak, T. E. Fischer, W. D. Robertson, "Surface Structure Analysis by Optical Simulation of LEED Patterns", *J. Applied Physics* **39**, 5658 (1968).

D. G. Fedak, J. V. Florio, W. D. Robertson, "The Interaction between Chlorine and the (100) Surface of Gold", to be published in *Structure and Chemistry of Solid Surfaces*, G. A. Somorjai et al., Eds., John Wiley and Sons, Inc., New York, 1969.

J. V. Florio, W. D. Robertson, "Chlorine Reactions on the Si(111) Surface", submitted to *Surface Science*, April 1969.

Invited Presentations

American Institute of Chemical Engineers, Annual Meeting, 1968.

Department of Materials Science, University of Pennsylvania, 1968.

International Nickel Company Research Laboratory, Sterling Forest, New York, 1968.

Kennecott Copper Corporation, Research Laboratory, Legermont, Massachusetts, 1968.

Naval Research Laboratory

STRESS-CORROSION CRACKING (General)

B. F. Brown

Objective

To present general and tutorial reviews of the subject.

Publications

"The Application of Fracture Mechanics to Stress-Corrosion Cracking," B. F. Brown, *Metallurgical Reviews* 13:129, Dec 1968, pp. 171-183

"Coping with the Problem of the Stress-Corrosion Cracking of Structural Alloys in Sea Water," B. F. Brown, *J. Ocean Engineering* 1:3, Feb 1969, pp. 291-296

"Interpreting Laboratory Stress-Corrosion Cracking Data in Materials Selection," B. F. Brown, presented at 1969 ASME Metals Engineering and Pressure Vessels & Piping Conference on Environmental Effects in Failure of Engineering Materials, Washington, D. C., 31 Mar 1969; ASME Preprint 69-MET-10

"Stress-Corrosion Cracking: A Perspective Review of the Problem," B. F. Brown, NRL Report 7130, 16 June 1970

"Corrosion Effects in Mechanical Failure; Corrosion Fatigue and Stress-Corrosion Cracking," B. F. Brown, Proc. of the 15th Meeting of the Mechanical Failures Prevention Group—MFPG Technical Report No. 8, Office of Naval Research, June 1, 1971

Presentations

"The Application of Fracture Mechanics to Stress Corrosion and Other Cracking Problems in Advanced Metallurgical Materials," B. F. Brown, presented to the Lehigh Valley Chapter, ASM, Bethlehem, Pa., 1 Nov 1968

"The Three Facets of Stress-Corrosion Cracking," B. F. Brown, presented to Washington Section, ASM, as the 1969 Burgess Memorial Lecture, Washington, D. C., 10 Feb 1969

"Relation of Corrosion to the Use of Modern Metallurgical Alloys in the Sea," B. F. Brown, presented at Department of Ocean Engineering, Florida Atlantic University, Boca Raton, Florida, 28 Feb 1969

"Environmental Effects on Fracture," B. F. Brown, presented at Seminar in Deformation and Fracture of Engineering Materials, Carnegie-Mellon University, Pittsburgh, Pa., 17 Mar 1969

"The Fundamentals of Stress Corrosion," B. F. Brown, Lecture to graduate students in corrosion at the University of Delaware, Newark, Delaware, 29 Mar 1969

"Mechanisms of Stress-Corrosion Cracking (SCC)," B. F. Brown, presented at Rice University, Houston, Texas, 28 Apr 1969

"Mechanisms of Stress-Corrosion Cracking (SCC)," B. F. Brown, presented at ARPA Materials Research Council Conference, Centerville, Mass., 15 July 1969

"Implication of Cathodic Reduction of Hydrogen to Stress-Corrosion Cracking," B. F. Brown, presented at the Symposium on Cathodic Processes and Effects of Hydrogen on Metal Properties, 136th National Meeting of The Electrochemical Society, Detroit, Michigan, 5-10 Oct 1969; to be published in Extended Abstract Book

"The ARPA Coupling Program on Stress-Corrosion Cracking," B. F. Brown, presented at the 1969 Tri-Service Meeting on Corrosion of Military Equipment, Annapolis, Md., 19-21 Nov 1969; to be published in Proceedings

"The Application of Fracture Mechanics to Stress-Corrosion Cracking," B. F. Brown, presented at the ASM Educational Conference on Fracture Control for Metal Structures, Philadelphia, Pa., 27 Jan 1970; Chicago, Ill., 21 May 1970

"Implications of Stress Corrosion Cracking in Materials Selection and Design," B. F. Brown, presented to the Department of Mechanical and Aerospace Engineering Seminar, University of Delaware, Newark, Delaware, 10 Apr 1970

"Advances in Stress Corrosion," B. F. Brown, The Institute of Materials Science Lecture Series, University of Connecticut, Storrs, Connecticut, 24 Apr 1970

"Stress-Corrosion Behavior of High Strength Alloy Systems," B. F. Brown, presented at the Session on Stress Corrosion, Air Force Materials Symposium '70, Miami Beach, Florida, 21 May 1970

"Studies on Occluded-Cell Corrosion Phenomena," B. F. Brown, The Gordon Research Conference on Corrosion, New London, N. Y., 26-31 July 1970

"Overview of Stress-Corrosion Cracking," B. F. Brown, presented at the ASM Educational Conference on Stress Corrosion, Philadelphia, Pa., 4 Aug 1970

"Stress-Corrosion Cracking," B. F. Brown, presented to Graduate Course on Behavior of Materials in the Ocean Environment, The Catholic University of America, Washington, D. C., 24-28 Aug 1970

"Mechanical Failures under the Combined Action of Stresses and Corrosive Environments," B. F. Brown, presented to the Meeting on Corrosion Effects in Mechanical Failure, Mechanical Failures Prevention Group, Dayton, Ohio, 14-15 Apr 1971

Naval Research Laboratory

STRESS-CORROSION CRACKING IN TITANIUM (General)

E. P. Dahlberg and B. F. Brown

Objectives

To present or publish, or both, general reviews on stress-corrosion cracking in titanium alloys.

Publications

"An Annotated Bibliography of Recent Papers and Reports on the Subject of Ambient Temperature Aqueous Stress-Corrosion Cracking of Titanium and Titanium Alloys," E. P. Dahlberg, NRL Bibliography Report 29, Oct. 1966

Presentations

"Theory and Technology of Stress-Corrosion Cracking in Titanium Alloys," B. F. Brown, presented at Bureau of Mines, College Park, Maryland, 30 Apr 1969

"Titanium Alloys in the Marine Environment," B. F. Brown, presented at the Symposium on Titanium for the Chemical Engineer, National Meeting of the American Institute of Chemical Engineers, Atlanta, Georgia, 15-18 Feb 1970; Monograph on Symposium on Titanium for the Chemical Engineer, in press

Naval Research Laboratory

CORROSION FATIGUE PROCESSES IN ALUMINUM ALLOY

D. A. Meyn

Objective

To examine the difference between the propagation of cracks in an inert environment and in (humid) air.

Approach

Crack propagation experiments were conducted on aluminum alloy in vacuum and in (humid) air using fracture mechanics to quantify the stress factor. The fracture surfaces were studied by replication electron fractography.

Publication

"The Nature of Fatigue-Crack Propagation in Air and Vacuum for 2024 Aluminum,"
D. A. Meyn, ASM Trans. 61:1, Mar 1968, pp. 52-61

Naval Research Laboratory

DIAGNOSTIC CRITERION FOR STRESS-CORROSION
CRACKING IN ALUMINUM ALLOYS

D. A. Meyn and J. E. Flint

Objective

To examine corrosion product films on Al-Zn-Mg stress-corrosion cracking specimens for indications to differentiate SCC from other fracture modes.

Achievements

The pattern of fractured corrosion product films known as "mud-crack pattern" is a reliable method for positive identification of SCC when it is seen, but it may be missing over a large portion of the SCC surface.

Publications

"Fractographic Diagnosis of Stress-Corrosion Cracking in Al-Zn-Mg," D. A. Meyn, *Corrosion* 26:10, Oct 1970, pp. 427-429

Naval Research Laboratory

ELECTROCHEMISTRY OF STRESS-CORROSION CRACK TIPS

B. F. Brown, E. P. Dahlberg, C. T. Fujii, M. H. Peterson, and J. A. Smith

Objective

To determine and analyze the electrochemical conditions within growing stress-corrosion cracks.

Approach

Three approaches have been tried in order to determine the thermodynamic conditions (pH and E) corresponding to either stress-corrosion cracking initiation or growth: 1) Potentiostating smooth stressed specimens in buffered solutions of known pH, 2) freezing (liquid N) specimens with growing cracks, opening crack wide, and analyzing corrodent as it thaws, and 3) theifing corrodent at intersection of crack with edge of specimen and making instantaneous determination of pH at crack front using antimony electrode or glass electrode.

Achievements

The pH at a growing crack tip in all alloy steels is about 4, as determined by pH papers, antimony electrode, and glass electrode. The acid condition is due to hydrolysis. Potentiostating to various potentials causes large changes in cracking kinetics, but regardless of alloy content, the minimum in kinetics is at about -0.85 or -0.9 volts SCE. This potential corresponds to that for the thermodynamic stability for iron in water. Regardless of alloy or potential, while cracking is occurring the conditions at the crack tip are favorable for the reduction of hydrogen, and only the hydrogen mechanism is required to explain SCC in high strength steels. There is no basic reason why a given area (e.g., the crack tip) cannot be simultaneously an anode for iron dissolution and a cathode for hydrogen reduction.

The pH at the tips of growing cracks in aluminum alloys is about 3.2-3.5, and in titanium alloys about 1.6. Cathodic polarization tends to neutralize this acidity and thereby to reduce cracking kinetics. The addition of CuCl_2 decreases cracking kinetics in titanium alloys, probably by substituting the reduction of copper for the reduction of hydrogen.

Publications

"A Technique for Measuring the pH of Aqueous Solutions Within a Propagating Stress-Corrosion Crack," E. P. Dahlberg, C. T. Fujii, and B. F. Brown, Rept/NRL Prog., Aug. 1968, pp. 28-29

"Methods for Studying the Solution Chemistry Within Stress Corrosion Cracks," B. F. Brown, C. T. Fujii, and E. P. Dahlberg, J. Electrochem Soc. 116:2, Feb 1969, pp. 218-219

"On the Electrochemistry of Stress-Corrosion Cracking of High Strength Steels," B. F. Brown, Bulletin of CEBELCOR 8, March 1969, pp. E. 76/1-4

"Solution Chemistry Within Stress-Corrosion Cracks in Alloy Steels," G. Sandoz, C. T. Fujii, and B. F. Brown, *Corrosion Science* 10:12, Dec 1970, pp. 839-845

"A Method for the Direct Measurement of the Electrochemical Conditions at an Advancing Crack Front," J. A. Smith and M. H. Peterson, *Rept/NRL Prog.*, Jan 1970, pp. 32-33

"On the Existence of a Threshold Stress for Corrosion Cracking in Titanium Alloys in Salt Water," B. F. Brown, *Journal of Materials* 5:4, Dec 1970, pp. 786-791

"Mechanism(s) of Stress Corrosion of High Strength Steels as Deduced Using Indicator Papers," B. F. Brown, *Acta Mexicana de Ciencia y Tecnologia*, in press

"Electrochemical Conditions at the Tip of an Advancing Stress Corrosion Crack in AISI 4340 Steel," J. A. Smith, M. H. Peterson, and B.F. Brown, *Corrosion* 26:12, Dec 1970, pp. 539-542

Invited Talks

"Thermodynamic Conditions at the Tips of Growing Stress-Corrosion Cracks in High Strength Steels," B. F. Brown, presented at the Belgian-American Symposium, CEBELCOR, Brussels, Belgium, 3-4 Sept 1969

"Solution Chemistry Within Stress-Corrosion Cracks in Titanium Alloys," B. F. Brown, presented at the ASM Materials Engineering Congress, Philadelphia, Pa., 15 Oct 1969

"Advances in Stress Corrosion," B. F. Brown, presented at the University of Connecticut, Storrs, Connecticut, 24 Apr 1970

"Solution Chemistry Within Stress-Corrosion Cracks in Titanium 8-1-1 Alloy," B. F. Brown, presented to the International Symposium on Stress Corrosion Mechanisms in Titanium Alloys, Atlanta, Georgia, 27-29 Jan 1971

Naval Research Laboratory

STEELS

G. Sandoz, M. H. Peterson, J. A. Smith, B. F. Brown, and E. P. Dahlberg

Objective

To determine the resistance of high strength steel to stress-corrosion cracking and to further extend our knowledge of the mechanisms involved.

Approach

Determine the threshold values of stress intensity for stress-corrosion cracking in salt water for high strength steels. Study the chemistry of reactions within propagating cracks. Study the effect of individual alloying elements.

Achievements

The susceptibility to stress-corrosion cracking in salt water of a number of high strength steels at various levels of yield strength was measured. The susceptibility of the steels increases with increasing yield strength. Among commercial steels, the higher alloy steels are generally superior, but there are wide variations within any one steel class because of sensitivity to processing variables. In quenched-and-tempered steels the elements C and Mn lower markedly the threshold stress intensity parameter for stress-corrosion cracking; the elements Cr, Ni, Co, Mo, S, and P have little effect.

It was shown that the solution within propagating stress-corrosion cracks in a wide variety of high strength steels has a pH of 3.6-3.8. The metallic elements are in the solution in about the same proportions as in the alloy. A mechanism involving embrittlement from hydrogen released by corrosion reaction explains the observations.

Publications

"Stress-Corrosion Cracking Resistance of an 18Ni 200 Grade Maraging Steel Base Plate and Weld," G. Sandoz and R. L. Newbegin, NRL Memorandum Report 1772, Mar 1967

"Analysis of Environmental Cracking in 4340 Steel by Scanning Electron Microscopy," E. P. Dahlberg and E. J. Brooks, Rept/NRL Prog, Jan 1969, pp. 23-24

"The Effect of Carbon Content on the Stress-Corrosion Cracking Susceptibility of Quenched-and-Tempered Low Alloy Steels," G. Sandoz, R. L. Newbegin, and B. F. Brown, Rept/NRL Prog, July 1969, pp. 28-29

"Effect of Some Elements on the Susceptibility to Stress-Corrosion Cracking," G. Sandoz, Navy Materials Bulletin III:3, Navy Advisory Council on Materials, Oct 1969, p. 7

"The Effect of Manganese Content on the Stress-Corrosion Cracking Susceptibility of Quenched-and-Tempered Fe-C-Mn Alloys in Salt Water," G. Sandoz and R. L. Newbegin, Rept/NRL Prog, Feb 1970, pp. 26-29

"The Effects of Sulfur Content on the Stress-Corrosion Cracking Susceptibility of Quenched-and-Tempered Steel Similar to AISI 4340," G. Sandoz and R. L. Newbegin, Rept/NRL Prog, May 1970

"Electrochemical Conditions at the Tip of an Advancing Stress-Corrosion Crack in AISI 4340 Steel," J. A. Smith, M. H. Peterson, and B. F. Brown, Corrosion 26:12, Dec 1970, pp. 539-542

"Solution Chemistry Within Stress-Corrosion Cracks in Alloy Steels," G. Sandoz, C. T. Fujii, and B. F. Brown, Corrosion Science 10:12, Dec 1970, pp. 839-845

"The Effects of Alloying Elements on the Susceptibility to Stress-Corrosion Cracking of Martensitic Steels in Salt Water," G. Sandoz, Metallurgical Transactions 2:4, Apr 1971, pp. 1055-1063

"Mechanism(s) of Stress Corrosion of High Strength Steels As Deduced Using Indicator Papers," B. F. Brown, Acta Mexicana de Ciencia y Tecnologia, in press

"Stress-Corrosion Cracking of High Strength Steels," B. F. Brown, Proceedings of the NATO Conference on the Theory of Stress Corrosion Cracking in Alloys, in press

"The Resistance of Some High Strength Steels to Slow Crack Growth in Salt Water," G. Sandoz, submitted to Journal of Materials

Presentations

"The Susceptibility to Slow Crack Growth of Some High Strength Steels in Salt Water," G. Sandoz, presented to the ASTM Fall Meeting, Atlanta, Georgia, 2 Oct 1968

"Fractographic Analysis of Stress-Corrosion Cracking in High Strength 4340 Steel," E. Philip Dahlberg, presented at 1969 WESTEC Conference, Los Angeles, California, 13 Mar 1969

"The 'Hydrogen-or-Nothing' Model for Environmental Cracking of Alloy Steels," B. F. Brown, presented at Naval Air Development Center, Philadelphia, Pa., 6 May 1969

"Implication of Cathodic Reduction of Hydrogen to Stress-Corrosion Cracking," B. F. Brown, presented at the Symposium on Cathodic Processes and Effects of Hydrogen on Metal Properties, 136th National Meeting of The Electrochemical Society, Detroit, Michigan, 5-10 Oct 1969

"Stress-Corrosion Cracking of High Strength Steels," G. Sandoz, presented at the 1970 Westec Conference, Session on Stress Corrosion, Los Angeles, California, 9-12 Mar 1970

"Mechanism(2) of Stress Corrosion of High Strength Steels As Deduced Using Indicator Papers," presented at the Latin American Colloquium on Corrosion and Protection of Materials, Mexico City, 8-10 June 1970

"Stress-Corrosion Cracking of High Strength Steels, B. F. Brown, presented at the NATO Conference on the Theory of Stress Corrosion Cracking in Alloys, Ericeira, Portugal, 29 Mar 1971

Naval Research Laboratory

DEVELOPMENT OF STRESS-CORROSION CRACKING SPECIMENS
AND TEST METHODS

E. P. Dahlberg, C. D. Beachem, J. E. Flint, G. Sandoz, and R. L. Newbegin

Objective

To develop specialized specimens for determining stress-corrosion cracking (SCC) characteristics for both research and technology.

Approach

Specimens were sought which would contain a precrack and would be analyzable by fracture mechanics methods.

Achievements

A small specimen suitable for SCC tests of sheet material was designed and compliance measurements were made. When the notched specimen is stressed by a wedge to a measured displacement and is then exposed to a corrosive, a stress-corrosion crack propagates until the crack tip has reached a region where the stress is too low to propagate the crack further. This condition is defined as $K_{I_{SCC}}$ for arrest, and the K number can be determined from the compliance calibration, the crack length, and the displacement. The specimen is thus similar to the Manjoine specimen which had been adopted by Rolfe for SCC testing, except that the present specimen is suitable for sheet material. An equivalent specimen was designed for thick plate and was stressed by an elastic ring which relaxed as the crack grew, again permitting a crack-arrest characterization. A simple constant K specimen has been demonstrated useful for SCC kinetic studies; this specimen, designated the double torsion specimen, can be made from sheet material with a minimum of machine work.

Presentations

None.

Publications

"Stress-Corrosion-Cracking Test Methods," E. P. Dahlberg, Rept/NRL Prog, Oct 1967, pp. 41-42

"Stress-Corrosion-Cracking Characteristics of Several Aluminum Alloys by a Crack-Arrest Method," E. P. Dahlberg, Rept/NRL Prog, Jan 1968, pp. 23-24

"A Self-Stressed Specimen for Measuring Stress-Corrosion Cracking in Aluminum Alloys," E. P. Dahlberg, Rept/NRL Prog, April 1968, pp. 25-27

"Characterizing Stress-Corrosion Cracking in a 7079-T651 Aluminum Alloy by Using a Self-Stressed Double Cantilever Beam Specimen," E. P. Dahlberg, Rept/NRL Prog, Aug 1968, pp. 25-28

"Compliance Measurements for a Simple (WOL) Stress-Corrosion Cracking Test Specimen," E. P. Dahlberg and J. E. Flint, Rept/NRL Prog, Oct 1968, pp. 20-21

"A Constant K Specimen for Stress Corrosion Cracking Testing," C. D. Beachem, J. A. Kies, and B. F. Brown, Materials Research & Standards 11:4, April 1971, p. 30

Naval Research Laboratory

SCC IN TITANIUM

G. Sandoz, E. P. Dahlberg, R. L. Newbegin, and D. A. Meyn

Objective

To determine the effects of various environments on titanium alloys and use this information to determine the mechanisms of stress-corrosion cracking.

Approach

Use the cantilever beam test or the wedge load-type specimen test, or both, to determine values of $K_{I_{SCC}}$.

Achievements

Found that dissolved hydrogen in titanium alloys produces effects similar to effects of some environments. Generally, a common fracture plane is favored, regardless of the environment. Environment may be organic and need not be an electrolyte to produce cracking. Values of threshold stress intensity are similar in all organic environments, but values in water and methanol are somewhat lower.

Publications

"Effects of Some Organics on the Stress Corrosion Susceptibility of Some Titanium Alloys," G. Sandoz, DMIC Memorandum 228, Battelle Memorial Institute, 6 Mar 1967, pp. 10-15

"Stress Corrosion Cracking Susceptibility of a Titanium Alloy in a Non-electrolyte," G. Sandoz, *Nature* 214, 8 April 1967, pp. 166-167

"Fractography and Crystallography of Subcritical Crack Propagation in High Strength Titanium Alloys," D. A. Meyn and G. Sandoz, *Trans. TMS/AIME* 245, June 1969, pp. 1253-1258

"Subcritical Crack Propagation in Ti-8Al-1Mo-1V Alloy in Organic Environments, Salt Water, and Inert Environments," G. Sandoz, *Proceedings of Conference on Fundamental Aspects of Stress Corrosion Cracking*, NACE, Houston (1969), pp. 684-690

"Thin Foil Electron Microscopy," E. P. Dahlberg, *Rept/NRL Prog*, Apr 1967, pp. 19-21

"Delayed Fracture Characteristics of Ti-8Al-1Mo-1V Alloy," G. Sandoz, *Rept/NRL Prog*, May 1967, pp. 31-32

"Effect of Specimen Breadth on Susceptibility to Stress-Corrosion Cracking of Ti-8Al-1Mo-1V Alloy in Salt Water," G. Sandoz and R. L. Newbegin, *Rept/NRL Prog*, Aug 1967, pp. 45-46

"Delayed Failure of Ti-7Al-2Cb-1Ta Under Mode III Loading in Air, Salt Water and Methanol," D. A. Meyn, *Rept/NRL Prog*, Nov 1967, pp. 33-34

"Effect of Hydrogen Content on Subcritical Crack Growth in Ti-8Al-1Mo-1V Alloy," G. Sandoz and R. L. Newbegin, Rept/NRL Prog, Nov 1967, pp. 35-36

"Stress-Corrosion Cracking Tests of Surface Flawed Specimens of Ti-7Al-2Cb-1Ta," R. W. Judy, Jr., and E. P. Dahlberg, Rept/NRL Prog, May 1968, pp. 30-31

"Effects of Hydrogen Content and Environment on Subcritical Crack Growth in Ti-7Al-2Cb-1Ta and Ti-6Al-4V Alloys," G. Sandoz and R. L. Newbegin, Rept/NRL Prog, Nov 1968, pp. 31-32

"Subcritical Cracking of Ti-8Al-1Mo-1V in Mercury," D. A. Meyn and E. P. Dahlberg, Rept/NRL Prog, Mar 1969, pp. 17-18

Presentations

"Evaluation of Some Stress-Corrosion Cracking Characteristics of Aluminum Alloys Using Pre-cracked Specimens," E. P. Dahlberg, presented to the ASTM Fall Meeting, Atlanta, Georgia, 3 Oct 1968

"Solution Chemistry Within Stress-Corrosion Cracks in Titanium 8-1-1 Alloy," B. F. Brown, presented to the International Symposium on Stress Corrosion Mechanisms in Titanium Alloys, Atlanta, Georgia, 27-29 Jan 1971

Naval Research Laboratory

TOPOLOGY OF STRESS-CORROSION CRACKING FRACTURES IN TITANIUM

D. A. Meyn

Objective

To examine the details of stress-corrosion cracks in titanium alloys.

Approach

Replica electron fractography was used on laboratory specimens and on a specimen from an Apollo fuel cell tankage failure analysis.

Achievements

The fracture of Ti-6Al-4V by SCC in methanol demonstrated that the relative proportion of cleavage, peculiar to SCC in Titanium alloys, and mechanical rupture (by microvoid coalescence) depends upon stress intensity K . When K is low, most of the fracture is by cleavage; when K is high, there is a high proportion of microvoid coalescence, and thus the total process is a mixture of two mechanisms.

Publications

"Effect of Crack Tip Stress Intensity on the Mechanism of Stress-Corrosion Cracking of Titanium-6Al-4V in Methanol," D. A. Meyn, *Corrosion Science* 7:10, Oct 1967, pp. 721-723

Naval Research Laboratory

THE CONCEPT OF THE OCCLUDED CORROSION CELL

B. F. Brown

Objective

To analyze the process of stress-corrosion cracking (SCC) and the other forms of localized corrosion, such as pitting, crevice corrosion, intergranular corrosion, filiform corrosion, and exfoliation.

Achievements

It is concluded that the corrodent within all these local corrosion cells is acid by reason of hydrolysis and that it remains acid because of the restricted communication with the outside environment. This acidity militates against repassivation. Cathodic protection is effective in both preventing and stopping this form of attack by increasing the pH to the level at which protective metal oxides or hydroxides will form. (In alloys susceptible to hydrogen cracking, cathodic protection against SCC may not be a satisfactory solution.) This work has led to the organization (largely by Dr. Roger Staehle of Ohio State University) of an International Conference on the Occluded Corrosion Cell to be held in December 1971.

Publications

"The Role of the Occluded Corrosion Cell in Stress-Corrosion Cracking of High Strength Steels," B. F. Brown, CEBELCOR's Rapports Techniques 112, Jan 1970, pp. RT 170/1-3

"The Concept of the Occluded Corrosion Cell," B. F. Brown, Corrosion 26:8, Aug 1970, pp. 249-250

Presentations

"New Light on the Solution Chemistry of Stress-Corrosion Cracking," B. F. Brown, presented as the RESA Lecture at the Naval Research Laboratory, Washington, D. C., 19 Nov 1968, consequent to the receipt of the E. O. Hulburt Award

"Three Forms of Occluded-Cell Corrosion," B. F. Brown, presented at National Bureau of Standards, Gaithersburg, Maryland, 14 Apr 1969

"Studies on Occluded-Cell Corrosion Phenomena," B. F. Brown, presented at the Gordon Research Conference on Corrosion, New London, N. Y., 26-31 July 1970

Naval Research Laboratory

APPLICATION OF TENSILE LIGAMENT INSTABILITY MODEL
TO STRESS-CORROSION PROBLEMS

J. M. Krafft and A. M. Sullivan

Objective

To apply the ligament instability model to studies of stress-corrosion in an attempt to provide a consistent explanation of observed time to fracture and crack growth rate data.

Approach

A model which attributes stress-corrosion crack growth rate to erosive surface attack of d_T size ligaments is proposed. The ratio of surface reaction rate V_s and crack growth rate V_c can readily be evaluated from details of the stress strain curve. Relative specimen life t_f can be estimated from the summation. The model is examined by comparing the life time, or crack velocities, of notched bend specimens in aggressive environments with bulk plastic flow properties.

Achievements

Using either time to fracture or crack velocity data, generated as functions of the stress intensity factor K_I , substantial agreement with the material property dependent V_c/V_s curve is evident. Thus, the validity of this essentially mechanical model is demonstrated. Indicating the essential V_c curve shape it provides a rationale both for the threshold and observed non-sensitivity of velocity to K_I level.

Estimates of surface reaction rates, V_s , are also possible which agree well with the few published values.

Further calculations combining ligament area and V_s can generate information concerning the weight of metal involved in the corrosion process, which has been confirmed by micro-chemical analysis.

Publications

"Role of Local Dissolution in Corrosion-Assisted Cracking of Titanium Alloys," J. M. Krafft, Rept/NRL Prog, March 1967, pp. 6-18

"Dissolution Velocities of Different Organic Media," A. M. Sullivan, Rept/NRL Prog, April 1967, pp. 18-19

"Tensile-Ligament Instability and the Growth of Cracks in High Strength Alloys," J. M. Krafft and J. H. Mulherin (Frankford Arsenal), Trans ASM, 62, 1 March 1969, pp. 64-81

"Weight of Metal Involved During Progress of a Stress Corrosion Crack," A. M. Sullivan, Rept/NRL Prog, March 1969, pp. 18-19

"Velocity of Stress-Corrosion Cracks," A. M. Sullivan, Rept/NRL Prog, July 1969, pp. 30-31

"Velocity of Cracks Extending Under Stress in an Adverse Environment," A. M. Sullivan, Proceedings of Second International Conference on Fracture, Brighton, England, April 1969

Presentations

"Environmental Effects on Crack Growth Rates with Sustained and Repeated Load Cycles," J. M. Krafft and A. M. Sullivan, Invited talk at Symposium on Practical Aspects of Fatigue and Fracture, Derby, England, March 1970

"Stress-Corrosion Crack Velocity in 4340 Steel," A. M. Sullivan, presented to the 4th National Symposium on Fracture Mechanics, Pittsburgh, Pennsylvania, Aug 1970; to be published in Journal of Engineering Fracture Mechanics

Naval Research Laboratory

DUAL SCC-RATIO ANALYSIS DIAGRAMS FOR HIGH STRENGTH STRUCTURAL MATERIALS

R. W. Judy, Jr., and R. J. Goode

Objective

The objective of the dual SCC-RAD approach was to provide interpretative procedures for relating laboratory K_{Isc} data to materials applications.

Approach

Fracture mechanics technology provides equations to relate K_{Ic} values determined in the laboratory to flaw size-stress level relationships for fracture. Ratio Analysis Diagram (RAD) procedures have been evolved to make engineering assessments of conditions for fast fracture of the entire strength range of high strength metals. Expression of stress-corrosion cracking (SCC) characteristics in fracture mechanics parameters permits the effects of hostile environments on the same structural metals to be included in the RAD framework.

Achievements

Dual SCC-RAD procedures were derived for high strength steels and for titanium alloys. The ASTM E24 Committee's recommendations for specimen dimensions in K_{Ic} testing were imposed for the SCC specimens to determine a thickness requirement. The thickness requirement was necessary to separate plane strain and plane stress fracture conditions. With these criteria, SCC data were added to the RAD for steels and the RAD for titanium alloys by using the existing K_{Ic} scales. The thickness criteria were included on the RADs in the form of lines of constant ratio K_{Isc}/σ_{ys} ; the value of the ratio depended on the thickness of the specimen involved. A region of SCC tunnelling was defined for which K_{Isc} values cannot be obtained. Below this region K_{Isc} measurements are possible, and engineering interpretation of flaw size-stress level conditions for SCC and for fast fracture can be made.

Publications

"Stress-Corrosion Cracking Characterization Procedures and Interpretations to Failure-Safe Use of Titanium Alloys," R. W. Judy, Jr. and R. J. Goode, NRL Report 6879, 8 April 1969; ASME Journal of Basic Engineering 91, Series D(4), Dec. 1969, pp. 614-617

"Procedures for Stress-Corrosion Cracking Characterization and Interpretation to Failure-Safe Design for High Strength Steels," R. W. Judy, Jr. and R. J. Goode, NRL Report 6988, 29 Nov. 1969

Naval Research Laboratory

EFFECTS OF HEAT-TREATMENT ENVIRONMENTS ON THE STRESS-CORROSION
CRACKING RESISTANCE OF TITANIUM ALLOYS

D. G. Howe and R. J. Goode

Objective

The objective was to determine the effects of heat-treatment environments on the salt water stress-corrosion cracking (SCC) characteristics of four titanium alloys.

Approach

Cantilever bend tests were conducted in 3 1/2% salt water environments for samples of Ti-8Al-1Mo-1V, Ti-7Al-1Mo-1V, Ti-6Al-4V, and Ti-7Al-2.5Mo alloys which had been heat treated and aged in helium or argon atmospheres or in vacuum. The $K_{I_{SCC}}$ data for the various environments were compared.

Achievements

The $K_{I_{SCC}}$ characteristics were determined for a variety of heat-treating conditions involving different furnace environments at each step. Vacuum solution annealing and cooling in a helium atmosphere resulted in material immune to salt water SCC for all four alloys. Heat treatments in argon or helium atmospheres resulted in $K_{I_{SCC}}$ values that were dependent on the solution annealing temperature rather than the heat treating environment. The results of chemical analyses of the interstitial hydrogen content of all materials tested indicated a conjunctive relationship between the salt water SCC resistance and the interstitial hydrogen content of the material.

Publications

"Effects of Heat Treating Environmental Conditions on the Stress-Corrosion Cracking Resistance of Several Titanium Alloys," D. G. Howe and R. J. Goode, ASTM STP 432, (1968) pp. 189-201

"Effects of Heat Treatment Environmental Conditions on Stress-Corrosion Cracking Resistance of Several Titanium Alloys," D. A. Howe, Rept/NRL Prog, Feb 1967, pp. 32-35

"Effects of Heat-Treatment on the Stress-Corrosion-Cracking Resistance of the Alloy Ti-6Al-6V-2.5Sn," D. G. Howe, Rept/NRL Prog, Sept 1967, pp. 51-52

Naval Research Laboratory

CHARACTERISTICS OF STRESS-CORROSION CRACKING RESISTANCE OF HIGH STRENGTH TITANIUM ALLOYS

R. W. Judy, Jr., R. J. Goode, and R. W. Huber

Objective

The objective of these studies was the determination of the effects of salt water (simulated seawater) environments on structural titanium alloys.

Approach

Cantilever bend tests were conducted for a wide variety of titanium alloys in a 3 1/2 wt-% salt water environment. The SCC threshold (K_{Isc}) values were compared with mechanical property data.

Achievements

Characteristic K_{Isc} values were determined for a wide variety of titanium alloy plate materials and metal-inert-gas (MIG) and electron-beam (EB) weldments. These represented one-inch-thick materials with variations of heat-treated conditions and welding parameters. It was shown that comparison of salt water SCC resistance of titanium alloys was not related to other mechanical properties of the material. Interpretation of the K_{Isc} data to predictions of critical flaw size for yield stress loading was summarized on a SCC-index diagram based on linear elastic fracture mechanics.

Publications

"Stress-Corrosion Cracking Characteristics of Alloys of Titanium in Salt Water," R. W. Judy, Jr., and R. J. Goode, NRL Report 6564, 21 July 1967

"Fracture Toughness and Stress-Corrosion Cracking of Some Titanium Alloy Weldments," R. W. Huber, R. J. Goode, and R. W. Judy, Jr., Welding Journal Research Supplement 32: 10, October 1967, pp. 1-9

"Fractographic Study of Titanium Alloy SEN Fracture Mechanics Specimens," R. W. Judy, Jr., and R. J. Goode, Rept/NRL Prog, Nov 1966, pp. 18-20

"Stress-Corrosion-Cracking Characterization Studies of High Strength Titanium Alloy Weldments," R. W. Judy, Jr., A. Friedland, and R. J. Goode, Rept/NRL Prog, Nov 1966, pp. 20-21

"Stress-Corrosion-Cracking Characteristics of Alloys of Titanium in Salt Water," R. W. Judy, Jr., and R. J. Goode, NRL Report 6564, 21 July 1967

"Stress-Corrosion-Cracking Behavior in Titanium Alloys," R. W. Judy, Jr., and R. J. Goode, Rept/NRL Prog, July 1967, pp. 38-40

"Fracture Toughness and Salt-Water Stress-Corrosion-Cracking Resistance of Titanium Alloy Weldments," R. W. Huber, R. J. Goode, and R. W. Judy, Jr., Rept/NRL Prog, Nov 1967, pp. 1-11

"Study of Notch Acuity on the SCC Characteristics of Titanium Alloys,"
R. W. Judy, Jr., and R. J. Goode, Rept/NRL Prog, Nov 1967, pp. 34-35

"Procedures for Stress-Corrosion Cracking Characterization and Interpretation
to Failure-Safe Design for High Strength Steels," R. W. Judy, Jr., and R. J.
Goode, NRL Report 6988, 29 Nov 1969

Naval Research Laboratory

IRON HYDRIDE PREPARATION

Forrest L. Carter and M. O'Hara

Objective

To prepare and characterize the iron hydrides which are logical precursors to the understanding of the role hydrogen plays in the stress-corrosion cracking of steels.

Approach

The preparation of the iron hydrides is being attempted by four different chemical methods involving glove box procedures to provide an inert working atmosphere. These are: 1) The Grignard reaction between phenylmagnesium bromide and an anhydrous iron chloride in the presence of purified hydrogen, 2) the reaction between pyrophoric aluminum triethyl and an iron chloride in the presence of hydrogen, 3) the electrolysis of ammonium chloride in liquid ammonia using iron electrodes, and 4) the sputtering of iron via argon-hydrogen bombardment. In this latter method it is hoped that the atomic iron produced by energetic argon ions will react with hydrogen while it is in the finely divided state.

Achievements

It has been shown that the earlier work using the Grignard-reaction (1, above) is in error in that one obtains not the transition metal hydrides, but rather transition metal ether complexes of low hydrogen content (as hydride). Using the second method involving triethyl aluminum, small quantities of a black crystalline paramagnetic powder have been obtained. This material, containing iron, hydrogen, and 10-20% aluminum, is readily indexed as BCC with a 3.30\AA cell edge compared with BCC iron, the unit cell volume is 50% greater, and generally appears to be related to the iron hydride sought. It is possible that the compound is stabilized by the incorporation of aluminum, for which well-characterized hydrides are known. An alternate synthesis of this "iron aluminum hydride" is being attempted via the reaction of iron trichloride with the alkali aluminum hydrides. A reaction intermediate involving tetrahydrofuran has been obtained using LiAlH_4 . The decomposition of this product will be attempted by refluxing in a hydrocarbon solvent. The electrolysis of ammonium chloride in liquid ammonia gave no detectable change in the x-ray powder pattern of an iron wire electrode. However, the electrolysis of a liquid ammonia-ammonium chloride electrolyte containing FeCl_3 did yield a brown deposition on a platinum wire cathode. Difficulties in the isolation of this deposit have prevented its characterization to date. Definitive results for the argon bombardment method are yet to be obtained.

Naval Research Laboratory

POTENTIOSTATIC BEHAVIOR AND PASSIVATION OF ANODIC REACTIONS OF IRON AND PLATINUM

S. Schuldiner

Objective

The electrochemical behavior of iron and platinum has been investigated in closed high purity systems. Especial attention was paid to determination of the mechanism of passivation.

Approach

Steady-state potentiostatic polarization curves were determined under conditions in which reactable impurities were reduced by pre-electrolysis to extremely low levels. Effects of added impurities were determined after the behavior under high purity conditions was determined. Effects of anion adsorption were determined under both steady-state and transient conditions.

Achievements

Over a dozen identifying characteristics due to small amounts of impurities were described and most of the interfering impurities were reduced to a level of less than one part in 10^{12} . Under these conditions, iron gave results similar to platinum and acted as a noble metal, showing no corrosion at any applied potential. Current densities were only a few percent of those given in the literature where iron corroded under conditions of ordinary purity. The high purity system can act as a standard for determining electrode reactions and the nature of passivation and was used here to evaluate quantitatively the effect of adding various amounts of chloride ion to the system, thus showing the initiation of corrosion and of passivity. A mechanism of inert anion adsorption on the passive behavior of the hydrogen oxidation reaction on platinum was demonstrated under both steady-state and transient conditions.

Publications

"Passivation of Anodic Reactions," S. Schuldiner, Rept/NRL Prog, March 1968, p. 21; J. Electrochem. Soc. 115, Sept 1968, p. 897; and NRL Report 6703, 30 Apr 1968

"Anodic Oxidation of Hydrogen on Iron and Platinum in Sodium Hydroxide Solution," S. Schuldiner and C. M. Shepherd, J. Electrochem. Soc. 115, Sept 1968 p. 916; and NRL Report 6718, 24 May 1968

"Potentiostatic Current-Potential Measurements on Iron and Platinum Electrodes in High-Purity Closed Alkaline Systems," C. M. Shepherd and S. Schuldiner, J. Electrochem. Soc. 115, 1968, p. 1124; and NRL Report 6748, 26 Aug 1968

"Effect of Chloride Ion on Corrosion of Iron," C. M. Shepherd and S. Schuldiner, submitted to Corrosion Science

"Characterization of Platinum Electrodes in Sulfuric Acid Solution. I. Transient Conditions," M. Rosen, D. R. Flinn, and S. Schuldiner, submitted to the Journal of the Electrochemical Society

Presentations

Each of the above papers has been given at technical meetings. In addition, the following have been presented:

"Passive Films," S. Schuldiner, presented at the ARPA-IDL Navy Briefing, NSRDC (David Taylor Model Basin), Nov 2, 1967

"Passivation of Platinum and Iron in High-Purity Systems," S. Schuldiner, presented at the Gordon Research Conference on Corrosion, July 24, 1968

"Mechanisms of Passivation of Anodic Reactions on Inert Electrodes," S. Schuldiner, presented at the University of Pennsylvania, Chemistry Seminar, Philadelphia, Pa., Nov 6, 1968

Naval Research Laboratory

ROLE OF CHLORIDE IONS IN STRESS-CORROSION CRACKING

T. A. Kovacina and D. L. Venezky

Objective

Determine distribution of chloride ion between liquid (sodium chloride solution) and solid [iron (IV) oxide] phases and determine the reaction mechanisms involved.

Approach

Specific ion electrodes (H^+ and Cl^-) and the radioisotope $^{36}Cl_{17}$ are used to monitor the effect of the addition of αFe_2O_3 to various aqueous solutions.

Achievements

Additions of pure αFe_2O_3 (<10 ppm total impurities) to carbon dioxide free water or aqueous sodium chloride solutions resulted in significant changes in the hydrogen ion concentrations of the solutions. The results are consistent with a postulated initial hydration of the solid oxide surface, followed by acidic or basic hydrolysis, depending on the environment. Although a much weaker base than the hydroxide ion, the chloride ion appears to successfully replace hydroxide ions on the hydrated oxide surface.

Publication

"Investigations of Selective Interactions of the Iron/Aqueous Sodium Chloride System. Part 1—The Adsorption of Chloride Ion by α -Iron (III) Oxide in Oxygen-Saturated Sodium Chloride Solutions at 30°C," T. Kovacina and D. L. Venezky, NRL Report 7264, May 1971

Naval Research Laboratory

EFFECT OF CHEMICAL ENVIRONMENT ON STRESS-CORROSION
CRACKING OF METALS

H. R. Baker and C. R. Singleterry

Objective

To define chemical factors influencing stress-corrosion cracking (SCC) of metals and to identify chemical inhibitors of SCC.

Approach

SCC of U-bend specimens is studied under conditions of controlled pH, temperature, and ionic environment. The effect of corrosion inhibitors on SCC is examined as a function of these variables.

Achievements

Conditions have been established for the rapid SCC of 4340 steel in various salt solutions. It has been shown that conventional inhibitors of steel corrosion are effective in preventing SCC of this alloy, but that the inhibitors must be present at much higher concentrations than are required for the prevention of surface corrosion. As could be expected from the observations of the characteristic pH encountered in stress-corrosion cracks, the presence of an adequate alkaline reserve, by itself or in conjunction with conventional inhibitors, exerted a marked inhibiting effect. A report of this work is in preparation. Suitable buffering of chromate solutions has also been shown to delay the SCC of 7075 T aluminum alloy. Corrosion of 4340 alloy in boiling NaCl solution lowers the solution pH with concurrent formation of Fe_3O_4 , thus accelerating corrosive processes.

Naval Research Laboratory

OXIDE FILM EFFECTS IN STRESS-CORROSION CRACKING

M. C. Bloom* and S. H. Smith, Jr.

(* Retired 1 July 1969)

Objective

To determine whether the presence or absence of an oxide film on a metal alters its SCC behavior and whether the electrical conductivity or some other physical or electrochemical property of the oxide is a factor.

Approach

Some suitable SCC evaluation test having been selected, a specimen would be coated with either conductive or insulating oxide and tested. Expected to be of importance would be porosity of the film and its dependence on the method of growth. Ease of hydrogen permeation might be germane too.

Achievements

A procedure was devised for preparing type 4340 steel specimens for cantilever beam tests, but it was necessary to start the required fatigue crack before heat treating and this impeded experimental control of oxide in the crack. Instead, the simpler U-bend technique was put to use.

Experiments have thus far shown no performance difference between conductive (Fe_3O_4) film coatings and insulating (MnFe_2O_4) ones, but these were porous films. Other specimens coated with Teflon to simulate the physical but not chemical presence of oxide have tended to crack where pits formed at the bottom of pores. Iron plating 0.002 to 0.030-in. -thick curtails SCC in either acid (pH 2-3) or alkaline (pH 6-9) media, but oxidation of this plate to Fe_3O_4 hastens it.

Naval Research Laboratory

SURFACE CHEMICAL STUDIES OF METAL SURFACES

L. B. Lockhart, Jr., and R. L. Patterson, Jr.

Objective

Radiochemical techniques are used to investigate the nature of the bonding between adsorbed molecules and active sites at the surface of ferrous metals and their alloys.

Approach

Adsorption/desorption studies are made of carbon-14-labeled stearic acid and octadecylamine on iron, steel, and glass surfaces to learn more about the extent of surface coverage, the effective surface area of highly polished surfaces, and the number and type of active adsorption sites present in the surface layer. Fire-polished soft glass is used as a reference surface.

Achievements

Procedures have been developed for the preparation of condensed monomolecular films of stearic acid-1-C¹⁴ on both soda-lime glass and ferrous metals using retraction from nitrobenzene solution. Desorption studies have shown that 20-40% of the adsorbed molecules are strongly bonded, presumably through chemical reaction with active surface sites. A relationship has been developed between the extent of surface coverage and the contact angle of the adsorbed film.

Publications

"A Study of the Adsorption of Carbon-14 Labeled Stearic Acid on Iron," C. O. Timmons, R. L. Patterson, Jr., and L. B. Lockhart, Jr., NRL Report 6553, June 2, 1967; also *J. Colloid and Interface Sci.* 26, Jan 1968, pp. 120-127

"The Adsorption of Carbon-14-Labeled Stearic Acid on Soda-Lime Glass," R. L. Patterson, Jr. and L. B. Lockhart, Jr., NRL Report 6901, May 23, 1969

Subject Index to Abstracts of Achievement

	<u>Page</u>
Aluminum Alloys	
Corrosion fatigue	41,129,160
Stress-corrosion cracking	
Alloy development	33
Basic structure and fractography	41,86,87,95,98,99, 105,106,107,161
Characterization of alloys	28,33,126
Effect of environments	36,41,78,79,88,104
Effect of heat treatment	29,30,32,35,36,98
Electrochemistry	136,139,162
Inhibitors	182
Other basic studies	36,104,146,183
Interpretation of Test Data	
Continuum mechanics	169,174
Correlation of smooth and precracked data on aluminum	28
Crack branching	46
Wedge-force loading compared with remote loading in corrosion fatigue	41
Mechanics (Continuum)	133,134
Miscellaneous Materials	
MgO	81
CuNi	110
CuAu	142
Ni	145
Mica	157
Glass	159
Reviews	
Subcritical flaw growth	139
Al-H system	155
H in Fe	156
SCC (General)	165
SCC in Ti	167
Oxidation of Ti	77
Ti-H	76
Anion effects in corrosion	78,79
SSC Test Methods	
DCB specimen for Al alloys	29,36,175
Procedures and specimens	48,50,52,54,55,64
Specimen thickness	132

Steels

Corrosion fatigue 134,135

Stress-corrosion cracking

Characterization of alloys 49,125,172
 Effect of composition and impurities 45,91,108,172
 Effect of grain size 43,89,92
 Effect of heat treatment 43,47,92,93,97
 Effect of processing variables. 43
 Effect of various environments 101,130
 Electrochemistry 130,170,187
 Inhibitors. 190
 Mechanisms 79,80,83,90,92,103,108,
 112,114,147,186

Surface Preparation Effects 96

Surface Science Studies

Adsorption on iron 192
 Auger spectroscopy of titanium 116
 Chemisorption 148,151
 Electrochemistry of crack tip 170
 Electrochemistry of iron 187
 Electron spin resonance 160,161,162
 Field emission microscopy 120
 Field ion microscopy 122
 Ion bombardment 150
 Low energy electron diffraction 116,163
 Mossbauer spectroscopy 153

Titanium

Corrosion fatigue 138

Stress-corrosion cracking

Effect of composition, heat treatment, and structure . . . 57,59,61,64,66,67,69,
 71,72,77,184
 Effect of various environments 65,133,176
 Mechanisms 56,63,65,76,86,100,118,
 170,176,178
 Physical metallurgy 56,61,71,84,94

ACKNOWLEDGMENTS

The author wishes to acknowledge with thanks the contributions of the following persons: The principal investigators in the various organizations who directed the research in those organizations and the reporting thereof—Dr. D. Piper at The Boeing Company, Professor R. Foley at American University, Professor H. Paxton at Carnegie-Mellon University, Professor E. Verink, Jr., at University of Florida, Professor R. Hochman at Georgia Institute of Technology, and Professor P. Paris and Dr. H. Leidheiser, Jr., at Lehigh University; Mrs. R. Anastasio and Mrs. B. Test, who organized, smoothed, and produced the typescript; Mr. E. J. Chapin, who assembled and checked the Abstracts of Achievements; Mr. W. Ramey, who advised in the production of an unusual form of final report; and Dr. J. Scully who made valuable technical criticisms. Dr. G. Sandoz of NRL provided valuable assistance in collecting material for the up-dated version.

This research was supported by the Advanced Research Projects Agency of the Department of Defense, NRL Problem M04-08A, and was monitored by the Naval Research Laboratory under Contract Nos. N00014-67-A-0370-0006, N00014-68-A-314-0008, N00014-66-C0365, N00014-67-A-0159-0007, N00014-68A-0245-0001, and N00014-68-A-0173-0003.

DOCUMENT CONTROL DATA - R & D

(Security classification of title, body of abstract and indexing annotation must be entered when the overall report is classified)

1. ORIGINATING ACTIVITY <i>(Corporate author)</i> Naval Research Laboratory Washington, D.C. 20390		2a. REPORT SECURITY CLASSIFICATION Unclassified	
		2b. GROUP	
3. REPORT TITLE ARPA COUPLING PROGRAM ON STRESS-CORROSION CRACKING (Final Technical Report: Second Edition)			
4. DESCRIPTIVE NOTES <i>(Type of report and inclusive dates)</i> A final report on the problem.			
5. AUTHOR(S) <i>(First name, middle initial, last name)</i> Brown, B. F.			
6. REPORT DATE October 27, 1971		7a. TOTAL NO. OF PAGES 200	7b. NO. OF REFS 0
8a. CONTRACT OR GRANT NO. NRL Problem M04-08A		9a. ORIGINATOR'S REPORT NUMBER(S) NRL Report 7329	
b. PROJECT NO. ARPA Order 878		9b. OTHER REPORT NO(S) <i>(Any other numbers that may be assigned this report)</i>	
c.			
d.			
10. DISTRIBUTION STATEMENT Approved for public release distribution unlimited.			
11. SUPPLEMENTARY NOTES		12. SPONSORING MILITARY ACTIVITY Department of Defense (Advanced Research Projects Agency) Washington, D.C. 20301	
13. ABSTRACT The technical background, organization, and <u>modus operandi</u> of the ARPA coupling program on stress-corrosion cracking are summarized. The problem of interpreting the data from smooth stress-corrosion cracking specimens is discussed. This is followed by a summary of technical achievement highlights in narrative form treating specimen types, titanium alloys, high strength steels, aluminum alloys, and surface sciences. An Abstracts of Achievements section (abstract arranged by organization) is the most important part of this report, for it gives not only indications of technical contributions but the literature citations where the interested reader can examine the detailed account of a given topical area. The Abstracts of Achievements section includes a subject index. The Program was one of multiple goals, including experimentation involving coupling the Naval Research Laboratory with academic personnel and amplifying NRL's capabilities by the addition of an industrial contractor. Since the present report is a purely technical one, it does not treat these nontechnical goals. The present report represents an updating of NRL Report 7168 to include material published during the phase-out year of the program.			

UNCLASSIFIED

14. KEY WORDS	LINK A		LINK B		LINK C	
	ROLE	WT	ROLE	WT	ROLE	WT
Stress-corrosion cracking High-strength steels Titanium alloys Aluminum alloys Electrochemistry Fracture mechanics Surface science						